U. PORTO

DOUTORAMENTO

BIOLOGIA MOLECULAR E CELULAR

Characterization of a novel family of AB toxins with potential to be used as antigen delivery vehicles

Inês Lua Freitas

D

2025

U. PORTO

Inês Lua Freitas. Characterization of a novel family of AB toxins with potential to be used as antigen delivery vehicles

D.ICBAS **2025**

Characterization of a novel family of AB toxins with potential to be used as antigen delivery vehicles

Inês Lua Araújo Dias Nunes de Freitas

INSTITUTO DE CIÊNCIAS BIOMÉDICAS ABEL SALAZAR

FACULDADE DE CIÊNCIAS

INÊS LUA FREITAS

CHARACTERIZATION OF A NOVEL FAMILY OF AB TOXINS WITH POTENTIAL TO BE USED AS ANTIGEN DELIVERY VEHICLES

Tese de Candidatura ao grau de Doutor em
Biologia Molecular e Celular;
Programa Doutoral da Universidade do Porto (Instituto de Ciências Biomédicas de Abel Salazar e Faculdade de Ciências)

Orientador – Doutor Nuno dos Santos
Categoria – Investigador Principal
Afiliação – Instituto de Investigação e Inovação em Saúde da Universidade do Porto e Instituto de Biologia Molecular e Celular.

Co-orientadora – Doutora Ana do Vale
Categoria – Investigadora Auxiliar
Afiliação – Instituto de Investigação e Inovação em Saúde da Universidade do Porto e Instituto de Biologia Molecular e Celular.

Co-orientador – Doutor Johnny Lisboa
Categoria – Investigador Júnior
Afiliação – Instituto de Investigação e Inovação em Saúde da Universidade do Porto e Instituto de Biologia Molecular e Celular.

DECLARATION OF HONOUR

Declaro que a presente tese é de minha autoria e não foi utilizada previamente noutro curso ou unidade curricular, desta ou de outra instituição. As referências a outros autores (afirmações, ideias, pensamentos) respeitam escrupulosamente as regras da atribuição, e encontram-se devidamente indicadas no texto e nas referências bibliográficas, de acordo com as normas de referenciação. Tenho consciência de que a prática de plágio e auto-plágio constitui um ilícito académico.

X 

Signed by: Inês Lua Freitas

De acordo com o disposto no ponto n.º 2 do Art.º 31º do Decreto-Lei n.º 74/2006, de 24 de Março, aditado pelo Decreto-Lei n.º 230/2009, de 14 de Setembro, o autor declara que nesta tese foram incluídos dados dos artigos publicados ou submetidos para publicação abaixo indicados. O autor esclarece que participou ativamente na conceção e execução das experiências que estiveram na origem dos resultados apresentados, assim como na sua interpretação, discussão e redação.

According to the relevant national legislation, the author declares that this thesis includes data from the articles published or submitted for publication indicated below. The author clarifies that she actively participated in the conception and execution of the experiments that led to the results presented, as well as in their interpretation, discussion and writing.

1. **Freitas IL**, Teixeira A, Loureiro I, Lisboa J, Saraiva A, dos Santos NMS, do Vale A. Susceptibility of Sea Bream (*Sparus aurata*) to AIP56, an AB-Type Toxin Secreted by *Photobacterium Damselae* subsp. *piscicida*. *Toxins*. 2022; 14(2):119. https://doi.org/10.3390/toxins14020119
2. **Freitas IL,** Macedo MF, Oliveira L, Oliveira P, do Vale A, dos Santos NMS. AIP56, an AB toxin secreted by *Photobacterium Damselae* subsp. *piscicida*, has tropism for myeloid cells. *Front. Immunol*. 2025; 15:1527088. https://doi.org/10.3389/fimmu.2024.1527088

ACKNOWLEDGEMENTS / AGRADECIMENTOS

This academically journey was not only challenging but also enriching and it would not have been possible without the support of several people who made this achievement possible, whom I would like to recognize and thank immensely.

Foremost, I would like to thank my supervisor, Dr. Nuno dos Santos, for having hosted me in his lab, for the guidance and corrections that have improved significantly my work.

I am sincerely grateful to my co-supervisor, Dr. Ana do Vale, who provided me an outstanding scientific orientation. Thank you also for sharing a part of your immensurable knowledge with me.

I am extremely thankful to my co-supervisor, Dr. Johnny Lisboa, for everything he taught me, for his wise advices and also his constant little jokes. Johnny was always patient and thoughtful with me. I am grateful for his daily encouragement and motivation about my work. Thank you for being my role model as a scientist!

I want to thank all the FIV group members and ex-members for all of their availability and for helping me in some way. I am deeply grateful to Alexandra, who was always willing to help me no matter what and was crucial to make my PhD journey lighter.

Also, I am grateful to Dr. Fátima Macedo and Dr. Liliana Oliveira for their important contributions to this work and for the fruitful discussions we had.

I want to acknowledge my colleagues from MM, CBBI and CAGE groups that shared the lab with me. Thank you for all the enjoyable conversations during lunch and coffee time and for creating a good environment. You helped me more than you can imagine.

I would like to express my sincere gratitude to Ângela for being my PhD buddy, for listening to all my dramas and for supporting me in my professional and personal ups and downs. Thank you for growing up with me during these 4 years.

I am thankful to my parents, my grandparents and my dear friends for all the support and encouragement, for being always present in my life and for believing in me.

Last but not least, I am sincerely thankful to my husband, Flávio. Thank you for being my strength and my shelter. Thank you for your unconditional support, for believing in my worth more than anyone else. Thank you for listening to me, for your patience, for all the praise and also for putting my feet on the ground. I couldn’t achieve this without you by my side.

TABLE OF CONTENTS

ABSTRACT 13
RESUMO 15
LIST OF ABBREVIATIONS 18
GENERAL INTRODUCTION 23
1. BACTERIAL PROTEIN TOXINS 25
1.1 Injected effectors 26
1.2 Toxins secreted into the extracellular milieu 27
1.2.1 Exotoxins acting at the host cell surface 27
1.2.2 Exotoxins with cytosolic target 28
2. AB TOXINS 28
2.1 Structural organization 29
2.2 Cell surface receptors 31
2.3 Endocytic pathways 33
2.4 Intracellular trafficking routes 35
2.4.1 Short-trip toxins 36
2.4.2 Long-trip toxins 36
3. AIP56 37
3.1 Structural and functional organization 37
3.2 Endocytosis and intracellular trafficking 39
3.3 AIP56-like and AIP56-related toxins 40
3.4 Biotechnological potential 43
4. AIMS 45
RESULTS 46
CHAPTER I 50
Susceptibility of Sea Bream (Sparus aurata) to AIP56, an AB-Type Toxin Secreted by Photobacterium Damselae subsp. piscicida 52
Abstract 54
1. Introduction 54
2. Results 56
2.1. aip56 is ubiquitous and conserved among sea bream and sea bass Phdp isolates 56
2.2. Sea bream and sea bass Phdp isolates secrete identical AIP56 toxins 58
2.3. AIP56 does not induce apoptosis or other signs of toxicity in sea bream peritoneal leukocytes ex vivo 58
2.4. AIP56 displays proteolytic activity against sea bream NF-κB p65 59
2.5. The internalization of AIP56-488 in sea bream peritoneal leukocytes is inefficient 60
2.6. Sea bream are highly resistant to AIP56 toxicity 62
3. Discussion 68
4. Materials and Methods 71
4.1. Production and fluorescence labeling of recombinant proteins 71
4.2. Determination of recombinant protein concentration 71
4.3. Fish 71
4.4. Cells 72
4.5. Cell intoxication assays 72
4.6. AIP56 internalization assays 72
4.7. Detection of aip56 in Phdp field isolates 72
4.8. Comparative analysis of AIP56 from different Phdp strains 73
4.9. Cloning sea bream NF-κB p65 73
4.10. NF-κB cleavage assay 74
4.11. In vivo toxicity tests 74
4.12. GenBank accession numbers 75
References 76

CHAPTER II 80
AIP56, an AB Toxin Secreted by Photobacterium Damselae subsp. piscicida, Has Tropism for Myeloid Cells 82
Abstract 84
1. Introduction 84
2. Results 86
2.1. AIP56 internalization by sea bass leukocytes 86
2.2. AIP56 internalization by mouse leukocytes 88
2.3. AIP56 internalization by human leukocytes 91
3. Discussion 92
4. Materials and Methods 95
4.1. Production and fluorescence labeling of recombinant proteins 95
4.2. Determination of recombinant protein concentration 96
4.3. Fish 96
4.4. Mice 96
4.5. Fish neutrophils 96
4.6. Fish lymphocytes 97
4.7. Isolation of splenocytes, bone marrow, peritoneal and blood cells from mice 97
4.8. Differentiation and polarization of mouse bone marrow derived macrophages 98
4.9. Isolation of human monocytes and lymphocytes 98
4.10. Polarization of human macrophages 99
4.11. Generation of human dendritic cells 99
4.12. Human neutrophils 100
4.13. AIP56-488 internalization assays 100
4.14. Flow cytometry 102
4.14.1. Sea bass: 102
4.14.2. Mouse: 103
4.14.3. Human: 103
4.15. NF-κB cleavage assay 104
4.16. Statistical analysis 104
5. Supplementary Data 105
References 112
CHAPTER III 118
LRP1 Is a Receptor for AIP56-Family Toxins 120
Abstract 122
1. Introduction 123
2. Results 126
2.1. AIP56, AIP56-like and AIP56-related toxins likely share a conserved receptor 126
2.2. LRP1 is involved in AIP56 internalization 129
2.3. Dl-LRP1X1-C4 has a preponderant role in AIP56 intoxication of sbPL 136
2.4. Residues K350 and R441 in AIP56 RBD are essential for binding to sea bass LRP1 139
3. Discussion 144
4. Materials and Methods 148
4.1. Ethics statement 148
4.2. Fish 148
4.3. Mice 148
4.4. Reagents and Antibodies 148
4.5. Cells 149
4.6. DNA constructs for recombinant protein production 149
4.7. Production of recombinant proteins 151
4.8. Determination of protein concentration 152
4.9. Fluorescent labelling of AIP56 153

4.10. Competition assays *153*
4.11. SDS-PAGE and western blotting *154*
4.12. Flow cytometry *154*
4.13. In vivo intoxication assays *155*
5. Supplementary Data *156*
References *163*
GENERAL DISCUSSION *172*
Supplementary Data *179*
REFERENCES *183*

ABSTRACT

AIP56 (apoptosis inducing protein of 56 kDa) is an AB-type toxin secreted by *Photobacterium Damselae* subsp. *piscicida* (*Phdp*), playing a crucial role in the pathogenesis of photobacteriosis, a disease that affects several marine fish species and has been causing major economic losses in aquaculture. Previous studies showed that AIP56 is able to enter and cleave NF-κB p65 in the cytosol of sea bass macrophages, leading to their death by apoptosis and thereby compromising inflammatory and immune responses. Beyond AIP56, homologous toxins (AIP56-like toxins) or toxins bearing a domain homologous to the receptor-binding domain of AIP56 (AIP56-related toxins) have been identified. These AIP56-family toxins were identified in the genome of several pathogenic or endosymbiont bacteria such as *Arsenophonus nasoniae*, *Shewanella psychrophile*, *Candidatus Symbiopectobacterium* and *Vibrio* species, including a strain of *Vibrio tarriae* isolated from humans, or in eukaryotic organisms, such as *Danaus plexippus* and *Drosophila bipectinata.* Thus, the relevance of this toxin family is extended to diverse organisms from distinct phylogenetic branches.

Although it is known that AIP56 target macrophages, there is no information concerning the (sub)populations that are susceptible to this toxin. Furthermore, until recently, the cell surface receptor targeted by this toxin family as well as the amino acid residues involved in toxin-receptor interactions remained to be identifyed. This thesis provides significant insights into the mechanisms underlying the host susceptibility to AIP56 and its receptor-mediated internalization pathways.

The first chapter focuses on the species-specific susceptibility of different fish species to AIP56. In this chapter, it is shown that while sea bass macrophages are highly susceptible to AIP56-induced apoptosis, sea bream phagocytes exhibit resistance due to inefficient internalization of the toxin. This discovery suggests the existance of variations in the expression of AIP56's receptor between species, or molecular specificities that result in differences in receptor interactions in different hosts.

The second chapter identifies the AIP56 target cell populations or subpopulations in sea bass, mice and humans. It is shown that, in all species tested, AIP56 has preferential tropism for myeloid cells, particularly macrophages. These findings underscore the toxin’s ability to effectively target immune cells in diverse hosts and suggest that AIP56 binds to an evolutionarily conserved receptor.

A major breakthrough that resulted from this study, presented in Chapter 3, was the identification and validation of low-density lipoprotein receptor-related protein 1 (LRP1) as

the primary receptor for AIP56-family toxins. Through *ex vivo* and *in vivo* assays, it was confirmed that they bind specifically to cluster 4 of LRP1. In sea bass, the isoform LRP1X1 was identified as the key mediator of intoxication. Two amino acid residues in the receptor-binding domain of AIP56 – K350 and R441 – were found to be critical for receptor interaction in this species. These findings constitute a significant contribution to the understanding of the mechanism of action of AIP56. The modular architecture of the AIP56-family toxins, which harbor a receptor-binding domain that targets myeloid cells, together with their intrinsic ability to reach the cells' cytosol, supports their potential to develop a platform for cytosolic delivery of antigens into antigen presenting cells (APCs). In this way, they could be harnessed to elicit cytotoxic immune responses against intracellular pathogens or tumor cells. Overall, this work substantially advances the understanding of AIP56-family toxins and their mechanism of action and opens new avenues for therapeutic development focused on immune modulation and antigen presentation.

RESUMO

AIP56 (proteína indutora de apoptose de 56 kDa) é uma toxina do tipo AB secretada pela *Photobacterium Damselae* subsp. *piscicida* (*Phdp*), desempenhando um papel crucial na patogénese da photobacteriose, uma doença que afeta diversas espécies de peixes marinhos e que tem causado grandes perdas económicas na aquacultura. Estudos anteriores mostraram que AIP56 é capaz de entrar nos macrófagos de robalo e clivar a subunidade p65 do NF-κB no citosol, levando à apoptose dessas células e comprometendo as respostas inflamatória e imunológica. Para além da AIP56, foram identificadas toxinas homólogas à AIP56 (toxinas AIP56-like), assim como proteínas contendo um domínio homólogo ao domínio de ligação ao recetor da AIP56 (toxinas AIP56-related). Essas toxinas da família AIP56 foram identificadas no genoma de várias bactérias patogénicas ou endossimbiontes, como *Arsenophonus nasoniae*, *Shewanella psychophila, Candidatus Symbiopectobacterium* e espécies de *Vibrio*, incluindo uma estirpe de *Vibrio tarriae* isolada de humanos. Além disso, também foram encontradas em organismos eucarióticos, como *Danaus plexippus* e *Drosophila bipectinata*. Isto indica que a relevância desta família de toxinas se extende a uma ampla diversidade de organismos filogeneticamente distintos.

Embora seja conhecido que a AIP56 tem como alvo macrófagos, não foram realizados estudos detalhados para identificar especificamente as (sub)populações celulares susceptíveis a esta toxina. Além disso, até recentemente, o recetor celular reconhecido por esta família de toxinas, assim como os resíduos aminoácidicos envolvidos na interação toxina-recetor permaneciam por identificar. Esta tese aporta informações relevantes para a compreensão dos mecanismos moleculares que determinam a especificidade de hospedeiro da AIP56 e as vias de internalização mediadas por receptores seguidas pela toxina durante a intoxicatção das células alvo.

O primeiro capítulo centra-se na suscetibilidade específica de diferentes espécies de peixes à AIP56. Neste capítulo, demonstra-se que embora os fagócitos de robalo sejam altamente suscetíveis à apoptose induzida pela toxina, os fagócitos de dourada exibem resistência devido à internalização ineficiente da AIP56. Esta descoberta sugere a existência de variações na expressão do recetor da AIP56 entre espécies, ou especificidades moleculares que se traduzem em diferenças na interação com o receptor em diferentes hospedeiros.

O segundo capítulo identifica as células alvo da AIP56 em robalos, ratinhos e humanos, mostrando que em todas estas espécies, a toxina tem um tropismo preferencial para as células mieloides, particularmente os macrófagos. Estas descobertas realçam a

capacidade da toxina para atingir eficazmente as células imunitárias em diversos hospedeiros, e sugerem que a AIP56 se liga a um receptor filogeneticamente conservado.

Uma das descobertas mais relevantes deste estudo, apresentada no terceiro capítulo, é a identificação e validação da proteína LRP1 (proteína 1 relacionada com o recetor de lipoproteínas de baixa densidade) como o principal recetor para a AIP56 e toxinas homólogas e com ela relacionadas. Através de ensaios *ex vivo* e *in vivo* confirmou-se que esta família de toxinas se liga especificamente ao cluster 4 do LRP1. No robalo, a isoforma LRP1X1 foi identificada como o principal mediador da intoxicação. Verificou-se ainda que dois resíduos aminoacídicos no domínio de ligação ao recetor da AIP56 - K350 e R441 – são críticos para a interação com o recetor nesta espécie. Estes resultados constituem um contributo significativo para a compreensão do mecanismo de ação da AIP56. A arquitetura modular das toxinas da família da AIP56, que contêm um domínio de ligação ao recetor que as direciona para células mielóides e possuem uma capacidade intrínseca de alcançarem o citosol, sustenta o seu potencial para o desenvolvimento de uma plataforma de entrega citosólica de antigénios a células apresentadoras de antigénios (APCs). Desta forma, poderão ser exploradas para despoletar respostas imunes citotóxicas contra patogénios intracelulares ou células tumorais. No seu conjunto, este trabalho representa um avanço substancial no conhecimento sobre as toxinas da família AIP56 e o seu mecanismo de ação, abrindo novas prespectivas para o desenvolvimento de estratégias terapêuticas centradas na modulação imunitária e na apresentação de antigénios.

LIST OF ABBREVIATIONS

AIP56	Apoptosis inducing protein of 56 kDa
A2MR	Alpha-2-macroglobulin receptor
ANOVA	Analysis of Variance
ANTXR	Anthrax receptors
ANTXR1	Anthrax receptor 1
ANTXR2	Anthrax receptor 2
AP	Adaptor proteins
AP1	Adaptor protein 1
AP2	Adaptor protein 2
APCs	Antigen presenting cells
APOER	Apolipoprotein E receptor
APSE	*Acyrthosiphon pisum* secondary endosymbiont
ATR	Ataxia telangiectasia and Rad3-related
AviTag	Automatic vehicle identification Tag
BAR	Bin/Amphiphysin/Rvs
BCIP	5-Bromo-4-chloro-3-indolyl phosphate
BLI	Biolayer interferometry
BMDM	Bone marrow derived macrophages
BoNTs	Botulinum neurotoxins
C2	*Clostridium botulinum* C2 Toxin
CD	Cluster of differentiation
CDT	Cytolethal distending toxin
CIE	Clathrin-independent endocytosis
CLIC	Clathrin-independent carriers
CME	Clathrin-mediated endocytosis
CMG2	Capillary morphogenesis 2
CNF	Cytotoxic necrotizing factor
CR3	Complement receptor 3
CRISPR	Clustered regularly interspaced short palindromic repeats
CST	*Clostridium spiroforme* Toxin
CT	Cholera toxin
DCs	Dendritic cells
DL	*Dicentrarchus labrax*
DMEM	Dulbecco's modified eagle medium

DNA	Deoxyribonucleic acid
Dnase	Deoxyribonuclease
DT	Diphtheria Toxin
DTT	Dithiothreitol
EDTA	Ethylenediaminetetraacetic acid
EE	Early endosome
EF	Edema factor
EGF	Epidermal growth factor precursor
ER	Endoplasmic reticulum
ETEC	Enterotoxigenic *Escherichia coli*
EV	Empty vector
FACS	Fluorescence-activated cell sorting
FBS	Fetal bovine serum
FSC-A	Forward scatter area
FSC-H	Forward scatter high
GAP	GTPase-activating protein
GD1	Ganglioside receptor
GEEC	GPI-enriched early endosomal compartments
GM1	Monosialotetrahexosylganglioside
GM-CSF	Granulocyte-macrophage colony-stimulating factor
GPI	Glycosylphosphatidylinositol
GRAF1	GTPase regulator associated with focal adhesion kinase
GTP	Guanosine triphosphat
HB-EGF	Heparin-binding epidermal growth factor precursor
HBSS	Hanks' balanced salt solution
HCL	Hydrochloric acid
HEK	Human embryonic kidney
Hsp90	Heat shock protein 90
iBMDM	Immortalized bone marrow derived macrophages
IFA	Incomplete Freunds’ adjuvant
IPTG	Isopropyl β-D-1-thiogalactopyranoside
KO	Knocked-out
LB	Luria Bertani
LCCM	L929 cell conditioned medium
LDL	Low-density lipoprotein
LDLR	Low-density lipoprotein receptors

LDLRA	Low-density lipoprotein receptors class A domain
LEE	locus of enterocyte effacement
LF	Lethal factor
LRP1	Low-density lipoprotein receptor-related protein 1
LRP1B	Low-density lipoprotein receptor-related protein 1B
LRP1B-C4	Cluster 4 of low-density lipoprotein receptor-related protein 1B
LRP1-C4	Cluster 4 of low-density lipoprotein receptor-related protein 1
LRP1X1	Isoform 1 of low-density lipoprotein receptor-related protein 1
LRP1X1-C4	Cluster 4 of the isoform 1 of low-density lipoprotein receptor-related protein 1
LRP1X2	Isoform 2 of low-density lipoprotein receptor-related protein 1
LRP1X2-C4	Cluster 4 of the isoform 2 of low-density lipoprotein receptor-related protein 1
LRP2	Low-density lipoprotein receptor-related protein 2
LRP4	Low-density lipoprotein receptor-related protein 4
LRP8	Low-density lipoprotein receptor-related protein 8
LT	Heat-labile enterotoxin
M0	Non-activated/resting macrophages
M1	Classically activated/proinflammatory macrophages
M2	Alternatively activated/anti-inflammatory macrophages
MAPK	Mitogen-activated protein kinase
MAPKK	Mitogen-activated protein kinase kinase
mBMDM	Mouse bone marrow derived macrophages
M-CSF	Macrophage colony-stimulating factor
MFI	Median fluorescence intensity
MHC	Major Histocompatibility Complex
moDCs	Monocyte-derived dendritic cells
NBT	Nitro blue tetrazolium
NF-κB	Nuclear factor κappa-light-chain-enhancer of activated B cells
Ni-NTA	Nickel-affinity chromatography
OD	Optical density
ORF	Open reading frame
p65	p65 subunit of NF-κB
PA	Protective Antigen
PBS	Phosphate buffered saline
PCR	Polymerase chain reaction
PE	*Pseudomonas aeruginosa* exotoxin A
PFT	Pore-forming toxins

Phdp	*Photobacterium Damselae* subsp. *piscicida*
PI	Propidium iodide
PI3K	Phosphoinositide 3-kinase
PL	Peritoneal leukocytes
PPI	Peptidylprolyl isomerase
PT	Pertussis Toxin
PUF	Protein of unknown function
RAP	Receptor-associated protein
RBD	Receptor-binding domain
RE	Recycling endosome
RHD	Rel homology domain
RPMI	Roswell Park Memorial Institute 1640 medium
RT	Room temperature
SAgs	Superantigens
sbPBS	Sea bass phosphate buffered saline
sbPL	Sea bass peritoneal leukocytes
SDS-PAGE	Sodium dodecyl sulfate-polyacrylamide gel electrophoresis
SEA-SEI	Staphylococcal enterotoxin A and Staphylococcal enterotoxin I
SMEZ	Streptococcal mitogenic exotoxin Z
SPEA	Streptococcal pyrogenic exotoxin A
SPEC	Streptococcal pyrogenic exotoxin C
SPEL	Streptococcal pyrogenic exotoxin L
SPEM	Streptococcal pyrogenic exotoxin M
SSA	Streptococcal Superantigen
SSC-A	Side scatter area
ST	Shiga toxin
T2SS	Type 2 secretion system
T3SS	Type 3 secretion system
TBS-T	Tris-buffered saline and Tween
TEM8	Tumor endothelial marker 8
TeNTs	Tetanus neurotoxin
TGN	Trans-Golgi-network
TSST	Toxic shock syndrome toxin-1
VLDL	Very-low-density lipoprotein receptor
WT	Wild-type

GENERAL INTRODUCTION

The references mentioned in this section are listed at the end of this document (Page 183).

1. BACTERIAL PROTEIN TOXINS

Toxins are intoxicating molecules produced and secreted by several bacteria, which target host cells and play crucial roles in the pathogenesis of a large variety of infections and diseases. The activity of toxins frequently determines the outcome of the infection, underscoring their major virulence roles [1,2]. The detailed study of their intoxication mechanisms allows the comprehension of the toxins' roles for pathogenesis and often leads to the development of numerous applications, that includes toxin-based vacines, the use of protein toxins as tools for the discovery of central cell biology processes and their use to fight different diseases including cancer and inflammatory and autoimmune disorders [2,3].

Bacterial protein toxins are extremely diverse in what concerns their structures and mode of action, but they can be classified into four different functional groups [2]: (A) toxins that are injected into the target cell through an injection apparatus from the bacterial pathogen; (B) toxins that bind the plasma membrane of the host cell through cell surface receptors and display their function by activating intracellular signalling pathways; (C) toxins that bind the host cell surface and damage the membrane through pore formation or phospholipase activity; and (D) AB toxins that enter the cell by receptor-mediated endocytosis and traffic to the cell's cytosol, where they perform an enzymatic activity [2,4].

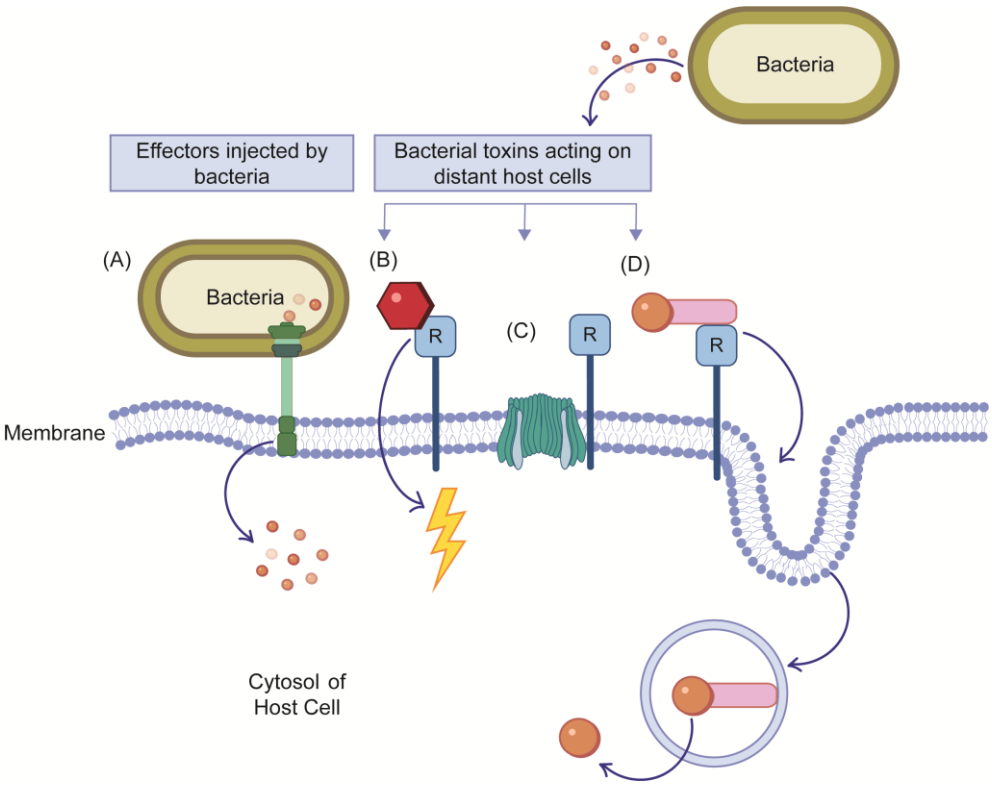

Figure 1. **Overview of the main types of bacterial toxins.** There are four main classes of bacterial protein toxins: **(A)** toxins that are injected directly from the bacterium into the cytosol of the target cell by an injection apparatus (e.g. type III secretion system) **(B)** toxins that bind cell surface receptors and trigger intracellular

signalling pathways; **(C)** toxins that bind the host cell surface and disrupt the membrane through pore formation or phospholipase activity; **(D)** AB toxins that undergo receptor-mediated endocytosis and traffic to the cell's cytosol, where they enzymatically modify cytosolic targets. **(A)** Requires direct contact between the bacteria and the host cell while **(B)**, **(C)** and **(D)** may act on distant host cells. Orange sphere: toxic factor; pink rectangle: receptor-binding/translocation component; red hexagone: Superantigens; R: receptor; Teal blue ring shape: pore. Figure done with Adobe Illustrator.

1.1 Injected effectors

Initially, it was thought that toxins were molecules that caused intoxication and promoted infection when secreted by bacterium into the body fluids of host organisms. Later, it became clear that some bacteria, such as *Salmonella*, *Shigella* and *Yersinia* [4], are able to intoxicate eukaryotic host cells by injecting proteinaceous effectors directly into the host cell's cytosol through contact-dependent secretion systems (Figure 1A). This is often achieved by using the specialized type III secretion system, present in many Gram-negative pathogens [5]. The injected effectors are very diverse (Table 1) and usually possesses catalytic activity, modifying host proteins through post-translational modifications or through other reversible molecular interactions, which can either disrupt or enhance host cell functions to support pathogen's survival and spread [2]. Type III secreted effectors are delivered in large amounts over a short period of time, interfering significantly with the host cell physiology [2].

Table 1. **Examples of type III secreted effectors.**

Bacteria	Effector Protein	Associated Function	References
Enteropathogenic *Escherichia coli*	EspF	Actin nucleation at the cell membrane	[6]
	NleE	Inhibition of NF-κB activation and pro-inflammatory cytokine production	[7]
	NleB1	NF-κB suppression	[7]
	NleH1	Inhibition of intrinsic apoptosis; mild stimulation of NF-κB	[8]
	NleD	Inhibition of intrinsic apoptosis and inhibition of MAPK signalling	[9]
	NleF	Suppression of death receptor-mediated extrinsic apoptosis	[10]
	NleC	Intrinsic and extrinsic apoptosis' inhibition; Inhibition of NF-κB signalling	[11]
Vibrio cholerae	VopF	Actin nucleation	[12]
Pseudomonas aeruginosa	ExoS	Disruption of the actin cytoskeleton	[13]

Pseudomonas syringae	AvrPtoB	Inhibition of programmed cell death	[14]
Salmonella enterica	SopE	Bacterial invasion of non-phagocytic cells	[15]
	SopA	Induction of inflammation	[16]
	SseL	Macrophages killing	[17]
	SopB	Modulation of vesicular trafficking; Akt activation	[18,19]
	SifA	Endosomal tubulation	[20]
***Shigella* spp.**	IpgB	Modulation of the actin cytoskeleton	[21]
	IpaA	Bacterial invasion of non-phagocytic cells and actin reorganization	[22]
***Yersinia* spp.**	YopE	Disruption of the actin cytoskeleton	[23]

1.2 Toxins secreted into the extracellular milieu

1.2.1 Exotoxins acting at the host cell surface

Some exotoxins act on the host cell's surface by interacting with receptors present on the plasma membrane, leading to activation of cell signaling pathways (Figure 1B), formation of pores at the cell membrane (Figure 1C) or cleavage of surface-exposed molecules [4].

Superantigens (SAgs), which lack enzymatic activity, cause harmful effects by promoting hyperstimulation of host's immune system through engagement of surface receptors on antigen presenting cells (APCs) and the major histocompatibility complex II (MHC II) on T-lymphocytes, affecting their interaction and corrupting intracellular pathways, ultimately resulting in severe inflammation [24,25]. SAgs embrace several secreted proteins, mostly produced by *Staphylococcus aureus* and *Streptococcus pyogenes*, such as SEA-SEI, TSST-1, SPEA, SPEC, SPEL, SPEM, SSA, and SMEZ [4].

Pore-forming toxins (PFTs) act by binding to the plasma membrane as monomers. Membrane-bound monomers oligomerize and form membrane pores, disturbing membrane permeability and causing ion imbalance [24–26]. There are two types of PFTs: α-PFTs that insert into the membrane as an α-helix, like colicins produced by *Escherichia coli (E. coli)*, and β-PFTs that insert into the membrane as β-sheets, such as cholesterol-dependent cytolysins produced by Gram-positive bacteria (*Listeria monocytogenes*, *Streptococcus pneumoniae*, and *Bacillus anthracis*) [25,26].

Molecules that target and enzymatically damage the cell membrane include bacterial hyaluronidases, collagenases, and phospholipases, such as the *Streptococcus pyogenes* streptokinase that hydrolyses plasminogen into plasmin, the clostridial collagenases, and the α-toxin of *Clostridium perfringens* that displays phospholipase C activity [4,27].

1.2.2 Exotoxins with cytosolic target

An important group of exotoxins are bacterial toxins that act inside the host cells by targeting cytosolic components (Figure 1D). To reach their targets at the cytosol, they are endocytosed by receptor-mediated endocytosis. These bacterial toxins, which are named AB toxins ("A" for "Active" and "B" for" "Binding" [28]), have enzymatic activity that can disrupt essential cellular processes, often leading to cell death or dysfunction [2,24]. AB toxins will be discussed in detail in the next section (2.).

2. AB TOXINS

AB toxins include a wide variety of structurally different toxins that share the common feature of being constituted by two components: an A subunit, which harbors the catalytic moiety of the toxin and displays enzymatic activity towards a cytosolic target, and a B subunit that contains the receptor binding moiety and is also typically involved in assisting the delivery of the A subunit into the cytosol of the host cells [4,25].

AB toxins interfere with several fundamental processes of eukaryotic cells, including protein synthesis, vesicle trafficking and actin polymerization [4] (Table 2). Generally, AB toxins are inactive when secreted by the bacteria and are then proteolytically activated by a host and/or a bacterial protease [25,29–31]. However, some AB toxins have the capacity of auto-proteolytic processing, including toxins A and B from *Clostridium difficile* (TcdA and TcdB), hemorrhagic and lethal toxins from *Clostridium sordellii* and the α-toxin from *Clostridium novyi* [32].

Table 2. **Examples of AB toxins. Adapted from** [24]**.**

Toxin	Source	Substrate	Effect on Cells	Disease
AIP56	*Photobacterium Damselae* subsp. *piscicida*	NF-κB	Induction of apoptosis	Photobacteriosis
Anthrax Toxin	*Bacillus anthracis*	MAPKK ATP	Immunosupression	Anthrax
BoNTs A-G (Botulinum Neurotoxins A-G)	*Clostridium botulinum*	Adaptor proteins	Block of neurotransmitter release	Botulism

CDT (*Clostridium difficile* Transferase)	*Clostridium difficile*	Actin	Depolymerization of F-actin	Enteritis
CNF (Cytotoxic Necrotizing Factor)	*Escherichia coli*	Rho-GTPases	Rho-signaling disturbed	Extraintestinal infections
CST (*Clostridium spiroforme* Toxin)	*Clostridium spiroforme*	Actin	Depolymerization of F-actin	Enteritis
CT (Cholera Toxin)	*Vibrio cholerae*	Heterotrimeric GTPases	Altered signal transduction	Cholera
C2 (*Clostridium botulinum* C2 Toxin)	*Clostridium botulinum*	Actin	Depolymerization of F-actin	-
DT (Diphtheria Toxin)	*Corynebacterium diphtheriae*	Elongation Factor-2	Inhibition of protein synthesis	Diphtheria
Exotoxin A	*Pseudomonas aeruginosa*	Elongation Factor-2	Inhibition of protein synthesis	Pneumonia
Iota Toxin	*Clostridium perfringens*	Actin	Depolymerization of F-actin	Enteritis
LT (Heat-Labile Enterotoxin)	*Escherichia coli* (ETEC)	Heterotrimeric GTPases	Altered signal transduction	Severe diarrhea
PT (Pertussis Toxin)	*Bordetella pertussis*	Heterotrimeric GTPases	Altered signal transduction	Pertussis (whooping cough)
TcdA (*Clostridium difficile* Toxin A)	*Clostridium difficile*	Rho-GTPases	Rho-signaling disturbed	Pseudomembranous colitis
TcdB (*Clostridium difficile* Toxin B)	*Clostridium difficile*	Rho-GTPases	Rho-signaling disturbed	Pseudomembranous colitis
TeNT (Tetanus Neurotoxin)	*Clostridium tetani*	Adaptor proteins	Enhanced neurotransmitter release	Tetanus

2.1 Structural organization

Some AB toxins are single polypeptide chains whereas others are multicomponent toxins composed by different combinations of A and B subunits (AB_5, A_2B_5, $AB_{7/8}$) (Figure 2). Single-chain AB toxins include Apoptosis Inducing Protein of 56 kDa (AIP56) [33], *diphtheria* toxin (DT), *Pseudomonas aeruginosa* exotoxin A (PE), tetanus neurotoxin (TeNT) and botulinum neurotoxins (BoNT/A-G) [25]. In most single chain AB toxins, the A and B components are adjacently connected until proteolytic cleavage occurs, resulting in a di-chain molecule with the A and B moieties linked by a disulphide bond [25]. Usually, the catalytic A domain is released when the toxin encounters reducing conditions at the cytosol, which are generated by metabolic oxidases (thioredoxin-1 and glutathione) found in this compartment to establish an environment for redox signaling [25,34].

Multicomponent toxins comprise one or two A subunits and a B subunit prearranged in a dimeric, pentameric or hepta/octameric form (AB_2, AB_5, A_2B_5 and $AB_{7/8}$). In AB_5 toxins, the gathering of A and B subunits occurs in the periplasmic compartment of the bacteria [25,35]. The A subunit is a single polypeptide chain that possesses two domains (A1 and A2) that are linked together through a disulfide bond. A1 includes the catalytic domain responsible for toxicity, while A2 promotes the non-covalent binding of the A subunit to the central cavity of the B pentamer. Examples of AB_5 toxins include shiga toxin (ST) and cholera toxin (CT) [30,35]. Other multicomponent toxins, such as anthrax and *Clostridium botulinum* C2 toxins, follow distinct activation and assembly processes. In the case of anthrax toxin, the B subunit, known as protective antigen (PA), first binds to the cell surface receptor and is subsequently cleaved by a furin-like protease, releasing a ~20 kDa fragment. This proteolytic cleavage triggers the oligomerization of the remaining ~63 kDa PA into a heptameric or octameric ring-shaped complex ($B_{7/8}$), which then recruits the A subunits, lethal factor (LF) and/or edema factor (EF), to form the complete multicomponent toxin complex for endocytosis [30,36–38]. Anthrax toxin can also undergo partial activation where oligomerization of the ~63 kDa PA occur prior to cell-binding and LF and/or EF can bind to the oligomer before or after receptor binding. Though, full activation and functional translocation only happen after receptor binding and internalization [37,38]. Similarly, C2 toxin undergoes activation first, followed by the oligomerization of the B subunit into $B_{7/8}$ complex, which then binds to the receptor. The A subunit is recruited only after receptor binding, leading to toxin internalization [30,36].

Some A_2B_5 and AB_2 toxins have also been reported. The typhoid toxin from *Salmonella enterica* serovar Typhi is an A_2B_5 toxin that has two A catalytic subunits (CdtB and PltA) covalently linked by a disulphide bond, and a pentameric B component composed of five PltB subunits. The delivery of CdtB and PltA to the host cell occurs simultaneously [39]. On the other hand, cytolethal distending toxin (CDT) - produced by several Gram-negative bacteria - is an AB_2 toxin [40]. CdtA and CdtC are two B subunits from CDT that bind the receptor on the host cell surface and assists translocation of the enzymatic A domain (CdtB) into the cytosol [41].

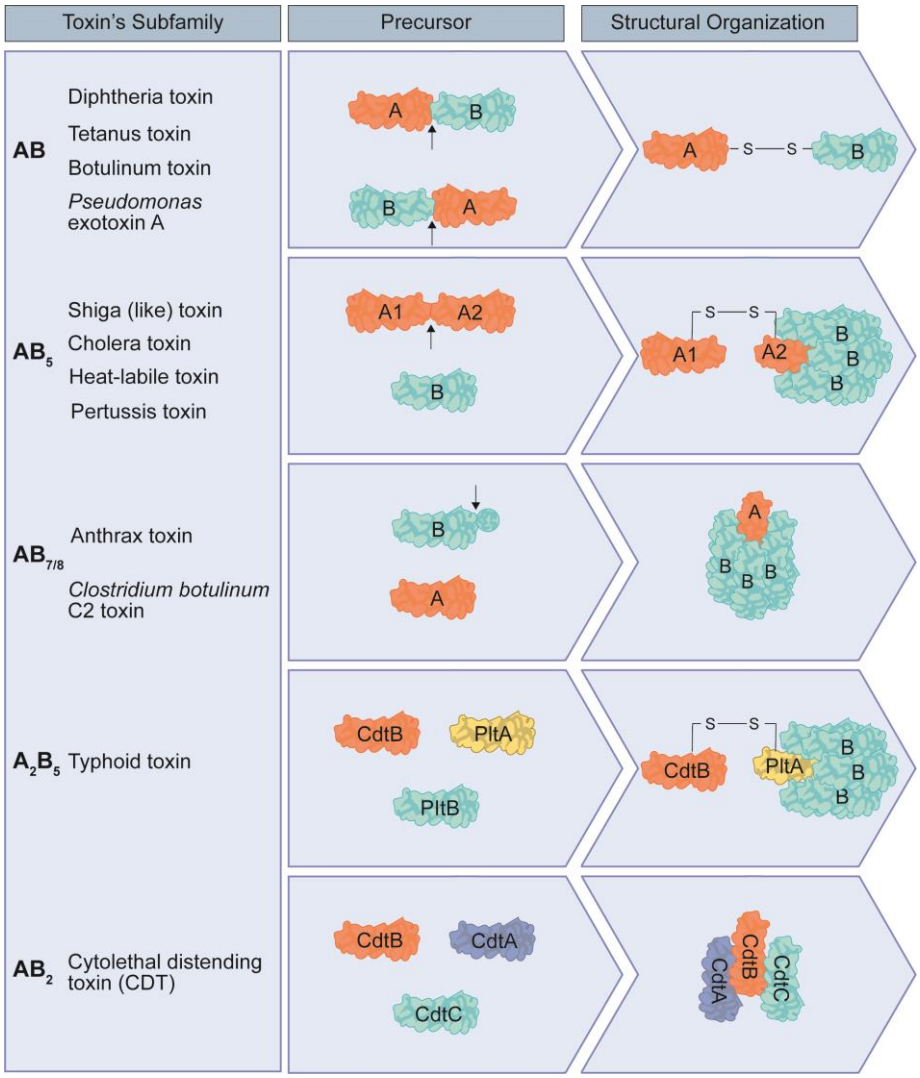

Figure 2. **Structural Organization of AB toxins.** AB toxins comprise a catalytic A subunit (orange or/and yellow), and a receptor-binding B subunit (cyan or/and blue) that also assists the delivery of the catalytic A domain into the host cell's cytosol. The A and B subunits can be part of a single polypeptide chain or form multicomponent toxins (AB_5, $AB_{7/8}$, A_2B_5, AB_2). Frequently, proteolytic cleavage (indicated by black arrows in the precursor column) promotes the toxin assembly ($AB_{7/8}$) or the activation of the toxin (AB, AB_5). Figure done with Adobe Illustrator.

2.2 Cell surface receptors

Endocytosis of AB toxins involves binding to a cell surface receptor that can be a lipid or a lipid derivative, a glycoprotein or a transmembrane protein [42,43]. Despite their diversity, all cell surface receptors comprise three domains: an extracellular recognition domain exposed on the cell membrane that binds the ligand(s); the membrane domain which is made of hydrophobic molecules, and the intracellular or coupling domain that is exposed at the cytoplasm [44].

The existence of specific receptors on a cell determines its sensitivity to a toxin able to recognise those receptors and offers a molecular basis for the toxin's cell specificity. Therefore, characterization of toxins' receptors is crucial to understand their modes of action. In order to consider a molecule as a toxin receptor, it is necessary to demonstrate that the molecule can bind directly and specifically to the toxin, and to show that the sensitivity of a cell to the toxin depends on the expression of the molecule proposed as receptor [45].

AB toxins can bind different receptors, with some recognizing a single receptor, while others interact with multiple receptors to enhance binding specificity and cell targeting. Toxins that bind to a single receptor rely on a high affinity interaction for cellular entry, whereas others use co-receptors or dual-receptor recognition to facilitate efficient uptake [45].

The well-studied cholera toxin (CT) has a pentameric B domain that binds to glycosphingolipid GM1 on mammalian intestinal epithelial cells, with CT subunit B (CTxB) binding to one GM1 molecule [46,47]. Despite GM1 has been described as the exclusive receptor, CTxB can bind to fucosylated glycoconjugates that are also implicated in its internalization and intoxication by CT [48]. In the case of shiga toxin (ST), its B pentamer binds to the glycosphingolipid globotriaosylceramide (Gb3) on endothelial cells, recruiting more Gb3 that lead to a stronger interaction of ST with the host cell. ST has high affinity for Gb3 because it contains 2-3 Gb3-binding sites per B monomer [49]. Concerning anthrax toxin, its B subunit, formed by the protective antigen (PA), can bind to two anthrax receptors (ANTXR) - tumor endothelial marker 8 (TEM8/ANTXR1) and capillary morphogenesis 2 (CMG2/ANTXR2) [47,50]. Heparin-binding epidermal growth factor precursor (HB-EGF), expressed on several mammalian cells, is the receptor for *diphtheria* toxin (DT) [45,51]. Considering botulinum neurotoxin type B, it binds to both a protein receptor (synaptotagmin-II) and a ganglioside receptor (GD1a) on nerve tissues, alone or simultaneously. It has a separate binding site for each of the receptors and the binding-affinity of one is not affected by the other [52]. Furthermore, adenylate cyclase toxin (CyaA), secreted by *Bordetella pertussis*, binds to a specific site of the inactive form of the integrin complement receptor 3 (CR3 – CD11b/CD18) that is not located on the CR3 I-domain (major binding site for endogenous ligands), avoiding triggering an immune response after CR3 binding [53]. Regarding the *Clostridium difficile* TcdA, it binds to a non-endocytic receptor (gp96, glycoprotein 96), which associates to an endocytic receptor that allows TcdA to be endocytosed [54]. This endocytic receptor is the low-density lipoprotein (LDL) receptor-related protein 1 (LRP1), a member of the LDL receptor (LDLR) family [54,55]. The extracellular domain of LRP1 contains 4 clusters of complement-like repeats responsible for ligand-binding. TcdA binds to clusters 2 and 4 of LRP1 [54,55]. After binding to LRP1,

TcdA is released from gp96 and the toxin-LRP1 complex is internalized [54]. Finally, cell-binding of *Pseudomonas aeruginosa* exotoxin A is mediated by its domain I, which binds to cluster 4 of LRP1 [56,57]. The toxin-LRP1 complex is internalized via clathrin coated pits [57]. This toxin is also able to use LRP1B as receptor [58].

2.3 Endocytic pathways

The process of internalization of extracellular ligands, soluble molecules or components of the cell membrane is called endocytosis and it is crucial for several cellular mechanisms in eukaryotic cells. Most AB toxins highjack host cells endocytic pathways to reach their targets at the cytosol [59]. In most cases, binding of an AB toxin to a specific cell surface receptor is followed by invagination of the cell membrane and formation of endocytic vesicles containing the toxin through different processes (Figure 3). These may be dependent or independent of dynamin and involve different adaptor proteins [42,60–64]. Some toxins appear to follow a single endocytic pathway, whereas others present endocytic plasticity and use several mechanisms simultaneously [65].

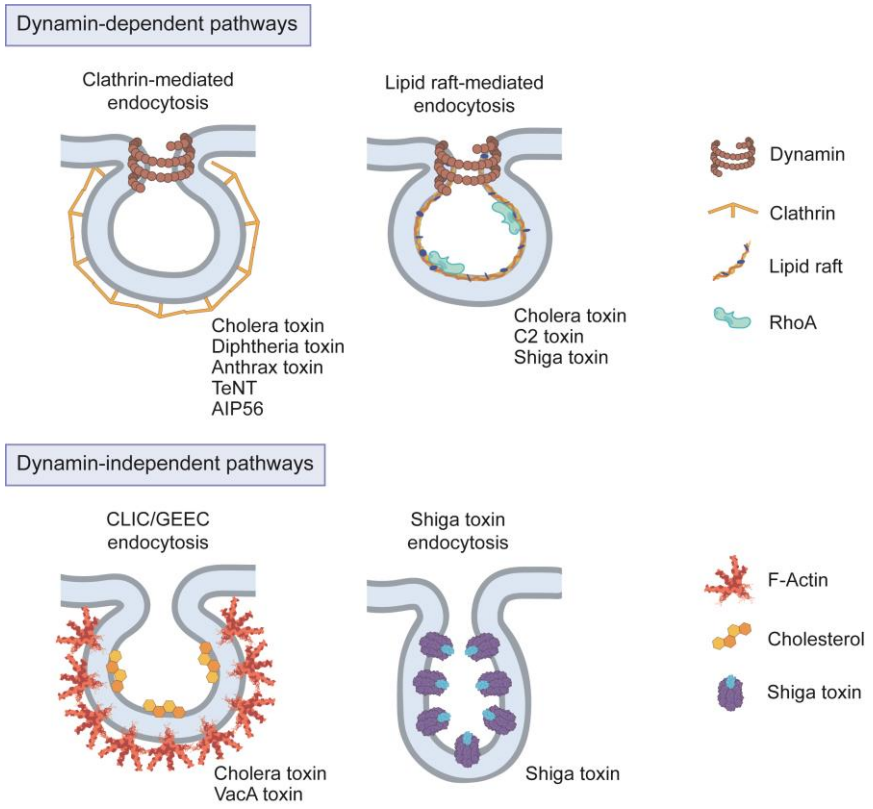

Figure 3. **Endocytic Pathways explored by different AB toxins.** AB toxins can be endocytosed by dynamin-dependent or -independent pathways that involve different coat proteins. Clathrin-dependent pathways are responsible for the endocytosis of CT, DT, Anthrax toxin, TeTN and AIP56. Additionally, CT can undertake other pathways, including lipid raft-mediated endocytosis and clathrin-independent carriers/GPI-enriched early endosomal compartments (CLIC/GEEC). C2 toxin is specifically internalized through lipid raft-mediated endocytic pathway. CLIC/GEEC also mediates VacA toxin endocytosis. ST follows its own specific dynamin-

independent pathway and, alternatively, can be internalized through lipid raft-mediated. Figure done in Adobe Illustrator.

Clathrin-mediated endocytosis (CME) is the most well-characterized endocytic pathway, and is the main endocytic mechanism mediating internalization of toxins that undergo receptor-mediated endocytosis [60]. CME allows internalization of several receptors and ligands and involves a coat of clathrin triskelion, that initiates the formation of clathrin-coated vesicles when accessory and adaptor proteins bind the cell-surface receptor [60,61]. Nucleation of clathrin at cell membrane and clathrin-coated vesicle maintenance demands the acquisition of cargo molecules by adaptor protein 2 (AP2) and its partners. Additionally, BAR (Bin/Amphiphysin/Rvs) domain-containing proteins enable the plasma membrane invagination. Then, dynamin is mandatory for the separation of these vesicles from the cell membrane because of its GTPase activity. Finally, clathrin-coated vesicles are uncoated and fuse with early endosomes [66].

DT, anthrax toxin and CT are example of toxins that hijack CME. DT and anthrax toxin use exclusively this pathway while CT can also follow clathrin-independent endocytic pathways, as explained bellow [65,67]. After binding to HB-EGF, DT is endocytosed in complex with its receptor through a process dependent on clathrin and AP2 but not on actin [68]. Anthrax toxin follows a more complex endocytic mechanism triggered by the binding of PA to ANTXR (ATR/TEM8 ou CMG2) on the plasma membrane. Afterward, transmembrane proteases cleave and consequently activate PA monomers to oligomerize into a heptameric/octameric pre-pore. Although the PA oligomer alone can be internalized, the binding of LF and/or EF enhances the efficiency of endocytosis by stabilizing the toxin-receptor complex. The toxin-receptor complex is endocytosed through a clathrin-dependent process that, contrary to the one used by DT, is dependent on actin and AP1, instead of the usual AP2 [69,70]. After endocytosis, the pre-pore is converted into a pore through conformational changes triggered by endosomal acidification. The PA pore forms a channel in the endosomal membrane, through which the A domain of anthrax toxin - LF and/or EF – translocate [70].

There are several endocytic mechanisms that do not rely on clathrin. Clathrin-independent endocytosis (CIE) embraces dynamin-dependent and -independent pathways. CIE depending on dynamin rely on lipid raft-mediated endocytosis and are usually related with small-scale invaginations [63,71,72]. Dynamin-independent pathways, which are associated with large-scale invaginations, such as macropinocytosis that exploit the cell membrane components like lipids and proteins to initiate membrane deformation, embraces also CLIC/GEEC (clathrin-independent carriers/GPI-enriched early endosomal compartments) and flotillin pathways [62–64,73]. This CLIC/GEEC endocytosis is dynamin-independent, despite one of the proteins implicated in the process – GRAF1 (GTPase

regulator associated with focal adhesion kinase) – can bind dynamin but here, GRAF1 primarly acts as a GTPase-activating protein (GAP) just to stabilize the CLICs [62,63,73].

Lipid raft-mediated endocytosis dependent on dynamin is used by toxins like CT, ST and C2 toxin [63,72–74]. It relies on cholesterol-rich lipid rafts and can also involve caveolae to internalize cargo without clathrin involvement. Toxins bind to specific glycosphingolipids on the plasma membrane, leading to clustering within lipid rafts [63,72–74]. RhoA, a small GTPase, plays a crucial role by regulating actin cytoskeleton remodeling, which facilitates vesicle formation and uptake in C2 toxin endocytosis [60,63,75]. RhoA signaling can enhance actin-driven vesicle trafficking but is not absolutely required for CT internalization. Once inside, vesicles fuse with early endosomes [63,72,73,76].

The CLIC/GEEC mainly internalizes glycosylphosphatidylinositol-anchored proteins (GPI-APs), fluid-phase markers, and bacterial toxins, such as CT and VacA (from *Helicobacter pylori*). Vesicle formation begins with actin-driven membrane invaginations, regulated by the GTPase Cdc42 and its effectors. GRAF1, a BAR-domain protein, helps sculpt these uncoated tubular carriers (CLICs) and functions as a GAP for Cdc42, facilitating vesicle scission. GPI-APs are enriched in these vesicles due to their association with specific lipid microdomains. Once formed, CLICs rapidly mature into GEECs, which then fuse with early endosomes [62–64,73].

Some toxins, like CT and ST, display endocytic plasticity [65]. ST binds to glycosphingolipid Gb3 in lipid-rafts through a complex mechanism and is also able to induce plasma membrane invagination, inducing its own endocytosis independent on dynamin [60]. The ST's endocytic vesicle dissociation from cell membrane is accomplished by a process dependent on endophilin-A2, actin and cholesterol [77]. After receptor binding and clustering in lipid-rafts, CT can enter the cell by both CME and CIE. Concerning CIE, it can follow CLIC/GEEC pathway and, alternatively, lipid raft/caveolae-mediated pathway, but CME is the main pathway hijacked by CT [60]. Furthermore, it has been proposed that CTxB internalization can be facilitated by cell membrane-associated proteins called flotillins that incite membrane invaginations in a dose-dependent way [61].

2.4 Intracellular trafficking routes

Once endocytosed, AB toxins can follow distinct endocytic pathways. The majority of them, at some point of their intracellular transport, localize in early endosomes and some of them follow later stages of trafficking [59,78].

Two main intracellular trafficking routes have been described for AB toxins (Figure 4): (A) a short-trip pathway, generally followed by single-chain and $AB_{7/8}$ toxins, that involves

translocation of the catalytic A domain through a pore formed by the B subunits(s) at the endosomal membrane in response to low pH; and (B) a long-trip pathway, commonly followed by AB_5 toxins, that pass from endosomes to the Golgi and then the ER, from where the translocation of the A domain occurs [59,78].

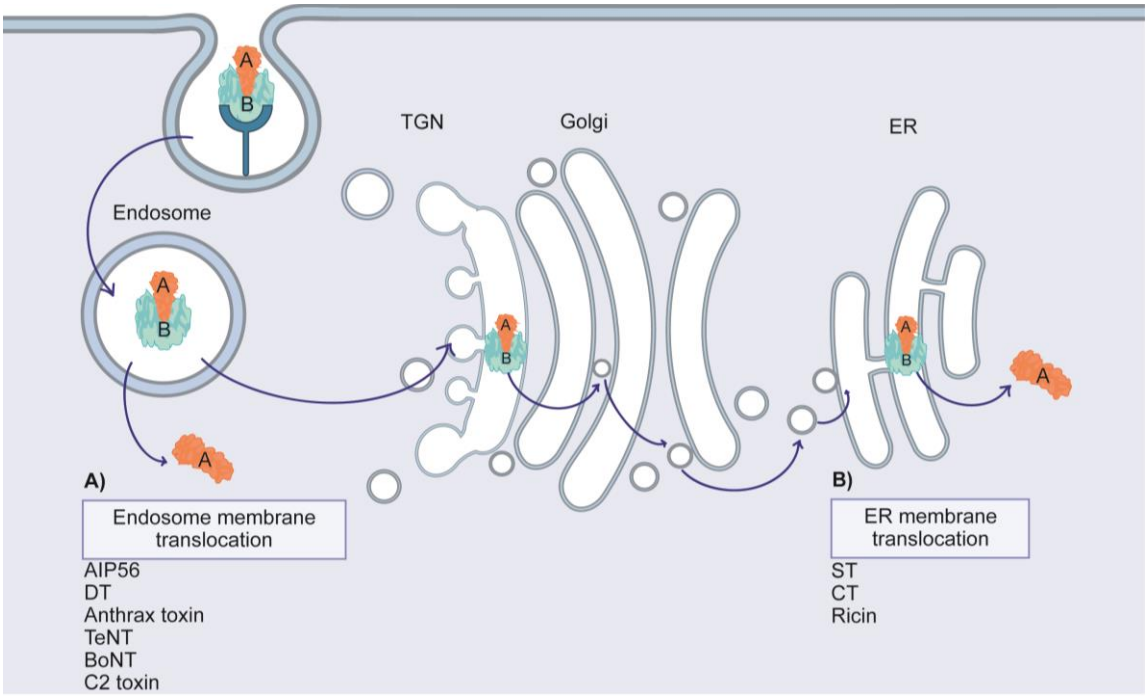

Figure 4. **Intracellular Trafficking Routes of Bacterial AB Toxins.** After endocytosis, some AB toxins, including AIP56, DT, anthrax toxin, TeNT, BoNT and C2 toxin, follow a short-trip route and reach the cytosol by translocating from endosomes **(A)**, whereas others, such as ST and CT follow a long-trip route in which they are retrogradely transported from endosomes to the Golgi and then to the ER, from where they translocate to reach the cytosol **(B)**. TGN: trans-Golgi-network; ER: endoplasmic reticulum.

2.4.1 Short-trip toxins

AB toxins that follow the short trip-pathway translocate from early or late endosomes through a process that requires endosome acidification [59,78]. AIP56, DT, anthrax toxin, TeNT, BoNT and C2 toxin are reported to use this route to reach the cytosol. After receptor binding and endocytosis, the short-trip toxins are known to undergo conformational changes induced by the low endosomal pH, resulting in the insertion of their B subunit into the endosomal membrane to form a pore through which the translocation of the respective catalytic domain takes place [59].

2.4.2 Long-trip toxins

Some toxins, like ST and CT, follow a longer pathway that does not depend on endosomal acidification, to reach their targets at the cytosol. After endocytosis, they undergo retrograde transport from early or recycling endosomes into the trans-Golgi-network (TGN) and then

from Golgi to the ER, where translocation of their enzymatic domain across the ER membrane occurs, after reduction of the disulphide bond that links the A1 and A2 domains [59,78]. The ER is a critical site for protein folding and assembly, and maintening ER homeostasis is essential for these processes. Misfolded proteins are degraded through retro-translocation via the Sec61 channel, followed by proteasomal degradation. Long-trip toxins can mimic misfolded proteins, exploiting the Sec61-mediated mechanism to translocate into the cytosol [79]. Once in the cytosol, these toxins avoid proteasomal degradation by refolding into a stable and active conformation or by lacking lysine residues required for ubiquitination. Since protein ubiquitination is a sign for proteasomal recognition, avoiding this modification allows long-trip toxins to escape proteasomal degradation and act on their cytosolic targets [79].

3. AIP56

Photobacterium Damselae subsp. *piscicida* (*Phdp*) is a Gram-negative bacterium that causes septicemic infections in marine warm water fish species, which result in necrotic lesions in several internal organs and in high mortality rates [80]. The major virulence factor that triggers the pathology associated with *Phdp* is the Apoptosis-Inducing Protein of 56 kDa (AIP56), an AB toxin that induces apoptosis of host phagocytes, leading to secondary necrosis of these cells [81,82]. The apoptotic pathway triggered by AIP56 involves the activation of caspases -8, -9 and -3, loss of mitochondrial membrane potential, translocation of cytochrome C to the cytosol and overproduction of reactive oxygen species in lysing phagocytes, which contribute to the occurrence of tissue damage and the histopathological changes characteristic of *Phdp* infections [83,84].

3.1 Structural and functional organization

AIP56 is encoded in a high-copy plasmid of approximately 10 kb (p*PHDP*10) found in virulent *Phdp* strains from different origins. The precursor form of the toxin has 520 amino acids and contains an N-terminal signal peptide of 23 amino acids that is cleaved during secretion, originating a 497 amino acid mature protein [81,85]. AIP56 has a modular structure (Figure 5) with an N-terminal domain containing a zinc-metalloprotease region linked to a C-terminal receptor-binding domain (RBD) through a small middle domain that contains a partially structured linker peptide flanked by a disulphide bridge (C^{262} and C^{298}) [81,86–89]. The middle domain is responsible for the transmembrane channel formation and requires the RBD for the translocation of the catalytic domain into the cytosol [89]. Remarkably, the fusion of three different genes seems to have originated AIP56: one, which encodes the toxin RBD, homologous to the gene encoding a protein of unknown function (Protein D) of the bacteriophage *Acyrthosiphon pisum* (*APSE*-2); a gene that encodes the

toxin catalytic domain, homologous to the gene encoding NleC, a type III secreted effector of several enteric bacteria associated with human diseases; and another, which encodes the middle domain, for which no homologs are known, which possibly evolved as an independent gene or, alternatively, from a gene/intergenic region of the recipient genome where the genes of RBD and catalytic domain were incorporated [88,90,91]

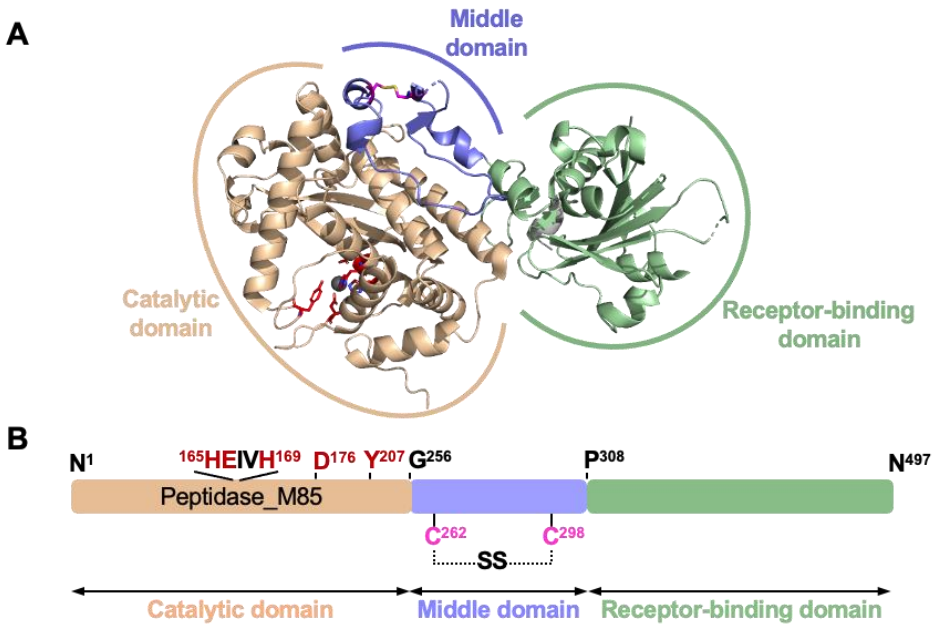

Figure 5. **AIP56 modular structure. (A)** Three-dimensional structure of AIP56 (WP_012954632; PDB: 7ZPF) [89]. **(B)** Schematic representation of mature AIP56. Catalytic domain (salmon); Middle domain (blue) and Receptor-binding domain (green). Zinc-metalloprotease signature residues (red stick), zinc ion (black sphere) and disulphide bond (SS, magenta stick). AIP56 is considered a member of the M85 metallopeptidase family because it contains the typical HEXXH metal-binding motif and depends on zinc for its proteolytic function.

The catalytic domain of AIP56 cleaves the p65 subunit of NF-κB, an evolutionarily conserved transcription factor that controls the expression of some inflammatory and anti-apoptotic genes and is a crucial regulator of innate immunity [87,92]. Silva *et al* (2013) [87], through the use of an AIP56 with a mutated zinc-binding motif (AIP56^{AAIVAA}), showed that disruption of the zinc metalloprotease signature is not associated with important structural changes in the toxin but eradicates its ability to cleave p65 and to induce phagocyte's apoptosis. In mammals, NF-κB comprises five members that associate to form different homodimers and heterodimers [92–94]: RelA/p65, RelB, c-Rel, p50 (NF-κB1), and p52 (NF-κB2). All these contain the Rel homology domain (RHD), a conserved N-terminal region that interacts with DNA and promotes subunit dimerization. AIP56 compromises NF-κB activity by cleaving an evolutionarily conserved peptide bond of NF-κB p65 RHD (Cys^{39}-Glu^{40}), removing residues essential for p65-DNA interaction [87]. Recently, it was found that the pH-sensing residues present upstream the linker, on the C-terminal end of the catalytic

domain of AIP56, are mandatory to control structural changes necessary for pore formation by middle and receptor-binding domains [89]. Thus, AIP56 does not have an independent translocation domain but rather elements involved in translocation spread across all its domains [89].

As in other single chain AB toxins, the disulphide bond that links the A and B subunits of AIP56 is essential for the intoxication process, since mutation of the two cysteine residues to serine abolished AIP56's toxicity [87,95]. However, in contrast to anthrax toxin, CT, ST, C2 toxin and BoNT [25,32], AIP56 does not require proteolytic activation to display toxicity and the linker region between the two cysteines must remain intact during the first steps of intoxication [87,96].

The AIP56's RBD is known to have specificity towards fish macrophages [81]. Competition assays using AIP56's C-terminal domain as a competitor showed that it inhibited AIP56 intoxication and AIP56-dependent NF-κB p65 cleavage in these cells, demonstrating that AIP56's C-terminal domain mediates receptor binding and subsequent cellular internalization of AIP56 [87]. Even though mammals are not susceptible to infection by *Phdp* [84,97], it has been shown that AIP56 is able to enter and cleave p65 in mouse macrophages [84]. These data suggest that AIP56 targets an evolutionary conserved cell surface receptor that has not been identified to date.

3.2 Endocytosis and intracellular trafficking

The RBD of AIP56 mediates binding to host macrophages and internalization through receptor-mediated and dynamin- and clathrin-dependent endocytosis (Figure 6), and follows an intoxication pathway that is independent on actin dynamics and microtubules [84,87]. A pool of endocytosed AIP56 follows a short-trip intracellular route, dependent on endosome acidification, that leads to the translocation from early/recycling endosomes into the cytosol (Figure 6) [82,84]. It has been shown that in acidic pH, AIP56 undergoes a reversible increase in hydrophobicity and has the ability to interact with lipid bilayer membranes [84]. The membrane activity of AIP56 is consistent with the formation of transient channels similar to the ones formed by the *Clostridium botulinum* and *Clostridium limosum* C3 toxins but not with the assembly of regular channels similar to the ones formed by some AB toxins, such as anthrax toxins [84,98,99]. It has been shown that pharmacological inhibition of heat shock protein 90 (Hsp90) and the PPIases cyclophilin A/D inhibits AIP56 intoxication [100]. Furthermore, it has been demonstrated that AIP56 interacts with those host cytosolic factors, and that the interaction is stronger when the catalytic domain is unfolded, suggesting that it happens during or shortly after translocation of the toxin to the cytosol [100].

A pool of AIP56 molecules that does not translocate into cytosol, follows the endosomal recycling pathway, being routed back out of the cells (Figure 6) through a mechanism that is independent on endosome acidification but requires the activity of PI3K, an evolutionarily conserved enzyme complex that phosphorylates phosphatidylinositol lipid substrates into 3-phosphoinositides and is crucial for several cellular processes [84,101]. Although essential for AIP56 recycling, PI3K activity is not required for AIP56 intoxication [84].

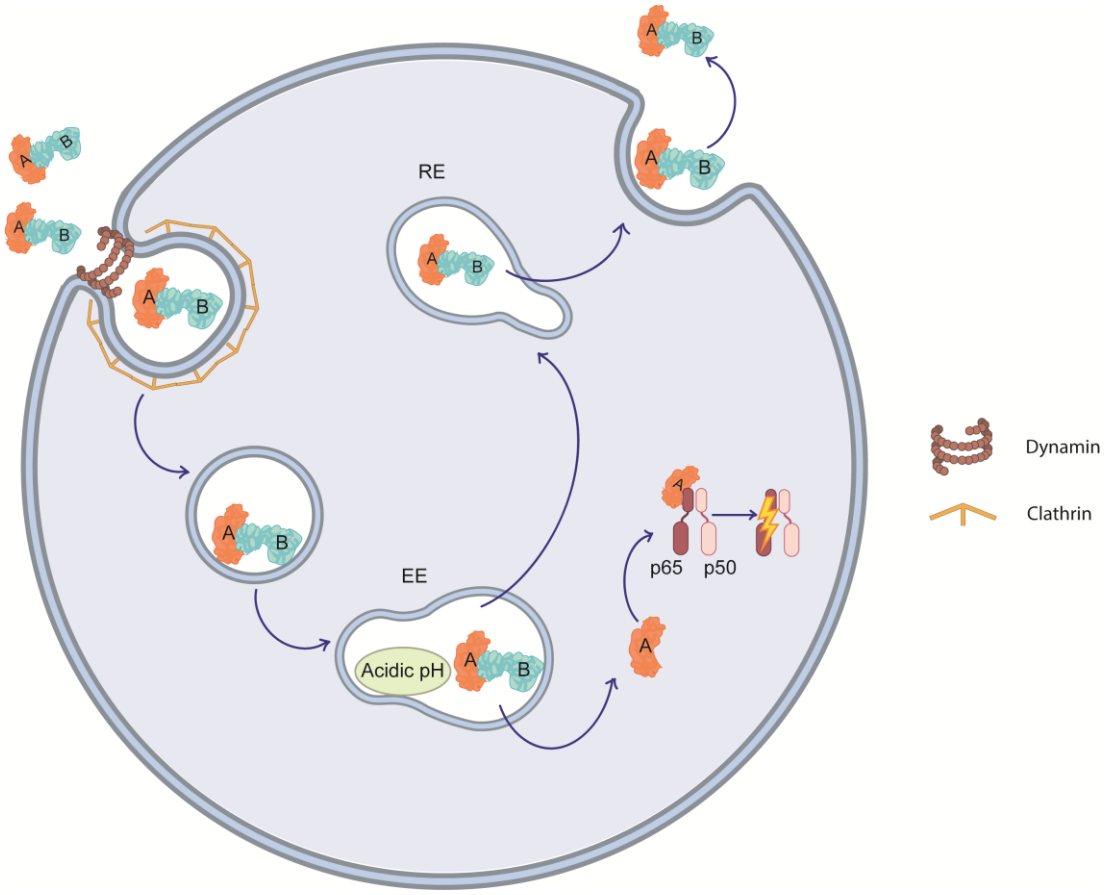

Figure 6. **Endocytosis and Intracellular Trafficking of AIP56.** After binding to an unknown cell surface receptor, AIP56 undergoes clathrin- and dynamin-dependent endocytosis. Once in early endosomes, AIP56 can translocate across the endosome membrane into the cytosol in response to endosome acidification, to reach its cytosolic target NF-κB p65. A pool of AIP56 can follows the recycling pathway, independent on endosomal acidification, back out of the cells. EE: early endosome; RE: recycling endosome.

3.3 AIP56-like and AIP56-related toxins

Since the discovery of AIP56 [81], several homologs to the full-length toxin (AIP56-like toxins) were identified in the genome of diverse pathogenic or endosymbiont bacteria such as *Arsenophonus nasoniae*, *Shewanella psychrophile*, *Candidatus* Symbiopectobacterium and various *Vibrio* species, including a strain of *Vibrio tarriae* isolated from human blood and stool [102,103] (Figure 7). Additionally, an increasing number of toxins with a domain homologous to the RBD of AIP56 and comprising distinct catalytic and translocation

domains (AIP56-related toxins) have been identified in the genome of different prokaryotic and eukaryotic organisms [104] (Figure 7). Two of these AIP56-related toxins contain putative catalytic domains with unknown function, including one from monarch butterfly - *Danaus plexippus* - and winter moth (*Operophtera brumata*), and another present in two bacteria (*Enterovibrio norvegicus*, isolated from turbot larvae [105], and *Shewanella* sp.). *Drosophila bipectinata* and *Drosophila ananassae* [104] contain another toxin with a domain homologous to AIP56's RBD fused to a catalytic domain that is homologous to CdtB, the catalytic domain of Cytolethal Distending Toxins (CDTs) and Typhoid toxin [106]. CdtB encoding genes were also identified in the genome of some insects and in *Acyrthosiphon pisum* secondary endosymbiont (APSE) phages [107]. CdtB is a catalytic subunit of the multicomponent CDT and Typhoid toxin, both of which comprise an independent multimeric B subunit - composed of CdtA and CdtC in CDT, and a pentamer of PltB in the typhoid toxin - that mediates the internalization of CdtB into cells, allowing it to display its DNase I-like activity [106]. Interestingly, in APSE-2, the gene encoding CdtB is immediately upstream of a gene encoding *protein D* [108] a homolog of the AIP56's RBD. However, it is not known if this results in a multicomponent toxin.

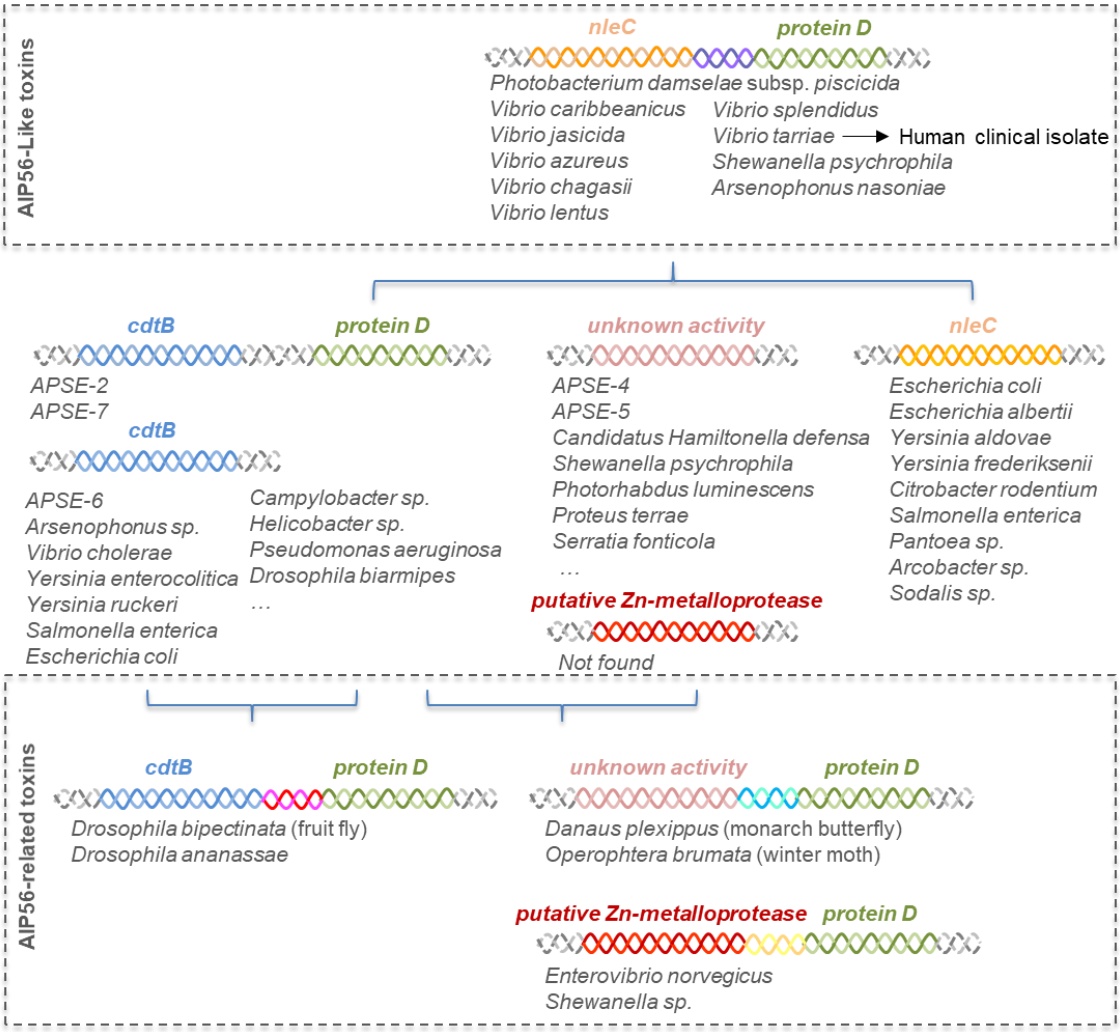

Figure 7. **AIP56-like and AIP56-related toxins.** Genes encoding AIP56 and AIP56 homologous toxins (AIP56-like toxins) as well as toxins that have a domain homologous to AIP56's receptor-binding domain fused to a (putative) catalytic domain different from that of NleC (AIP56-related toxins) are boxed. Genes encoding each of the domains present in the AIP56-like and AIP56-related toxins, but found isolated (not fused to other genes) are also shown (middle). Homologous genes/sequences are shown with the same color. The names below the schemes correspond to the species in which the genes/sequences were identified. *nleC*: non-LEE-encoded effector C (LEE: locus of enterocyte effacement); *cdtB*: cytolethal distending toxin subunit B; APSE: *Acyrthosiphon pisum* secondary endosymbiont.

All these findings suggest that genes encoding domains homologous to the receptor-binding domain of AIP56 have been horizontally transferred between diverse organisms and fused to distinct catalytic moieties and middle domains, resulting in new toxins that constitute a novel family of AB toxins, which has AIP56 as its founding member. It remains to be investigated if the domains homologous to the AIP56's RBD present in AIP56-like and -related toxins are also functionally equivalent and interact with the same cell-surface receptor.

3.4 Biotechnological potential

It has been shown that the receptor-binding and translocation domain of AIP56 is able to deliver polypeptides other than its own catalytic domain into the cytosol of APCs [109,110]. This ability is not exclusive of AIP56, as has also been demonstrated for CyaA, which also has tropism for APCs [111]. It has been shown that CyaA can tolerate the insertion of an antigen of considerable size within its catalytic domain maintaining the capacity of translocation into cytosol and consequent induction of an adaptive immune response against the inserted antigen [111]. These characteristics led to the development of potent vaccine vehicles that required inactivation of its enzymatic activity through mutations in the N-terminal [111,112]. The ability to deliver exogenous antigens and/or drugs has also been shown for other AB toxins, including DT, CT, anthrax toxin, ST and *Pseudomonas* exotoxin A (Table 3). AIP56-family toxins contain a domain homologous to the RBD of AIP56 and, similarly to the above-mentioned toxins, may be engineered as vehicles for antigen delivery, to trigger specific cytotoxic T-lymphocyte immune responses against intracellular pathogens or cancer specific antigens [110]. The great advantage of the AIP56 family toxins lie in their diversity. The existence of several AIP56-like and -related toxins with structurally and functionally similar but antigenically different RBDs, suggests that they can be used for the development of an antigen delivery platform comprising alternative delivery vehicles. This could be a great asset for situations that require multiple immunizations, because the switch of vehicles may overcome the immunogenicity problems that are often associated to multiple immunizations with the same vehicle.

Table 3. **Examples of AB toxins used as vehicles to deliver molecules into eukaryotic cells.**

Toxin	Bacterium	Type of chimeras	References
Adenylate cyclase toxin (CyA)	*Bordetella pertussis*	Fusion of proteins	[111,112]
Diphtheria toxin (DT)	*Corynebacterium diphtheriae*	Fusion of proteins	[113,114]
Cholera toxin (CT)	*Vibrio cholerae*	Drug conjugates, fusion of peptides	[115,116]
Anthrax toxin	*Bacillus anthracis*	Fusion of proteins/toxins	[117–119]
Shiga toxin (ST)	*Shigella dysenteriae*	Drug conjugates, fusion of toxins	[120–122]
Pseudomonas exotoxin A	*Pseudomonas aeruginosa*	Fusion of proteins	[123]

4. AIMS

AIP56 is an AB toxin that plays a key virulence role in infections of marine fish species caused by *Photobacterium Damselae* subsp. *piscicida* (*Phdp*). Although previous studies have revealed important aspects of AIP56's structure and mode of action, several critical questions remain unanswered.

To date, knowledge about the cellular specificity of AIP56 remains limited, with its toxicity reported only in sea bass and murine macrophages. Therefore, one of the objectives of this work is to investigate wether other immune cell types are also targeted by AIP56. In this context, it is particularly relevant to correlate cellular susceptibility to AIP56 with the host-specificity of the toxin, as studies in sea bass have shown that AIP56-mediated depletion of macrophages facilitates bacterial survival and dissemination, contributing to the pathogenesis of *Phdp* infections.

Although AIP56 is known to be internalized by receptor-mediated endocytosis, the identity of the receptor recognized by the toxin remains unknown. Moreover, there are toxins homologous to AIP56 (AIP56-like), or containing a domain homologous to the receptor-binding domain of AIP56, suggesting they may recognise a common receptor(s). The identification of the receptor(s) to which AIP56 - and potentially AIP56-like and -related toxins - bind is therefore another objective of this PhD project. Building on this, the project also aims to characterize the interaction between the toxin and its receptor(s), specifically by identifying the amino acid residues involved in receptor binding.

Achieving these objectives will make a significant contribution to unraveling essential aspects of the biology of these toxins and understanding the pathology they cause. Furthermore, identifying the susceptible cell populations and elucidating the molecular mechanisms of toxin-target cell interactions will also be valuable for the development of antigen delivery platforms based on the receptor-binding and translocation domains of these toxins.

RESULTS

This section comprises the following chapters:

- **Susceptibility of Sea Bream (*Sparus aurata*) to AIP56, an AB-Type Toxin Secreted by *Photobacterium Damselae* subsp. *piscicida*.** The toxicity of AIP56 had only been studied in sea bass. In this study, the toxicity of AIP56 for sea bream was investigated. It was shown that sea bream phagocytes are resistant to AIP56 cytotoxicity due to an inefficient internalization of AIP56. Accordingly, sea bream is more resistant to AIP56-induced lethality than sea bass. This work was published in Toxins (2022) 14(2): 119. https://doi.org/10.3390/toxins14020119.

- **AIP56, an AB Toxin Secreted by *Photobacterium Damselae* subsp. *piscicida*, Has Tropism for Myeloid Cells**. Although previous studies had shown that AIP56 was toxic to macrophages from sea bass and mice, the cellular specificity of the toxin remained undisclosed. This study shows that AIP56 preferentially targets myeloid cells, particularly macrophages, not only from sea bass but also from mice and human. This work was published in Frontiers in Immunology (2025) 15:1527088. https://doi.org/10.3389/fimmu.2024.1527088.

- **LRP1 is a receptor for AIP56-Family Toxins.** This study shows that low density lipoprotein receptor-related protein 1 (LRP1) works as the common receptor of AIP56, AIP56-like and -related toxins, and identifies amino acid residues of the toxins required for receptor interaction. This research was done in collaboration with Min Dong's lab (https://donglab.hms.harvard.edu/), which was responsible for the CRISPR/Cas9 screening and the Biolayer interferometry (BLI) analysis (results shown in boxes 2, 3, 4, 5 and 6 of this section). It includes data generated in the context of this thesis, namely *ex vivo* and *in vivo* competition and intoxication assays for validation of LRP1 as a receptor for AIP56-family toxins.

CHAPTER I

Susceptibility of Sea Bream (*Sparus aurata*) to AIP56, an AB-Type Toxin Secreted by *Photobacterium Damselae* subsp. *piscicida*

Susceptibility of Sea Bream (*Sparus aurata*) to AIP56, an AB-Type Toxin Secreted by *Photobacterium Damselae* subsp. *piscicida*

Inês Lua Freitas[1,2,3], Alexandra Teixeira[1,2], Inês Loureiro[1,2], Johnny Lisboa[1,2], Aurélia Saraiva[4,5], Nuno M.S. dos Santos[1,2,], Ana do Vale[1,2,]

[1]Fish Immunology and Vaccinology Group, IBMC - Instituto de Biologia Molecular e Celular, Universidade do Porto, Porto, Portugal

[2]Fish Immunology and Vaccinology Group, i3S - Instituto de Investigação e Inovação em Saúde, Universidade do Porto, Porto, Portugal

[3]McBiology Doctoral Program, ICBAS – Instituto de Ciências Biomédicas Abel Salazar, Universidade do Porto, Porto, Portugal

[4]Faculty of Sciences, Biology Department, Universidade do Porto, Porto, Portugal

[5]CIIMAR - Interdisciplinary Center of Marine and Environmental Research of the University of Porto, Matosinhos, Portugal

Abstract

Photobacterium Damselae subsp. *piscicida* (*Phdp*) is a Gram-negative bacterium that infects a large number of marine fish species in Europe, Asia and America, both in aquacultures and in the natural environment. Among the affected hosts are economically important cultured fish, such as sea bream (*Sparus aurata*), sea bass (*Dicentrarchus labrax*), yellowtail (*Seriola quinqueradiata*) and cobia (*Rachycentron canadum*). The best characterized virulence factor of *Phdp* is the Apoptosis-Inducing Protein of 56 kDa (AIP56), a secreted AB-type toxin that has been shown to induce apoptosis of sea bass phagocytes during infection. AIP56 has an A subunit that displays metalloprotease activity against NF-κB p65 and a B subunit that mediates binding and internalization of the A subunit in susceptible cells. Despite the fact that the *aip56* gene is highly prevalent in *Phdp* isolates from different fish species, the toxicity of AIP56 has only been studied in sea bass. In the present study, the toxicity of AIP56 for sea bream was evaluated. *Ex vivo* assays showed that sea bream phagocytes are resistant to AIP56 cytotoxicity and that resistance was associated to an inefficient internalization of the toxin by those cells. Accordingly, *in vivo* intoxication assays revealed that sea bream is much more resistant to AIP56-induced lethality than sea bass. These findings, showing that the effect of AIP56 is different in sea bass and sea bream, set the basis for future studies to characterize the effects of AIP56 and to fully elucidate its virulence role in different *Phdp* susceptible hosts.

1. Introduction

AIP56 (Apoptosis-Inducing Protein of 56 kDa) is an AB toxin secreted by virulent strains of *Photobacterium Damselae* subsp. *piscicida* (*Phdp*) [1], a Gram-negative bacterium that causes a septicemic infection that leads to high mortalities in a large number of wild and cultured warm water marine fish species in Europe, Asia, and North America [2]. *Phdp* is a ubiquitously distributed pathogen resistant to many antimicrobials that constitutes a serious threat for the aquaculture production of economically important species, such as sea bream (*Sparus aurata*) [3], sea bass (*Dicentrarchus labrax*) [4], sole (*Solea senegalensis* and *Solea solea*) [5], yellowtail (*Seriola quinqueradiata*) [6], and cobia (*Rachycentron canadum*) [7]. *Phdp* infections are characterized by the occurrence of generalized bacteremia and extensive cytopathology with abundant tissue necrosis [8]. Whitish tubercle-like lesions of about 0.5 to 3.5 mm in diameter, consisting of accumulations of bacteria, apoptotic cells, and necrotic cell debris are often present in several internal organs of infected fish [8–12]. Many of the *Phdp*-induced pathological changes have been attributed to AIP56, an exotoxin secreted in high amounts by the T2SS of *Phdp* [1,13]. Studies in sea bass have shown that AIP56 is secreted and systemically

disseminated during infection and causes apoptosis of macrophages and neutrophils, ultimately leading to their extensive lysis by post-apoptotic secondary necrosis [1,8,14]. This disarms the host phagocytic defense and allows the massive extracellular proliferation of the pathogen, thereby contributing to establishment of the infection [8]. Additionally, the massive lysis of host phagocytes induced by the toxin results in the release of highly cytotoxic molecules, including neutrophil elastase, a situation that induces tissue damage and contributes to the genesis of the necrotic lesions characteristic of *Phdp* infections [8,14]. Previous *ex vivo* and *in vitro* studies have shown that AIP56 is a short-trip AB toxin that displays toxicity towards sea bass and mouse macrophages [15,16]. AIP56 toxicity involves the activity of its zinc-metalloprotease domain that catalyzes the proteolytic cleavage of NF-κB p65 in susceptible cells, leading to depletion of this transcription factor and, ultimately, to the cell's apoptosis [1,16]. To reach the cytosol, where its substrate is located, AIP56 follows a multi-step process that starts by the binding to a so far unknown receptor at the surface of the target cell, followed by receptor mediated endocytosis of the toxin [15]. Translocation into the cytosol has been proposed to occur from early/recycling endosomes, by a mechanism that requires endosome acidification [15] and the participation of host cell Hsp90 [17].

Although *aip56* is almost 100% prevalent in *Phdp* isolated from disease outbreaks in different fish species over last three decades [18]; the effects of AIP56 have only been studied in sea bass. In this study, the toxicity of AIP56 for sea bream, another economically important fish species susceptible to *Phdp* infections, was investigated. *Ex vivo* assays showed that sea bream phagocytes are resistant to AIP56-induced cytotoxicity, which is in agreement with the results obtained *in vivo* showing that sea bream is highly resistant to AIP56-induced lethality. The here reported differences in the susceptibility to AIP56 between sea bass and sea bream emphasize the need for additional studies to determine the susceptibility to the toxin and its role for virulence in other *Phdp* susceptible hosts. The clarification of the host-specific effects of the toxin will allow understanding the relative contribution of AIP56 for the establishment of *Phdp* infections in different hosts, which will likely impact the design of preventive and therapeutic measures against this bacterial disease.

2. Results

2.1. *aip56* is ubiquitous and conserved among sea bream and sea bass *Phdp* isolates

A previous study [18] analyzed 103 *Phdp* strains isolated between 1963 and 2015 from different host species and geographical locations, revealing an almost 100% prevalence of the *aip56* gene, which was only absent in six of the isolates, two of them (ATCC29690 and EPOY8803-II) previously shown to be non-virulent [19]. Here, the analysis of the distribution of *aip56* was extended to 49 *Phdp* field isolates recovered from sea bream or sea bass during outbreaks occurred between 2014 and 2020 in different European countries (Table 1, rows 5–53). As shown in Figure 1, all these isolates tested positive for *aip56*.

***Table 1. Photobacterium Damselae* subsp. *piscicida* strains used in this study.**

	Strain	Host Species	Year	Geographical origin
1	ATCC29690	*Seriola quinqueradiata*	1972	Japan
2	EPOY8803-II	*Epinephelus akaara*	1988	Japan
3	DI21	*Sparus aurata*	1990	Spain
4	MT1415	*Dicentrarchus labrax*	unknown	Italy
5	SPSA14-1	*Sparus aurata*	2014	Spain
6	SPDL15-1	*Dicentrarchus labrax*	2015	Spain
7	SPSA16-1	*Sparus aurata*	2016	Spain (Mediterranean)
8	SPDL17-1	*Dicentrarchus labrax*	2017	Spain (Atlantic)
9	SPDL17-3	*Dicentrarchus labrax*	2017	Spain (Atlantic)
10	SPDL17-5	*Dicentrarchus labrax*	2017	Spain (Atlantic)
11	SPDL17-2	*Dicentrarchus labrax*	2017	Spain (Canary Islands)
12	SPDL17-4	*Dicentrarchus labrax*	2017	Spain (Mediterranean)
13	GRDL17-1	*Dicentrarchus labrax*	2017	Greece
14	SPSA18-1	*Sparus aurata*	2018	Spain (Canary Islands)
15	SPSA18-2	*Sparus aurata*	2018	Spain (Mediterranean)
16	SPDL18-1	*Dicentrarchus labrax*	2018	Spain (Atlantic)
17	SPDL18-2	*Dicentrarchus labrax*	2018	Spain (Mediterranean)
18	SPDL18-3	*Dicentrarchus labrax*	2018	Spain (Mediterranean)
19	SPDL18-4	*Dicentrarchus labrax*	2018	Spain (Mediterranean)

20	SPDL18-5	*Dicentrarchus labrax*	2018	Spain (Mediterranean)
21	SPDL18-6	*Dicentrarchus labrax*	2018	Spain (Mediterranean)
22	SPDL18-7	*Dicentrarchus labrax*	2018	Spain (Mediterranean)
23	ITDL18-1	*Dicentrarchus labrax*	2018	Italy
24	SPSA19-1	*Sparus aurata*	2019	Spain
25	SPSA19-2	*Sparus aurata*	2019	Spain (Canary Islands)
26	GRSA19-1	*Sparus aurata*	2019	Greece
27	SPDL19-2	*Dicentrarchus labrax*	2019	Spain
28	SPDL19-3	*Dicentrarchus labrax*	2019	Spain (Atlantic)
29	SPDL19-4	*Dicentrarchus labrax*	2019	Spain (Canary Islands)
30	SPDL19-1	*Dicentrarchus labrax*	2019	Spain (Mediterranean)
31	SPDL19-5	*Dicentrarchus labrax*	2019	Spain (Mediterranean)
32	SPDL19-6	*Dicentrarchus labrax*	2019	Spain (Mediterranean)
33	SPDL19-7	*Dicentrarchus labrax*	2019	Spain (Mediterranean)
34	SPDL19-8	*Dicentrarchus labrax*	2019	Spain (Mediterranean)
35	SPDL19-9	*Dicentrarchus labrax*	2019	Spain (Mediterranean)
36	SPDL19-10	*Dicentrarchus labrax*	2019	Spain (Mediterranean)
37	GRDL19-1	*Dicentrarchus labrax*	2019	Greece
38	GRDL19-2	*Dicentrarchus labrax*	2019	Greece
39	ITDL19-1	*Dicentrarchus labrax*	2019	Italy
40	SPSA20-1	*Sparus aurata*	2020	Spain (Mediterranean)
41	SPSA20-2	*Sparus aurata*	2020	Spain (Mediterranean)
42	GRSA20-1	*Sparus aurata*	2020	Greece
43	SPDL20-1	*Dicentrarchus labrax*	2020	Spain (Atlantic)
44	SPDL20-2	*Dicentrarchus labrax*	2020	Spain (Atlantic)
45	SPDL20-5	*Dicentrarchus labrax*	2020	Spain (Atlantic)
46	SPDL20-6	*Dicentrarchus labrax*	2020	Spain (Atlantic)
47	SPDL20-3	*Dicentrarchus labrax*	2020	Spain (Mediterranean)
48	SPDL20-4	*Dicentrarchus labrax*	2020	Spain (Mediterranean)
49	SPDL20-7	*Dicentrarchus labrax*	2020	Spain (Mediterranean)
50	SPDL20-8	*Dicentrarchus labrax*	2020	Spain (Mediterranean)
51	GRDL20-1	*Dicentrarchus labrax*	2020	Greece

52	GRDL20-2	*Dicentrarchus labrax*	2020	Greece
53	PTDL20-1	*Dicentrarchus labrax*	2020	Portugal

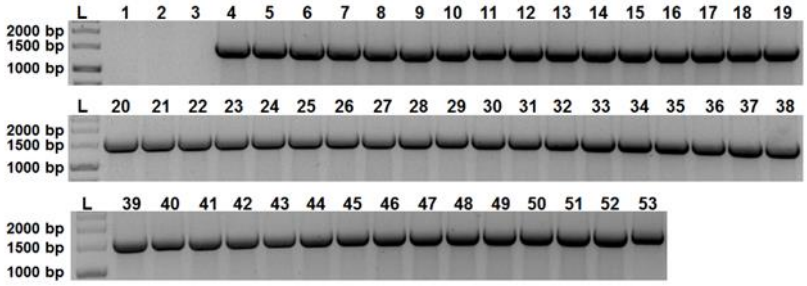

***Figure 1. aip56* is widespread amongst *Phdp* field isolates recovered from diseased sea bream and sea bass.** Colony-PCR for *aip56* gene. L, DNA ladder marker (GeneRuler 1 kb DNA Ladder, Thermo Scien-tific™); 1, EPOY8803-II strain (negative control); 2, ATCC29690 strain (negative control); 3, no template (negative control); 4, MT1415 strain (positive control); 5-53, field isolates (see Table 1).

2.2. Sea bream and sea bass *Phdp* isolates secrete identical AIP56 toxins

To evaluate if sea bream and sea bass isolates secrete identical AIP56 toxins, the *aip56* ORF from 3 sea bream (DI21, GRSA19-1 and SPSA20-2) and 3 sea bass (MT1415, GRDL19-1 and SPDL20-5) strains isolated in different geographical locations were sequenced and the nucleotide and deduced amino-acid sequences compared. The results revealed that the *aip56* ORF from those strains are 100% identical, indicating that they secrete identical AIP56 toxins.

2.3. AIP56 does not induce apoptosis or other signs of toxicity in sea bream peritoneal leukocytes *ex vivo*

The susceptibility of sea bream leukocytes to AIP56 was tested using peritoneal leukocytes collected from resting peritoneal cavities or from peritoneal cavities that were stimulated with Incomplete Freunds' Adjuvant (IFA) 12 days prior to leukocytes' collection. The peritoneal leukocyte populations from resting sea bream consisted mainly of neutrophilic and acidophilic granulocytes (47.96 ± 0.09% and 44.15 ± 0.09%, respectively), with small numbers of macrophages (4.10 ± 0.03%) and lymphocytes (3.7 ± 0.01%), whereas leukocyte populations collected from inflamed peritoneal cavities were composed mainly of monocytes/macrophages (88.09 ± 0.04%), with small numbers of neutrophils (1.20 ± 0.01%), acidophilic granulocytes (5.77 ± 0.02%), and lymphocytes (4.93 ± 0.03%). To test the susceptibility of the cells to AIP56, they were incubated with the toxin for 5 h and the occurrence of apoptosis or other signs of toxicity was evaluated by analyzing cytospin preparations by light microscopy (Figure 2). Sea bass leukocytes collected from inflamed

peritoneal cavities, mainly composed of macrophages (82.6 ± 0.08%) and containing small numbers of neutrophils (7.64 ± 0.05%), eosinophilic granular cells (2.10 ± 0.01%), and lymphocytes (7.40 ± 0.03%) were used as a positive control, because it is well established that sea bass macrophages are highly susceptible to AIP56 and undergo apoptosis in response to intoxication [8,20]. As shown in Figure 2, incubation of resting or inflamed sea bream peritoneal leukocytes with AIP56 did not lead to an increase in the percentage of cells with apoptotic morphology or with any other morphological alterations indicative of toxicity, when compared to untreated cells. In contrast, and as expected, most sea bass leukocytes were apoptotic after incubation with AIP56 (Figure 2), confirming that the toxin was active. These results suggest that sea bream peritoneal leukocytes are resistant to AIP56 intoxication.

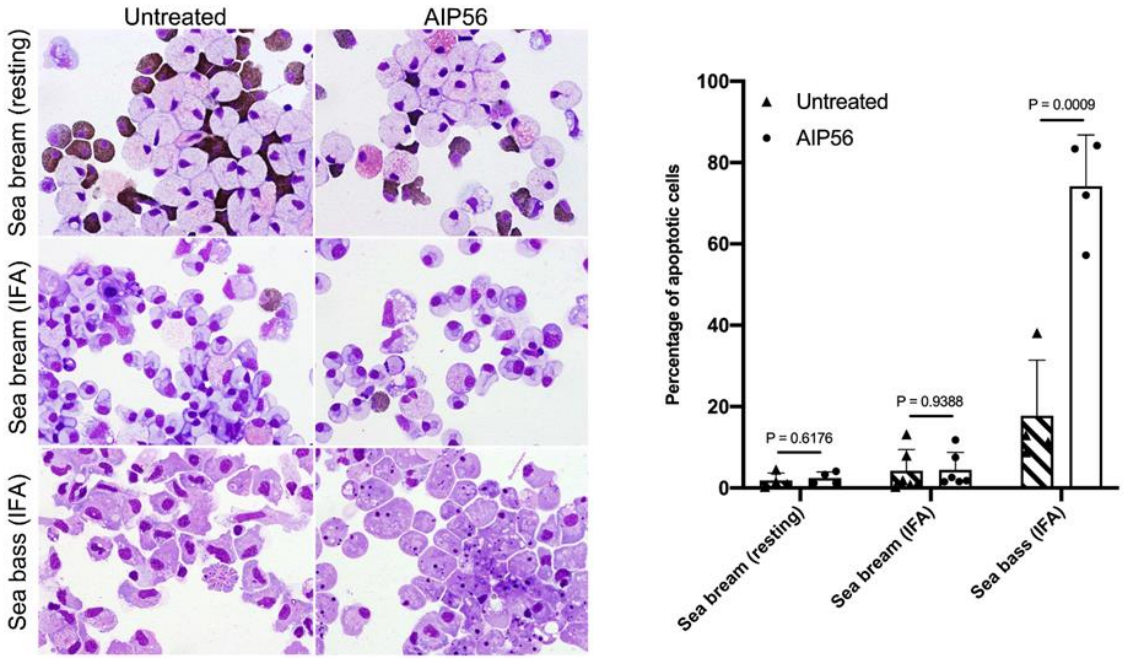

Figure 2. **Sea bream leukocytes are resistant to AIP56 intoxication.** Peritoneal leukocytes collected from resting or IFA-stimulated sea bream (Batch IV, 65-173 g) or from IFA-stimulated sea bass (Batch II, 202-367 g) were left untreated or incubated for 5 h at 22°C with 10 µg/mL AIP56. Images show representative microscopic fields of cytospin preparations stained with Hemacolor after labeling the neutrophils' peroxidase (brown). Note that after incubation with the toxin, most sea bass leukocytes were apoptotic, whereas no signs of toxicity were detected in sea bream leukocytes. The percentage of apoptotic leukocytes, determined by morphological analysis of at least 300 cells, is depicted in the graph. Results are expressed as mean ± SD (n= 4 for sea bream resting, n=6 for sea bream IFA-stimulated, n=4 for sea bass IFA-stimulated). Statistical analysis involved performing two-tailed Student's *t*-test.

2.4. AIP56 displays proteolytic activity against sea bream NF-κB p65

Previous studies have shown that in susceptible cells (e.g., sea bass peritoneal macrophages

and mouse macrophages), AIP56 cleaves NF-κB p65 at a conserved Cys–Glu peptide bond located at the REL homology domain, leading to depletion of this transcription factor and apoptotic death of the cells [1,16]. A possible explanation for the lack of toxicity of AIP56 for sea bream leukocytes could be the inability of the toxin to cleave NF-κB p65 of this fish species. To investigate this possibility, we performed a multiple alignment of the translated amino-acid sequences of NF-κB p65 REL homology domain from different species (Figure 3A), which showed that AIP56 cleavage site is conserved in sea bream NF-κB p65, suggesting that this protein is also susceptible to AIP56 cleavage. To confirm this suggestion, ^{35}S-labeled sea bream NF-κB p65 was incubated *in vitro* with AIP56, and cleavage accessed by autoradiography. ^{35}S-labeled sea bass NF-κB p65 was used as a positive control [16]. As shown in Figure 3B, AIP56 cleaves sea bream and sea bass NF-κB p65 with similar efficiency. As expected, no cleavage occurred after incubation with the catalytically inactive AIP56^{AAIVAA} [16]. These results clearly show that sea bream NF-κB p65 is susceptible to proteolytic cleavage by AIP56.

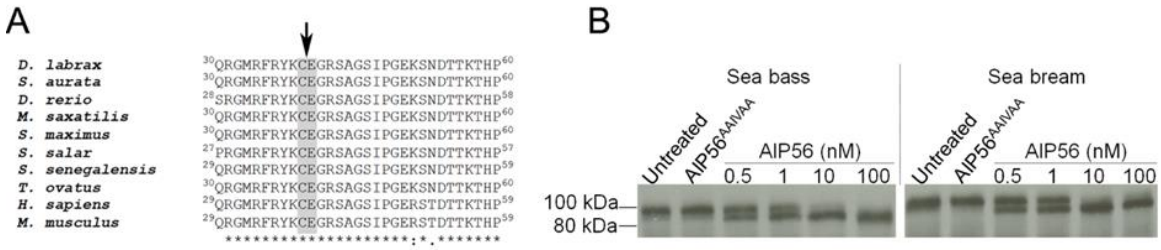

Figure 3. Sea bream NF-κB p65 is susceptible to AIP56 cleavage. **(A)** Alignment of the p65 N- terminal region from different species. *Dicentrarchus Labrax* sequence (DLAgn_00141590) was retrieved from [21] and the remaining sequences were obtained from GenBank (Accession numbers: *Sparus aurata*, XP_030285950; *Danio rerio*, NP_001001839; *Morone saxatilis*, XP_035530725; *Scophthalmus maximus*, XP_035483131; *Salmo salar*, XP_014062259; *Solea senegalensis*, XP_043876337; *Trachinotus ovatus*, QJQ40092; *Homo sapiens*, XP_011543508; *Mus musculus*, NP_033071). AIP56 cleavage site (Cys/Glu) is indicated with an arrow and shaded in grey. Alignment was performed using Clustal Omega [22]. (B) ^{35}S-labeled NF-κB p65 from sea bream or sea bass (positive control) were left untreated or incubated for 2 h at 20 ◦C with 0.5, 1, 10, or 100 nM AIP56 or with 100 nM of the catalytically inactive AIP56^{AAIVAA} and cleavage of p65 assessed by autoradiography. Result shown is representative of 3 independent experiments.

2.5. The internalization of AIP56-488 in sea bream peritoneal leukocytes is inefficient

Studies performed in sea bass and mouse macrophages have shown that intoxication by AIP56 is a multi-step process that begins with clathrin-dependent endocytosis, followed by low pH-dependent translocation of the toxin from the endosomes into the cytosol, where it cleaves NF-κB p65 [15]. Since the resistance of sea bream leukocytes to AIP56 toxicity cannot be explained by an inability to cleave sea bream NF-κB p65, we decided to

investigate if it could be related to an incapacity of the toxin to enter sea bream cells. For this, peritoneal leukocytes collected from resting or inflamed peritoneal cavities of sea bream were incubated with fluorescent-labeled AIP56 (AIP56-488) for 15 min on ice, followed by 15 min at 22 ˚C and the internalization of the toxin was analyzed by flow cytometry. Peritoneal leukocytes collected from IFA-stimulated sea bass, which are known to internalize AIP56 [15], were used as a positive control. In these experiments, we used cells from the same batches of fish used for collecting cells for the *in vitro* toxicity tests (Figure 2), i.e., sea bream Batch IV (75–158 g) and sea bass Batch II (202–367 g), but also cells collected from sea bream Batch II (6.6–14.8 g) or sea bass Batch I (43–65 g). As shown in Figure 4A,B, almost no AIP56-488-positive cells were detected in sea bream leukocytes collected from resting peritoneal cavities, which may explain the observed resistance of those cells to AIP56-induced cytotoxicity (Figure 2). Additionally, only a minority of sea bream leukocytes collected from IFA-stimulated sea bream (17.7% and 29.7% for Batch II and IV, respectively) became positive for AIP56-488 (Figure 4A,B), indicating that most sea bream macrophages that are recruited to the peritoneal cavity in response to IFA stimulation are unable to internalize the toxin. This contrasts with the results obtained in IFA-stimulated sea bass peritoneal leukocytes, in which toxin internalization was detected in more than 70% of the cells (75.9% and 74.2% for Batch I and II, respectively). Moreover, the intensity of fluorescence in sea bass cells positive for AIP56-488 was higher than in AIP56-488-positive cells from sea bream (Figure 4C), suggesting that the toxin binds and is internalized more efficiently by sea bass macrophages. The lower efficiency of AIP56 internalization in sea bream macrophages may contribute to the fact that even though the toxin is internalized by some sea bream macrophages, no AIP56-induced toxicity was detected in these cells.

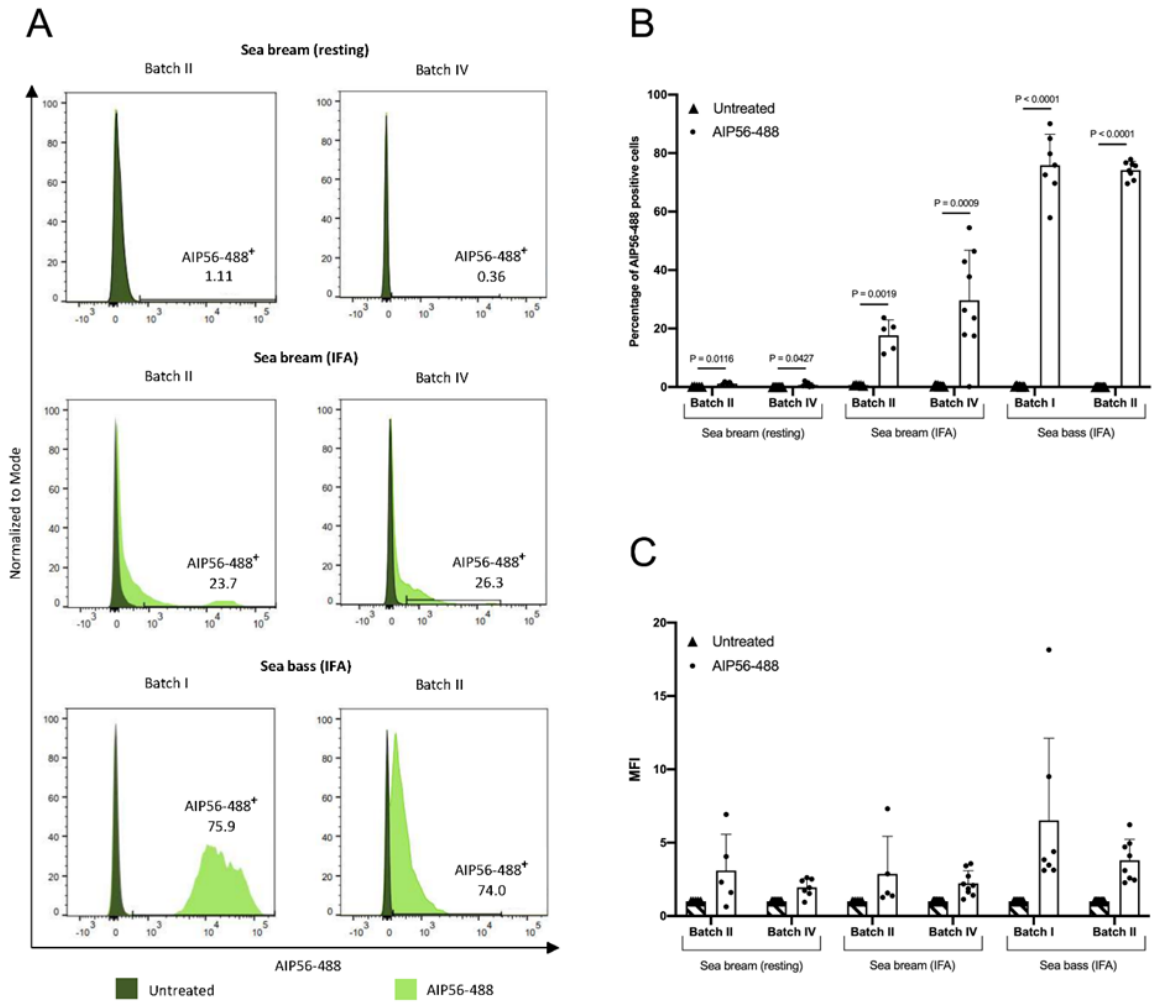

Figure 4. **Internalization of AIP56 by sea bream peritoneal leukocytes.** Peritoneal leukocytes collected from resting or IFA-stimulated sea bream, or from IFA-stimulated sea bass were left untreated or incubated with 5 µg/mL AIP56-488 (15 min on ice + 15 min at 22ºC) and the percentage of AIP56-488-positive cells quantified by flow cytometry. **(A)** Representative flow cytometry plots. **(B)** Quantification of the percentage of AIP56-488-positive cells (n=7 for resting sea bream/Batch II, n=9 for IFA-stimulated sea bream/Batch II, n=5 for resting and IFA-stimulated sea bream/Batch IV, n=8 for sea bass/Batch I, n=7 for sea bass/Batch II). Statistical analysis involved performing two-tailed Student's *t*-test. (C) Mean fluorescence intensity (MFI) of AIP56-488 in the AIP56-488-positive cells, relative to untreated cells. Results are expressed as mean ± SD.

2.6. Sea bream are highly resistant to AIP56 toxicity

To investigate the susceptibility of gilthead sea bream to AIP56, six independent experiments were performed (Table 2). In each experiment, groups of sea bream were injected intra-peritoneally (i.p.) with different doses of AIP56 followed by lethality assessment. Groups of sea bass, which are known to be susceptible to AIP56 [8], were injected in parallel to confirm that the AIP56 was active. In all experiments, the injection of AIP56 in sea bass resulted in mortality. In this species, toxin doses ranging from 0.3–1.0 µg/g body weight resulted in 100% mortality and 60–90% mortality was observed for doses ranging from

0.005–0.2 µg/g body weight. In contrast, no sea bream mortality was observed in experiments 1, 2, 3, 5, and 6, after i.p. injection of AIP56 in doses ranging from 0.9–4.2 µg/g body weight, indicating that this fish species is highly resistant to AIP56 toxicity. Sea bream mortality was however observed in experiment 4, in which 2.2 or 0.2 µg AIP56/g body weight resulted in 100% and 30% mortality, respectively. Nevertheless, despite the increased susceptibility of this batch of sea breams to AIP56, the results of experiment 4 confirmed the higher resistance of sea bream to intoxication, when compared to sea bass, as 90% mortality was observed after injection of sea bass with 0.2 µg AIP56/g body weight, compared to the 30% mortality obtained in sea bream with the same dose. The observed sea bream mortality was caused by the toxin and involved its catalytic activity, as no mortality was observed after injection of the vehicle or 2.2 µg/g body weight of the catalytically inactive AIP56^{AAIVAA}.

Table 2. **Results of the *in vivo* AIP56 lethality tests.**

Experiment	Species	Average weight (g)	Batch	Treatment	Dose (µg/g body weight)	Mortality
1	*Sparus aurata*	11.4 ± 2.6	I	AIP56	0.9	0% (0/10)
				AIP56	0.09	0% (0/10)
	Dicentrarchus labrax	9.6 ± 2.1	I	AIP56	1	100% (10/10)
				AIP56	0.1	60% (6/10)
2	*Sparus aurata*	12.0 ± 2.0	I	AIP56	4.2	0% (0/10)
				AIP56	0.8	0% (0/10)
	Dicentrarchus labrax	10.4 ± 2.1	I	AIP56	1	100% (10/10)
				AIP56	0.1	90% (9/10)
3	*Sparus aurata*	16.0 ± 3.8	I	AIP56	3.1	0% (0/10)
	Dicentrarchus labrax	14.8 ± 6.6	I	AIP56	0.7	100% (10/10)
				AIP56	0.07	70% (7/10)
				Vehicle	x	0% (0/10)
4	*Sparus aurata*	11.6 ± 2.8	II	AIP56	2.2	100% (10/10)
				AIP56	0.2	30% (3/10)
				AIP56^{AAIVAA}	2.2	0% (0/10)
				Vehicle	x	0% (0/10)
	Dicentrarchus labrax	53.6 ± 12.5	I	AIP56	0.2	90% (9/10)
5	*Sparus aurata*	34.4 ± 4.5	III	AIP56	2.9	0% (0/6)
	Dicentrarchus labrax	177.8 ± 23.2	II	AIP56	0.06	100% (5/5)
6	*Sparus aurata*	53.9 ± 14.5	IV	AIP56	1.9	0% (0/5)
	Dicentrarchus labrax	183.4 ± 41.0	II	AIP56	0.005	80% (4/5)

The high resistance of sea bream to AIP56 intoxication suggested that the pathological effects of the toxin for this fish species were mild or even absent. To assess this, spleen, head-kidney and liver samples of fish injected with AIP56 (or vehicle, as control) were collected for histological examination. The first batch of samples were from experiment 3 (Table 2), and included samples from sea bream injected with 3.1 µg AIP56/g body weight, in which no mortality was observed, from sea bass injected with 0.7 µg AIP56/g body weight, that led to 100% mortality, and vehicle controls. The second batch of samples were collected in experiment 4 and included samples from sea bream injected with 2.2 µg AIP56/g body weight, in which 100% mortality was observed, and vehicle controls. Organs collected from sea bass and sea bream injected with vehicle presented a typical histological structure (Figure 5, micrographs 1, 3 and 5; Figure 6, micrographs 1, 4 and 7). Hepatic steatosis, a common phenomenon in farmed fish, was evident in both species (Figure 5, micrographs 5; Figure 6, micrograph 7). In agreement with previous studies [8], i.p. inoculation of AIP56 in sea bass resulted in major histopathological changes in the spleen, head-kidney, and liver (Figure 5). Changes in the spleen included disorganization of the parenchyma architecture, red pulp atrophy, and multifocal necrosis (Figure 5, micrograph 2). A marked disorganization of parenchyma's structure was also evident in the head-kidneys of AIP56-injected sea bass. In this organ, multifocal necrosis of the hematopoietic tissue was evident at 36 h post-injection (Figure 5, micrograph 4) and generalized necrosis was observed in moribund fish. Injection of AIP56 in sea bass resulted also in severe alterations in the liver, including loss of hepatic structure with occurrence of massive hepatocellular necrosis (Figure 5, micrograph 6) and pancreatic atrophy.

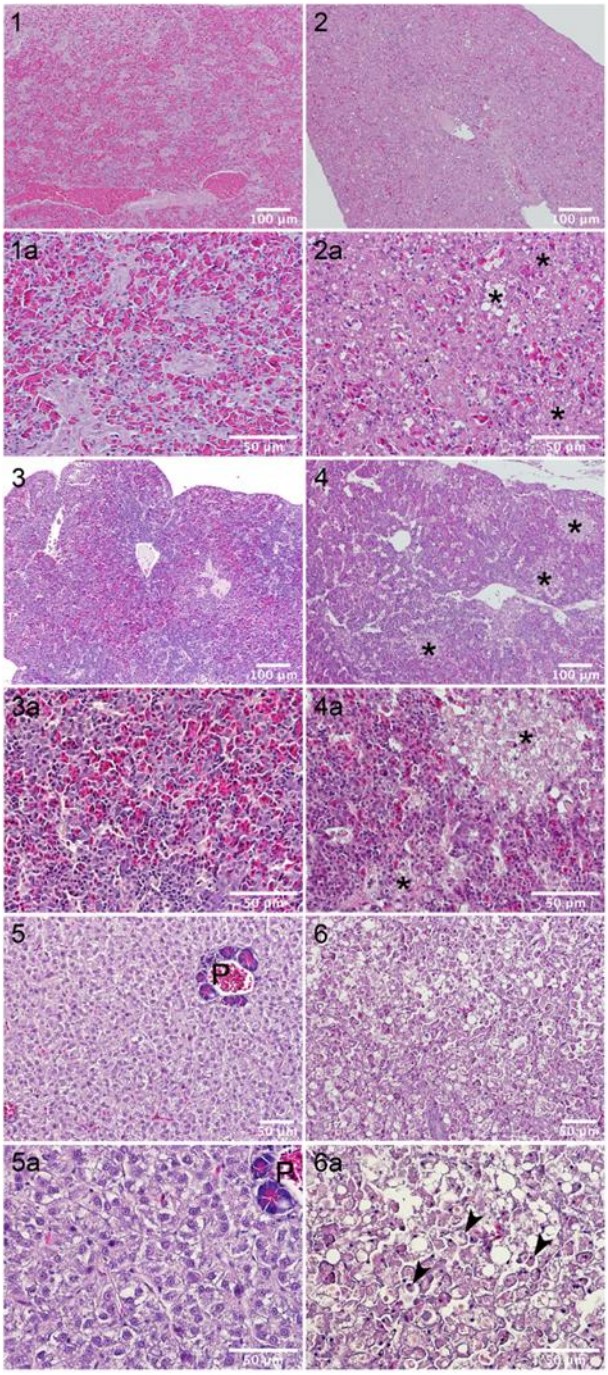

Figure 5. **Histopathological changes induced by AIP56 in sea bass. (1)** Spleen from a control fish (injected with vehicle); **(2)** Spleen collected 36 h after injection of AIP56 (0.7 µg AIP56/g body weight); **(3)** Head-kidney from a control fish (injected with vehicle); **(4)** Head-kidney collected 36 h after injection of AIP56 (0.7 µg AIP56/g body weight); **(5)** Liver from a control fish (injected with vehicle); **(6)** Liver collected 36 h after injection of AIP56 (0.7 µg AIP56/g body weight). Each panel labeled with "a" corresponds to a higher magnification of the panel with the respective number. Asterisks indicate necrotic foci and arrows indicate pyknotic/degenerated cells. P-pancreatic tissue.

In comparison, and in agreement with the lethality results, the pathological alterations induced by AIP56 in sea bream were less prominent (Figure 6). Spleens from AIP56-injected sea breams presented a normal histological structure (Figure 6, panels 2 and 3). In head-kidneys collected from AIP56-injected sea breams from experiment 3, histological alterations, including the presence of degenerated cells and occurrence of multifocal necrosis, were observed in 4 out of 9 specimens (one collected at 36 h and three collected at 60 h post-injection). In experiment 4, pathological alterations were observed in all head-kidneys from AIP56-injected sea breams and were more exacerbated, with higher number of degenerated cells and more frequent and extensive necrotic foci (Figure 6, micrographs 5 and 6). Livers from sea bream injected with AIP56 in experiment 3 presented a normal histological structure, whereas degenerated cells and spotty/focal necrosis (Figure 6, micrographs 8 and 9) were present in all livers from AIP56-injected sea bream from experiment 4. Overall, these observations confirm that the pathology induced by AIP56 in sea bream is milder than in sea bass, while showing that the occurrence of sea bream mortality in response to toxin injection in experiment 4 was associated with histopathological changes in the head-kidney and liver.

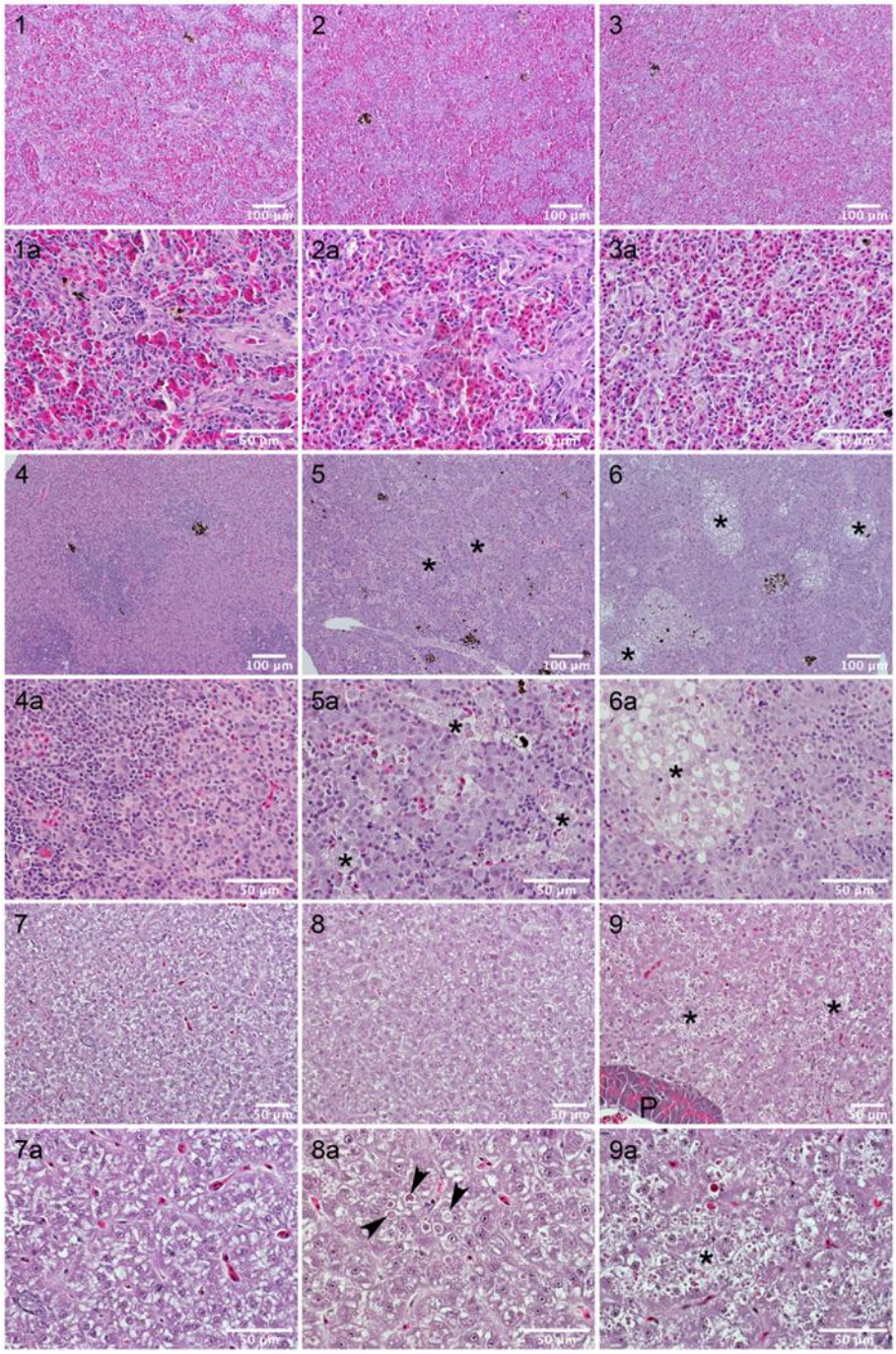

Figure 6. **Histopathological changes induced by AIP56 in sea bream. (1)** Spleen from a control fish (injected with vehicle); **(2)** Spleen collected 60 h after injection of AIP56 (Experiment 3, 3.1 µg AIP56/g body weight); **(3)** Spleen collected 30 h after injection of AIP56 (Experiment 4, 2.2 µg AIP56/g body weight) (4) Head-kidney from a control fish (injected with vehicle); **(5)** and **(6)** Head-kidneys collected 60 h after injection of AIP56 (Experiment 4, 2.2 µg AIP56/g body weight); **(7)** Liver from a control fish (injected with vehicle); **(8)** and **(9)** Livers collected 60 h after injection of AIP56 (Experiment 4, 2.2 µg AIP56/g body weight). Each panel labeled with "a" corresponds to a higher magnification of the panel labeled with the respective number. Asterisks indicate necrotic foci and arrows indicate necrotic cells. P-pancreatic tissue.

3. Discussion

AIP56 is a plasmid encoded exotoxin abundantly secreted by virulent strains of *Phdp in vitro* and *in vivo* [1,8,13]. It has been shown that during *Phdp* infections in sea bass, AIP56 is systemically distributed and plays a major virulence role, by triggering the destruction of the sea bass professional phagocytes, macrophages and neutrophils [23], by post-apoptotic secondary necrosis, a process that culminates in massive phagocytes' lysis [8]. This not only leads to impairment of the host phagocytic defense and, consequently, to unrestricted extracellular multiplication of *Phdp*, but also to the exposure of the host tissues to the highly cytotoxic molecules released from lysing phagocytes that likely participate in the genesis of the necrotic lesions typically associated to *Phdp* infections. Although a similar histopathology has been reported in advanced *Phdp* infections of different fish species, including striped bass (*Morone saxatilis*), sea bream, sea bass, and sole [8,10,24], to date, the contribution of AIP56 for the establishment of the infection in other *Phdp* hosts, apart from sea bass, has not been characterized.

In this work, the toxic effects of AIP56 for sea bream were investigated. We started by analyzing the susceptibility of the sea bream professional phagocytes—acidophilic granulocytes, which are the functional equivalents to mammalian neutrophils, and macrophages [25–27]—to AIP56 *ex vivo*. For this, we used peritoneal leukocytes collected from undisturbed peritoneal cavities, composed mainly by neutrophilic and eosinophilic granulocytes (approximately 48 and 44%, respectively) or leukocytes collected 12 days after i.p. injection of IFA, that were highly enriched in monocytes/macrophages (88% of the total population). Both leukocyte populations were found to be resistant to AIP56 toxicity. The resistance of the resting peritoneal leukocytes (e.g., neutrophilic and eosinophilic granulocytes) agrees with the results obtained in the toxin internalization assays, which showed that AIP56 is not internalized by those cells. For these studies, we used an AIP56 carrying a 6-histidine tag at the C-terminus, but it is unlikely that this could explain the lack of toxicity of AIP56 for sea bream cells, because previous studies have shown that his-tagged AIP56 remains toxic for sea bass [15,16], mouse [15] and human macrophages (unpublished results). The most likely explanation for the inability of sea bream neutrophilic and eosinophilic granulocytes to internalize the toxin is the lack of expression of the AIP56 receptor in those cells, since previous studies in sea bass and mouse macrophages revealed that the entry of AIP56 in the target cells is initiated by binding to a cell surface receptor that remains unidentified [15]. In agreement with this, in the present study, the percentage of sea bass IFA-stimulated peritoneal leukocytes that internalized the AIP56-488 (approximately 76 and 74% for Batch I and Batch II, respectively) was similar to the percentage of cells that underwent apoptosis in

response to intoxication (approximately 74% for Batch II). In what concerns IFA-stimulated peritoneal leukocytes from sea bream, there was no concordance between toxin internalization and cytotoxicity, as they were found to be resistant to AIP56-induced toxicity, despite the fact that internalization of AIP56-488 was detected in a significant percentage of cells (approximately 18% and 30% for Batch II and Batch IV, respectively). There are two main hypotheses that can contribute to this discrepancy. On the one hand, the lower amounts of AIP56 internalized in sea bream macrophages, when compared to the sea bass counterparts, may not be sufficient to decrease the NF-κB p65 levels. On the other hand, since it is known that the consequences of NF-κB p65 downregulation in different cells may differ [28], it cannot be excluded that even if AIP56 is able to lower the levels of NF-κB p65 in some sea bream macrophages, they do not die in response to intoxication. In this work, although it was shown that AIP56 cleaves sea bass and sea bream NF-κB p65 with similar efficiency *in vitro*, it was not possible to determine the extent of p65 cleavage in AIP56-treated sea bream macrophages, due to the lack of antibodies able to recognize sea bream NF-κB p65. This is an important aspect that must be addressed in the future. Additionally, it would also be important to analyze the presence (e.g, by immunohistochemistry) of AIP56 in phagocytes from sea bream naturally infected with *Phdp*, to confirm the here reported *in vitro* observations in a more biologically relevant scenario.

In agreement with the observed low susceptibility of sea bream leukocytes to AIP56-induced toxicity, *in vivo* intoxication assays, performed with different batches of fish, revealed that sea bream are much less susceptible to AIP56-induced lethality than sea bass. In sea bass, mortality was observed in 6 out of 6 experiments, with toxin doses ranging from 0.005–1.0 µg/g body weight resulting in 60–100% mortality, whereas in sea bream, mortality occurred only in 1 out of 6 experiments. In this experiment, injection of sea bream with 0.2 or 2.2 µg AIP56/g body weight resulted in 30% and 100% mortality, respectively, whereas the mortality induced in sea bass by the lowest dose (0.2 µg AIP56/g body weight) reached 90%. Accordingly, the histopathological alterations induced by the toxin in sea bream were milder than in sea bass. The most striking difference was observed in the spleen. In sea bass, marked pathological changes were detected in this organ after injection of 0.7 µg AIP56/g body weight, a dose that led to 100% lethality. In contrast, no histological changes were observed in sea bream spleens even after injection of toxin dose that also led to 100% mortality (2.2 µg AIP56/g body weight). In line with these findings, the histological alterations detected in the head-kidneys and livers of sea bream injected with 2.2 µg AIP56/g body weight were less prominent than the alterations detected in sea bass injected with 0.7 µg AIP56/g body weight. The molecular basis of the high resistance of sea bream to AIP56 is currently unknown, but the results of the *ex vivo* experiments

suggest that it may be related to differences in the expression levels of the AIP56 receptor in sea bream cells, both at the level of cell populations and individual cells, and/or to the existence of evolutionary differences between the sea bass and sea bream receptors that result in different binding affinities to AIP56. The elucidation of these possibilities is worth pursuing, but will require the identification of the AIP56 receptor.

Taken together, the results of the *ex vivo* and *in vivo* experiments indicate that sea bream is more resistant to AIP56 intoxication than sea bass, which may suggest that the toxin plays a less important virulence role during *Phdp* infections in sea bream. However, the screening of 49 *Phdp* isolates recovered between 2014 and 2020 from diseased sea bream and sea bass in different European countries showed a 100% prevalence of the AIP56-encoding gene. This result, which is in agreement with previous studies reporting a ubiquitous distribution of the *aip56* gene in *Phdp* strains recovered worldwide from different fish species in the last 30 years [18,29,30], suggests the existence of selective pressure to maintain the toxin gene and supports the hypothesis that in the majority of hosts the toxin may be required for virulence. However, it cannot be excluded that, in some hosts, AIP56 may have a less important contribution for virulence and that other virulence determinants, so far unidentified, may assume a more prominent virulence role. In this context, the in-depth characterization of the pathogenic role played by AIP56 in different *Phdp* hosts is of outmost importance to gain a more complete understanding of *Phdp* pathogenicity. So far, that characterization has been hampered by the lack of isogenic mutants deficient in *aip56* due to technical drawbacks mainly related to the fact that the toxin is encoded in a high copy plasmid.

In conclusion, the results reported in this work disclose the existence of differences in the susceptibility to AIP56 between sea bass and sea bream and emphasize the need for additional studies, to not only determine the susceptibility to this toxin and its role for virulence in other *Phdp* susceptible hosts, but also the contribution of other virulence factors for *Phdp*-induced lethality. Uncovering the relevance of the toxin in the context of the *Phdp* infections and the dissection of the specific effects triggered in different hosts is highly relevant for supporting future development of therapeutic and prophylactic measures against *Phdp* infections.

4. Materials and Methods

4.1. Production and fluorescence labeling of recombinant proteins

Full-length His-tagged AIP56 (AIP56) or catalytically inactive AIP56 ($AIP56^{AAIVAA}$) were expressed and purified as previously described [16]. Briefly, the sequence encoding AIP56 from the MT1415 strain was cloned in pET28a(+) in frame with a C-terminal His-tag and expressed in *E. coli* BL21 (DE3) cells at 17ºC. Induced bacterial cells were lysed by sonication, centrifuged, and the recombinant protein was purified from the supernatant using nickel-affinity chromatography (Ni-NTA agarose, ABT) followed by size exclusion chromatography (Superose 12 10/300 GL, GE Healthcare). $AIP56^{AAIVAA}$ was purified from inclusion bodies by metal-affinity chromatography under denaturing conditions, refolded, and subjected to size exclusion chromatography [16]. Purified protein batches were analyzed by SDS-PAGE and purities, determined by densitometry of Coomassie blue-stained gels, were ≥ 90%. Recombinant AIP56 labelled with Alexa Fluor 488 (AIP56-488) was prepared using the Molecular Probes® Alexa Fluor protein labelling kit (Thermo Fisher Scientific), following the manufacturer's instructions.

4.2. Determination of recombinant protein concentration

Protein concentrations were determined by spectrophotometry by measuring absorbance at 280 nm using NanoDrop 1000 (Thermo Fisher Scientific), considering the extinction coefficients and the molecular weights, calculated by the ProtParam tool (http://www.expasy.org/tools/protparam.html).

4.3. Fish

Four different lots of sea bream (*S. aurata*) and two lots of sea bass (*D. labrax*) with no previous history of *Phdp* infection were purchased from commercial hatcheries, and maintained in 600 L seawater aquaria. Water temperature was maintained at 20 ± 2°C, salinity at 23-28‰ and the photoperiod was 14 h light: 10 h dark. Water quality was maintained with mechanical and biological filtration and ozone-disinfection and the fish were fed on commercial pellets (Skretting), adjusting the food intake to fish species/size and water temperature, according to the supplier's recommendations. All experimental protocols were carried out in accordance with European and Portuguese legislation for the use of animals for scientific purposes (Directive 2010/63/EU; Decreto-Lei 113/2013) and were licensed by the DGAV (Lic. 0421/000/000/2021).

4.4. Cells

Peritoneal leukocytes were obtained from resting or inflamed peritoneal cavities of sea bream (weighting between 6.6 g and 173 g) or sea bass (weighting between 43 g and 367 g), following a procedure described in detail elsewhere [22,30]. Inflammation was induced by intraperitoneal (i.p.) injection of 100 µL of Incomplete Freund's Adjuvant (IFA) 12 days before collecting the cells [31]. Cells were used at a density of 2 x 10^6 cells/mL in L-15 medium (Gibco) adjusted to 322 mOsm and supplemented with 2.5% fetal bovine serum (FBS, Gibco), 1% penicillin/streptomycin (P/S, Gibco) and 20 U/mL heparin (Braun).

4.5. Cell intoxication assays

Intoxication assays were performed by incubating peritoneal leukocytes suspensions from sea bream (Batch IV, 65-173 g) or sea bass (Batch II, 202-367 g) with 10 µg/mL of AIP56 for 5 h at 22°C. Untreated cells were used as controls. Occurrence of apoptosis and other signs of toxicity was assessed as described [20], through morphological analysis by light microscopy of at least 300 cells in cytospin preparations stained with Hemacolor (Merck), after labelling the neutrophils' peroxidase using the Antonow's technique [22,30].

4.6. AIP56 internalization assays

To assess AIP56 internalization, peritoneal leukocyte suspensions collected from sea bream (Batch II, 6.6-14.8 g and Batch IV, 75-158 g) or sea bass (Batch I, 43-65 g and Batch II, 202-367 g) were incubated with 5 µg/mL AIP56-488 in L-15 medium adjusted to 322 mOsm and supplemented with 2.5% FBS, 1% P/S and 20 U/mL heparin for 15 min on ice. Cell suspensions were centrifuged (5 min, 500 g, 4ºC), the supernatant discarded, and the cells resuspended in the same medium without toxin and incubated for 15 min at 22ºC. Cells were washed thrice with sea bass PBS (sbPBS; 50 mM phosphate buffer pH 7.2 + 184 mM NaCl), resuspended in 0.2 mL FACS buffer (sbPBS + 2% FBS), filtered through a 35 µm nylon mesh cell strainer into flow cytometry tubes and analyzed by flow cytometry on a BD FACSCanto™ II (BD Biosciences, San Jose, CA). PI (5 µg/mL) was added to access cell viability and fluorescence were collected through a 530/30 nm (FITC) and 695/40 nm (PerCP-Cy5.5) detection filters. Ten thousand events per sample were analyzed at medium flow rate. All data were analyzed using FlowJo™ software v10.6.1 (San Diego, CA).

4.7. Detection of *aip56* in *Phdp* field isolates

The presence of *aip56* was evaluated in 49 isolates recovered during *Phdp* outbreaks occurred in Europe between 2014 and 2020 (Table 1). Strains ATCC29690 and EPOY8803-

II, both lacking *aip56* [1,18], were used as negative controls, and strain MT1415 was used as a positive control. Bacterial stocks that were kept at -80ºC were plated in Tryptic Soy Agar (TSA, Difco) supplemented with NaCl to a final concentration of 1% (TSA-1) and grown for 48 h at 25ºC. A single colony of each strain was picked, with a sterile tip, and dipped into NZYTaq II 2x Green Master Mix (NZYTech). Colony-PCR was carried out with primers: 5'-GCATGACAGCAATATTTTCT-3' (forward) and 5'-TTAATTAATGAATTGTGGCG-3'(reverse) and the following program: a) denaturation for 3 min at 95ºC, b) 35 cycles of denaturation at 95ºC for 30 s, annealing at 55ºC for 30 s, elongation at 72ºC for 1 min and c) a final elongation step at 72ºC for 10 min. PCR products were analyzed by electrophoresis in an 1% agarose gel.

4.8. Comparative analysis of AIP56 from different *Phdp* strains

Nucleotide sequences of *aip56* genes from *Phdp* strains isolated from sea bass (GRDL19-1, and SPDL20-5) and sea bream (DI21, GRSA19-1, SPSA20-2) were determined by Sanger sequencing at Eurofins Genomics or GATC Company. AIP56 ORFs were amplified by PCR using NZYProof DNA polymerase (NZYTech) and primers 5'-GCGCCATGGCGGTATATTAACAGGATGTCACAGTG-3' (forward) and 5'-CGGCTCGAGCGGTTCTACTTCTACAAAATTTTGCGGC-3' (reverse) and cloned into pET28a(+) using the NcoI and XhoI restriction sites. The sequence of *aip56* from MT1415 was obtained from GenBank (Accession number: TJZ88254.1). The DNA sequences were translated into protein using ExPASy translate tool (https://web.expasy.org/translate/) on the basis of standard genetic code. Multiple alignments of nucleotide/amino acid sequences were performed by Clustal Omega program [32].

4.9. Cloning sea bream NF-κB p65

To amplify and clone sea bream NF-κB p65 coding sequence, a sea bream was stimulated i.p. with 150 µL of a suspension of UV-killed *Phdp* MT1415 cells (OD600nm=0.9) and total RNA was extracted from the head-kidney using TripleXtractor reagent (Grisp) according to the manufacturer's instructions. Briefly, 100 mg of the tissue were homogenized with TripleXtractor, chloroform was added to the homogenate and the aqueous phase collected. Following precipitation with isopropanol, the total RNA was washed with 70% ethanol and dissolved in RNAse-free water. cDNA synthesis was carried out using the PrimeScript RT Reagent Kit (Takara) according to the manufacturer's instructions. The cDNA was then amplified using NZYProof DNA Polymerase (NZYTech) and primers 5'-GCGCCATGGAGGGTGGGTTTGGATGGAGCC-3' (forward) and 5'-GCGCTCGAGAGTTGGGTGTCCTGACACAAACC-3' (reverse) and cloned into pET28a(+) using the NcoI and XhoI restriction sites.

4.10. NF-κB cleavage assay

Sea bass and sea bream ^{35}S-labeled NF-κB p65 synthetized *in vitro* using the TNT T7 Quick Coupled Transcription/Translation system (Promega), as previously described [16], were incubated in 10 mM Tris-HCl pH 8.0 + 300 mM NaCl for 2 h at 20°C with different concentrations of AIP56 (0.5, 1, 10 and 100 nM) or with 100 nM of AIP56^{AAIVAA}. Samples were subjected to SDS-PAGE, transferred to nitrocellulose membranes (Amersham Protran) and p65 cleavage analyzed by autoradiography.

4.11. *In vivo* toxicity tests

The *in vivo* toxicity of AIP56 was tested in 6 independent experiments, using 4 different batches of sea bream and 2 batches of sea bass, as specified in Table 3. In each experiment, groups of sea bream were injected with the indicated concentrations of AIP56, the catalytically inactive AIP56^{AAIVAA} or vehicle, in 100 µL of sbPBS. Sea bass, which are known to be susceptible to AIP56 [8], were injected in parallel. Injections were performed under anesthesia induced by immersion in 0.03% (v/v) ethylene glycol monophenyl ether. Injected fish were monitored at least 4 times a day and mortalities recorded. Any fish showing signs of advanced disease (darkening of body color, lethargy, erratic swimming and loss of equilibrium) were euthanized, by immersion in 0.06% (v/v) of ethylene glycol monophenyl ether followed by sectioning of the ventral aorta, and counted as dead.

In experiments 3 and 4, in parallel to the groups used for assessing lethality, groups were included for collecting samples for histological analysis. Two sampling times were established, at 36 and 60 h post-injection, for collecting the head-kidney, spleen and liver. Five animals from each group were euthanized and sampled at 36 h and the remaining fish were sampled at 60 h. In experiment 3, two sea bass injected with AIP56 were found dead at 35 and 59 h after injection and three sea bass from the same group become moribund at 14, 18 and 24 h. These moribund fish were euthanized and organs collected. Tissues were fixed in 10% buffered formalin, routinely processed in an automated system, embedded in paraffin, sectioned at 3 µm and stained with hematoxylin and eosin (H&E).

Table 3. **Description of the *in vivo* assays.**

Experiment	Species	Average Weight (g)	Batch	Treatment	Dose (µg/g body weight)	Lethality	Histopathology
1	*Sparus aurata*	11.4 ± 2.6	I	AIP56	0.9	Yes (n=10)	No
				AIP56	0.09	Yes (n=10)	No

	Dicentrarchus labrax	9.6 ± 2.1	I	AIP56	1	Yes (n=10)	No
				AIP56	0.1	Yes (n=10)	No
2	*Sparus aurata*	12.0 ± 2.0	I	AIP56	4.2	Yes (n=10)	No
				AIP56	0.8	Yes (n=10)	No
	Dicentrarchus labrax	10.4 ± 2.1	I	AIP56	1	Yes (n=10)	No
				AIP56	0.1	Yes (n=10)	No
3	*Sparus aurata*	16.0 ± 3.8	I	AIP56	3.1	Yes (n=10)	Yes (n=10)
				Vehicle	x	No	Yes (n=10)
	Dicentrarchus labrax	14.8 ± 6.6	I	AIP56	0.7	Yes (n=10)	Yes (n=10)
				AIP56	0.07	Yes (n=10)	No
				Vehicle	x	Yes (n=10)	Yes (n=10)
4	*Sparus aurata*	11.6 ± 2.8	II	AIP56	2.2	Yes (n=10)	Yes (n=10)
				AIP56	0.2	Yes (n=10)	No
				$AIP56^{AAIVAA}$	2.2	Yes (n=10)	No
				Vehicle	x	Yes (n=10)	Yes (n=10)
	Dicentrarchus labrax	53.6 ± 12.5	I	AIP56	0.2	Yes (n=10)	No
5	*Sparus aurata*	34.4 ± 4.5	III	AIP56	2.9	Yes (n=6)	No
	Dicentrarchus labrax	177.8 ± 23.2	II	AIP56	0.06	Yes (n=5)	No
6	*Sparus aurata*	53.9 ± 14.5	IV	AIP56	1.9	Yes (n=5)	No
	Dicentrarchus labrax	183.4 ± 41.0	II	AIP56	0.005	Yes (n=5)	No

4.12. GenBank accession numbers

The nucleotide sequences of *aip56* from strains DI21, GRSA19-1, GRDL19-1, SPSA20-2 and SPDL20-5 were deposited in the GenBank database under accession numbers OM056532, OM056531, OM056529, OM056530, OM056528, respectively.

References

1. do Vale, A.; Silva, M.T.; dos Santos, N.M.S.; Nascimento, D.S.; Reis-Rodrigues, P.; Costa-Ramos, C.; Ellis, A.E.; Azevedo, J.E. AIP56, a novel plasmid-encoded virulence factor of *Photobacterium Damselae* subsp. *piscicida* with apoptogenic activity against sea bass macrophages and neutrophils. *Mol. Microbiol.* 2005, *58*, 1025–1038.
2. Andreoni, F.; Magnani, M. Photobacteriosis: Prevention and diagnosis. *J. Immunol. Res.* 2014, *2014*, 793817.
3. Colloca, F.; Cerasi, S. *Sparus aurata*. Cultured Aquatic Species Information Programme. Available online: https://www.fao.org/fishery/en/culturedspecies/sparus_aurata/en (accessed on 14 December 2021).
4. Bagni, M. *Dicentrarchus labrax*. Cultured Aquatic Species Information Programme. Available online: https://www.fao.org/fishery/en/culturedspecies/dicentrarchus_labrax/en (accessed on 14 December 2021).
5. Colen, R.; Ramalho, A.; Rocha, F.; Dinis, M.T. *Solea solea*. Cultured Aquatic Species Information Programme. Available online: https://www.fao.org/fishery/en/culturedspecies/solea_spp/en (accessed on 14 December 2021).
6. Dhirendra, P.T. *Seriola quiqueradiata*. Cultured Aquatic Species Information Programme. Available online: https://www.fao.org/fishery/en/culturedspecies/seriola_quinqueradiata/en (accessed on 14 December 2021).
7. Kaiser, J.B.; Holt, J.G. *Rachycentron canadum*. Cultured Aquatic Species Information Programme. Available online: https://www.fao.org/fishery/en/culturedspecies/rachycentron_canadum/en (accessed on 14 December 2021).
8. do Vale, A.; Costa-Ramos, C.; Silva, A.; Silva, D.S.; Gartner, F.; dos Santos, N.M.; Silva, M.T. Systemic macrophage and neutrophil destruction by secondary necrosis induced by a bacterial exotoxin in a Gram-negative septicaemia. *Cell. Microbiol.* 2007, *9*, 988–1003.
9. Tung, M.-C.T.; Tsai, S.S.; Ho, L.-F.; Huang, S.T.; Chen, S.C. An acute septicemic infection of *Pasteurella* organism in pond-cultured Formosa snake-head fish (*Channa maculata* Lacepeda) in Taiwan. *Fish Pathol.* 1985, *20*, 143–148.
10. Hawke, J.P.; Plakas, S.M.; Minton, R.V.; McPhearson, R.M.; Snider, T.G.; Guarino, A.M. Fish pasteurellosis of cultured striped bass (*Morone saxatilis)* in coastal Alabama.

Aquaculture 1987, *65*, 193–204.

11. Noya, M.; Magarinos, B.; Toranzo, A.E.; Lamas, J. Sequential pathology of experimental pasteurellosis in gilthead seabream *Sparus aurata*. A light- and electron-microscopic study. *Dis. Aquat. Org.* 1995, *21*, 177–186.
12. Magarinos, B.; Toranzo, A.E.; Romalde, J.L. Phenotypic and pathobiological characteristics of *Pasteurella piscicida*. *Annu. Rev. Fish Dis.* 1996, *6*, 41–64.
13. do Vale, A.; Pereira, C.; Osorio, C.R.; dos Santos, N.M.S. The Apoptogenic Toxin AIP56 Is Secreted by the Type II Secretion System of *Photobacterium Damselae* subsp. *piscicida*. *Toxins* 2017, *9*, 368.
14. Silva, M.T.; do Vale, A.; dos Santos, N.M. Secondary necrosis in multicellular animals: An outcome of apoptosis with pathogenic implications. *Apoptosis* 2008, *13*, 463–482.
15. Pereira, L.M.; Pinto, R.D.; Silva, D.S.; Moreira, A.R.; Beitzinger, C.; Oliveira, P.; Sampaio, P.; Benz, R.; Azevedo, J.E.; dos Santos, N.M.S.; et al. Intracellular trafficking of AIP56, an NF-κB cleaving toxin from *Photobacterium Damselae* subsp. *piscicida*. *Infect. Immun.* 2014, *82*, 5270–5285.
16. Silva, D.S.; Pereira, L.M.G.; Moreira, A.R.; Ferreira-da-Silva, F.; Brito, R.M.; Faria, T.Q.; Zornetta, I.; Montecucco, C.; Oliveira, P.; Azevedo, J.E.; et al. The Apoptogenic Toxin AIP56 is a Metalloprotease A-B Toxin that Cleaves NF-κb P65. *PLoS Pathog.* 2013, *9*, e1003128.
17. Rodrigues, I.S.; Pereira, L.M.G.; Lisboa, J.; Pereira, C.; Oliveira, P.; Dos Santos, N.M.S.; do Vale, A. Involvement of Hsp90 and cyclophilins in intoxication by AIP56, a metalloprotease toxin from *Photobacterium Damselae* subsp. *piscicida*. *Sci. Rep.* 2019, *9*, 9019.
18. Abushattal, S.; Vences, A.; Osorio, C.R. A virulence gene typing scheme for *Photobacterium Damselae* subsp. *piscicida*, the causative agent of fish photobacteriosis, reveals a high prevalence of plasmid-encoded virulence factors and of type III secretion system genes. *Aquaculture* 2020, *521*, 735057.
19. Magarinos, B.; Romalde, J.L.; Bandin, I.; Fouz, B.; Toranzo, A.E. Phenotypic, antigenic, and molecular characterization of *Pasteurella piscicida* strains isolated from fish. *Appl. Environ. Microbiol.* 1992, *58*, 3316–3322.
20. do Vale, A.; Marques, F.; Silva, M.T. Apoptosis of sea bass (*Dicentrarchus Labrax L.*) neutrophils and macrophages induced by experimental infection with *Photobacterium Damselae* subsp. *piscicida*. *Fish Shellfish Immunol.* 2003, *15*, 129-144.
21. Draft Assembly of *Dicentrarchus Labrax* Genome (dicLab v1.0c). Available online: http://seabass.mpipz.mpg.de/ (accessed on 18 October 2021).
22. Sievers, F.; Wilm, A.; Dineen, D.; Gibson, T.J.; Karplus, K.; Li, W.; Lopez, R.; McWilliam, H.; Remmert, M.; Söding, J.; et al. Fast, scalable generation of high-quality protein

multiple sequence alignments using Clustal Omega. *Mol. Syst. Biol.* 2011, *7*, 539.

23. do Vale, A.; Afonso, A.; Silva, M.T. The professional phagocytes of sea bass (*Dicentrarchus Labrax L.*): Cytochemical characterisation of neutrophils and macrophages in the normal and inflamed peritoneal cavity. *Fish Shellfish Immunol.* 2002, *13*, 183–198.
24. Toranzo, A.E.; Barreiro, S.; Casal, J.F.; Figueras, A.; Magarinos, B.; Barja, J.L. Pasteurellosis in cultured gilthead seabream (*Sparus aurata*): First report in Spain. *Aquaculture* 1991, *99*, 1–15.
25. Chaves-Pozo, E.; Muñoz, P.; López-Muñoz, A.; Pelegrín, P.; García Ayala, A.; Mulero, V.; Meseguer, J. Early innate immune response and redistribution of inflammatory cells in the bony fish gilthead seabream experimentally infected with *Vibrio anguillarum*. *Cell Tissue Res.* 2005, *320*, 61–68.
26. Sepulcre, M.; Pelegrín, P.; Mulero, V.; Meseguer, J. Characterisation of gilthead seabream acidophilic granulocytes by a monoclonal antibody unequivocally points to their involvement in fish phagocytic response. *Cell Tissue Res.* 2002, *308*, 97–102.
27. Sepulcre, M.P.; Lopez-Castejon, G.; Meseguer, J.; Mulero, V. The activation of gilthead seabream professional phagocytes by different PAMPs underlines the behavioural diversity of the main innate immune cells of bony fish. *Mol. Immunol.* 2007, *44*, 2019–2026.
28. Hodgson, A.; Wan, F. Interference with nuclear factor kappaB signaling pathway by pathogen-encoded proteases: Global and selective inhibition. *Mol. Microbiol.* 2016, *99*, 439–452.
29. Pham, T.H.; Cheng, T.-C.; Wang, P.-C.; Chen, S.-C. Genotypic diversity, and molecular and pathogenic characterization of *Photobacterium Damselae* subsp. *piscicida* isolated from different fish species in Taiwan. *J. Fish Dis.* 2020, *43*, 757–774.
30. Baseggio, L.; Silayeva, O.; Buller, N.; Landos, M.; Englestädter, J.; Barnes, A.C. Complete, closed and curated genome sequences of *Photobacterium Damselae* subsp. *piscicida* isolates from Australia indicate mobilome-driven localized evolution and novel pathogenicity determinants. *Microb. Genom.* 2021, *7*, 000562.
31. ProtParam Tool on the Expasy Server. Available online: http://www.expasy.org/tools/protparam.html (accessed on 18 Octo- ber 2021).
32. Afonso, A.; Ellis, A.E.; Silva, M.T. The leucocyte population of the unstimulated peritoneal cavity of rainbow trout (*Oncorhynchus mykiss*). *Fish Shellfish Immunol.* 1997, *7*, 335–348.
33. Costa-Ramos, C.; do Vale, A.; Ludovico, P.; dos Santos, N.M.S.; Silva, M.T. The bacterial exotoxin AIP56 induces fish macrophage and neutrophil apoptosis using mechanisms of the extrinsic and intrinsic pathways. *Fish Shellfish Immunol.* 2011, *30*, 173–181.

34. Translate Tool on the Expasy Server. Available online: https://web.expasy.org/translate/ (accessed on 18 October 2021).
35. Madeira, F.; Park, Y.m.; Lee, J.; Buso, N.; Gur, T.; Madhusoodanan, N.; Basutkar, P.; Tivey, A.R.N.; Potter, S.C.; Finn, R.D.; et al. The EMBL-EBI search and sequence analysis tools APIs in 2019. *Nucleic Acids Res.* 2019, *47*, W636–W641.

CHAPTER II

AIP56, an AB Toxin Secreted by *Photobacterium Damselae* subsp. *piscicida*, Has Tropism for Myeloid Cells

AIP56, an AB Toxin Secreted by *Photobacterium Damselae* subsp. *piscicida*, Has Tropism for Myeloid Cells

Inês Lua Freitas[1,2,3], Maria Fátima Macedo[4,5], Liliana Oliveira[4,5], Pedro Oliveira[6], Ana do Vale[1,2], Nuno M.S. dos Santos[1,2]

[1]Fish Immunology and Vaccinology Group, IBMC - Instituto de Biologia Molecular e Celular, Universidade do Porto, Porto, Portugal

[2]Fish Immunology and Vaccinology Group, i3S - Instituto de Investigação e Inovação em Saúde, Universidade do Porto, Porto, Portugal

[3]McBiology Doctoral Program, ICBAS – Instituto de Ciências Biomédicas Abel Salazar, Universidade do Porto, Porto, Portugal

[4]Cell Activation and Gene Expression, IBMC – Instituto de Biologia Molecular e Celular, Universidade do Porto, Porto, Portugal

[5]Cell Activation and Gene Expression, i3S – Instituto de Investigação e Inovação em Saúde, Universidade do Porto, Porto, Portugal

[6]EPIUnit, ICBAS-Instituto de Ciências Biomédicas Abel Salazar, Universidade do Porto, Porto, Portugal

Abstract

The AB-type toxin AIP56 is a key virulence factor of *Photobacterium Damselae* subsp. *piscicida* (*Phdp*), inducing apoptosis in fish immune cells. The discovery of AIP56-like and AIP56-related toxins in diverse organisms, including human-associated Vibrio strains, highlights the evolutionary conservation of this toxin family, suggesting that AIP56 and its homologs may share conserved receptors across species. These toxins have potential for biotechnological applications, such as therapeutic protein delivery and immune modulation. Herein, the cell specificity of AIP56 for immune cells in sea bass, mice, and humans was characterized.

Whether AIP56 interacts directly or indirectly with sea bass neutrophils was never investigated. Here, it was shown that only a small population of sea bass neutrophils internalized AIP56, indicating that most of the neutrophilic destruction during *Phdp* infection and/or AIP56 intoxication does not result from the direct action of the toxin. Moreover, the cellular tropism of AIP56 for myeloid cells was observed in the three species, including its preference for macrophages. Further, mouse and human M0 and

M2-like macrophages internalized more toxin than M1-like macrophages. Despite the limited interaction of lymphoid cells with AIP56, mouse B1-cells were able to internalize the toxin, possibly due to its myeloid features. These findings are relevant for both pathogenicity and biomedical contexts.

1. Introduction

Photobacterium Damselae subsp. *piscicida* (*Phdp*) is a Gram- negative bacterium that infects a large number of warm saltwater fish species, including sea bass, sea bream, sole and yellowtail, with high impact for the aquaculture industry (1–3). A crucial virulence factor of this pathogen is AIP56 (Apoptosis-Inducing Protein of 56 kDa), a plasmid-encoded AB-type toxin secreted through T2SS (type 2 secretion system) (4–6). It has been reported that the systemic distribution of the toxin in infected animals is associated to the death of fish macrophages and neutrophils by post-apoptotic secondary necrosis, causing the release of highly cytotoxic molecules that likely contribute to the typical necrotic lesions of *Phdp* infections (4, 7). The AIP56-associated systemic elimination of the host phagocytes facilitates the extracellular proliferation of the pathogen, leading to septicemia and death of the infected host (7). Passive immunization with rabbit anti-AIP56 serum protected sea bass from *Phdp* infections, further supporting that AIP56 is a key virulence factor of this pathogen (4). Although *Phdp* is unable to grow at 37°C and has a strict salt dependency (4), making it incapable to infect mammals, AIP56 displays high toxicity for mouse macrophages (8).

The three-dimensional structure of AIP56 has been recently solved, showing that it has a three-domain organization (9). The N-terminal domain is homologous to NleC (non LEE-encoded effector C), a T3SS effector secreted by several enteric bacteria associated with human diseases (10–12) and displays metalloprotease activity for NF-κB p65 (6), a transcription factor that promotes the expression of anti-apoptotic and inflammatory genes (13). Thus, AIP56-mediated cleavage of NF-κB p65 will likely lead to decreased expression of anti-apoptotic genes and consequently apoptotic death of the host cells (6–8). The small middle domain is mostly composed by a 35-aa long partially structured linker peptide, whose ends are bound by a disulfide bridge necessary for intoxication (8), and is likely involved in transmembrane channel formation (9). The C-terminal domain is responsible for binding to as yet unidentified receptor(s) (6) and is also required for pore-formation (9). Studies performed in sea bass and mouse macrophages showed that, to reach its molecular target in the cytosol, AIP56 is internalized by clathrin-dependent endocytosis followed by acidic-dependent translocation from the endosomal compartment into the cytosol, in a process involving Hsp90 and Cyclophilin A/D (6, 8, 14). An increasing number of putative toxins homologous to AIP56 (AIP56-like toxins) is being annotated in the genomes of organisms that have hosts from different phylogenetic groups such as *Shewanella psychrophila*, *Arsenophonus nasoniae*, *Candidatus* Symbiopectobacterium and several *Vibrio* species, including strains that have been isolated from human blood and stool (15, 16). Also, toxins that have a domain homologous to the receptor-binding domain of AIP56 but distinct catalytic and middle domains (AIP56-related toxins) can be found in the genomes of prokaryotic and eukaryotic organisms such as *Enterovibrio norvegicus*, *Shewanella woodyi*, *Shewanella nanhaiensis*, *Neisseria gonorrhoeae*, *Danaus plexippus*, *Danaus chrysippus*, *Operophtera brumata*, *Thrips palmi*, *Drosophila ananassae* (17) and *Drosophila bipectinata*. Moreover, proteins homologous to the AIP56's receptor- binding domain are also present in the genome of *Acyrthosiphon pisum* secondary endosymbiont 2 (APSE-2) and 7 (APSE-7) bacteriophages. AlphaFold predictions indicate that the homologous domain present in all these putative toxins is structurally similar to the receptor-binding domain of AIP56 (9). This, together with the fact that AIP56 is toxic to both sea bass and mouse macrophages (8, 14), suggests that they likely bind to a phylogenetically conserved receptor and target similar cell populations.

In this work, a detailed characterization of the specificity of AIP56 for cells involved in the immune response in sea bass, humans and mice was performed. Identification of AIP56 target cells is not only important for understanding the biology of intoxication, with eventual extension to other members of the AIP56-toxin family, but also relevant from the biotechnological and/or biomedical point of view. In fact, AB toxins naturally evolved as

autonomous systems capable of delivering their catalytic domain into the cytosol of target cells and are top candidates for delivering therapeutic proteins to the cytosol of human cells to treat many diseases and conditions (17, 18). The modular structure of these toxins allows replacing their domains or grafting other moieties to diversify their functions or redirect them to different cell types. In the case of AIP56, it has been shown that the delivery region (middle and receptor-binding domains) is capable of delivering b-lactamase into the cytosol of mouse macrophages (9, 14). The here reported characterization of the cellular susceptibility to AIP56 in humans (and mice, as a model species) is of relevance when considering the future use of AIP56 and AIP56-like and/or -related toxins as biotechnological/ biomedical tools.

2. Results

2.1. AIP56 internalization by sea bass leukocytes

The occurrence of apoptosis of macrophages and neutrophils after injection of sea bass with *Phdp* or AIP56 is well documented (4, 7). However, whereas it has been shown that AIP56 directly targets macrophages leading to their apoptosis (8, 19), a similar causal correlation has not been established for neutrophils. Thus, it was important to evaluate if AIP56 is also able to directly target other sea bass immune cells, namely neutrophils and lymphocytes. The study was not extended to other cellular populations or subsets due to the lack of specific markers/antibodies for sea bass cells.

Sea bass neutrophils can hardly be manipulated outside the host as they die quickly. To circumvent this, the internalization of AIP56 in sea bass neutrophils was studied *in vivo*, in inflamed peritoneal cavities. UV-killed *Phdp* MT1415 cells were injected intraperitoneally (ip) to attract neutrophils to the peritoneal cavity and, after 6 h, fluorescent- labelled AIP56 (AIP56-488) was ip injected in the fish. After 15 min, peritoneal cells were collected and the percentage of neutrophils and macrophages with internalized AIP56-488 analyzed by flow cytometry. Data showing that the flow cytometry protocols used only detect cells with endocytosed toxin are shown in Supplementary Figure S1. The populations of gated neutrophils and macrophages analyzed were selected based on their high side (cell complexity) and forward (cell size) scatter profiles, typical of neutrophils and macrophages. Cell sorting and positive or negative detection of intracellular peroxidase activity (20) confirmed that > 95% of the gated cells were neutrophils and > 99% were macrophages, respectively (Supplementary Figure S2). Approximately 82% of macrophages and 13% of neutrophils were positive for AIP56-488 (Figure 1, Supplementary Table 1), showing that AIP56 is internalized by the majority of macrophages, but only by a minoritarian population of neutrophils. A population of small mononucleated cells was also observed in these sea

bass inflamed peritoneal cavities, which is composed by lymphocytes and thrombocytes (21). No AIP56-488 positive cells were identified in this population (data not shown). Lymphocytes and thrombocytes cannot be distinguished by flow cytometry based on their cell complexity and size (21), therefore, to study the internalization of AIP56 by sea bass lymphocytes, cell suspensions enriched in lymphocytes were obtained from sea bass spleen or thymus by centrifugation on a Percoll gradient. Cell suspensions were then incubated with AIP56-488 for 15 min on ice followed by 15 min at 22°C to allow toxin internalization (8, 19).The percentage of AIP56-488 positive cells was then analyzed by flow cytometry using anti-sea bass IgM antibody (19) to identify splenic IgM^+ B-cells and thymic IgM^- cells [putatively thymocytes, since ~ 74.9% thymus IgM^- cells are thymocytes (22–24)]. After incubation with AIP56, only a very small percentage of AIP56-488 positive IgM^+ B-cells was detected and the Median Fluorescence Intensity (MFI) of AIP56-488 positive cells was low, indicating that most sea bass lymphoid cells appear unable to internalize the toxin.

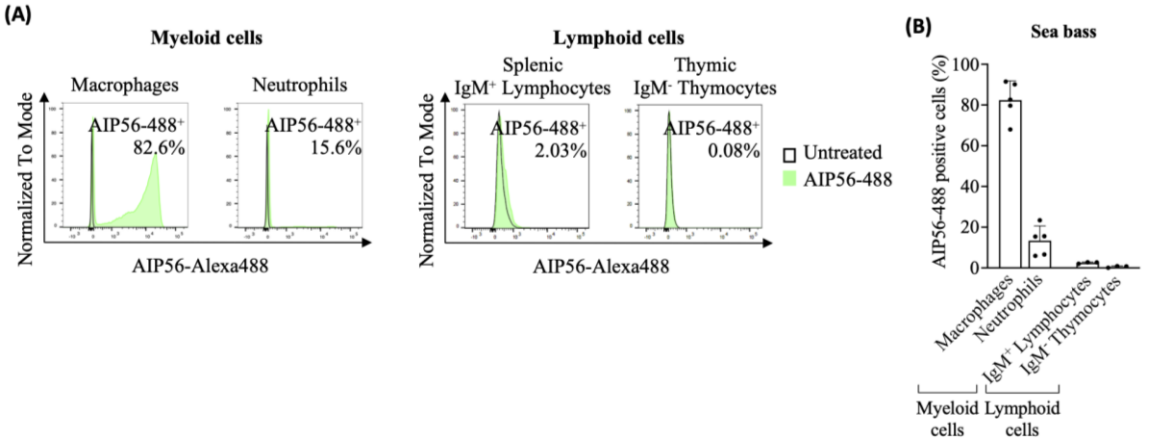

Figure 1. **Internalization of AIP56 by sea bass cells. (A)** Representative flow cytometry plots and **(B)** quantification of AIP56-488 internalization by sea bass macrophages (n=5), neutrophils (n=5) and lymphoid cells (n=3). Macrophages and neutrophils were collected from sea bass inflamed peritoneal cavity 15 min after injection of AIP56-488. Lymphoid cells obtained from sea bass spleen or thymus were left untreated or incubated with AIP56- 488 for 15 min on ice followed by 15 min at 22°C. The percentage of $AIP56\text{-}488^+$ cells was quantified by flow cytometry after gating the different cell populations (Supplementary Figure S2). Flow cytometry source data is shown in Supplementary Material Data Sheet 1.

2.2. AIP56 internalization by mouse leukocytes

Given the existence of a putative AIP56-like toxin in *Vibrio tarriae* isolated from humans (15, 16) and the potential of AIP56 and AIP56-like and -related toxins as biotechnological/biomedical tools, the study was extended to mouse and human immune cells. Mouse myeloid cells were obtained from bone marrow (BM) (macrophages, monocytes, eosinophils and neutrophils), spleen (macrophages, monocytes and dendritic cells (DCs)), peritoneum (macrophages and neutrophils) and blood (neutrophils). Spleen was also the source of lymphoid cells (B-cells and T-cells). The cells were incubated for 15 min on ice with AIP56- 488, followed by 30 min at 37°C to allow toxin internalization (8, 19). Mouse cell types were identified with established fluorescent cell markers (Supplementary Figures S3–S5) and the percentage of AIP56-488-labeled cells analyzed by flow cytometry.

The results (Figures 2A, B, Supplementary Table S2) showed that on average 73 to 98% of macrophages became positive for AIP56-488, regardless of whether they were obtained from the BM, spleen or peritoneum. More than 20% of BM and spleen monocytes as well as DCs from spleen also became positive for AIP56-488. Moreover, the MFI in AIP56-488 positive monocytes and DCs was high, and even higher in macrophages (Supplementary Table S2). Less than 4% of mouse BM eosinophils and neutrophils, and around 9% and 7% of peritoneal and blood neutrophils, and respectively, were positive for AIP56-488, although the MFI of these cells was lower than that in AIP56-488 positive monocytes, DCs and macrophages (Figures 2A, B, Supplementary Table S2).

Regarding mouse lymphocytes (Figures 2A, B, Supplementary Table S2), approximately 8% of AIP56-488 positive B-cells were detected, being the percentage of positive B1-cells (~ 34%) three times higher than the percentage of positive B2-cells (~ 11%). In turn, almost no internalization of AIP56-488 was detected in mouse T-cells, with less than 1.11% cytotoxic T-cells and helper T-cells becoming positive for the toxin. These results suggest that there is a small population of B cells that internalize AIP56. To investigate whether the internalization of AIP56 by B-cells (~ 8%) leads to NF- kB p65 cleavage, mouse B-cells were incubated with inactive AIP56- 488 and the B-cells positive for inactive AIP56-488 were sorted and subsequently incubated with wild-type AIP56 to evaluated p65 cleavage by Western Blotting (WB). However, p65 cleavage was not detected when AIP56-488 positive B-cells were incubated with AIP56 (Figure 2C). It remains to be investigated if this results from a defective translocation or refolding mechanism of AIP56 in the cytosol of these cells, or to other, so far unknown, specificities of these cells.

Considering the preference of AIP56 to intoxicate macrophages and the distinct role of macrophage subpopulations in the immune response (25–28) the susceptibility of M0 (non-

activated/resting), M1-like (classically activated/proinflammatory) and M2-like (alternatively activated/anti-inflammatory) mBMDM to AIP56 was investigated by assessing both internalization (Figures 2D, E, Supplementary Table S2) and p65 cleavage (Figure 2F). Interestingly, there appears to be a preference for the internalization of AIP56 in M0 macrophages and, especially, in M2-like, when compared to M1-like macrophages (Figures 2D, E, Supplementary Table S2). Accordingly, the cleavage of p65 was less pronounced in M1-like macrophages (Figure 2F), especially compared to M0-like macrophages.

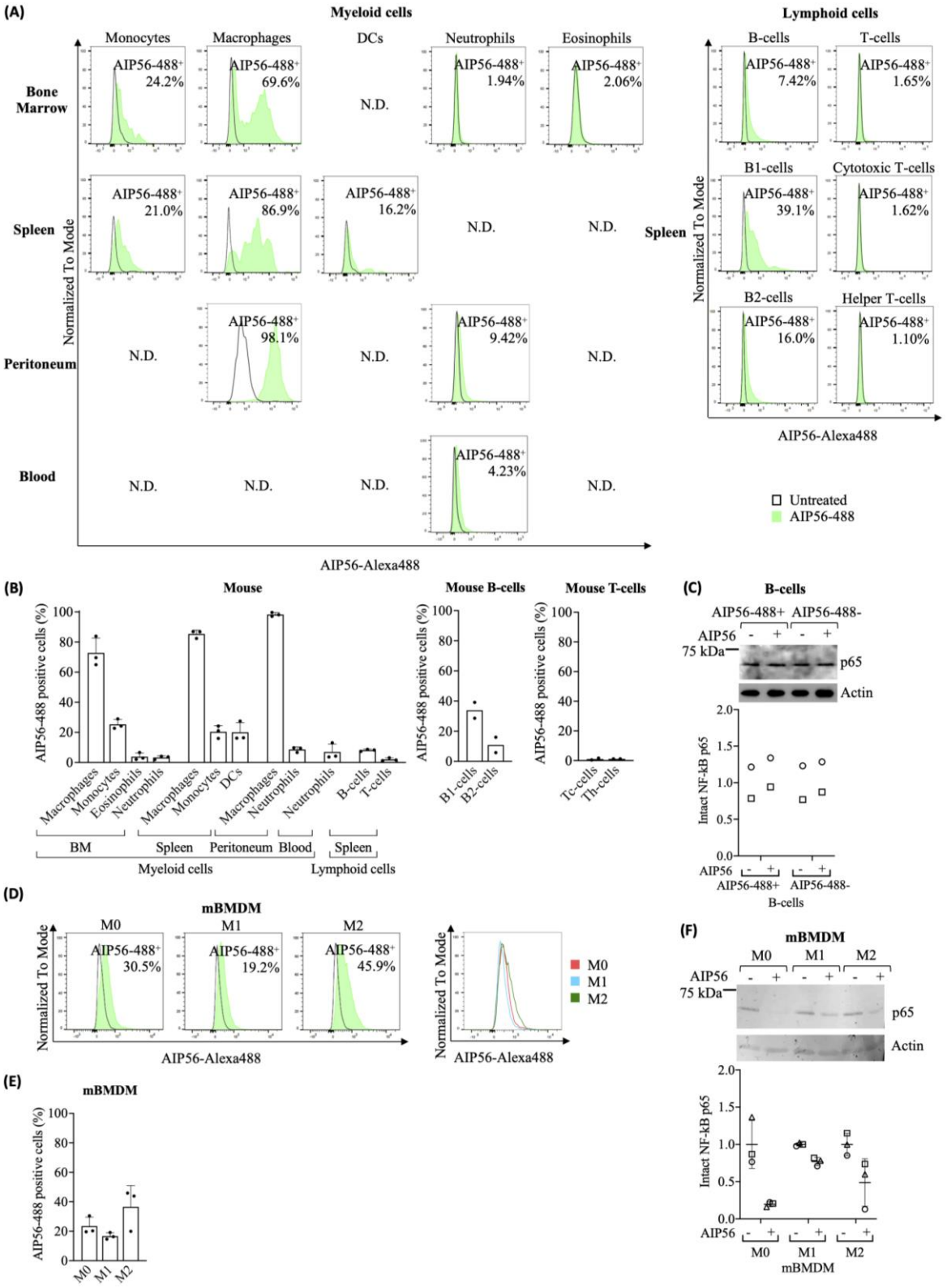

Figure 2. **Internalization of AIP56 by mouse leukocytes. (A)** Representative flow cytometry plots (N.D.: not done) and **(B)** quantification of AIP56-488 internalization by mouse myeloid (n=3) and lymphoid cells (n=3, except B1-cells, B2-cells, cytotoxic T-cells (Tc-cells) and helper T-cells (Th-cells): n=2). B1-cells, B2-cells, Tc-cells and helper Th-cells were analyzed from spleen. **(C)** Representative WB analysis of NF-κB p65 cleavage in mouse AIP56-488^{+} and AIP56-488^{-} B-cells intoxicated with AIP56 (n=2). **(D)** Representative flow cytometry plots of AIP56 internalization by mBMDM polarized into M0, M1-like or M2-like phenotypes and comparison of

representative flow cytometry plots of AIP56-488$^+$ cells (overlay plot, right panel). **(E)** Quantification of AIP56 internalization by mBMDM polarized into M0, M1-like or M2-like phenotypes (n=3) **(F)** Representative WB analysis of NF-κB p65 cleavage in M0, M1-like or M2-like mBMDM incubated with AIP56 (n=3). For toxin internalization **(A, B, D, E)** cells were left untreated or incubated with AIP56-488 for 15 min on ice followed by 30 min at 37°C and the percentage of AIP56-488$^+$ cells quantified by flow cytometry after gating the different cell populations with specific cell markers (Supplementary Figures S3–S5). For NF-κB p65 cleavage **(C, F)**, cells were incubated with AIP56 for 15 min on ice followed by 4 h at 37°C, and subjected to WB to quantify inta NF-κB p65 bands; loading correction was achieved by dividing the density of p65 band by the density of actin band from the same sample; results are presented as fold-change relative to the untreated control. Different symbols represent independent experiments. Flow cytometry and WB source data is shown in Supplementary Material Data Sheet 1.

2.3. AIP56 internalization by human leukocytes

Human monocytes and B and T lymphocytes were isolated from human buffy coats. Monocytes were directly used or differentiated to M0, M1-like or M2-like macrophages, or monocyte-derived dendritic cells (moDCs). Human neutrophils were obtained from peripheral blood. The percentages of AIP56- 488-labeled cells were analyzed essentially as described for mouse cells, but using human cell markers for cell type identification (Supplementary Figures S6, S7).

The results of the internalization assay covering myeloid cells showed that on average over 92% of monocytes, M0, M1-like and M2-like macrophages, became positive for AIP56-488, and more than 72% of moDCs internalized the toxin (Figures 3A, B, Supplementary Table S3). Although the percentages of AIP56-488 positive cells did not differ among the different macrophage phenotypes, the MFI was higher in M0 and M2 macrophages, suggesting that these cell subtypes internalize the toxin with higher efficiency. However, no differences in the AIP56-induced cleavage of p65 among human macrophages subtypes were detected. Cleavage of NF-κB p65 was also detected in monocytes and moDCs incubated with AIP56 (Figure 3C). Finally, contrary to what was observed in mice, a large percentage of human neutrophils (~ 61%) internalized AIP56-488 (Figures 3A, B, Supplementary Table S3).

Regarding human lymphocytes (Figures 3A, B, Supplementary Table S3), a similar result to that obtained for mouse lymphocytes was observed, with ~ 7% of B-cells positive for AIP56-488 and almost no AIP56-488 positive T-cells (~ 1%). Nevertheless, the MFI of AIP56-488 positive B- and T-cells was very low, indicating low internalization of the toxin in these cells.

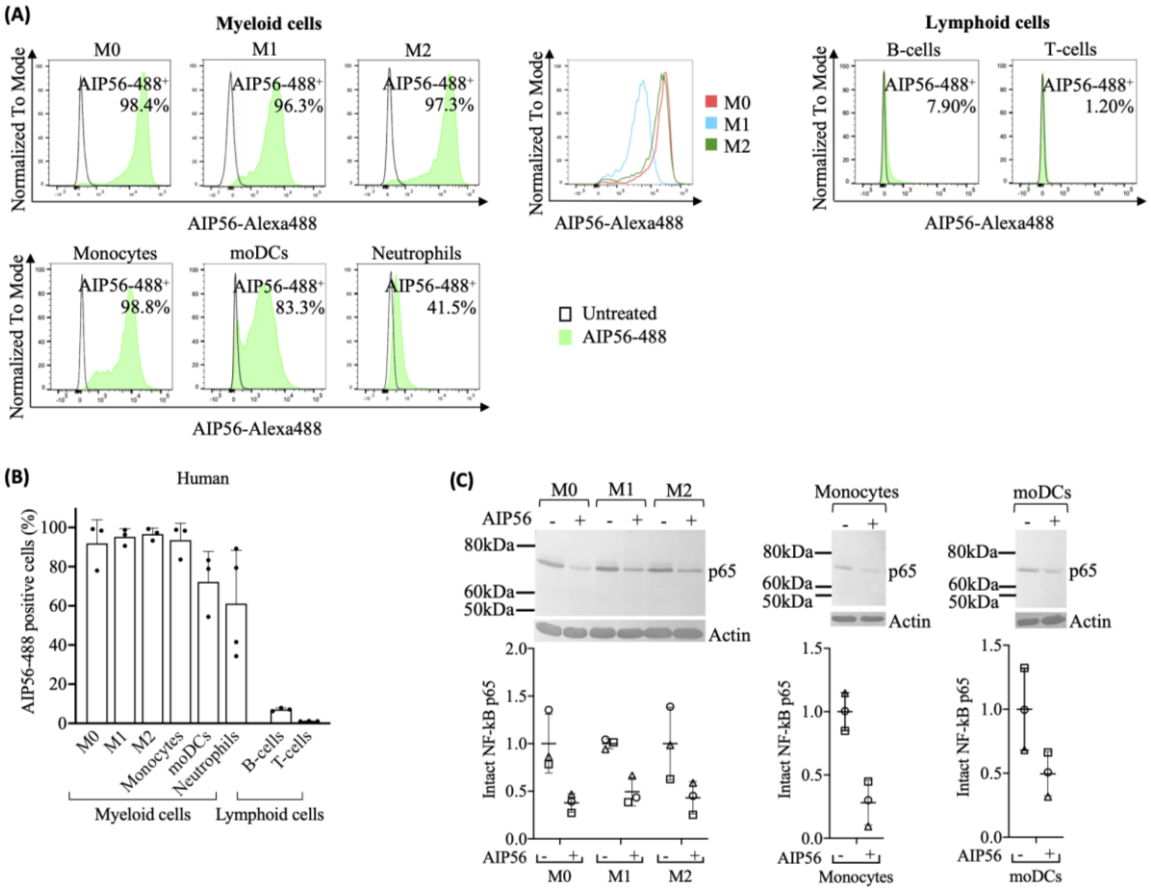

Figure 3. **Internalization of AIP56 by human leukocytes. (A)** Representative flow cytometry plots of AIP56-488 internalization by human myeloid and lymphoid cells and comparison of representative flow cytometry plots of AIP56-488$^+$ cells from human monocyte derived macrophages M0 (red), M1-like (blue), M2-like (green). **(B)** Quantification of AIP56-488 internalization by human myeloid (n=3 except neutrophils, for which n=4) and lymphoid cells (n=3). For assessing internalization, leukocytes were left untreated or incubated with AIP56-488 for 15 min on ice followed by 30 min at 37°C and the percentage of AIP56-488$^+$ cells quantified by flow cytometry after gating the different cell populations with specific cell markers (Supplementary Figures S6, S7). **(C)** Representative WB analysis of NF-κB p65 cleavage in human M0, M1-like or M2-like macrophages, monocytes and moDCs incubated with AIP56 for 15 min on ice followed by 6 h (macrophages) or 4 h (monocytes and moDCs) at 37°C and quantification of intact NF-κB p65 bands (n=3). Loading correction was achieved by dividing the density of p65 band by the density of actin band from the same sample. Results are presented as fold-change relative to the untreated control. Different symbols represent independent experiments. Flow cytometry and WB source data is shown in Supplementary Material Data Sheet 1.

3. Discussion

Sea bass is one of the main fish species targeted by *Phdp* virulent strains and has been widely used experimentally to study the virulence factors and mechanisms behind the disease caused by this pathogen. Pathogenic strains of *Phdp* secrete AIP56 in large quantities, which plays a crucial role in the virulence and pathological hallmarks observed during the disease (4–7). Among these, the elimination of macrophages and neutrophils by

post-apoptotic secondary necrosis stands out, disarming the host's innate immune response against the pathogen and contributing to the occurrence of extensive tissue destruction (4, 7). However, while the direct intoxication of macrophages by AIP56 has been well documented (6, 8, 19), it remained to be investigated if it directly affects neutrophils and other immune cells.

In this work, it was shown that sea bass macrophages internalize AIP56 with high efficiency, corroborating their elimination by the toxin in infected animals (4, 7). In contrast, despite the extensive neutrophil apoptosis observed during *Phdp* infection (7) or AIP56 intoxication (4, 7), only a small subset of neutrophils became positive for AIP56 after incubation with the toxin, indicating that most of the observed neutrophil destruction during *Phdp* infection may not result from the direct toxicity of AIP56. Instead, it may be a consequence of cell death pathways that occur during the participation of neutrophils in the inflammatory response (29, 30) triggered by *Phdp* or its components. In the absence of live macrophages to clear dying neutrophils, they lyse and release highly cytotoxic molecules that likely contribute to the extensive necrotic lesions typically found in *Phdp* infected fish (4, 7). The availability of monoclonal antibodies against sea bass IgM (31) also allowed to evaluate the internalization of AIP56 in lymphoid cells. The fact that only a very low percentage of B-cells became positive for AIP56, with relatively low MFI, and almost no AIP56-488 positive IgM^- thymocytes were observed, suggests that sea bass lymphocytes lack or have low levels of the receptor(s) for the toxin, supporting why no significant alterations in these cell types have been reported during *Phdp* infection or AIP56 intoxication.

Altogether, these data show that, in sea bass, AIP56 targets myeloid cells, having greater tropism for macrophages. The myeloid lineage is an essential component of the innate immune response, playing a key role in the initial response against infections (32, 33). Furthermore, myeloid cells bridge innate and adaptive immunity through antigen processing and presentation, mainly by dendritic cells and macrophages, thus triggering the adaptive immune response (32, 33). Thus, by disabling key cells of the myeloid lineage, AIP56 evades both arms of the immune response, facilitating bacterial proliferation and subsequent septicemia and death of the host (7, 34).

As observed in sea bass, the results also indicate that AIP56 has specificity for human and mouse myeloid cells, preferably macrophages. In mice, there appears to be a greater tropism for peritoneal macrophages (AIP56-positive cells), accompanied by greater toxin content (MFI), compared to those in the spleen and BM. Peritoneal macrophages have been described as the most mature, followed by splenic and then BM macrophages (35). In the present study, peritoneal macrophages were obtained 6 h after proinflammatory stimulation.

In this condition, it has been described that resident peritoneal macrophages are in an active/mature state and a small population of peritoneal macrophages derive from recruited circulating monocytes that, in later stages of the inflammation, eliminate resident macrophages and acquire mature resident identity (36–38). Thus, the preference of AIP56 may depend on the maturation/activation status of macrophages, which likely correlates with differential expression of AIP56 receptor(s). Furthermore, it may also correlate with the monocytic origin of some of the peritoneal macrophages present after the proinflammatory stimuli. Indeed, in humans, it was observed that AIP56 has high affinity not only for macrophages but also for dendritic cells, which have been both derived from circulating monocytes.

Regarding the affinity of AIP56 for classically categorized macrophage subpopulations (39), there appears to be a preference to M0- (resting) and M2-like (anti-inflammatory) over M1-like (pro-inflammatory) macrophages. This is mostly supported by results in mice, where a lower percentage of AIP56-positive cells and weaker p65 cleavage was observed in M1-like macrophages. On the other hand, in humans, only a greater internalization efficiency (higher MFI) was observed in M0- and M2-like macrophage subsets. Considering that the macrophage subsets were derived *ex vivo* from different cellular compartments, it is not possible to discern whether the observed differences are species specific or actually result from their distinct origin. Although the existence of subpopulations equivalent to mammalian M1- and M2-like macrophages has been described in fish (40), the lack of specific antibodies to distinguish these subpopulations did not allow to investigate their susceptibility to AIP56 and the consequences for infection.

In mice, in agreement to what was observed in sea bass, only a low percentage of neutrophils (<10%) internalized AIP56 regardless of their source (BM, blood and peritoneum). When compared to neutrophils isolated from BM, higher internalization appears to occur in blood neutrophils and peritoneal neutrophils recruited after inflammatory stimulation, which suggests greater expression of the AIP56 receptor(s) in activated neutrophils (41). In contrast to what was observed in mice, a much higher percentage of human blood neutrophils (61%) internalized AIP56. This indicates species-specific differences in the expression of the AIP56 receptor(s), which agrees with the documented differences between human and mice neutrophils, including a distinct receptor repertoire (30). Finally, some mouse and human B lymphocytes (7-8%) internalized AIP56. Interestingly, the results obtained in mice show that the toxin has greater affinity for B1 lymphocytes, which express transcription factors and surface markers that confers them myeloid characteristics (42, 43). In fact, while B2 lymphocytes originate from the bone marrow, mature in the blood and secondary lymphatic organs, and play an essential role in

the adaptive immune response by producing memory cells and high- affinity antibodies (44, 45), B1 lymphocytes originate from fetal liver progenitors, have self-renewal capacity, and play a role in the innate immune response, including phagocytic and antigen presentation capabilities (42, 44, 46). However, AIP56 internalization in B-cells did not result in detectable NF-κB p65 cleavage, suggesting that AIP56 may not be fully functional in these cells or that additional factors are required for its activity.

Overall, it can be concluded that the efficient internalization of AIP56 by sea bass, mouse and human macrophages and subsequent cleavage of NF-κB p65 points to the evolutionary conservation of its receptor(s) and mechanism of action across species. This finding is relevant as it raises the possibility that AIP56-like and -related toxins may also play a role in pathogenesis, with particular interest in the context of the AIP56-like toxin identified in human-associated *Vibrio* strains (15, 16). Furthermore, the here reported cell specificity of AIP56 is relevant when considering the potential biotechnological/biomedical use of these toxins, either to inactivate NF-κB in situations where this transcription factor plays an important role or to deliver therapeutic proteins or antigens into the cytosol of myeloid cells.

4. Materials and Methods

4.1. Production and fluorescence labeling of recombinant proteins

Full-length His-tagged AIP56 (AIP56) and His-tagged AIP56 metalloprotease mutant (AIP56^{AAIVAA}), corresponding to a full- length inactive version of the toxin were expressed and purified as previously described (6). Briefly, the sequence encoding AIP56 from the MT1415 strain was cloned in pET28a(+) in frame with a C- terminal His-tag and expressed in *E. coli* BL21 (DE3) cells at 17°C. The mutant was generated by site directed mutagenesis using QuickChange Site-Directed Mutagenesis Kit (Stratagene) following manufacturer's instructions. Induced bacterial cells were lysed by sonication, centrifuged, and the recombinant AIP56 was purified from the supernatant using nickel-affinity chromatography (Ni-NTA agarose, ABT) followed by size exclusion chromatography (Superose 12 10/300 GL, GE Healthcare). Inactive AIP56 was purified from inclusion bodies by metal affinity chromatography under denaturing conditions, refolded and subjected to size exclusion chromatography. Purified protein batches were analyzed by SDS-PAGE and purities, determined by densitometry of Coomassie blue-stained gels, were ≥ 90% (Supplementary Figure S8). Recombinant AIP56 or inactive AIP56 labelled with Alexa Fluor 488 were prepared using the Molecular Probes® Alexa Fluor protein labelling kit (Thermo Fisher Scientific), following the manufacturer's instructions, but with higher toxin:Alexa488 ratio (57 nM:1 vial), as the recommended ratio inhibited AIP56-488 cell binding and NF-κB p65

cleavage. The activity of the used batch was confirmed by performing NF-κB p65 cleavage assay in sea bass macrophages (Supplementary Figure S1).

4.2. Determination of recombinant protein concentration

Protein concentrations were determined by spectrophotometry by measuring absorbance at 280 nm using NanoDrop 1000 (Thermo Fisher Scientific), considering the extinction coefficients and the molecular weights, calculated by the ProtParam tool (http://www.expasy.org/tools/protparam.htmL).

4.3. Fish

Sea bass (*Dicentrarchus labrax*) were purchased from commercial hatcheries, and maintained in 600 L seawater aquaria. Water temperature was maintained at 20 ± 1 °C, salinity at 23-28‰ and the photoperiod was 14 h light:10 h dark. Water quality was maintained with mechanical and biological filtration and ozone-disinfection and the fish were fed with commercial pellets (Skretting), adjusting the food intake to fish size and water temperature, according to the supplier's recommendations.

4.4. Mice

C57BL/6 mice were bred and housed at the IBMC/i3S animal facility. They were fed sterilized food and water ad libitum. Four-week-old male mice were used exclusively to derive macrophages from bone marrow. To collect spleens, femurs and tibias, mice were euthanized by CO_2 followed by cervical dislocation. To collect blood, mice were anesthetized with isoflurane and, after confirmation of the inexistence of reflexes, cardiac puncture was performed. After terminal blood collection, cervical dislocation was done.

4.5. Fish neutrophils

A suspension of UV-killed *Phdp* MT1415 virulent strain (OD 600 nm of 0.9), obtained as previously reported (47), was injected ip in sea bass (100 ml per fish) in order to induce inflammation and enrich the peritoneal leukocytes (PL) in neutrophils. After 6 h, fish were injected with 500 µL sea bass PBS (sbPBS; 50 mM phosphate buffer pH 7.2 + 184 mM NaCl) containing 10 µg/mL AIP56-488 or the same volume of sbPBS. After 15 min, PL were collected following a procedure described elsewhere (20). Cells were centrifuged (5 min, 250 × *g*, 4°C) and distributed in a 96-well plate (U-bottom). Dead cells were labeled with FVD (eFLuorTM 506 fix viability dye 1:1000 in sbPBS) for 20 min on ice in the dark, centrifuged as above and fixed with 1% paraformaldehyde (PFA) at room temperature (RT)

for 15 min. Cells were washed and filtered into FACS tubes. Live neutrophils were selected by differential gating (see section 4.14. bellow).

4.6. Fish lymphocytes

Lymphoid cells were obtained from thymus or spleen of sea bass (88.4 - 107.3 g body weight). Fish were euthanized by immersion in 0.06% (v/v) 2-fenoxyethanol, followed by exsanguination, and the organs were removed and placed in isolation medium (L-15 medium (Gibco) adjusted to 322 mOsm and supplemented with 2% fetal bovine serum (FBS, Gibco), 1% penicillin/streptomycin (P/S, Gibco) and 20 U/mL heparin (Braun)). Cell suspensions were obtained by macerating the organs through a 100 µm nylon mesh with isolation medium. Cell suspension was carefully added onto Percoll gradient (45% and 31% Percoll) and centrifuged (45 min, 400 × *g*, 4°C, without break). The leukocytes remaining at the interface were collected and washed twice with culture medium (L- 15 medium adjusted to 322 mOsm and supplemented with 10% fetal bovine serum, 1% P/S and 20 U/mL heparin). The cells were then adjusted to a density of 3×10^6 cells/mL in culture medium and plated in 96-well plate with U-bottom (100 µL/well). Lymphocytes were selected through flow cytometry by differential gating (see section 4.14. bellow).

4.7. Isolation of splenocytes, bone marrow, peritoneal and blood cells from mice

Splenocytes were obtained by macerating spleens through a 100 µm nylon mesh with complete DMEM [cDMEM: supplemented with 10% FBS, 10 mM L-glutamine, 10 mM HEPES, 1 mM sodium pyruvate and 1% P/S (all from Gibco)]. Then, in the case of splenocytes that were used for cell sorting, red blood cells (RBC) were eliminated by incubation of the cell pellet with 5 mL of RBC lysis buffer (BioLegend) for 5 min at RT. Cell suspension was washed with PBS and centrifuged (5 min, 280 × *g*, 4°C).

To collect the bone marrow, muscle from mice femurs and tibias was removed, the extremities of the bones cut and the bone marrow cavities flushed with 5 mL of ice-cold cDMEM per bone using a syringe with a 26G needle.

Recruitment of neutrophils into the peritoneal cavity was achieved by the ip injection of 2.5 mL 3% thioglycolate (48). After 6 h, mice were euthanized as described in section 4.4. and 5 mL RPMI with 5% FBS were injected in the peritoneal cavity and left for 1 min before collecting the cells by aspiration with a Pasteur pipette.

Blood was collected by cardiac puncture with a 25G needle on a 1 mL syringe coated with heparin and placed in an Eppendorf with 20 µL heparin. RBC were eliminated by incubation

of blood with 10 mL of RBC lysis buffer for 5 min at RT. Cell suspension was washed with 20 mL of PBS and centrifuged (250 × *g*, 10 min, 4°C).

Splenocytes, bone marrow, peritoneal and blood cells were centrifuged (280 × *g*, 10 min, 4°C), resuspended in cDMEM and plated at a density of 1 × 10^6 cells/well in U-bottom 96-well plates for internalization assays. Instead, the pellet of splenocytes to be sorted was resuspended in 3 mL of cDMEM.

4.8. Differentiation and polarization of mouse bone marrow derived macrophages

Mouse macrophages were derived from the bone marrow, following an established protocol (49). Bone marrow cells were obtained as previously described, but using Hanks' balanced salt solution (HBSS) (Gibco) to flush the bone marrow cavities, instead of cDMEM. Cell suspension was centrifuged (250 × *g*, 10 min, 4°C) and the resulting pellet was resuspended in cDMEM with 10% L929 cell conditioned medium (LCCM) as a source of M-CSF (50). Cells were incubated overnight on a cell culture dish at 37°C in a 7% CO_2 atmosphere to remove fibroblasts. Non-adherent cells were collected in HBSS, centrifuged, resuspended in cDMEM with 10% LCCM and plated at a density of 5 × 10^5 cells/well in a 24-well plate with 1 mL per well. After 3 days, 10% (v/v) LCCM was added to each well and, at day 7, the medium was renewed. At day 10, the medium was removed and cDMEM with cytokines was added to the wells to polarize the primary macrophages. Five µg/mL of LPS and 300 U/mL of IFNg were used to induce M1-like phenotype, 20 ng/ mL of IL-4 was added to promote M2-like differentiation, and cDMEM alone was used to achieve M0. Mouse M0, M1-like and M2-like macrophages were used after 48 h incubation at 37°C in a 7% CO_2 atmosphere.

4.9. Isolation of human monocytes and lymphocytes

Peripheral blood mononuclear cells (PBMCs) were isolated from human buffy coats from healthy blood donors. Buffy coats were diluted 1:1 in PBS and gently layered over Histopaque®-1077 (Sigma). After centrifuging (30 min, 400 × *g*, RT, without break), the whitish ring containing PBMCs was collected and washed with PBS (10 min, 250 × *g*, RT). Cells were resuspended in RBC lysis buffer, incubated for 10 min at RT to eliminate red blood cells and washed with PBS. Magnetic Activated Cell Sorting (MACS) system was used to isolate the desired leukocytes, using nano-sized magnetic beads. Basically, cell pellet was resuspended in PBS and washed in MACS buffer (PBS with 0.5% BSA and 2 mM EDTA). MACS buffer (530 µL) and CD14 beads (70 µL) (MicroBeads human 2 mL 130-050-201) were added per each 100 × 10^6 PBMCs and incubated for 20 min on ice. PBMCs were washed twice in MACS buffer and resuspended in the same buffer at a density of 100

× 10^6 cells/mL. To isolate monocytes, the suspension of PBMCs with CD14 beads was gravity run through Low-Shear (LS) columns pre- equilibrated with MACS buffer. The run-through was collected to isolate lymphocytes, as described below. The CD14 cells remaining in the column were then flushed, washed with PBS, and (i) either resuspended in RPMI 1640 (Gibco) supplemented with 10% FBS, 1% non-essential amino acids, 1 mM sodium pyruvate and 1% kanamycin (all from Gibco) and plated at a density of 0.4 × 10^6 cells/well in 96-well plate for flow cytometry or 1 × 10^6 cells/well in 24-well plate for p65 cleavage assays, or (ii) used for obtaining macrophages and DCs as described in sections 4.10 and 4.11, respectively.

Lymphocytes were isolated from the run through of the suspension of PBMCs with CD14 beads, containing CD14- negative cells. Per each 100 × 10^6 cells from this suspension, 560 µL MACS buffer and 140 µL CD19 beads (MicroBeads human 2mL 130-050-301) were added following by incubation for 20 min on ice. The suspension was then run through LS columns, the flow through collected for acquiring a population enriched in T-cells and the B-cells flushed from the column. After washing with PBS, B- and T-lymphocytes were resuspended in RPMI 1640 supplemented as referred above and plated as described for monocytes.

4.10. Polarization of human macrophages

Macrophages were generated following a procedure described elsewhere (51). Monocytes isolated as referred above, were resuspended in RPMI 1640 supplemented with 10% FBS, 1% P/S and 50 ng/mL of M-CSF (ImmunoTools, Friesoythe, Germany) and plated at a density of 0.3 × 10^6 cells/well in 24-well plates with glass coverslips. Cells were incubated for 7 days at 37°C with 5% CO_2. Medium was replaced by fresh RPMI 1640 supplemented with 10% FBS and 1% P/S. After 3 days, the medium was replaced by fresh RPMI 1640 supplemented with 10% FBS, 1% P/S to maintain M0 phenotype or with the same medium supplemented with 100 ng/mL of LPS (Sigma-Aldrich, St. Louis, MO, USA) and 25 ng/mL of IFNg (ImmunoTools, Friesoythe, Germany) to polarize into M1-like macrophages or with 20 ng/mL of IL-4 to polarize into M2-like macrophages. Cells were incubated for 24-48 h at 37°C, 5% CO_2 before use.

4.11. Generation of human dendritic cells

Dendritic cells were generated as described elsewhere (52). Isolated monocytes were resuspended in RPMI 1640 supplemented with 10% FBS, 1% non-essential amino acids, 1 mM sodium pyruvate, 1% kanamycin, 50 ng/mL IL-4 and 50 ng/mL GM-CSF, plated at a density of 3 × 10^6 cells/well in 6-well plates and incubated for 4 days at 37°C with 5% CO_2.

Half of the medium was removed and replaced by fresh RPMI 1640 supplemented as above, but containing 150 ng/mL IL-4 and 150 ng/mL GM-CSF. After 7 days, the medium was discarded and cells were harvested with PBS by pipetting the cultured cells out of the 6-well plate into a tube. Cells were centrifuged (10 min, 250 × *g*, RT), resuspended in RPMI supplemented with 10% FBS, 1% non-essential amino acids, 1 mM sodium pyruvate and 1% kanamycin and plated at a density of 0.4 × 10^6 cells/well in 96-well plate (U-bottom) for flow cytometry or 0.5–1× 10^6 cells/well in 24-well plate for p65 cleavage assays.

4.12. Human neutrophils

Human leukocytes were isolated from whole peripheral blood of healthy volunteers collected into EDTA-collection tubes and slowly agitated. Each subject signed a written informed consent before blood collection. To eliminate erythrocytes, 10 mL of pre-warmed (37°C) RBC lysis buffer were added per each 500 µL of blood, followed by immediate vortexing and incubation for 10 min at RT. After washing (350 × *g*, 5 min, RT) twice with PBS, the cell pellet was resuspended in the same volume of RPMI 1640 supplemented with 10% FBS as the volume of blood used initially, and 100 µL-aliquots were distributed in wells of a 96-well plate (U-bottom). Neutrophils were identified through flow cytometry by differential gating (see section 4.14. bellow).

4.13. AIP56-488 internalization assays

To assess AIP56 internalization, sea bass lymphocytes, mouse and human leukocytes were incubated for 15 min on ice with 89 nM AIP56-488 in the respective medium (see above). For sorting of AIP56-488^+ B-cells, the same procedure was followed in mouse splenocytes, but using the fluorescent-labelled inactive AIP56. Cells were centrifuged (3 min, 250 × *g*, 4°C), the supernatant discarded and the pellet resuspended in the same medium without toxin and incubated for 15 min at 22°C (sea bass lymphocytes) or 30 min at 37°C (human and mouse cells) to allow toxin internalization (Supplementary Figure S1). Cells were washed twice with sbPBS (sea bass lymphocytes) or commercial PBS (Gibco) (mouse and human cells). Mouse cells were incubated with FVD (1:1000 in commercial PBS) for 20 min on ice in the dark to label dead cells, centrifuged (3 min, 250 g, 4°C) and the supernatant discarded. Sea bass lymphocytes were labeled with the anti-IgM monoclonal antibody WDI3 (31) (1:50 in sbPBS, 1 h on ice) followed by a Cyanine 5 (Cy5) fluorescent goat anti-mouse IgG secondary antibody (1:200 in sbPBS, 20 min on ice in the dark), both in sea bass FACS buffer (sbPBS + 2% FBS). Human and mouse cells were labelled with fluorescent antibodies (Table 1) diluted in FACS buffer (PBS + 2% FBS) for 20 min on ice in the dark in a final volume of 50 mL except for splenocytes to be sorted as AIP56-488^+ B-cells, which were incubated in a final volume of 2 mL because the cell density was higher. Cells were

washed with its respective FACS buffer, fixed with 1% PFA for 15 min at RT and washed again with FACS buffer. In the case of mBMDM, cells were incubated for 10 min at RT with permeabilization buffer (0.1% saponin in FACS buffer), centrifuged and incubated for 30 min at 4°C with antibody anti-mouse CD206-APC in permeabilization buffer. Cells were resuspended in its corresponding FACS buffer and filtered through a 35 µm nylon mesh cell strainer into flow cytometry tubes. Propidium iodide (PI; 5 µg/mL; PercP-Cy5.5) was added exclusively to sea bass lymphocytes to access cell viability (instead of FVD). Fluorescence was analyzed by flow cytometry. Both inactive AIP56- 488^{+} and inactive AIP56-488^{-} B-cells from mouse splenocytes were isolated into 15 mL tubes through the BD FACSARIA™ II cell sorter, centrifuged (10 min, 250 × *g*, 4°C), resuspended in 400 µL of cDMEM without FBS and distributed into 2 wells of 96-well plates (U-bottom) at a density of ≈ 1 × 10^{6} cells/well to perform NF-κB p65 cleavage assay.

Table 1. **Antibodies used for flow cytometry.**

Cells	Antibodies	Dye	Clone	Company/Ref
Sea bass lymphocytes	Mouse IgG1 anti-sea bass IgM	Unlabeled	n/a	(31)
	Goat anti-mouse IgG	Cy5	n/a	Jackson ImmunoResearch/AB_2338714
Mouse leukocytes	Rat anti-mouse CD45	PercP-Cy5.5	I3/2.3	BioLegend/147706
	Rat anti-mouse/human CD11b	PE	M1/70	BioLegend/101208
	Rat anti-mouse F4/80	APC-Cy7	BM8	BioLegend/123118
	Armenian hamster anti-mouse CD11c	Pacific Blue	N418	BioLegend/117321
	Rat anti-mouse CD19	APC	6D5	BioLegend/115511
	Rat anti-mouse CD5	PE-Cy7	53-7.3	BioLegend/100621
	Rat anti-mouse CD3	APC-Cy7	17A2	BioLegend/100221
	Rat anti-mouse CD4	PE	GK1.5	BioLegend/100407
	Rat anti-mouse CD8	Pacific Blue	53-6.7	BioLegend/100728
	Rat anti-mouse Ly6G	Pacific Blue	1A8	BioLegend/127612
	Rat anti-mouse Siglec-F	A647	E50-2440	BD Biosciences/562680
	Rat anti-mouse CD86	PE	GL1	eBiosciences/12-0862-82
	Rat anti-mouse CD38	FITC	90	BioLegend/102705
	Rat anti-mouse CD206	APC	C068C2	BioLegend/141707
Human leukocytes	Mouse anti-human CD14	PE-Cy7	61D3	eBiosciences/25-0149-42
	Mouse anti-human CD19	PE-Cy7	HIB19	Invitrogen/25-0199-42
	Mouse anti-human CD3	PercP-Cy5.5	OKT3	eBiosciences/45-0037-42

	Mouse anti-human CD11c	PE-Cy7	3.9	eBiosciences/25-0116-42
	Mouse anti-human HLA-DR	APC	LN3	eBiosciences/17-9956-42
	Mouse anti-human CD40	PE	HI40a	Immunotools/21270404
	Mouse anti-human CD86	APC	BU63	BioLegend/374207
	Mouse anti-human CD163	BV421	GHI/61	BioLegend/333611
	Mouse anti-human CD206	PE	15-2	BioLegend/321105

4.14. Flow cytometry

Flow cytometry data were acquired on a BD FACSCanto™ II (BD Biosciences, San Jose, CA). Ten thousand events per sample for sea bass and human cells and twenty thousand events per sample for mouse cells were analyzed at medium flow rate. All data were analyzed using FlowJo™ software v10.6.1 (San Diego, CA).

4.14.1. Sea bass:

Sea bass peritoneal granulocytes and lymphoid cells from spleen and thymus (Supplementary Figure S2) were first selected by differential gating based on their side scatter area (SSC-A; cell complexity) and forward scatter area (FSC-A; cell size) profile, followed by forward scatter high (FSC-H) and FSC-A profile for elimination of duplets. As neutrophils are the major cell population in sea bass peritoneal cells 6 h after injection of UV-killed MT1415 (20, 53), the granulocytes selected based on high SSC-A and FSC-A were assumed as neutrophils and macrophages were identified as intermediate SSC-A and high FSC-A. Then, the viable neutrophils or macrophages were identified as FVD^- cells. To confirm the identity of sea bass neutrophils and macrophages, the selected populations were sorted separately (BD FACSARIA™ II cell sorter) into 1.5 mL tubes at a density of approximately 2×10^5 cells/tube. Sorted cells were used to perform cytospins, which were then stained for peroxidase using the Antonow technique that specifically labels neutrophils (20, 54), followed by heamacolor (Supplementary Figure S2). Regarding lymphoid cells, viable B- cells were selected from splenic lymphocytes by the specific IgM marker WDI3 ($WDI3^+$ cells) (23, 31) combined with a Cy5 fluorescent goat anti-mouse IgG secondary antibody and PI (PI^- cells) gating. $WDI3^-$ and PI^- thymic lymphoid cells were considered viable putative thymocytes, since around 74.9% of the thymic IgM^- cells are thymocytes (22–24).

4.14.2. Mouse:

Mouse leukocytes were first selected through SSC-A vs FSC-A and FSC-H vs FSC-A, followed by selection of viable mature leukocytes for the specific leukocyte marker CD45 ($CD45^+$ positive cells) and viable dye FVD^- negative cells. Then, in mouse bone marrow samples (Supplementary Figure S3), neutrophils were identified as $CD11b^+$ and $Ly6G^+$ cells and eosinophils as $CD11b^+$ and $Siglec\text{-}F^+$ cells. Within $CD11b^+$ and $Ly6G^-$ cells, macrophages were identified as $F4/80^+$ and $CD11b^{high}$, and monocytes as $F4/80^+$ and $CD11b^{intermediate}$. In mouse spleen samples (Supplementary Figure S3), B-cells were identified as $CD19^+$ lymphocytes with B1- cells identified as $CD5^+$, whereas B2-cells were assumed as $CD5^-$. The $CD19^-$ population was used to select $SSC\text{-}A^-$ and $F4/80^+$ cells for identification of spleen macrophages ($F4/80^+$; $CD11b^{high}$) and monocytes ($F4/80^+$; $CD11b^{intermediate}$). $CD11b^+/F4/80^+/CD11c^+$ cells were categorized as DCs. After selecting the viable spleen leukocytes, T-cells ($CD3^+$) were also identified and then, helper T- cells ($CD4^+$ and $CD8^-$) and cytotoxic T-cells ($CD8^+$ and $CD4^-$) were selected. In mouse peritoneal and blood samples (Supplementary Figure S3), neutrophils were identified as $CD11b^+$ and $Ly6G^+$ cells and macrophages were also identified in peritoneal cells as $F4/80^+$ and $CD11b^{high}$.

The mBMDM M0, M1-like and M2-like phenotypes were confirmed by analyzing the expression of specific cell markers through flow cytometry (Supplementary Figure S4). mBMDM were first selected through SSC-A vs FSC-A and singlets were identified through FSC-H vs FSC-A plot. Then, CD86, CD38 and CD206 were analyzed. Mouse M1-like macrophages were confirmed by a higher expression of CD86 and CD38 than M0 and M2-like, whereas M2-like phenotype was confirmed by a higher expression of CD206 than in M0 and M1-like cells.

BD FACSARIA™ II cell sorter (BD Biosciences, San Jose, CA) was used to identify and isolate mouse $AIP56\text{-}488^+$ and $AIP56\text{-}488^-$ B-cells (Supplementary Figure S5). First, mouse leukocytes were selected by differential gating based on SSC-A vs FSC-A and duplets were eliminated though FSC-H vs FSC-A plot. B-cells were identified as $CD19^+$. Then, $AIP56\text{-}488^+$ and $AIP56\text{-}488^-$ B-cells were isolated. Around 2 million events of $AIP56\text{-}488^+$ B-cells and 4 million events of $AIP56\text{-}488^-$ B-cells were sorted.

4.14.3. Human:

Regarding human monocyte derived macrophages (Supplementary Figure S6), after assessing the viable subset of cells based on their SSC-A vs FSC-A profile and eliminating the duplets (FSC-H vs FSC-A), macrophages were identified as $CD40^+$ and $CD86^+$, with

higher expression of these markers in M1-like followed by M2-like and M0. CD163 was very low in M0 and M2- like and absent in M1-like. Besides that, M2-like phenotype was confirmed through the higher expression of CD206 than M0 and M1-like, because of M2-like polarization with IL-4. The phenotype of the other human myeloid and lymphoid cells used was confirmed as follows (Supplementary Figure S7): neutrophils from peripheral blood were selected based on the SSC-A^{high} vs FSC-A^{high} profile after eliminating duplets (FSC-H vs FSC-A), considering that 95% of the total pool of circulating granulocyte are neutrophils (55, 56); monocytes were $CD14^+$; moDCs were HLA-DR^+ and $CD11c^+$; B- cells were identified as $CD19^+$ and T-cells as $CD3^+$.

4.15. NF-κB cleavage assay

Human cells (macrophages, monocytes, moDCs and lymphocytes), mBMDM (M0, M1-like and M2-like) and mouse AIP56-488^+ B-cells or AIP56-488^- B-cells were left untreated or incubated for 15 min on ice with 179 nM of AIP56, followed by a 4 h (human monocytes, moDCs and lymphocytes and mouse cells) or 6 h (macrophages) incubation at 37°C in 5% CO_2. Cells were washed and lysed in SDS-PAGE loading buffer (50 mM Tris-HCl pH 8.8, 2% SDS, 0.05% bromophenol blue, 10% glycerol, 2 mM EDTA and 100 mM DTT). Samples were heated at 95°C for 5 min, subjected to 10% SDS-PAGE using Laemmli discontinuous buffer system (57) and transferred into nitrocellulose membranes (GE Healthcare Life science, Buckinghamshire, UK). Staining with Ponceau S was used to verify loading and transfer efficiency. Membranes were then blocked with 5% (w/v) skimmed powder milk in TBS-T (tris- buffered saline, 0.1% Tween) for 1 h at RT followed by incubation with an anti-NF-κB p65 rabbit antibody (sc-372, Santa Cruz Biotechnology) diluted 1:3000 in blocking solution. After 3 washes of 5 min with TBS-T, membranes were incubated for 1 h with alkaline phosphatase conjugated secondary anti-rabbit antibody (A9919, Sigma Aldrich) (human cells and mBMDM) or HRP conjugated secondary anti-rabbit antibody (AP311, the Binding Site) (mouse AIP56-488^+ B-cells), both secondary antibodies were diluted 1:10000 in blocking solution. After 3 washes, immunoreactive bands were detected using nitroblue tetrazolium–5-bromo-4-chloro-3-indolylphosphate (NBT/BCIP) (Promega, Madison, WI, USA), for human cells and mBMDM, or with ECL Dura (34075, Thermo Scientific™) for mouse AIP56-488^+ B-cells.

4.16. Statistical analysis

Data were analyzed through one-way analysis of variance. Since the results were expressed as percentages, the arcsine transformation was used. As homogeneity of variances was not observed, the Kruskal-Wallis non-parametric test was used. Although there were statistically significant results across groups (conditions), when the pairwise

Bonferroni correction was applied for multiple comparisons, it did not yield significant results in a vast majority of the comparisons. This can be explained by the low number of individuals per condition (n=3). Since the figures by themselves are quite explanatory, we decided not to present the statistical results bearing in mind the limitation just mentioned.

5. Supplementary Data

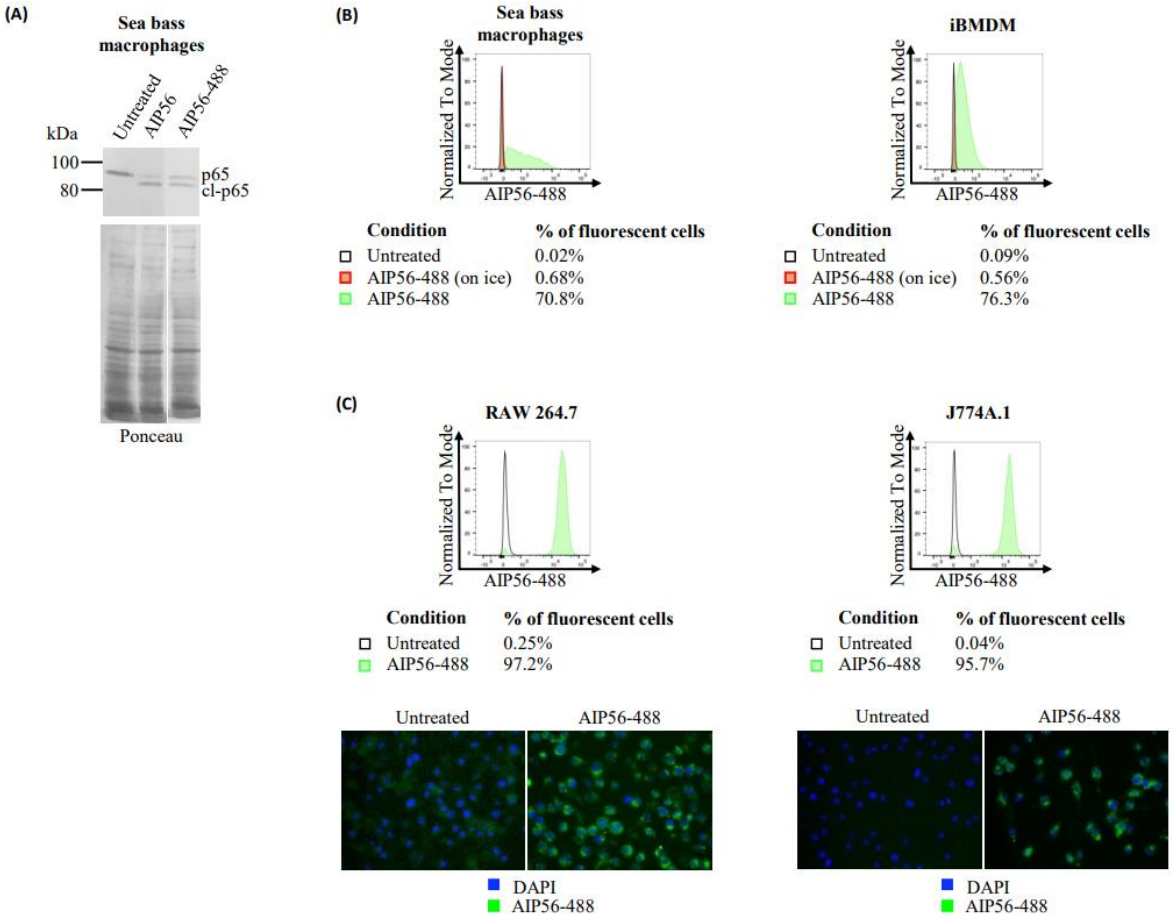

Figure S1. **AIP56-488 is successfully internalized by the cells. (A)** Representative WB analysis of NF-κB p65 cleavage in sea bass macrophages left untreated or incubated with AIP56 or AIP56-488 for 15 min on ice followed by 4 h at 22°C. NF-κB p65 was cleaved by both toxins. **(B)** Sea bass macrophages and immortalized bone marrow derived macrophages (iBMDM) were incubated with AIP56-488 on ice, washed, and either kept on ice to inhibit endocytosis (see e.g., Weigel and Oka 1981 Journal of Biological Chemistry 256:2615-2617. https://doi.org/10.1016/S0021-9258(19)69656- 0 and Szewczyk-Roszczenko et al 2023 Cells 12:2312. https://doi.org/10.3390/cells12182312), or transferred to 22ºC for 15 min or to 37ºC for 30 min, for sea bass or mammalian cells, respectively. When analyzed by flow cytometry, AIP56-488-positive cells were only detected in sea bass or mammalian cells incubated at 22ºC or 37ºC, respectively. This confirms that the flow cytometry protocol used only detects cells with endocytosed toxin, in agreement with microscopy results reported in Pereira et al 2014 (Infect Immun 82:5270–5285. doi: 10.1128/IAI.02623-14), showing that in cells incubated with AIP56-488, fluorescence can only be detected after internalization and concentration of AIP56-488 in the endocytic compartment. **(C)** Representative flow cytometry plots and correspondent fluorescence microscopy images of AIP56-488 internalization by mouse RAW 264.7 and J774A.1 cell lines. Cells were left untreated or incubated

with AIP56-488 for 15 min on ice followed by 30 min at 37°C. AIP56-488-positive cells were detected by flow cytometry or fluorescence microscopy after staining the nuclei with DAPI (blue).

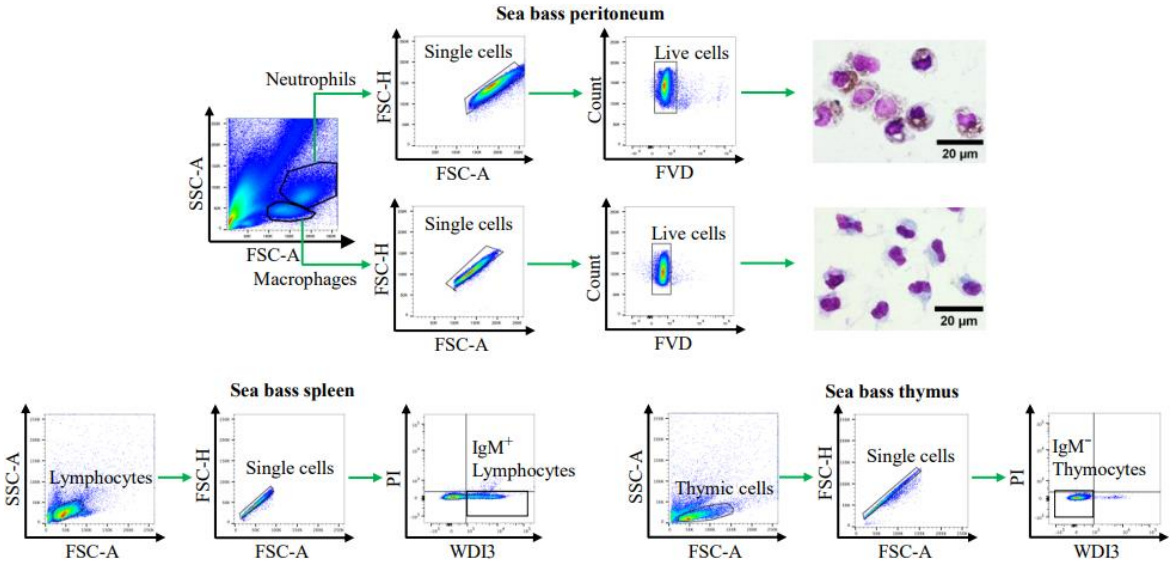

Figure S2. Gating strategy applied to identify sea bass neutrophils and macrophages from peritoneum and IgM+ lymphocytes (B-cells) and IgM- cells (putative thymocytes) from sea bass spleen and thymus samples, respectively, after Percoll gradient. Neutrophils were assessed based on their morphology (FSC-A vs SSC-A) considering that the analyzed samples were from inflamed peritoneal cavities after 6 h injection of UV-killed MT1415, where neutrophils are the majority of the granulocytes. Macrophages from the same cavities were also assessed based on FSC-A vs SSC-A and analyzed as control. After selecting viable neutrophils and macrophages, cells were sorted and cytospins were performed to confirm the identity of the selected cells. Hemacolor technique was performed and Antonow was used for peroxidase detection to stain neutrophils (brown), allowing to distinguish between these two cell types. Lymphoid cells were selected based on their morphology (SSC-A vs FSC-A) and IgM expression. Fixable viability dye (FVD) and propidium iodide (PI) were used to identify viable neutrophils/macrophages and lymphoid cells, respectively.

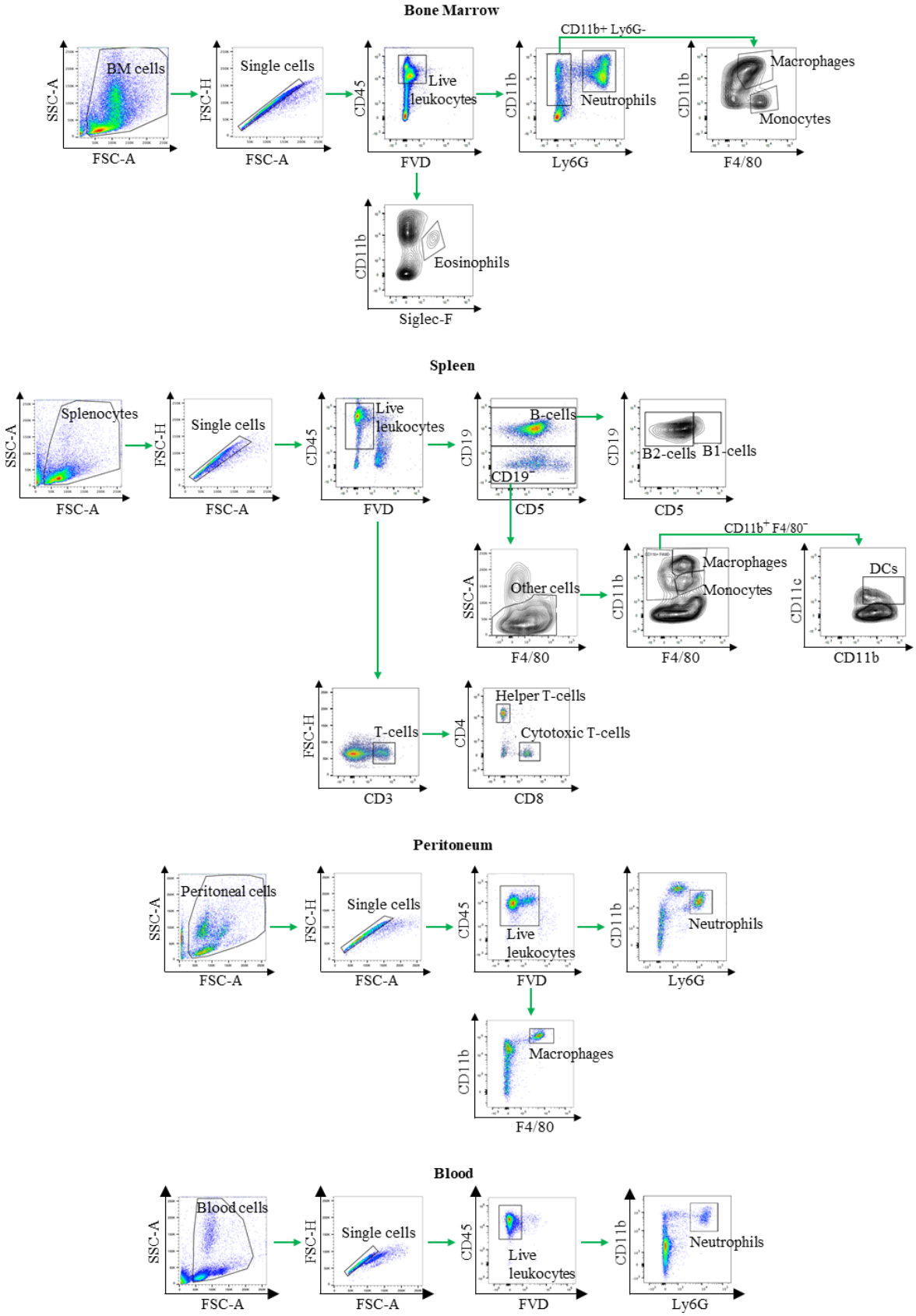

Figure S3. Gating strategy applied to identify different mouse leukocytes from bone marrow (BM), spleen, peritoneum (inflamed with thioglycolate for 6 h) and blood samples, after identifying general cell population by morphological parameters (SSC-A vs FSC-A) and eliminating duplets (FSC-H vs FSC-A).

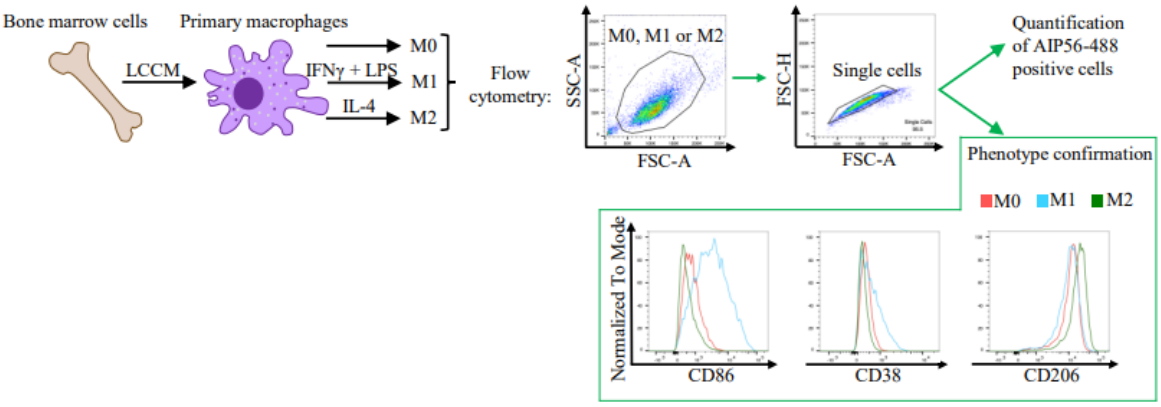

Figure S4. Schematic description of mBMDM differentiation and polarization. Representative plots of the gating strategy applied to confirm M0, M1-like and M2-like phenotype, after identifying general cell population by morphological parameters (SSC-A vs FSC-A) and eliminating duplets (FSC-H vs FSC-A), based on their expression of CD86, CD38 and CD206, respectively.

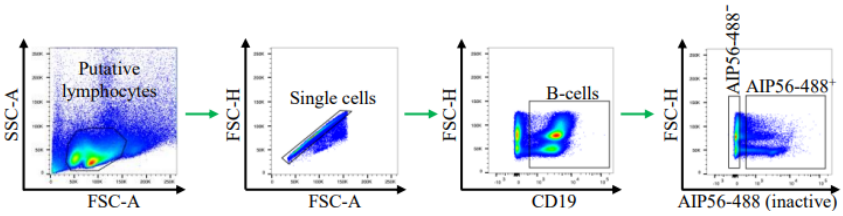

Figure S5. Gating strategy applied to isolate mouse AIP56-488+ and AIP56-488^{-} B-cells from spleen, after identifying general cell population by morphological parameters (SSC-A vs FSC-A), eliminating duplets (FSC-H vs FSC-A) and selecting B-cells (CD19+).

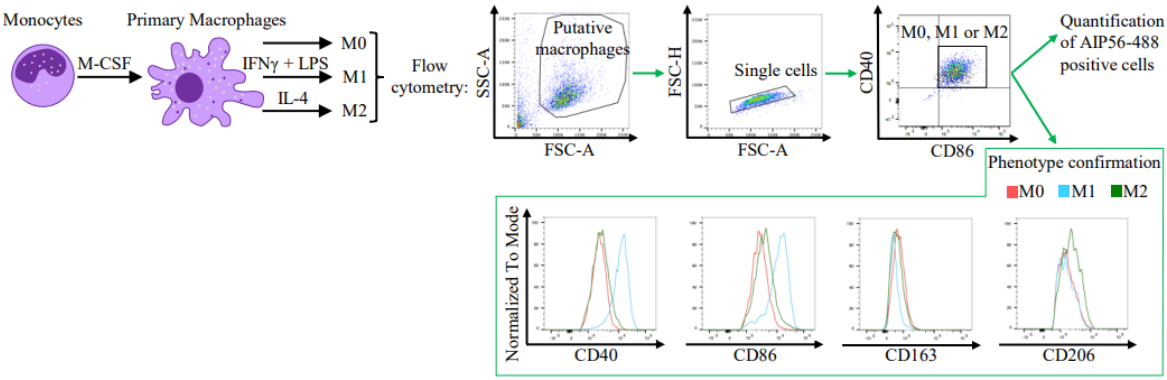

Figure S6. Schematic description of human monocytes differentiation into macrophages and their polarization. Representative plots of gating strategy applied to identify human macrophages, after selecting the general cell population through morphological parameters (SSC-A vs FSC-A) and eliminating duplets (FSC-H vs FSC-A). Macrophages subtypes (M0, M1-like and M2-like) were confirmed based on their expression of CD40, CD86, CD163 and CD206, respectively.

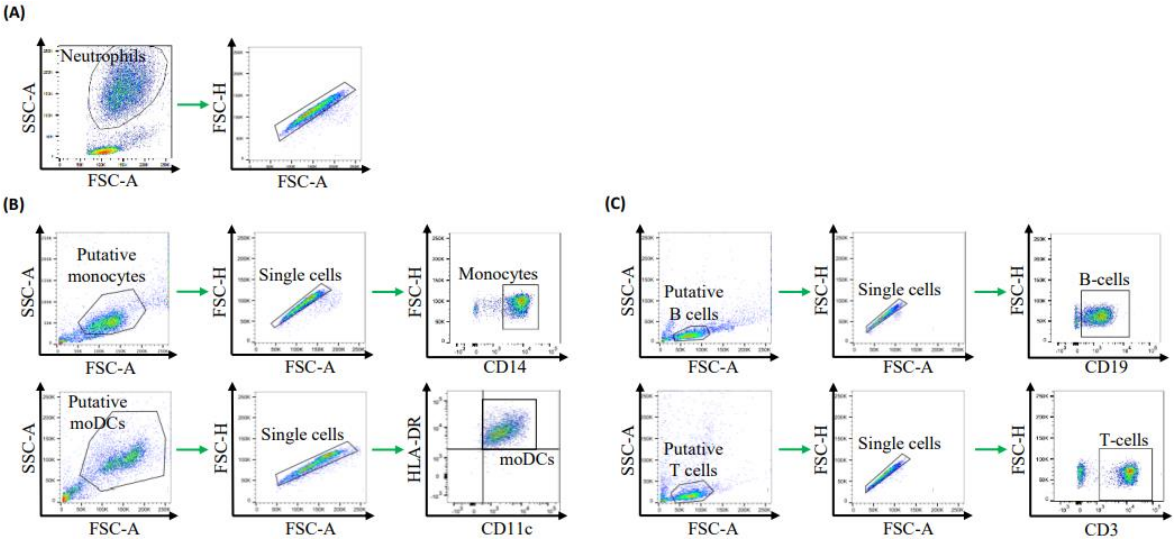

Figure S7. **Gating strategy applied to identify different and viable human leukocytes. (A)** Neutrophils were analyzed from whole peripheral blood, where neutrophils are the majority of the granulocytes. Neutrophils were gated based on morphological parameters (SSC-A vs FSC-A) and then, duplets were eliminated (FSC-H vs FSC-A). **(B)** Monocytes were isolated from buffy coats by MACS system, using CD14 beads and moDCs were derived from these cells. **(C)** The portion of cells that were negatively selected by CD14 beads were divided in B-cells and T-cells also by MACS system, using CD19 beads. **(B, C)** Gating strategy to identify the obtained monocytes, moDCs, B-cells and T-cells after selecting the general cell population through morphological parameters (SSC-A vs FSC-A) and eliminating duplets (FSC-H vs FSC-A).

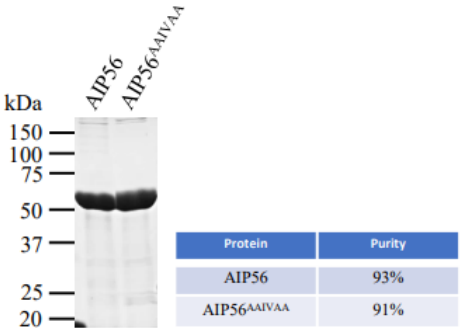

Protein	Purity
AIP56	93%
AIP56^{AAIVAA}	91%

Figure S8. SDS-PAGE analysis of purified recombinant proteins used in this study. Each lane was loaded with 10 µg of the indicated recombinant protein and the gel was stained with Coomassie Blue. Purity of the proteins was determined by densitometry using Image Lab software (Bio-Rad).

Table S1. **AIP56-488 internalization by sea bass leukocytes.**

Sea bass cell populations			% of fluorescent cells		MFI[1]
Lineage	**Source**	**Cell type**	**Untreated cells**	**AIP56-488 treated cells**	**AIP56-488 treated cells**
Myeloid	Peritoneum	Macrophages	0.06 ± 0.13	82.38 ± 9.44	46.83 ± 16.66
		Neutrophils	0.01 ± 0.02	13.40 ± 7.25	2.14 ± 0.90
Lymphoid	Spleen	IgM^+ Lymphocytes	0.67 ± 0.87	2.53 ± 0.43	1.36 ± 0.09
	Thymus	IgM^- Thymocytes	0.10 ± 0.07	0.58 ± 0.44	1.29 ± 0.19

[1]MFI (Median Fluorescence Intensity) results are presented as fold-change in fluorescence intensity to the untreated cells (control). Values from each individual experiment are shown in Supplementary Material data sheet 1.

Table S2. **AIP56-488 internalization by mouse leukocytes.**

Mouse cell populations				% of fluorescent cells		MFI[1]
Lineage	**Source**	**Cell type**		**Untreated cells**	**AIP56-488 treated cells**	**AIP56-488 treated cells**
Myeloid	BM	Macrophages		0.31 ± 0.20	72.83 ± 9.86	6.47 ± 1.63
		Monocytes		0.82 ± 0.46	25.30 ± 3.29	2.12 ± 0.14
		Eosinophils		0.59 ± 0.56	3.87 ± 2.44	1.25 ± 0.12
		Neutrophils		0.18 ± 0.04	3.28 ± 1.17	1.16 ± 0.37
		mBMDM	M0	2.93 ± 0.48	23.50 ± 6.07	1.67 ± 0.23
			M1	2.08 ± 0.75	16.70 ± 2.33	2.07 ± 0.17
			M2	2.13 ± 0.69	36.60 ± 14.41	2.13 ± 0.41
	Spleen	Macrophages		0.38 ± 0.65	85.37 ± 2.57	8.86 ± 3.12
		Monocytes		1.11 ± 1.39	20.40 ± 4.13	2.24 ± 0.57
		DCs		0.00 ± 0.00	20.05 ± 6.45	3.32 ± 0.19
	Peritoneum	Macrophages		1.28 ± 0.19	98.30 ± 1.31	28.66 ± 9.41
		Neutrophils		0.28 ± 0.13	8.61 ± 1.72	0.95 ± 0.28
	Blood	Neutrophils		0.00 ± 0.01	7.00 ± 5.29	1.92 ± 0.18
Lymphoid	Spleen	B-cells		0.58 ± 0.96	8.17 ± 0.68	2.43 ± 0.88
		B1-cells		2.83 ± 3.68	33.85 ± 7.43	5.76 ± 0.64
		B2-cells		0.62 ± 0.74	10.89 ± 7.23	2.87 ± 0.41
		T-cells		0.09 ± 0.13	1.99 ± 0.99	1.19 ± 0.06
		Tc-cells		0.00 ± 0.00	1.02 ± 0.86	1.16 ± 0.09
		Th-cells		0.08 ± 0.08	1.11 ± 0.01	1.10 ± 0.02

[1]MFI (Median Fluorescence Intensity) results are presented as fold-change in fluorescence intensity to the untreated cells (control). Values from each individual experiment are shown in Supplementary Material data sheet 1.

Table S3. **AIP56-488 internalization by human leukocytes.**

Human cell populations		% of fluorescent cells		MFI[1]
Lineage	**Cell type**	**Untreated cells**	**AIP56-488 treated cells**	**AIP56-488 treated cells**
Myeloid	M0	1.18 ± 0.76	91.87 ± 12.02	20.98 ± 4.17
	M1	0.48 ± 0.32	95.19 ± 4.16	7.66 ± 4.87
	M2	1.62 ± 1.18	96.62 ± 3.03	25.15 ± 10.87
	Monocytes	0.07 ± 0.06	93.57 ± 8.64	9.59 ± 4.44
	moDCs	0.47 ± 0.25	72.20 ± 15.57	5.30 ± 2.35
	Neutrophils	3.76 ± 6.04	61.10 ± 27.25	2.83 ± 0.91
Lymphoid	B-cells	0.16 ± 0.24	7.07 ± 0.85	1.50 ± 0.59
	T-cells	0.05 ± 0.03	1.10 ± 0.10	1.15 ± 0.10

[1]MFI (Median Fluorescence Intensity) results are presented as fold-change in fluorescence intensity to the untreated cells (control). Values from each individual experiment are shown in Supplementary Material data sheet 1.

References

1. Romalde JL. *Photobacterium Damselae* subsp. *piscicida*: an integrated view of a bacterial fish pathogen. *Int Microbiol*. (2002) 5:3–9. doi: 10.1007/S10123-002-0051-6
2. Zorrilla I, Balebona MC, Moriñigo MA, Sarasquete C, Borrego JJ. Isolation and characterization of the causative agent of pasteurellosis, *Photobacterium damsela* ssp. *piscicida*, from sole, *Solea Senegalensis* (Kaup). *J Fish Dis*. (1999) 22:167–72. doi: 10.1046/J.1365-2761.1999.00157.X
3. Liu PC, Lin JIY, Lee KK. Virulence of *Photobacterium Damselae* subsp. *piscicida* in cultured cobia *Rachycentron canadum*. *J Basic Microbiol*. (2003) 43:499–507. doi: 10.1002/JOBM.200310301
4. do Vale A, Silva MT, dos Santos NMS, Nascimento DS, Reis-Rodrigues P, Costa-Ramos C, et al. AIP56, a novel plasmid-encoded virulence factor of *Photobacterium Damselae* subsp. *piscicida* with apoptogenic activity against sea bass macrophages and neutrophils. *Mol Microbiol*. (2005) 58:1025–38. doi: 10.1111/j.1365-2958.2005.04893.x
5. do Vale A, Pereira C R, Osorio C, dos Santos NMS. The Apoptogenic Toxin AIP56 Is Secreted by the Type II Secretion System of *Photobacterium Damselae* subsp. *piscicida*. *Toxins (Basel)*. (2017) 9:368. doi: 10.3390/toxins9110368
6. Silva DS, Pereira LMG, Moreira AR, Ferreira-Da-Silva F, Brito RM. The apoptogenic toxin AIP56 is a metalloprotease A-B toxin that cleaves NF-κB P65. *PloS Pathog*. (2013) 9:1003128. doi: 10.1371/journal.ppat.1003128
7. do Vale A, Costa-Ramos C, Silva A, Silva DSP, Gärtner F, dos Santos NMS, et al. Systemic macrophage and neutrophil destruction by secondary necrosis induced by a bacterial exotoxin in a Gram-negative septicaemia. *Cell Microbiol*. (2007) 9:988–1003. doi: 10.1111/J.1462-5822.2006.00846.X
8. Pereira LMG, Pinto RD, Silva DS, Moreira AR, Beitzinger C, Oliveira P, et al. Intracellular trafficking of AIP56, an NF-κB-cleaving toxin from *Photobacterium Damselae* subsp. *piscicida. Infect Immun*. (2014) 82:5270–85. doi: 10.1128/IAI.02623-14
9. Lisboa J, Pereira C, Pinto RD, Rodrigues IS, Pereira LMG, Pinheiro B, et al. Unconventional structure and mechanisms for membrane interaction and translocation of the NF-κB-targeting toxin AIP56. *Nat Commun*. (2023) 14:1–16. doi: 10.1038/s41467-023-43054-z
10. Turco MM, Sousa MC. The structure and specificity of the type III secretion system effector nleC suggest a DNA mimicry mechanism of substrate recognition. *Biochemistry*. (2014) 53:5051–198. doi: 10.1021/bi500593e
11. Baruch K, Gur-Arie L, Nadler C, Koby S, Yerushalmi G, Ben-Neriah Y, et al. Metalloprotease type III effectors that specifically cleave JNK and NF-κB. *EMBO J*.

(2011) 30:221–31. doi: 10.1038/EMBOJ.2010.297
12. Yen H, Ooka T, Iguchi A, Hayashi T, Sugimoto N, Tobe T. NleC, a type III secretion protease, compromises NF-κB activation by targeting p65/relA. *PloS Pathog*. (2010) 6:e1001231. doi: 10.1371/JOURNAL.PPAT.1001231
13. Gilmore TD, Wolenski FS. NF-κB: Where did it come from and why? *Immunol Rev*. (2012) 246:14–35. doi: 10.1111/j.1600-065X.2012.01096.x
14. Rodrigues IS, Pereira LMG, Lisboa J, Pereira C, Oliveira P, dos Santos NMS, et al. Involvement of Hsp90 and cyclophilins in intoxication by AIP56, a metalloprotease toxin from *Photobacterium Damselae* subsp. *piscicida*. *Sci Rep*. (2019) 9:1–13. doi: 10.1038/s41598-019-45240-w
15. Liang K, Islam MT, Hussain N, Winkjer NS, Im MS, Rowe LA, et al. Draft Genome Sequences of Eight *Vibrio* sp. Clinical Isolates from across the United States That Form a Basal Sister Clade to *Vibrio cholerae*. *Microbiol Resour Announc*. (2019) 8. doi: 10.1128/MRA.01473-18
16. Islam MT, Liang K, Orata FD, Im MS, Alam M, Lee CC, et al. *Vibrio tarriae* sp. nov., a novel member of the *Cholerae* clade. *Int J Syst Evol Microbiol*. (2022) 72. doi: 10.1099/IJSEM.0.005571
17. Verster KI, Cinege G, Lipinszki Z, Magyar LB, Kurucz É, Tarnopol RL, et al. Evolution of insect innate immunity through domestication of bacterial toxins. *Proc Natl Acad Sci U.S.A*. (2023) 120:e2218334120. doi: 10.1073/PNAS.2218334120/
18. Piot N, Gisou van der Goot F, Sergeeva OA. Harnessing the membrane translocation properties of AB toxins for therapeutic applications. *Toxins*. (2021) 13:36. doi: 10.3390/TOXINS13010036
19. Freitas IL, Teixeira A, Loureiro I, Lisboa J, Saraiva A, dos Santos NMS, et al. Susceptibility of Sea Bream (*Sparus aurata*) to AIP56, an AB-Type Toxin Secreted by *Photobacterium Damselae* subsp. *piscicida*. *Toxins (Basel)*. (2022) 14. doi: 10.3390/TOXINS14020119
20. do Vale A, Afonso A, Silva MT. The professional phagocytes of sea bass (*Dicentrarchus Labrax L.*): cytochemical characterisation of neutrophils and macrophages in the normal and inflamed peritoneal cavity. *Fish Shellfish Immunol*. (2002) 13:183–98. doi: 10.1006/FSIM.2001.0394
21. Esteban M Á, Muñoz J, Meseguer J. Blood cells of sea bass (*Dicentrarchus Labrax L.*). Flow cytometric and microscopic studies. *Anat Rec*. (2000) 258:80–9. doi: 10.1002/(SICI)1097-0185(20000101)258:1
22. Scapigliati G, Mazzini M, Mastrolia L, Romano N, Abelli L. Production and characterisation of a monoclonal antibody against the thymocytes of the sea bass *Dicentrarchus labrax*(L.) (*Teleostea, Percicthydae*). *Fish Shellfish Immunol*. (1995) 5:393–

405. doi: 10.1006/FSIM.1995.0039
23. dos Santos NMS, Romano N, De Sousa M, Ellis AE, Rombout JHWM. Ontogeny of B and T cells in sea bass (*Dicentrarchus labrax*, L.). *Fish Shellfish Immunol*. (2000) 10:583–96. doi: 10.1006/FSIM.2000.0273
24. Picchietti S, Buonocore F, Guerra L, Belardinelli MC, De Wolf T, Couto A, et al. Molecular and cellular characterization of European sea bass CD3e + T lymphocytes and their modulation by microalgal feed supplementation. *Cell Tissue Res*. (2021) 1:3. doi: 10.1007/s00441-020-03347-x
25. Ma RY, Black A, Qian BZ. Macrophage diversity in cancer revisited in the era of single-cell omics. *Trends Immunol*. (2022) 43:546–63. doi: 10.1016/J.IT.2022.04.008
26. Lendeckel U, Venz S, Wolke C. Macrophages: shapes and functions. *ChemTexts*. (2022) 8:12. doi: 10.1007/S40828-022-00163-4
27. Martinez FO, Gordon S. The M1 and M2 paradigm of macrophage activation: Time for reassessment. *F1000Prime Rep*. (2014) 6:1–13. doi: 10.12703/P6-13
28. Franken L, Schiwon M, Kurts C. Macrophages: Sentinels and regulators of the immune system. *Cell Microbiol*. (2016) 18:475–87. doi: 10.1111/cmi.12580
29. Singhal A, Kumar S. Neutrophil and remnant clearance in immunity and inflammation. *Immunology*. (2022) 165:22–43. doi: 10.1111/IMM.13423
30. Nauseef WM. Human neutrophils ≠ murine neutrophils: Does it matter? *Immunol Rev*. (2022) 314:442–56. doi: 10.1111/IMR.13154
31. dos Santos NMS, Taverne N, Taverne-Thiele AJ, De Sousa M, Rombout JHWM. Characterisation of monoclonal antibodies specific for sea bass (*Dicentrarchus labraxL.*) IgM indicates the existence of B cell subpopulations. *Fish Shellfish Immunol*. (1997) 7:175–91. doi: 10.1006/FSIM.1996.0073
32. Stegelmeier AA, van Vloten JP, Mould RC, Klafuric EM, Minott JA, Wootton SK, et al. Myeloid cells during viral infections and inflammation. *Viruses*. (2019) 11. doi: 10.3390/V11020168
33. McDaniel MM, Meibers HE, Pasare C. Innate control of Adaptive Immunity and Adaptive Instruction of Innate Immunity: Bi-Directional flow of information. *Curr Opin Immunol*. (2021) 73:25. doi: 10.1016/J.COI.2021.07.013
34. Pidwill GR, Gibson JF, Cole J, Renshaw SA, Foster SJ. The role of macrophages in *staphylococcus aureus* infection. *Front Immunol*. (2020) 11:620339. doi: 10.3389/FIMMU.2020.620339
35. Wang C, Yu X, Cao Q, Wang Y, Zheng G, Tan TK, et al. Characterization of murine macrophages from bone marrow, spleen and peritoneum. *BMC Immunol*. (2013) 14. doi: 10.1186/1471-2172-14-6
36. Louwe PA, Badiola Gomez L, Webster H, Perona-Wright G, Bain CC, Forbes SJ, et

al. Recruited macrophages that colonize the post-inflammatory peritoneal niche convert into functionally divergent resident cells. *Nat Commun*. (2021) 12:1–15. doi: 10.1038/s41467-021-21778-0

37. Wang J, Kubes P. A reservoir of mature cavity macrophages that can rapidly invade visceral organs to affect tissue repair. *Cell*. (2016) 165:668–78. doi: 10.1016/J.CELL.2016.03.009
38. Bou Ghosn EE, Cassado AA, Govoni GR, Fukuhara T, Yang Y, Monack DM, et al. Two physically, functionally, and developmentally distinct peritoneal macrophage subsets. *Proc Natl Acad Sci U.S.A*. (2010) 107:2568–73. doi: 10.1073/PNAS.0915000107/SUPPL_FILE/PNAS.200915000SI.PDF
39. Bassler K, Schulte-Schrepping J, Warnat-Herresthal S, Aschenbrenner AC, Schultze JL. The myeloid cell compartment-cell by cell. *Annu Rev Immunol*. (2019) 37:269–93. doi: 10.1146/ANNUREV-IMMUNOL-042718-041728/CITE/REFWORKS
40. Geert Wiegertjes F, Philip Elks M. Fish macrophages. *Principles Fish Immunology: From Cells Molecules to Host Prot*. (2022), 203–27. doi: 10.1007/978-3-030-85420-1_6
41. Tsai JM, Shoham M, Fernhoff NB, George BM, Marjon KD, McCracken MN, et al. Neutrophil and monocyte kinetics play critical roles in mouse peritoneal adhesion formation. *Blood Adv*. (2019) 3:2713. doi: 10.1182/BLOODADVANCES.2018024026
42. Popi AF, Longo-Maugeŕi IM, Mariano M. An overview of B-1 cells as antigen-presenting cells. *Front Immunol*. (2016) 7:138/BIBTEX. doi: 10.3389/FIMMU.2016.00138/BIBTEX
43. Popi AF. B-1 phagocytes: the myeloid face of B-1 cells. *Ann N Y Acad Sci*. (2015) 1362:86–97. doi: 10.1111/NYAS.12814
44. Tangye SG. To B1 or not to B1: that really is still the question! *Blood*. (2013) 121:5109–10. doi: 10.1182/BLOOD-2013-05-500074
45. Kuby. *Immunology*. *7th ed*. New York: W. H. Freeman and Company (2012) p. 81–7. doi: 10.1007/s13398-014-0173-7.2
46. Smith FL, Baumgarth N. B-1 cell responses to infections. *Curr Opin Immunol*. (2019) 57:23–31. doi: 10.1016/J.COI.2018.12.001
47. do Vale A, Marques F, Silva MT. Apoptosis of sea bass (*Dicentrarchus Labrax L.*) neutrophils and macrophages induced by experimental infection with *Photobacterium Damselae* subsp. *piscicida*. *Fish Shellfish Immunol*. (2003) 15:129–44. doi: 10.1016/S1050-4648(02)00144-4

48. Oliveira L, Silva MC, Gomes AP, Santos RF, Cardoso MS, Nóvoa A, et al. CD5L as a promising biological therapeutic for treating sepsis. *Nature Communications*. (2024) 15. doi: 10.1038/s41467-024-48360-8
49. Gomes MS, Fernandes SS, Cordeiro JV, Gomes SS, Vieira A, Appelberg R. Engagement of Toll-like receptor 2 in mouse macrophages infected with *Mycobacterium avium* induces non-oxidative and TNF-independent anti-mycobacterial activity. *Eur J Immunol*. (2008) 38:2180–9. doi: 10.1002/eji.200737954
50. Englen MD, Valdez YE, Lehnert NM, Lehnert BE. Granulocyte/macrophage colony-stimulating factor is expressed and secreted in cultures of murine L929 cells. *J Immunol Methods*. (1995) 184:281–3. doi: 10.1016/0022-1759(95)00136-X
51. Loureiro JP, Cruz MS, Cardoso AP, Oliveira MJ, Macedo MF. Human iNKT cells modulate macrophage survival and phenotype. *Biomedicines*. (2022) 10:1723. doi: 10.3390/BIOMEDICINES10071723/S1
52. Pereira CS, Pérez-Cabezas B, Ribeiro H, Maia ML, Cardoso MT, Dias AF, et al. Lipid antigen presentation by CD1b and CD1d in lysosomal storage disease patients. *Front Immunol*. (2019) 10:1264/BIBTEX. doi: 10.3389/FIMMU.2019.01264/BIBTEX
53. Ferreira IA, Peixoto D, Losada AP, Quiroga MI, do Vale A, Costas B. Early innate immune responses in European sea bass (*Dicentrarchus Labrax L.*) following *Tenacibaculum maritimum* infection. *Front Immunol*. (2023) 14:1254677/FULL. doi: 10.3389/FIMMU.2023.1254677/FULL
54. Afonso A, Lousada S, Silva J, Ellis AE, Silva MT. Neutrophil and macrophage responses to inflammation in the peritoneal cavity of rainbow trout *Oncorhynchus mykiss.* A light and electron microscopic cytochemical study. *Dis Aquat Organ*. (1998) 34:27–37. doi: 10.3354/dao034027
55. Krouse JH. Introduction to allergy. *Managing Allergic Patient*. (2008), 1–17. doi: 10.1016/B978-141603677-7.50005-4
56. Prinyakupt J, Pluempitiwiriyawej C. Segmentation of white blood cells and comparison of cell morphology by linear and naïve Bayes classifiers. *BioMed Eng Online*. (2015) 14:1–19. doi: 10.1186/S12938-015-0037-1/TABLES/8
57. Laemmli UK. Cleavage of structural proteins during the assembly of the head of bacteriophage T4. *Nature*. (1970) 227:680–5. doi: 10.1038/227680a0

CHAPTER III

LRP1 Is a Receptor for AIP56-Family Toxins

LRP1 Is a Receptor for AIP56-Family Toxins

Inês Lua Freitas[1,2,3], Johnny Lisboa[1,2], Ana do Vale[1,2], Nuno M.S. dos Santos[1,2]

[1]Fish Immunology and Vaccinology Group, IBMC - Instituto de Biologia Molecular e Celular, Universidade do Porto, Porto, Portugal

[2]Fish Immunology and Vaccinology Group, i3S - Instituto de Investigação e Inovação em Saúde, Universidade do Porto, Porto, Portugal

[3]McBiology Doctoral Program, ICBAS – Instituto de Ciências Biomédicas Abel Salazar, Universidade do Porto, Porto, Portugal

Abstract

The AB-type toxin AIP56 is a key virulence factor of *Photobacterium Damselae* subsp. *piscicida (Phdp)*, a bacterial fish pathogen that causes lethal infections in several warmwater marine fish species. The toxin is secreted into the extracellular space via the type II secretion system of *Phdp*, targets sea bass macrophages and cleaves NF-κB p65 in these cells, leading to their death via post-apoptotic secondary necrosis. AIP56 has a modular structure that includes a receptor-binding domain responsible for the binding of the toxin to a specific receptor on its target cells. Importantly, toxins homologous to AIP56 (AIP56-like toxins) and toxins containing a domain homologous to the AIP56 receptor-binding domain (AIP56-related toxins), but distinct putative catalytic and translocation domains, have been identified in diverse organisms, suggesting they may target an evolutionarily conserved receptor.

A CRISPR-Cas9 screen, conducted in collaboration with Min Dong's lab identified low-density lipoprotein receptor-related protein 1 (LRP1) as the top candidate receptor for AIP56. This study validates LRP1 as a receptor for not only AIP56 but also for AIP56-like and -related toxins. Competition assays with some of these toxins suggest that they bind the same receptor, and biolayer interferometry (BLI) analyses demonstrate specific binding to cluster 4 of LRP1. The essential role of this interaction for toxin internalization was confirmed through further competition assays where RAP inhibited AIP56 internalization in mBMDMs and the cluster 4 of sea bass LRP1 was able to inhibit AIP56 internalization and p65 cleavage in sea bass cells.

This research revealed that the amino acid residues K350 and R441 in the receptor-binding domain of AIP56 are essential for binding sea bass LRP1, while K350 and K365 are required for binding to human LRP1.

Altogether, these findings suggest that AIP56, AIP56-like and AIP56-related toxins use LRP1 as a receptor, providing mechanistic insights into their pathogenicity. Clarifying this crucial step of intoxication may allow developing toxin blockers to prevent cell intoxication by these toxins.

1. Introduction

Apoptosis Inducing Protein of 56 kDa (AIP56) is an AB-type toxin secreted by *Photobacterium Damselae* subsp. *piscicida* (*Phdp*) [1–3], a bacterium that causes high mortality rates in a diversity of wild and farmed salt water fish species [4–7]. AIP56 is known to target sea bass macrophages and to cleave NF-κB p65 in the cytosol of these cells [8,9]. The depletion of this anti-apoptotic transcription factor [10] culminates in the elimination of intoxicated cells by post-apoptotic secondary necrosis [1,3,8,11]. Although mammals are not infected by *Phdp* [1], mouse and human macrophages and other myeloid cells are susceptible to AIP56 [9,12], suggesting that AIP56 recognizes a phylogenetically conserved receptor.

The gene encoding AIP56 appears to have resulted from the fusion of 3 genes [13]: (i) a gene homologous to nleC (non LEE-encoded effector C) [14,15], encoding a metalloprotease catalytic domain that cleaves NF-κB p65 [8][7]; (ii) a gene for which no homologues are known, which encodes the middle domain, involved in transmembrane channel formation [13,16]; and (iii) a gene homologous to the gene coding for Protein D of bacteriophage APSE-2 and APSE-7 [17], encoding the receptor-binding domain (RBD) that, in addition to mediate receptor interaction, is also required for pore formation [8,13].

A growing number of toxins homologous to AIP56 (AIP56-like toxins) have been identified in diverse bacteria, including *Symbiopectobacterium*, *Arsenophonus nasoniae*, *Shewanella psychrophila* and several *Vibrio* species, the latter including a strain of *Vibrio tarriae*, a member of the Cholera clade, isolated from human blood and stool [18,19]. Most of those toxins are found in secondary endosymbiont bacteria of insects, often providing an ecologically-contingent benefit [20], or in bacteria pathogenic for aquatic organisms. Their genetic and predicted structural homology [13] suggests that they act similarly to AIP56, whether in pathogenic or symbiotic processes [20]. Likewise, the number of toxins with a domain homologous to AIP56's RBD fused to distinct putative catalytic and translocation domains (AIP56-related toxins) identified in several prokaryotes and eukaryotes is also increasing [21]. These include: (i) two toxins that have putative catalytic domains with no functional homologues, one present in monarch butterfly (*Danaus plexippus*) and winter moth (*Operophtera brumata*), and the other in two bacteria (*Enterovibrio norvegicus*, isolated from turbot larvae [22], and in *Shewanella* sp.); and (ii) a toxin present in *Drosophila bipectinata* and *D. ananassae*, that contains a catalytic domain homologous to CdtB [21,23], the later present in Cytolethal Distending Toxins (CDTs) and Typhoid toxin [32] and also encoded in the genome of some insects and APSE phages [24]. Remarkably, in the APSE-2 genome, *cdtB* is immediately upstream of *protein D* (AIP56's RBD homologue) [23].

Whether Protein D combines with CdtB to form the production of a functional toxin remains to be determined, but it has been advanced that toxins produced by APSE bacteriophages play key roles in anti-parasitoid defense conferred by aphid bacterial symbionts [25].

The identification of host cell receptors used by bacterial toxins is crucial for understanding their mechanism of action and developing targeted therapeutics. Herein, the validation of Low-density lipoprotein (LDL) receptor-related protein 1 (LRP1) as a receptor for AIP56, as well as for a set of AIP56-like and -related toxins, has been performed, highlighting the role of this receptor in toxin internalization.

LDL receptor (LDLR) family members have numerous common and different ligands and are involved in diverse functions, from receptor-mediated endocytosis and cellular trafficking to signal transduction and modulation [26–29]. The binding of such a multitude of structurally unrelated macromolecules to these receptors is also promoted by their association with co-receptors [29]. Remarkably, the LDL receptors are highly conserved across species, with primitive multicellular organisms such as *Caenorhabditis elegans* encoding in its genome several large and small LDLR family members that are almost identical to their human counterparts [27,29]. LRP1 (alpha-2-macroglobulin receptor (A2MR), apolipoprotein E receptor (APOER) or cluster of differentiation 91 (CD91)) is one of the seven core members of the LDLR family [30] (LDLR itself, very-low-density lipoprotein receptor (VLDL), LRP1, LRP1B, LRP2, LRP4 and LRP8) (Figure 1), which are closely related and structurally homologous [26,30]. LRP1 is a type 1 transmembrane protein that, after processing by furin-like proteases in the trans-Golgi compartment, comprises a mature two-chain structure [30–33]. LRP1 extracellular α-chain contains 4 clusters of complement-like repeats (C1, C2, C3 and C4, numbered from the N-terminal) responsible for ligand-binding, intercalated by epidermal growth factor (EGF)-like repeats, and tyrosine-tryptophan-threonine-aspartate (YWTD) residues [26,28,30]. LRP1 transmembrane and intracellular β-chain provides binding sites for signaling adaptor proteins and several tyrosine residues, which requires phosphorylation for LRP1-mediated signal transduction [26,28,30].

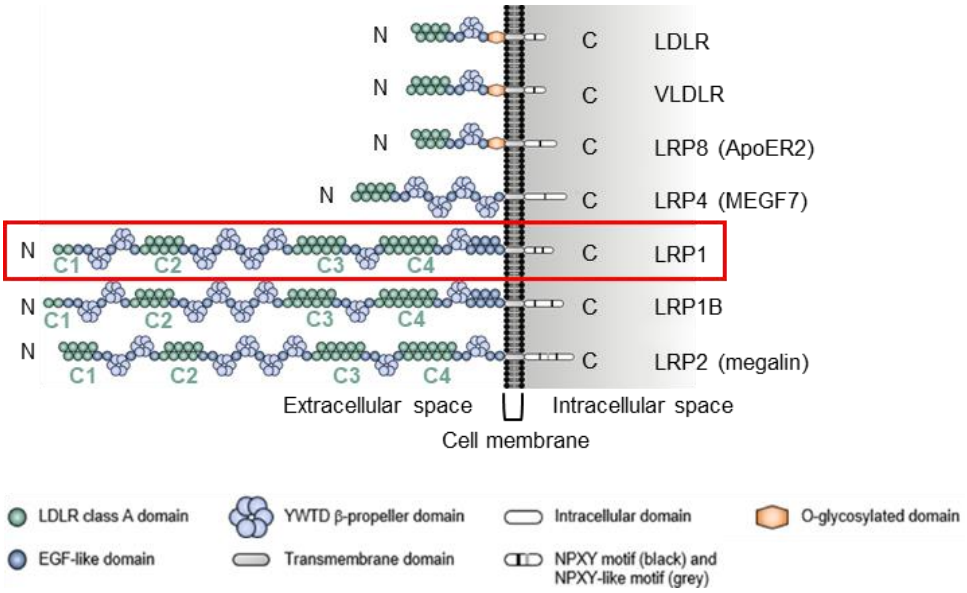

Figure 1. **Schematic representation of the domain organization of human LDLR family members.** Clusters of LDLR class A domains (complement-like repeats) are numbered from C1 to C4 in LRP1, LRP1B and LRP2. Figure adapted from [26].

In this study, the *in vivo* and *ex vivo* validation of LRP1 as a receptor for AIP56 has been performed using sea bass and sea bass cells, the main study models for AIP56. Moreover, it was investigated whether AIP56-like and -related toxins target the same receptor as AIP56. Also, it was analyzed which sea bass LRP1 isoform has (higher) affinity for AIP56 and which amino acid residues in the AIP56 receptor-binding domain are responsible for the interaction with the receptor.

2. Results

2.1. AIP56, AIP56-like and AIP56-related toxins likely share a conserved receptor

The fact that AIP56-like and -related toxins harbor a domain genetically homologous to the AIP56 receptor-binding domain (RBD), suggests that they all share an evolutionarily conserved cell surface receptor. Importantly, the structure of the putative AIP56-related toxin from *Enterovibrio norvegicus* and the putative RBD of the AIP56-related toxin from *Danaus plexippus plexippus* were recently solved, showing that these receptor-binding domains have a structure similar to that of AIP56 RBD (Box 1), further supporting that they may target the same receptor.

Box 1. The receptor-binding domain (RBD) of the AIP56-related toxins from *Enterovibrio norvegicus* and *Danaus plexippus* are structurally similar to the RBD of AIP56.

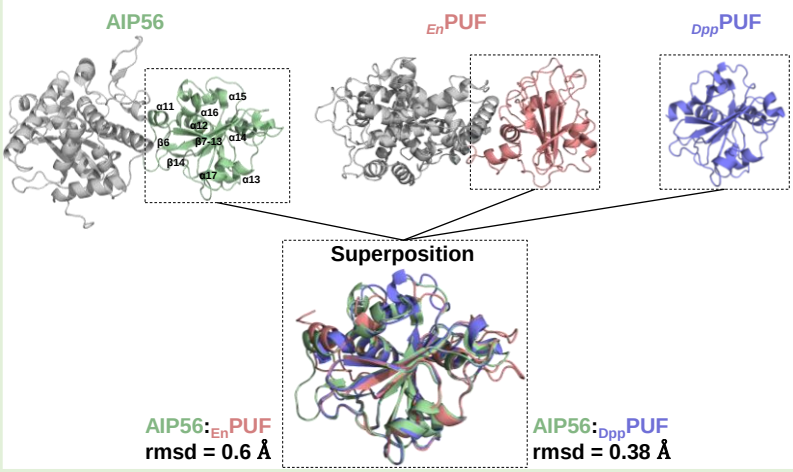

Unpublished data from Johnny Lisboa et al. (FIV group, i3S).

The structure of AIP56 was recently solved [89] as well as the structure of the RBD of two AIP56-related toxins: (i) $_{En}$PUF, *Enterovibrio norvegicus* Protein of Unknown Function and (ii) $_{Dpp}$PUF, *Danaus plexippus plexippus* Protein of Unknown Function. The superposition of the putative RBD of $_{En}$PUF and $_{Dpp}$PUF with the one of AIP56 [11], confirmed that the structure of these domains is similar, featuring a central antiparallel seven-stranded β-sheet (β7-β13) flanked by four helices on one side (α11, α12, α15 and α16) and three helices on the other (α13, α14 and α17). Additionally, two short β-strands (β6 and β14) are present, forming a small β-sheet oriented perpendicularly to the large one. Notably, the RBD of these AIP56-related toxins are characterized by an exceptionally high proportion of aromatic and hydrophobic amino acid residues, a feature also shared with AIP56.

To investigate whether these and other AIP56-related and AIP56-like toxins target the same receptor as AIP56, competition assays were first performed in sea bass peritoneal leukocytes (sbPL) using the putative RBDs of some AIP56-like toxins (from *Vibrio tarriae*: $_{Vt}$AIP56$^{S321\text{-}S518}$; *Vibrio azureus*: $_{Va}$AIP56$^{S321\text{-}R518}$; and *Arsenophonus nasoniae*: $_{An(WP919)}$AIP56$^{H295\text{-}L486}$, $_{An(WP251)}$AIP56$^{R318\text{-}I515}$ and $_{An(WP127)}$AIP56$^{I376\text{-}L579}$) and AIP56-related toxins (proteins with unknown function (PUF) from *E. norvegicus*: $_{En}$PUF$^{A513\text{-}L704}$; *D. plexippus plexippus*: $_{Dpp}$PUF$^{L244\text{-}S422}$; *Drosophila bipectinata*: $_{Db}$PUF$^{K258\text{-}S458}$; and Protein D

(ProtD) from APSE-2: $_{APSE\text{-}2}$ProtD$^{P49\text{-}S237}$ and from APSE-7: $_{APSE\text{-}7}$ProtD$^{M1\text{-}N219}$) (Figure 2). Briefly, sbPL were incubated 15 min on ice with the competitor at 400-fold molar excess relative to AIP56, followed by incubation with AIP56 at room temperature (RT) for 4 h in the presence of the competitor. AIP56 RBD (AIP56$^{T299\text{-}N497}$) was used as a positive control. Cleavage of NF-κB p65 was analyzed by western blotting and used as a read-out for intoxication. As expected, when AIP56$^{T299\text{-}N496}$ was used as competitor, AIP56-mediated cleavage of NF-κB p65 was inhibited (Figure 2A-B). Likewise, the cleavage of NF-κB p65 by AIP56 was also inhibited when the RBD of the AIP56-like toxins $_{Vt}$AIP56$^{S321\text{-}S518}$ and $_{Va}$AIP56$^{S321\text{-}R518}$ and the AIP56-related toxins $_{En}$PUF$^{A513\text{-}L704}$, $_{Dpp}$PUF$^{L244\text{-}S422}$ and $_{APSE\text{-}2}$ProtD$^{P49\text{-}S237}$ were used as competitors, supporting that these toxins share a common receptor(s). However, it should be noted that, although $_{Vt}$AIP56 competes for the same receptor of AIP56 in sbPL, it is not lethal *in vivo* for sea bass (Supplementary Figure 1). On the other hand, the putative RBD of the AIP56-like toxins $_{An(WP919)}$AIP56$^{H295\text{-}L486}$, $_{An(WP251)}$AIP56$^{R318\text{-}I515}$ and $_{An(WP127)}$AIP56$^{I376\text{-}L579}$, and the AIP56-related toxins $_{Db}$PUF$^{K258\text{-}S458}$ and $_{APSE\text{-}7}$ProtD$^{M1\text{-}N219}$ did not inhibit cleavage of p65 by AIP56, suggesting that they may have a distinct receptor or co-receptor. Alternatively, they may have evolved to recognize a receptor orthologous to that of AIP56, but have low or no affinity to the AIP56 receptor in sea bass cells.

To complement this study and understand the behavior of these toxins in sea bass, *in vivo* competitions were performed. For that, sea bass were injected with AIP56 alone or mixed with a 300-fold molar excess of the RBD of some AIP56-like and -related toxins. AIP56 mixed with a 300-fold molar excess of its own RBD (AIP56$^{T299\text{-}N497}$) or its catalytic domain (AIP56$^{N1\text{-}G256}$) were injected as positive and negative controls, respectively. In contrast to AIP56$^{T299\text{-}N497}$, which slightly inhibited AIP56-induced lethality, the RBDs of AIP56-like and -related toxins did not inhibit the mortality induced by AIP56. In fact, contrary to what was observed in the *ex vivo* competition tests in sbPL, in the presence of $_{Vt}$AIP56$^{S321\text{-}S518}$, $_{An(WP251)}$AIP56$^{R318\text{-}I515}$, $_{En}$PUF$^{A513\text{-}L704}$ and $_{Dpp}$PUF$^{L244\text{-}S422}$, sea bass mortality was higher than that caused by AIP56 alone. The reason for the discrepancy between the results obtained *ex vivo* and *in vivo* remains undetermined, but a plausible hypothesis is that these toxins may also bind to an alternative receptor or co-receptor expressed in cell types other than macrophages, losing their competitive effect in the more complex *in vivo* environment.

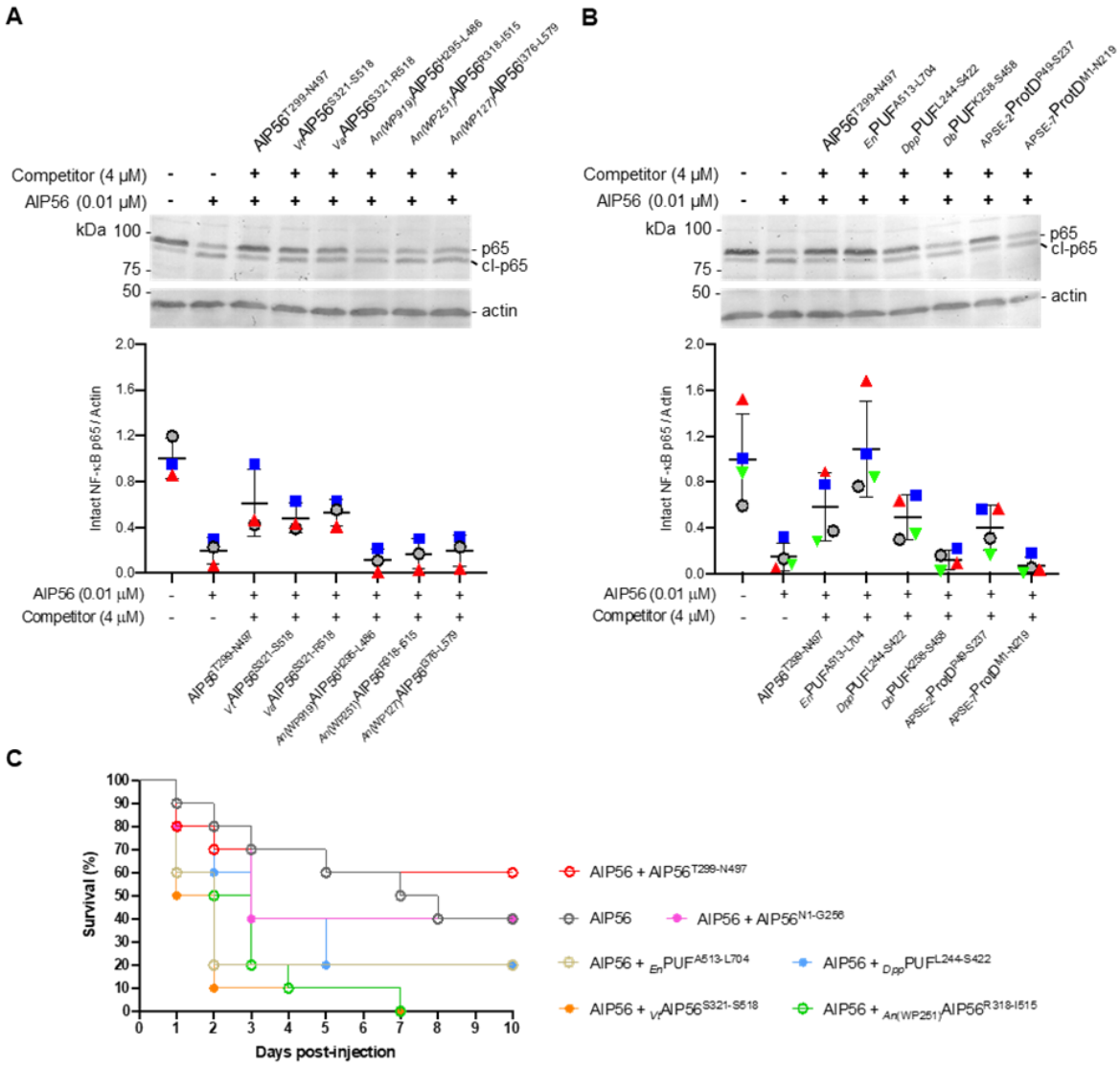

Figure 2. **The RBDs of AIP56-like and AIP56-related toxins recognize the same evolutionarily conserved receptor targeted by AIP56. (A)** Competition of the RBDs of AIP56-like toxins for AIP56 receptor. The blot shown is representative of three independent experiments (n = 3). **(B)** Competition of the RBDs of AIP56-related toxins for AIP56 receptor. The blot shown is representative of four independent experiments (n = 4). Sea bass peritoneal leukocytes (sbPL) were pre-incubated on ice for 15 min with 4 µM of RBD of AIP56-like toxins ($_{Vt}$AIP56$^{S231-S518}$, $_{Va}$AIP56$^{S321-R518}$, $_{An(WP919)}$AIP56$^{H295-L486}$, $_{An(WP251)}$AIP56$^{R318-I515}$ or $_{An(WP127)}$AIP56$^{I376-L579}$) or AIP56-related toxins ($_{En}$PUF$^{A513-L704}$, $_{Dpp}$PUF$^{L244-S422}$, $_{Db}$PUF$^{K258-S458}$, $_{APSE-2}$ProtD$^{P49-S237}$ and $_{APSE-7}$ProtD$^{M1-N219}$) and, after adding 0.01 µM AIP56, incubated for further 4 h at 22 ºC. Cleavage of NF-κB p65 was accessed by western blotting. Untreated cells or cells pre-incubated with AIP56's RBD (AIP56$^{T299-N497}$) were used as negative and positive controls, respectively. For quantification, loading correction was achieved by dividing the density of intact p65 band by the density of actin band from the same lane. Results shown in the graphs correspond to fold-changes in the normalized density of p65 band relative to the untreated control. Results from each independent experiment are represented by the same symbol/color. **(C)** Kaplan-Meyer survival curves of sea bass injected with 0.3 µg/g of body weight of AIP56 or AIP56 mixed with 300-fold molar excess of the RBD of AIP56 (AIP56$^{T299-N497}$), the catalytic domain of AIP56 (AIP56$^{N1-G256}$) or the RBD of AIP56-like ($_{Vt}$AIP56$^{S231-S518}$ and $_{An(WP251)}$AIP56$^{R318-I515}$) or of AIP56-related ($_{En}$PUF$^{A513-L704}$ and $_{Dpp}$PUF$^{L244-S422}$) toxins (10 fish/treatment).

2.2. LRP1 is involved in AIP56 internalization

Since the identification of the receptor for AIP56, AIP56-like and -related toxins was essential to better understand the cellular tropism and internalization process of these toxins as well as to study in detail the toxin-receptor interactions, a genome-wide CRISPR-Cas9 screening was performed in collaboration with Min Dong's Lab (https://donglab.hms.harvard.edu/), to retrieve AIP56 receptor candidates. This screening identified LRP1, a member of the LDLR family [30], as a putative receptor for AIP56 (Box 2).

Box 2. Genome-wide CRISPR-Cas9-mediated loss-of-function screen identified LRP1 as putative receptor for AIP56.

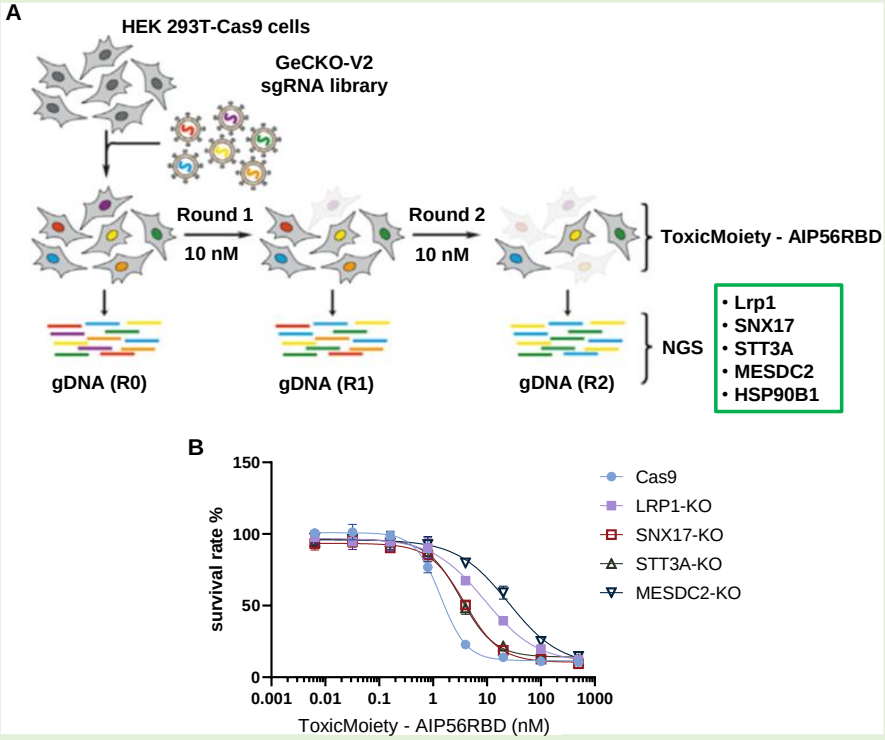

Unpublished data from Pengsheng Chen, Huan Wang and Min Dong.

(A) A cell line that stably expresses Cas9 (HEK 293T-Cas9) was transduced with lentiviral GeCKO-V2 sgRNA library. Cells were then selected by two rounds of intoxication with 10 nM of the chimera ToxicMoiety-AIP56RBD, composed of a toxic moiety fused to AIP56 receptor-binding domain (RBD). After each round, cells were harvested and single guide RNA (sgRNA) sequences were identified by next-generation sequencing (NGS). Cells not treated with ToxicMoiety-AIP56RBD served as a control (R0). Of the identified genes (boxed), LRP1 and proteins directly or indirectly related to LRP1 stood out: (i) SNX17 (Sorting Nexin 17) interacts with members of the LDLR family and modulates endocytosis of the LDLR [56]; (ii) STT3A (oligosaccharyl transferase complex catalytic subunit A), one of the catalytic subunits of the oligosaccharyltransferase (OST) complex, which functions in the endoplasmic reticulum (ER) and catalyzes the first step in N-linked glycosylation during co-translational protein modification [57]; (iii) MESDC2 (Mesoderm Development LRP Chaperone) that helps LDLR family proteins fold their beta-propeller and EGF modules correctly [58], ensuring these receptors can function properly; and (iv) HSP90B1/Grp94 (Heat Shock Protein 90 kDa Beta Member 1/Glucose-regulated protein 94), an ER chaperone whose loss is associated with increasing proprotein convertase subtilisin/kexin type 9 (PCSK9) expression, leading to the degradation of LDLRs, including LRP1 [59,60]. **(B)** Knocking out LRP1 and proteins involved in its mechanism of action reduces intoxication of 293T cells by ToxicMoiety-AIP56RBD, validating LRP1 as AIP56 receptor.

Biolayer interferometry (BLI) assays showed that AIP56 interacted with cluster 4 of human LRP1 (Hs-LRP1-C4) in a calcium-dependent manner (Box 3). Additionally, other AIP56-like and -related toxins also interacted with (Hs-LRP1-C4) (Box 3). To validate LRP1 as receptor for AIP56, additional *ex vivo* and *in vivo* studies were performed.

Box 3. AIP56, AIP56-like and AIP56-related toxins bind to LRP1 cluster 4 (LRP1-C4).

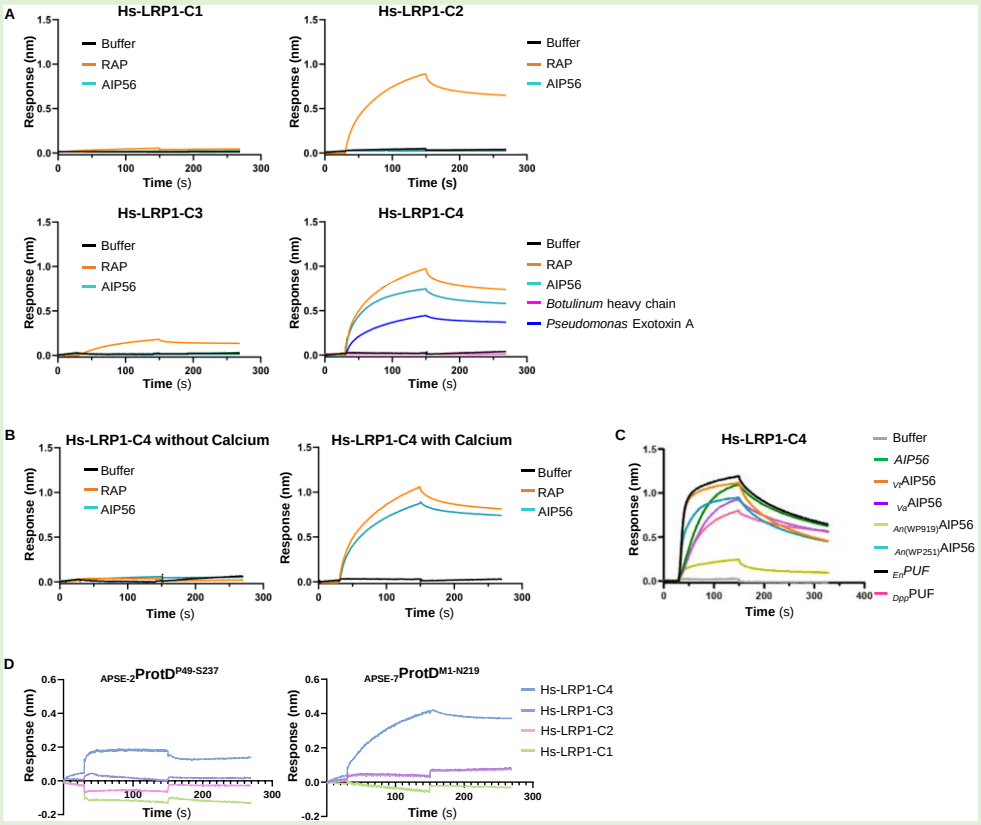

Unpublished data from Pengsheng Chen, Huan Wang and Min Dong.

Full-length LRP1 has a large size, is highly glycosylated and is rich in cysteines, being very difficult to express. Therefore, studies on LRP1 have been carried out using soluble isolated clusters [56,140]. The interaction of different toxins with human Fc-tagged LRP1 (Hs-LRP1) clusters was evaluated using biolayer interferometry (BLI) assays. **(A)** Interaction with AIP56 with the indicated clusters immobilized onto capture biosensors. Receptor-associated protein (RAP) and *Pseudomonas* exotoxin A, which binds to LRP1-C4 [56], were used as positive controls. Buffer alone and *Botulinum* heavy chain, which does not bind to LRP1, were used as negative controls. AIP56 showed robust binding to Hs-LRP1-C4, but do not bind to other LRP1 clusters. **(B)** Interaction of AIP56 with Hs-LRP1-C4 is calcium-dependent. **(C)** Interaction of AIP56-like and -related toxins with immobilized Hs-LRP1-C4. $_{Vt}$AIP56, $_{Va}$AIP56, $_{An(WP919)}$AIP56 and $_{An(WP251)}$AIP56, $_{En}$*PUF* and $_{Dpp}$*PUF* bind Hs-LRP1-C4 with different affinities, indicating that they also have LRP1 as receptor. **(D)** Interaction of immobilized $_{APSE-2}$ProtD$^{P49-S237}$ and $_{APSE-7}$ProtD$^{M1-N219}$ with the indicated human LRP1 clusters. Both proteins bind exclusively to Hs-LRP1-C4 albeit with different affinities.

It is known that RAP (Receptor-Associated Protein) binds to LDLR in the early secretory pathway to prevent premature interaction of the receptors with intracellular ligands in the endoplasmic reticulum (ER), allowing the effective delivery of the LDLR to the cell surface [34,35]. Before LDLR couple to the cell membrane, RAP dissociates from the receptors in an acidic-dependent manner [34,35]. RAP binds strongly to C2 and C4 and weakly to C3 of LRP1 through its domain 3 (RAP-D3) [36]. Due to its tight binding to LDLR members, RAP (or RAP-D3) has been widely used in biochemical and cellular assays as universal antagonist/inhibitor for ligand binding studies [31,35,37].

Thus, considering that LRP1 is phylogenetically conserved and that AIP56 is internalized both by sbPL [9,12,38] and mouse bone marrow derived macrophages (mBMDM) [9,12], the ability of human RAP (Hs-RAP) to inhibit the internalization of fluorescence-labeled AIP56 (AIP56-488) in mBMDM and sbPL was analyzed by flow cytometry (Figure 3A and B; Supplementary Table 1). AIP56$^{T299\text{-}N497}$ was used as positive control. Although pre-incubation of sbPL with Hs-RAP did not change the percentage of AIP56-488 positive cells, it led to a decrease in fluorescence intensity, indicating a lower number of AIP56-488 molecules internalized per cell. In mBMDM, the inhibitory effect of Hs-RAP was stronger, resulting in a marked reduction both in the percentage of AIP56-488 positive cells as well as in the number of AIP56-488 molecules internalized per cell. To complement these flow cytometry-based experiments, the capacity of Hs-RAP to inhibit AIP56 intoxication was also analyzed using cleavage of p65 as read-out. In agreement with the minor effect in internalization of AIP56 in sbPL detected by flow cytometry, Hs-RAP did not inhibit AIP56-dependent p65 cleavage in these cells (Figure 3C). The effect of Hs-RAP in p65 cleavage in mBMDM could not be evaluated because the higher concentration of AIP56 needed to induce p65 cleavage in these cells requires the use of competitors at a concentration that leads to their precipitation. Therefore, the ability of Hs-RAP to inhibit AIP56-mediated p65 cleavage was evaluated in human embryonic kidney (HEK) 293T cells (Box 4A), confirming that, in line to what was observed in the flow cytometry experiments with mBMDM, pre-incubation with Hs-RAP leads to decreased p65 cleavage in HEK 293T cells. Altogether, these results suggest that, despite the phylogenetic conservation of LRP1, there is species-specific affinity of RAP for LRP1. Whether this holds true for other LRP1 ligands remains to be investigated.

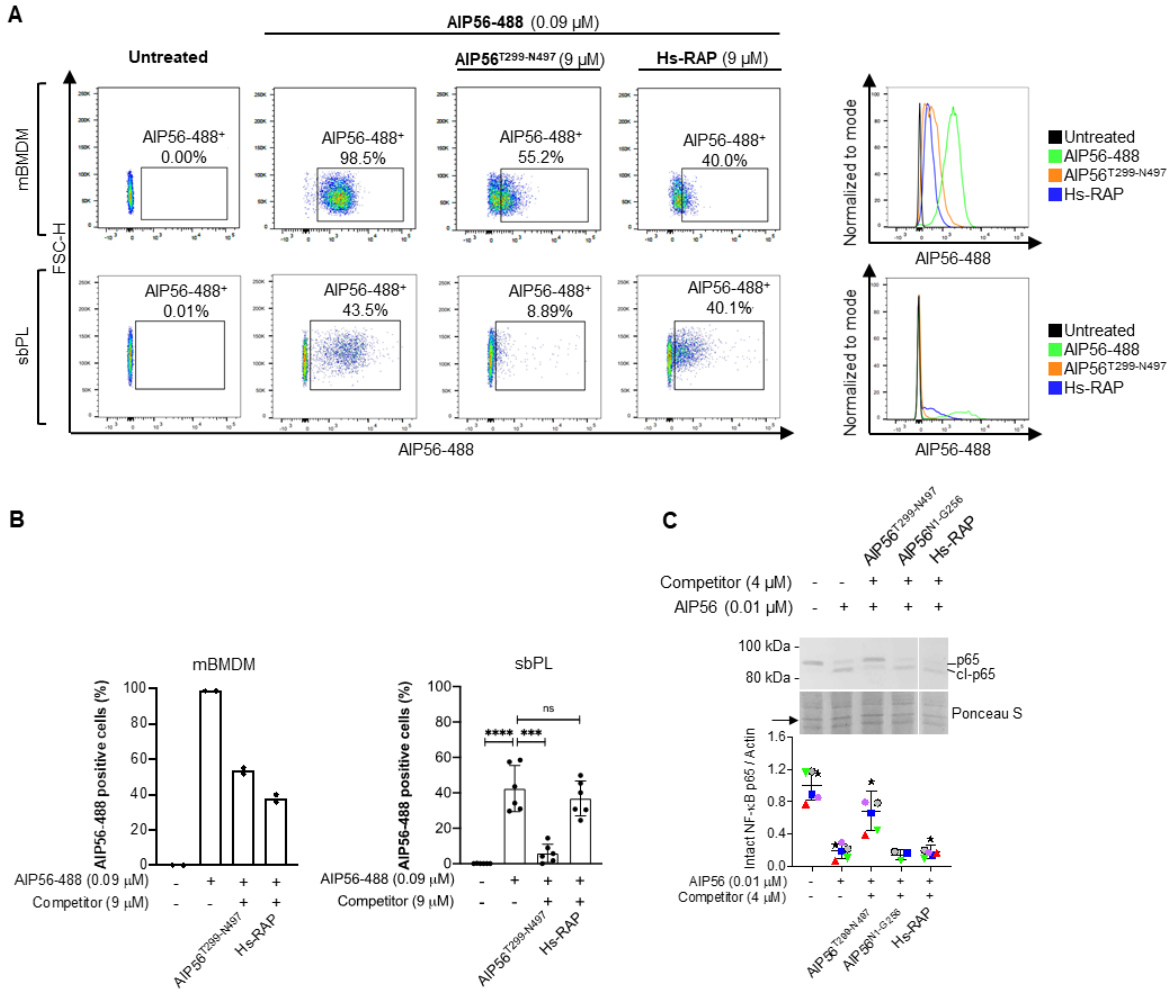

Figure 3. **Inhibitory effect of human RAP in AIP56 internalization in mBMDM and sbPL. (A)** Representative flow cytometry plots of competition assays for AIP56-488 internalization in mBMDM and sbPL showing the percentage of AIP56-488 positive cells (left panel) and the fluorescence intensity of AIP56-488 positive cells (right panel). **(B)** Quantification of mBMDM AIP56-488 positive cells (n = 2) and sbPL AIP56-488 positive cells assessed by flow cytometry as in (A). Statistical significance was tested by Brown-Forsythe one-way ANOVA. **(A, B)** SbPL and mBMDM were pre-incubated with the indicated doses of Hs-RAP for 15 min on ice. Then, AIP56-488 was added to the cells and incubated for 15 min on ice followed by other 15 min at 22 ºC (sbPL) or 30 min at 37 ºC (mBMDM). Untreated cells or cells pre-incubated with AIP56$^{T299-N497}$ were used as negative and positive controls, respectively. **(C)** Representative blot of competition assays for AIP56 intoxication in sbPL. SbPL were pre-incubated on ice for 15 min with the indicated concentrations of Hs-RAP, followed by addition of AIP56 and incubation for 4 h at 22 ºC. NF-κB p65 cleavage was analyzed by western blotting. Untreated cells and cells pre-incubated with AIP56's catalytic domain (AIP56$^{N1-G256}$) was used as negative controls and cells pre-incubated with AIP56's RBD (AIP56$^{T299-N497}$) were used as positive controls. For quantification, loading correction was achieved by dividing the density of intact p65 band by the density of Ponceau S. (band signaled by an arrow) from the same lane. Results shown in the graph correspond to fold-changes in the normalized density of p65 band relative to the untreated control. Results from each independent experiment are represented by the same symbol/color.

Additionally, the ability of Hs-RAP to inhibit death of wild type and *Lrp1* KO HEK 293T cells incubated with the ToxicMoiety-AIP56RBD chimera, was tested (Box 4B). Remarkably, Hs-RAP not only inhibited death in wild-type HEK 293T but also in HEK 293T lacking LRP1, suggesting that AIP56 may also bind to other(s) LDLR(s). Of the LDLR family, LRP1 and LRP1B are the most similar (Figure 1), raising the hypothesis that, similarly to *Pseudomonas aeruginosa* exotoxin A (ExoA) [39,40], AIP56 could use both LRP1 and LRP1B as receptors. However, preliminary experiments in which a mini LRP1B receptor containing cluster 4 (mLRP1B-C4) was overexpressed in the OVCAR-8 cell line, which does not express or expresses LRP1 and LRP1B at low levels [41], suggest that it is unlikely that LRP1B mediates AIP56 internalization into cells, as no AIP56-dependent p65 cleavage was observed in those cells (Supplementary Figure 2).

Box 4. Possible redundancy of LDLR.

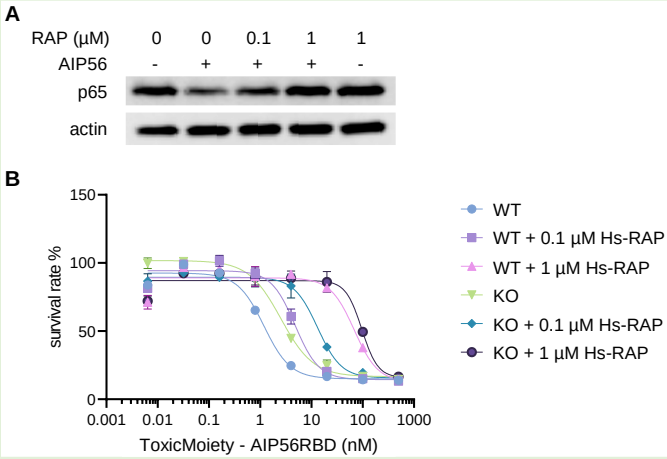

Unpublished data from Pengsheng Chen, Huan Wang and Min Dong.

(A) Hs-RAP inhibited NF-κB p65 cleavage by AIP56 in the HEK 293T cell line. **(B)** Inhibiting ToxicMoiety-AIP56RBD binding to LRP1 by Hs-RAP reduces intoxication of both wild type (WT) and *Lrp1* knockout (KO) HEK 293T cells, suggesting that AIP56 recognizes other(s) LDLR family member(s).

Since Hs-RAP only inhibited AIP56 intoxication in mammalian cells, the domain 3 of sea bass RAP (Dl-RAP-D3) was cloned, recombinantly expressed and purified, in order to test whether it would inhibit the internalization and cleavage of p65 in sbPL. Human RAP domain 3 (Hs-RAP-D3) was also produced and used as control.

As previously observed for Hs-RAP, Hs-RAP-D3 did not inhibit the internalization of AIP56-488 (Figure 4A and B) or AIP56-dependent p65 cleavage (Figure 4C) in sbPL, even when used at a dose 4-fold higher (Figure 4D and E) than the one required for inhibiting intoxication in mammalian cells (Figure 3A and B). Unexpectedly, the same result was obtained with DL-RAP-D3 (Figure 4A-E). This result cannot be attributed to alternative sea bass RAP isoforms that could be responsible for the binding to LRP1 since in the sea bass genome there is only one gene coding for a RAP-homologous protein.

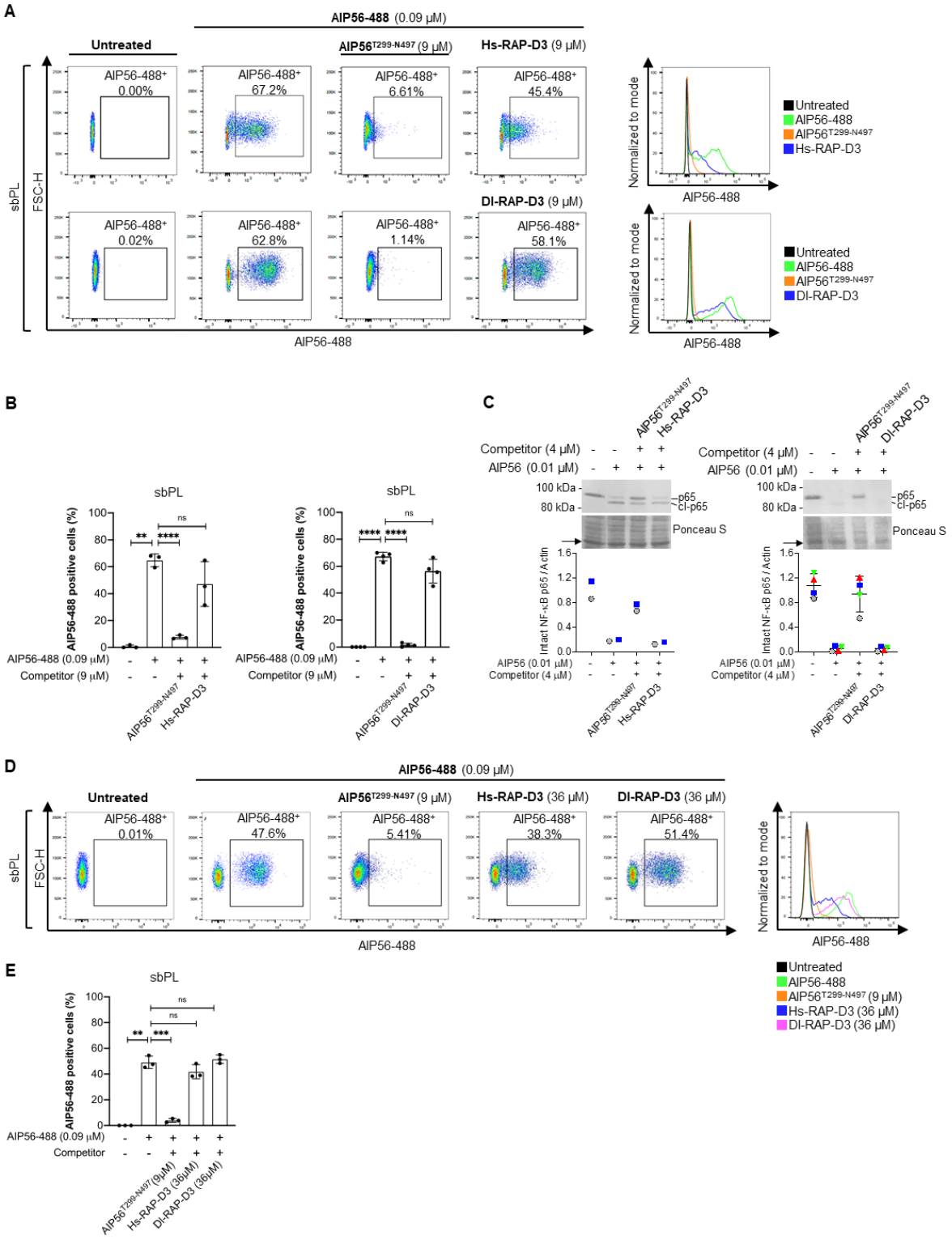

Figure 4. **Inhibitory effect of human and sea bass RAP-D3 in AIP56 internalization in sbPL. (A, D)** Representative flow cytometry plots of competition assays for AIP56-488 internalization in sbPL showing the percentage of AIP56-488 positive cells (left panel) and the fluorescence intensity of AIP56-488 positive cells (right panel). **(B, E)** Quantification of sbPL AIP56-488 positive cells (n = 3) assessed by flow cytometry as in (A, D). Statistical significance was tested by Brown-Forsythe one-way ANOVA. **(A, B, D, E)** SbPL were pre-incubated with the indicated doses of AIP56$^{T299-N497}$, Hs-RAP-D3 or Dl-RAP-D3 for 15 min on ice. Then, AIP56-488 was added and cells incubated for further 15 min on ice followed by 15 min at 22 ºC. Untreated cells or cells

pre-incubated with AIP56$^{T299-N497}$ were used as negative and positive controls, respectively. **(C)** Representative blot of competition assays for AIP56 intoxication in sbPL. SbPL were pre-incubated on ice for 15 min with the indicated dose of AIP56$^{T299-N497}$, Hs-RAP-D3 or Dl-RAP-D3. Then, AIP56 was added, followed by incubation for 4 h at 22 ºC. NF-κB p65 cleavage was analyzed by western blotting. Untreated cells or cells pre-incubated with AIP56's RBD (AIP56$^{T299-N497}$) were used as negative and positive controls, respectively. Quantification was performed as for Figure 3. Results from each independent experiment are represented by the same symbol/color.

2.3. Dl-LRP1X1-C4 has a preponderant role in AIP56 intoxication of sbPL.

Sea bass has two LRP1 isoforms: Dl-LRP1X1 and Dl-LRP1X2. Considering the phylogenetic conservation of LRP1 and the fact that AIP56 binds to C4 of Hs-LRP1, the C4 of both sea bass LRP1 isoforms (Dl-LRP1X1-C4 and Dl-LRP1X2-C4) were recombinantly produced and first used in molecular interaction studies by BLI assays. These tests showed that AIP56 interacts with C4 of both sea bass LRP1 isoforms, with slightly greater affinity for Dl-LRP1X1-C4 (Box 5).

Box 5. AIP56 binds to Dl-LRP1-C4 and Dl-LRP1X1-C4 *in vitro*.

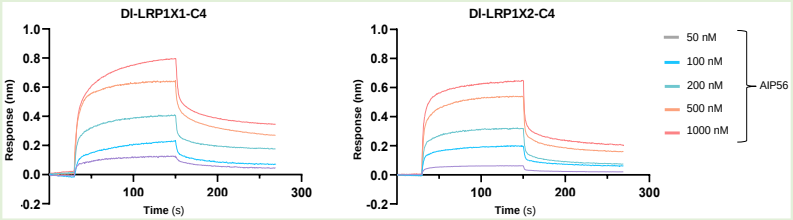

Unpublished data from Pengsheng Chen, Huan Wang and Min Dong.

The interactions of AIP56 with C4 of the two isoforms of sea bass LRP1 (Dl-LRP1X1-C4 and Dl-LRP1X2-C4) were evaluated by BLI assays. For that, increasing concentrations of AIP56 were incubated with Fc-tagged Dl-LRP1X1-C4 and Dl-LRP1X2-C4 immobilized onto capture biosensors. BLI analysis showed that AIP56 interact with both DL-LRP1X1-C4 and DL-LRP1X2-C4, in agreement with the BLI analysis previously performed with Hs-LRP1-C4.

The interaction of AIP56 with these two LRP1 isoforms was subsequently evaluated in sbPL using two different approaches: in the first approach, cells were co-incubated with AIP56-488 and Dl-LRP1X1-C4 or Dl-LRP1X2-C4 at 1:400 molar ratio, and cellular internalization of AIP56-488 assessed by flow cytometry. The RBD of AIP56 (AIP56$^{T299-N497}$) was used as positive control. Hs-LRP1-C4, which binds to AIP56 *in vitro* (Box 3), was also tested to compare its affinity with that of its sea bass counterparts. These results showed that pre-incubation of AIP56-488 with Dl-LRP1X1-C4 resulted in almost complete inhibition of AIP56-488 uptake by sbPL, at a similar extent as that observed with AIP56$^{T299-N497}$ (Figure 5A and B; Supplementary Table 2). On the other hand, although both Dl-LRP1X2-C4 and Hs-LRP1-C4 decreased the number of AIP56 molecules internalized per cell, as supported by a decrease in median fluorescence intensity (MFI), they did not cause major changes in the

percentages of AIP56 positive cells. Considering that AIP56 interacts with Dl-LRP1X2-C4 and Hs-LRP1-C4 *in vitro*, the low ability of Dl-LRP1X2-C4 and Hs-LRP1-C4 to inhibit the internalization of AIP56-488 into cells suggests that the toxin has higher affinity for Dl-LRP1X1 present in the cells than for the recombinant truncated forms used as inhibitors.

In the second approach, the ability of Dl-LRP1X1-C4 and Dl-LRP1X2-C4 to inhibit sbPL intoxication by AIP56 was evaluated through competition assays similar to those described above but involving analysis of NF-κB p65 cleavage by western blotting. These results corroborated the results of AIP56 internalization described before, i.e., Dl-LRP1X1-C4 strongly inhibited NF-κB p65 cleavage by the toxin, while no inhibition was observed with Dl-LRP1X2-C4 and Hs-LRP1-C4 (Figure 5C). Altogether, these results suggest that the Dl-LRP1X1 isoform plays a major role in intoxication of sbPL by AIP56.

Finally, the *in vitro* and *ex vivo* experiments were complemented with *in vivo* competition experiments, to determine whether the C4 of Dl-LRP1X1 could function as a blocker/inhibitor of AIP56 toxicity in sea bass. Two independent experiments have been performed, in which sea bass were injected with AIP56 alone or mixed with a 400-fold (experiment 1; Figure 5D top graph) or 300-fold (experiment 2; Figure 5D bottom graph) molar excess of Dl-LRP1X1-C4. AIP56 mixed with a 300-fold molar excess of its own RBD ($AIP56^{T299\text{-}N497}$) was injected as positive control. AIP56 mixed with a 300-fold molar excess of its catalytic domain ($AIP56^{N1\text{-}G256}$) and DL-LRP1X1-C4 alone (experiment 1) or inactive AIP56 ($AIP56^{AAIVAA}$) mixed with Dl-LRP1X1-C4 (experiment 2) were injected as negative controls. In both experiments (Figure 5D), Dl-LRP1X1-C4 failed to inhibit sea bass mortality induced by AIP56. This may be due to the fact that *in vivo* there are many LRP1 ligands, with affinities for LRP1-C4 similar or higher than that of AIP56, available to bind to Dl-LRP1X1-C4 co-injected with AIP56, removing the intended competition effect. In contrast, when AIP56 was co-injected with $AIP56^{T299\text{-}N497}$, a 10% (experiment 1) and 50% (experiment 2) reduction in mortality was observed, consistent with *in vivo* results previously obtained (section 2.1) and those observed in the *ex vivo* experiments (Figure 5A-C).The discrepancy in $AIP56^{T299\text{-}N497}$-induced protection observed between the two experiments is most likely related to the susceptibility of the sea bass to the intoxicating dose of AIP56 used, since in experiment 1 it induced low mortality, reducing the detection threshold between fish injected with AIP56 and injected with AIP56 combined with $AIP56^{T299\text{-}N497}$.

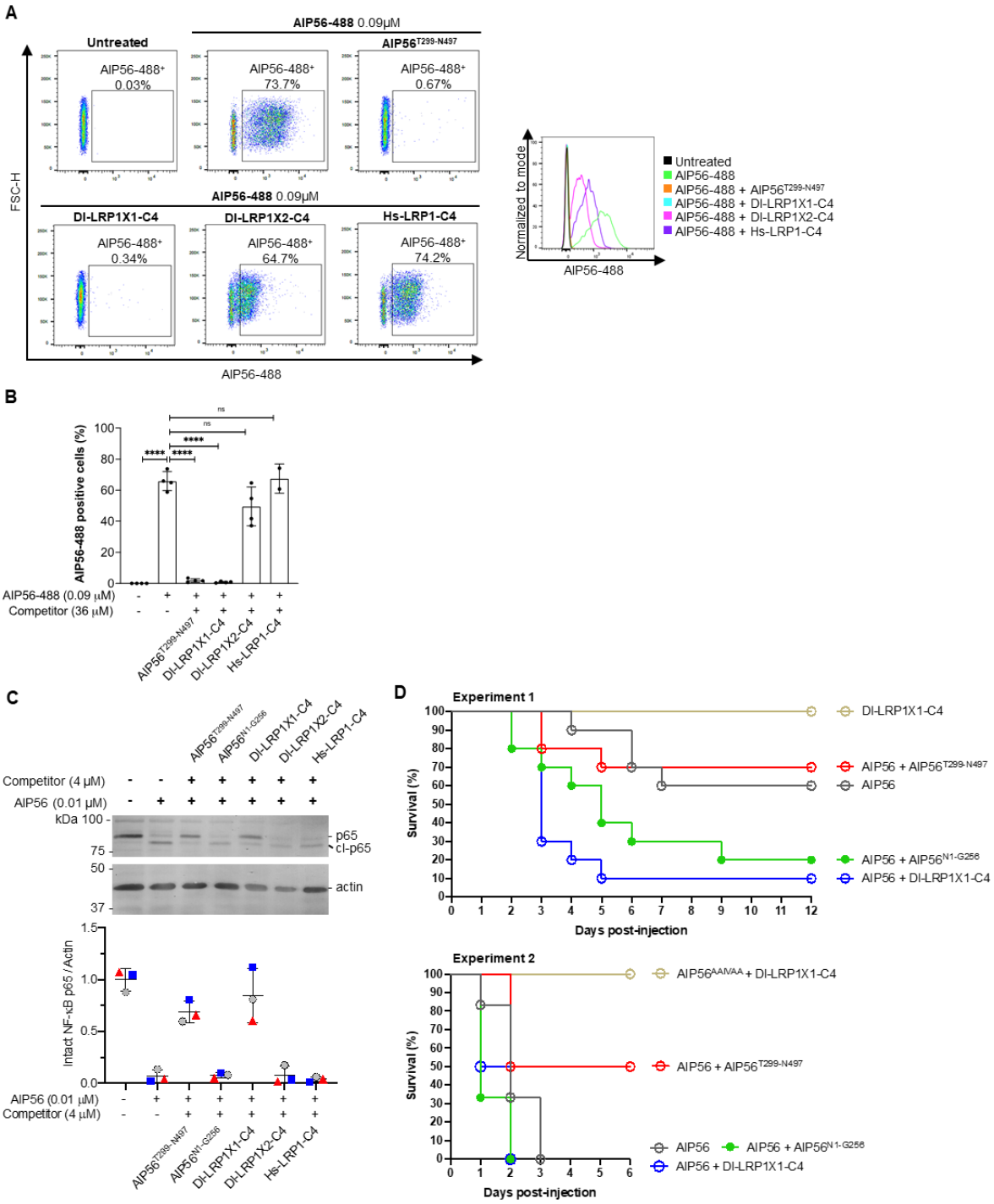

Figure 5. **DI-LRP1X1-C4 has a preponderant role in intoxication of sbPL by AIP56. (A)** Representative flow cytometry plots of competition assays for AIP56-488 internalization in sbPL showing the percentage of AIP56-488 positive cells (left panel) and the fluorescence intensity of AIP56-488 positive cells (right panel). **(B)** Quantification of sbPL AIP56-488 positive cells (n = 4) assessed by flow cytometry as in (A). Statistical significance was tested by Brown-Forsythe one-way ANOVA. **(A, B)** The indicated concentration of AIP56-488 was incubated with 36 µM of DI-LRP1X1-C4, DI-LRP1X2-C4 or Hs-LRP1-C4 for 15 min on ice. This mixture was added to the cells, which were then incubated for 15 min at 22 ºC. The percentage of AIP56-488 positive cells was quantified by flow cytometry. Untreated cells or cells pre-incubated with AIP56$^{T299-N497}$ for 15 min on ice were used as negative and positive controls, respectively. **(C)** Competition assays for AIP56 intoxication. The

indicated concentration of AIP56 was incubated with Dl-LRP1X1-C4, Dl-LRP1X2-C4 or Hs-LRP1-C4 for 15 min on ice. This mix was added to the cells followed by incubation for 4 h at 22 ºC. NF-κB p65 cleavage was analyzed by western blotting. Untreated cells were used as negative control and cells pre-incubated for 15 min on ice with AIP56 RBD ($AIP56^{T299\text{-}N497}$) were used as positive control. A blot representative of three independent experiments is shown. The graph shows the quantification of the results from 3 independent experiments (n=3). Loading correction was achieved by dividing the density of intact p65 band by the density of actin band from the same lane. Values in the graph correspond to fold-changes in the normalized density of p65 band relative to the untreated control. Results from each independent experiment are represented by the same symbol/color. **(D)** Kaplan-Meyer survival curves of sea bass (10 fish/treatment – experiment 1 or 6 fish/treatment – experiment 2) injected with 0.2 or 0.3 μg/g of fish body weight of AIP56 or AIP56 mixed with 400-fold (experiment 1) or 300-fold (experiment 2) molar excess of $AIP56^{T299\text{-}N497}$ or $AIP56^{N1\text{-}G256}$ as positive and negative controls, respectively. Dl-LRP1X1-C4 alone (experiment 1), inactive AIP56 ($AIP56^{AAIVAA}$) mixed with 300-fold molar excess of Dl-LRP1X1-C4 (experiment 2) were also injected as negative controls.

2.4. Residues K350 and R441 in AIP56 RBD are essential for binding to sea bass LRP1

To better understand the interaction between AIP56 and LRP1, it is important to identify the toxin's residues that interact with the receptor. This knowledge is also important for the development of toxin inhibitors/blockers and to eventually redirect the toxin to other cellular receptors after genetic manipulation.

Box 6. Residues of AIP56 essential for binding to LRP1.

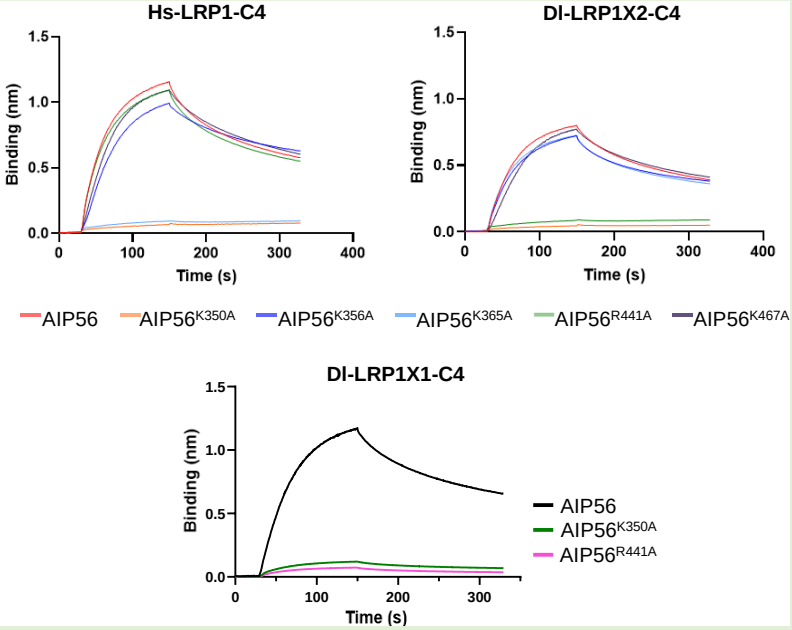

Unpublished data from Pengsheng Chen, Huan Wang and Min Dong.

Binding of AIP56 and AIP56 mutants carrying amino-acid substitutions in the receptor-binding domain ($AIP56^{K350A}$, $AIP56^{K356A}$, $AIP56^{K365A}$, $AIP56^{R441A}$ and $AIP56^{K467A}$) to Hs-LRP1-C4, Dl-LRP1X2-C4 and Dl-LRP1X1-C4 was analyzed by BLI assays with Fc-tagged Hs-LRP1-C4, Dl-LRP1X2-C4 and Dl-LRP1X1-C4 immobilized onto capture biosensors.

It has been reported that the interaction of a ligand with LRP1 is typically mediated by pairs of lysine and/or arginine residues that interact with negatively charged amino acid residues in the LRP1 complement-like repeats [30]. Additionally, hydrophobic residues on the surface of the ligand may be involved in this interaction [30]. In order to analyze which

residues in the AIP56 RBD could bind to LRP1, we first analyzed the presence of conserved lysine and arginine residues in the RBD of AIP56 and AIP56-like and -related toxins (Figure 6A). Residues K350, K356, K365, R441, and K467 met the criteria of potential interacting residues, as they are located on the surface of the AIP56 RBD (Figure 6B) and are therefore available to interact with LRP1. Thus, those residues were mutated to alanine and the impact of the mutations for the interaction of AIP56 with human and sea bass LRP1-C4 evaluated by BLI (Box 6). Similarly to what has been observed with other LRP1 ligands [42–46], this analysis confirmed that the interaction between AIP56 RBD and human LRP1-C4 is carried out by a pair of lysine residues (K350 and K365). However, from these two residues, only K350 is essential for the interactions of the AIP56 RBD and Dl-LRP1X1-C4 or Dl-LRP1X2-C4, together with R441. This suggests that although AIP56-like and -related toxins have LRP1 as a receptor, the interaction between the RBD of each of the toxins with LRP1 may be species-specific.

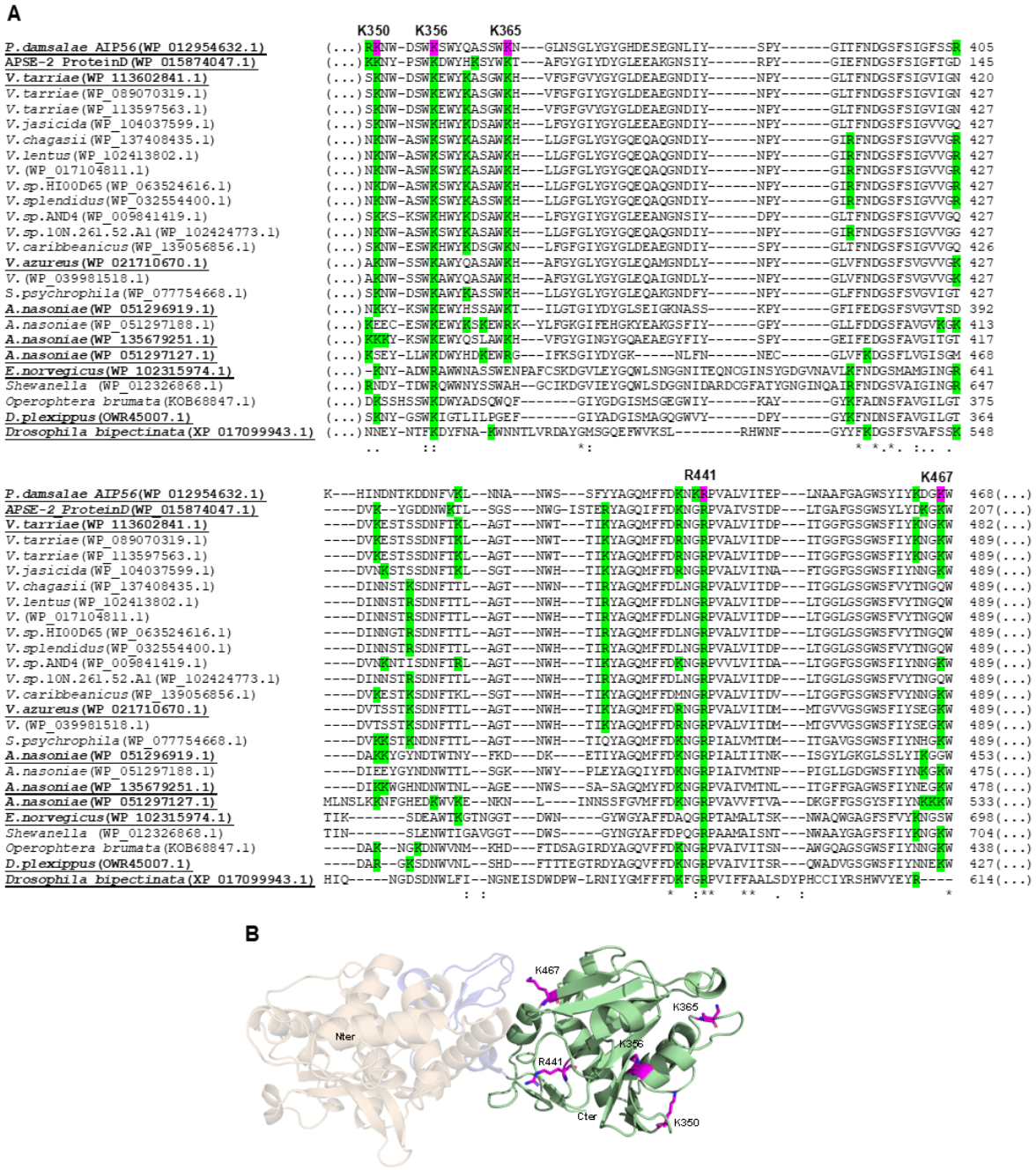

Figure 6. **Identification of lysine/arginine residues of the RBD of AIP56, AIP56-like and AIP56-related toxins potentially involved in the interaction with LRP1. (A)** Sequence alignment of the complete proteins was performed by Clustal Omega, with default parameters. Proteins used in this study are in bold and underlined. Only the regions of the RBDs with the highest number of lysine/arginine residues (highlighted in green) are shown. Residues mutated in AIP56 are highlighted in pink. **(B)** 3D structure of AIP56 showing the position of K350, K356, K365, R441 and K467 amino acid residues (pink sticks) in the RBD (green). Faded region includes the catalytic (beige) and middle (blue) domains.

To support the BLI results, *ex vivo* intoxication assays in sbPL were then performed, using the five AIP56 single mutants, as well as a double mutant in K350 and R441 ($AIP56^{K350A/R441A}$) (Figure 7A). These results showed that both $AIP56^{R441A}$ and

AIP56K$^{350A/R441A}$ were less toxic to sbPL than WT AIP56, having only residual NF-κB p65-cleavage activity. Surprisingly, AIP56^{K350A}, which did not interact with Hs-LRP1C4 and Dl-LRP1X2-C4 in the BLI assay, retained the ability to cleave p65 in sbPL, similarly to AIP56^{K356A}, AIP56^{K365A} and AIP56^{K467A}, suggesting that R441 has a preponderant role for intoxication of sbPL by AIP56. However, the result with AIP56^{K350A} was not supported by *in vivo* experiments, in which the sea bass mortalities induced by the wild type toxin and the toxin mutants were compared (Figure 7B). In this case, the mortalities induced by AIP56^{K356A} (90%), AIP56^{K365A} (80%) and AIP56^{K467A} (90%) were similar to the ones obtained after injection of the wild type toxin (90%), suggesting that these residues are not essential for toxicity. However, the mortalities induced by AIP56^{K350A} and AIP56^{R441A} were much lower (20-40%), and almost no mortality occurred after injection of the double mutant AIP56K$^{350A/R441A}$ (0-10% mortality). These findings, further supported by additional *in vivo* tests using higher doses of mutants (Supplementary Figure 3), indicate that K350 and R441 are required for efficient intoxication of sea bass by AIP56. The definite reason for the discrepancy between the *ex vivo* and *in vivo* experiments requires further investigation. Altogether, the results obtained so far indicate that K365 is required for interaction with human LRP1 but is dispensable for interaction with sea bass LRP1X2 (Box 6), intoxication of sea bass peritoneal leukocytes (Figure 7A), and sea bass lethality (Figure 7B), suggesting that the RBD of these toxins may have coevolved to adapt more specifically to the LRP1 of the respective host species.

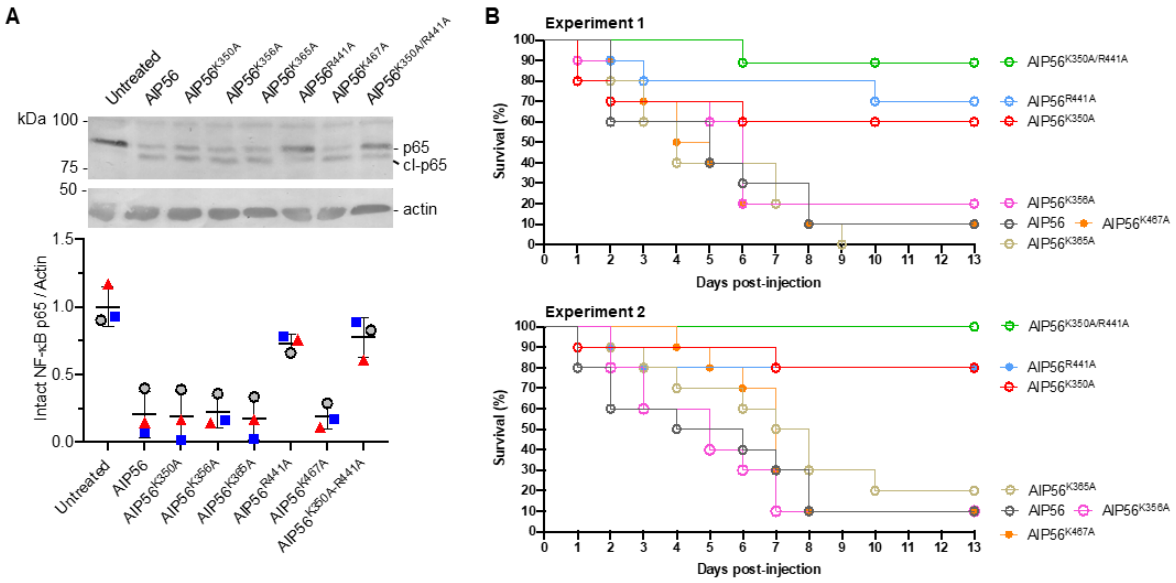

Figure 7. **Residues K350 and R441 are essential for AIP56 toxicity in sea bass. (A)** *Ex vivo* intoxication assays. SbPL were pre-incubated on ice for 15 min with 0.5 nM of AIP56, AIP56^{K350A}, AIP56^{K356A}, AIP56^{K365A}, AIP56^{R441A}, AIP56^{K467A} or AIP56$^{K350A/R441A}$ followed by 4 h incubation at 22 ºC, and the cleavage of NF-κB p65 analyzed by western blotting. Untreated cells were used as negative control. A blot representative of three

independent experiments is shown. The graph shows the quantification of the results from 3 independent experiments (n=3). Quantification was performed as for Figure 5. Results from each independent experiment are represented by the same symbol/color. **(B)** Kaplan-Meyer survival curves of sea bass injected with 0.15 µg/g of body weight (experiment 1) or 0.1 µg/g of body weight (experiment 2) of AIP56 or AIP56 mutants. The two independent experiments were performed using 10 fish/treatment.

The results showing that binding of AIP56 to its receptor is mediated by lysine/arginine residues led to the question of whether free lysine and arginine amino acids could be used to inhibit AIP56 toxicity. To test this, sbPL intoxication assays were performed in culture medium supplemented with lysine and arginine, to evaluate if the presence of these amino-acids inhibited AIP56-induced p65 cleavage (Figure 8). The RBD of AIP56 (AIP56$^{T299\text{-}N497}$) was included as positive control, while untreated cells and cells incubated with free lysine and arginine alone were used as negative controls. The results show that both amino acids, particularly lysine, inhibit p65 cleavage. These findings are promising as they suggest that dietary supplementation of lysine and arginine in sea bass could potentially confer protection against AIP56 intoxication, thereby mitigating the pathogenic effects of *Phdp* infection.

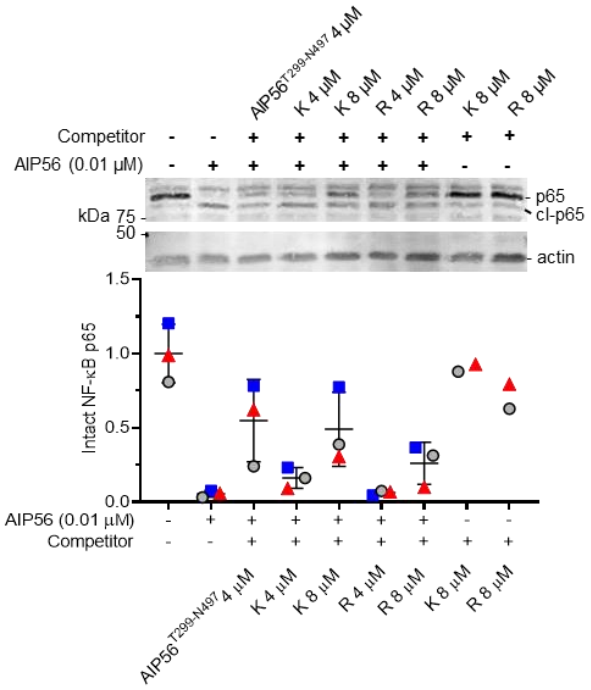

Figure 8. **Free lysine (K) and arginine (R) decrease AIP56 toxicity for sbPL.** A representative blot of three independent experiments (n = 3) is shown. SbPL were pre-incubated on ice for 15 min with the indicated concentrations of lysine or arginine followed by incubation with AIP56 for 4 h at 22 ºC and the cleavage of NF-κB p65 was analyzed by western blotting. Untreated cells and cells incubated with free lysine or arginine alone were used as negative controls. Cells pre-incubated with AIP56's RBD (AIP56$^{T299\text{-}N497}$) were used as positive controls. The graph shows the quantification of the results from three independent experiments (n=3) with the exception of cells incubated with free lysine or arginine alone that are from two independent experiments (n=2).

Loading correction was achieved by dividing the density of intact p65 band by the density of actin band from the same lane. Values in the graph correspond to fold-changes in the normalized density of p65 band relative to the untreated control. Results from each independent experiment are represented by the same symbol/color.

3. Discussion

In this study, LRP1 was identified as a receptor for AIP56 and the toxin-receptor interaction was characterized, showing that it plays a crucial role in the intoxication process. The results also indicate that LRP1 is the receptor for a set of AIP56-like and -related toxins.

LRP1 is an endocytic receptor that binds more than 30 ligands, including proteases, protease inhibitor complexes, extracellular matrix proteins, growth factors, viral proteins and bacterial toxins [30,32,48,49], such as *Pseudomonas* exotoxin A [50], *Clostridium perfringens* large cytotoxin [51], *Clostridioides difficile* toxin A [52], *Clostridium novyi* alpha-toxin [53] and *Pasteurella multocida* toxin [54]. Although LRP1 can transiently localize to lipid rafts, the receptor migrates in the plasma membrane to clathrin-coated pits, undergoing constitutive endocytosis and recycling between endosomes and the cell membrane [30,37]. In most cells, including macrophages, ligands bound to LRP1 dissociate under endosomal acidic pH and are transferred to lysosomes for degradation [30,37]. This trafficking route is ideal for some cargos, such as viruses and bacterial AB toxins, which utilize LRP1 to enter into target cells. The trafficking pathway of LRP1 cargoes mirrors the initial steps of the intracellular trafficking of AIP56, which targets myeloid cells, preferentially macrophages [12], and is internalized through receptor-mediated clathrin-dependent endocytosis [9]. However, once in endosomes, a pool of AIP56 translocates to the cytosol in response to acidification, while the remaining pool is recycled back to the extracellular compartment, escaping lysosomal degradation and eventually becoming available to intoxicate other or the same cell [9].

As with other members of the LDLR family, ligand binding to LRP1 is calcium-dependent and mediated by pairs of LDLRA domains (complement-like repeats) [53,55], which are organized in clusters in the extracellular region of the receptor (Figure 1) [35–37]. Most ligands bind to LRP1 clusters 2 and/or 4 [30,40,49,51,54], with all ligands studied so far binding via pairs of positively charged arginine and/or lysine residues [56–59]. Using individual functional clusters of human LRP1 in BLI assays (Box 3), AIP56 was found to bind exclusively to cluster 4 in a calcium-dependent manner, via residues K350 and K365 of its RBD (Box 6). This aligns with what has been shown for *Clostridium perfringens* TpeL toxin [51], *Pasteurella multocida toxin* [54] and *Pseudomonas exotoxin* A [40], which also bind preferentially or exclusively to this cluster, which is sufficient for their internalization and cytotoxicity. Accordingly, AIP56 was also shown to bind to cluster 4 of both sea bass

LRP1 isoforms, with the highest affinity for cluster 4 of LRP1X1 (Box 5). This preference was corroborated by *ex vivo* experiments in sbPLs, in which only cluster 4 of LRP1X1 was able to inhibit AIP56 internalization (Figure 4A and B) and the concomitant cleavage of p65 (Figure 4C). However, attempts to block AIP56 toxicity *in vivo* by preincubating the toxin with LRP1X1-C4 prior to inoculation into fish were unsuccessful. Although the reason for this remains unknown, the intoxication experiments performed with *Lrp1*-KO human cells (Box 2 and 4) suggest that AIP56 may use alternative receptor(s). The binding of alternative receptors, if mediated by different toxin regions/residues could explain the inability of LRP1X1-C4 to inhibit toxicity *in vivo*. Alternatively, it is possible that under physiological *in vivo* conditions, endogenous LRP1 ligands that are not present in cell culture conditions outcompete AIP56 for LRP1X1-C4 binding, creating a competitive-ligand binding scenario in which AIP56 becomes free to bind LRP1 on the cell membrane and exert its cytotoxic effect.

The residues in AIP56 RBD that interact with sea bass LRP1 were determined for cluster 4 of Dl-LRP1X2 and confirmed for Dl-LRP1X1 (Box 6), showing that AIP56 binds to both LRP1 isoforms of sea bass differently than to human LRP1-C4: while K350 is involved in both cases, the second residue in sea bass is R441 whereas in humans is K365. Thus, although LRP1 is phylogenetically conserved, interactions of AIP56 with different LRP1 orthologues rely on different residue pairs, supporting the occurrence of receptor-ligand coevolution. In agreement with this, experiments using human and sea bass RAP/RAP-D3 as inhibitors of AIP56 internalization and cytotoxicity showed that despite the high phylogenetic conservation of RAP (Supplementary Figure 4), human RAP inhibited AIP56 internalization in mBMDMs (Figure 3) and intoxication by the ToxicMoiety-AIP56RBD chimera in human HEK 293T cells (Box 4), but not AIP56 intoxication in sbPL (Figure 4). Surprisingly, sea bass RAP-D3 also failed to prevent internalization and p65 cleavage by AIP56 in these cells (Figure 4). Although the explanation for these results is currently unavailable, it is possible that the ratio of RAP:AIP56 (300:1) used was insufficient, as previous works reported the use of higher ratios (1000:1) to block intoxication by other toxins [51]. Alternatively, the inability of RAP to inhibit AIP56 toxicity could be due to a lower affinity of RAP to bind sea bass LRP1s, when compared to the affinity of AIP56, or to the recognition, by RAP, of different clusters/regions in sea bass LRP1s than the ones involved in AIP56 binding.

A particularly relevant finding of the present work with translational potential was the ability lysine and, to some extent, arginine, to inhibit AIP56 toxicity for sbPL, likely by competing with AIP56 for LRP1 binding. In face of these results, it would be highly relevant to test if dietary supplementation with lysine and/or arginine is able to confer protection against

AIP56 toxicity *in vivo* and, more importantly, against *Phdp* infection, as it could lead to novel approaches to prevent the high mortalities and economic losses caused by *Phdp* in marine aquaculture [7]. In this context, the results showing that the RBD of AIP56 per se can block AIP56-induced mortality in sea bass are also very promising and support its potential for therapeutic development. Exploring these approaches could allow reducing or even eliminate the use of antibiotics for treating *Phdp* infections [60,61], benefiting antibiotic resistance, management animal welfare, human health, and the environment [62,63].

Finally, the implications of this study go beyond AIP56. Several lines of evidence suggest that the RBDs of AIP56-like and -related toxins are functionally equivalent to that of AIP56. First, structural predictions of AIP56-like toxins [13] and structural analysis of AIP56 [13] and AIP56-related toxins from *D. plexippus* and *E. norvegicus* (Box 1) confirmed the structural similarity of their RBDs. Second, both AIP56 and all tested AIP56-like and -related toxins bound to human LRP1 cluster 4 in BLI assays (Box 3), suggesting that they recognize LRP1 orthologs expressed in their respective hosts. Third, the putative RBDs of some of those toxins inhibited AIP56 toxicity in sea bass leukocytes (Figure 1A-B), possibly by blocking AIP56 binding to LRP1. However, protection of sea bass from AIP56-induced lethality was only achieved using AIP56 RBD as competitor, in contrast to the aggravated mortality observed when a molar excess of the RBDs of some AIP56-like and -related toxins was co-injected with AIP56 (Figure 1C). The reason why some AIP56-like and -related toxins, despite interacting with human LRP1 cluster 4 in BLI assays, fail to compete in the *ex vivo* tests with sbPL and why all failed to protect fish from AIP56 toxicity *in vivo* remains to be clarified. One possible explanation is that the toxins have distinct affinities for different LRP1 orthologues due to toxin-host co-evolution. Indeed, the results of the BLI assays (Box 3) revealed that different toxins have different affinities for human LRP1 cluster 4. It is reasonable to speculate that their affinity for sea bass LRP1 also varies, which might explain the inability of the toxins to inhibit AIP56 in *ex vivo* and *in vivo* conditions. It is also possible that they may bind to regions of cluster 4 that do not interfere with AIP56 binding, as suggested above for sea bass RAP-D3. It also cannot be ruled out that binding to LRP1 by these toxins involves distinct combinations of receptors. In fact, the wide range of structurally unrelated macromolecules that bind to LDL receptors, including LRP1, is often promoted by their association with co-receptors [29]. Therefore, it is possible that these toxins may share one receptor but rely on different co-receptor(s). Considering this scenario, it is possible that *ex vivo*, some of the AIP56-like and -related toxins may block AIP56 interaction by blocking its binding to LRP1 on macrophages but are unable to block AIP56 toxicity in the more complex *in vivo* context. This could be due to these toxins binding

to LRP1 expressed on a wide variety of cells that lack the specific co-receptor(s) required for AIP56 interaction, thereby dispersing their competitive effect.

As a concluding remark, it can be stated that the identification of LRP1 as a receptor for AIP56 and related toxins is a significant breakthrough that will open doors to the characterization of the cellular specificity and internalization process of the growing family of AIP56-like and -related toxins, as well as on the detailed study of the toxins-receptor interactions. Some of these toxins are produced by bacteria that cause great economic losses in the aquaculture industry (e.g., AIP56 in *Phdp*), while others are produced by symbiotic bacteria of insects (e.g., AIP56-like toxin of *Arsenophonus nasoniae*) that are agricultural pests or by pollinating insects (e.g, AIP56-related toxin of *Danaus plexippus*) necessary for the production of all fruit and most vegetable crops. Although there is no information available on the possible infection caused by *Vibrio tarriae*, the presence of an AIP56-like toxin in this strain of *Vibrio* isolated from human blood and stool raises the question of the role that the toxin may eventually play. Thus, disclosing the molecular details underlying toxin-receptor interaction will have an extensive impact for understanding the biology of those organisms and their hosts as well as on (co)evolutionary aspects resulting from the toxin-receptor interaction. It will also be an asset for the rational development of prophylactic and therapeutic strategies, such as vaccines able to induce production of antibodies that block toxin-receptor binding or drugs that inhibit toxin-receptor interactions. Furthermore, it can support the elaboration of strategies for biological control of herbivorous pests and/or protection of pollinating insects with impact for agriculture, aquaculture, or even human health.

4. Materials and Methods

4.1. Ethics statement

This study was carried out in accordance with European and Portuguese legislation for the use of animals for scientific purposes (Directive 2010/63/EU; Decreto-Lei 113/2013). The work was approved by Direcção-Geral de Alimentação e Veterinária, the Portuguese authority for animal protection (Lic. 0421/000/000/2021).

4.2. Fish

Sea bass (*Dicentrarchus labrax*) with no previous history of *Phdp* infection were purchased from commercial hatcheries, and maintained in 600 L seawater aquaria. Water temperature was maintained at 20 ± 1 °C, salinity at 23–28‰, and the photoperiod was 14 h light: 10 h dark. Water quality was maintained with mechanical and biological filtration and ozone-disinfection and the fish were fed with commercial pellets from Skretting, according to the supplier's instructions. Euthanasia was performed using with an overdose of 2-phenoxyethanol (Panreac; 5 mL/10 L) followed by bleeding.

4.3. Mice

C57BL/6 mice were bred and housed at the IBMC/i3S animal facility. They were fed sterilized food and water *ad libitum*. Four-week-old male mice were used exclusively to derive macrophages from bone marrow. Mice were euthanized by CO_2 followed by cervical dislocation.

4.4. Reagents and Antibodies

Hanks' balanced salt solution (HBSS, 14060-040), fetal bovine serum (FBS, 10500064), phosphate buffered saline (PBS, 14040-091), TripLE, Leibovitz's L-15 medium (L-15, 11415-049), DMEM, L-glutamine, sodium pyruvate and HEPES were all from Gibco™. Penicillin/streptomycin (P/S, DE17-602E) was purchased from Lonza. Heparin was purchased from B. Braun. Isopropyl β-D-1-thiogalactopyranoside (IPTG, MB026) was purchased from NZYTech. Incomplete Freund's Adjuvant (IFA, F5506) was purchased from Sigma. The anti-sea bass NF-κB p65 rabbit serum was produced using a peptide (SIFNSGNPARFVS) located at the C-terminal region of sea bass p65 as antigen [67]. The anti-sea bass actin primary mouse monoclonal antibody is from Santa Cruz Biotechnology (clone C-4, sc-47778). The goat anti-rabbit IgG (A9919) and goat anti-mouse IgG (A2429) secondary antibodies conjugated to alkaline phosphatase were purchased from Sigma.

4.5. Cells

Sea bass peritoneal leukocytes (sbPL) were obtained from inflamed peritoneal cavities 12 days after intraperitoneal administration of 100 µl IFA, as previously described [124], and used at a density of 2 x 10^6 cells/mL in L-15 medium adjusted to 322 mOsm and supplemented with 10% (v/v) FBS, 1% (v/v) P/S and 20 U mL^{-1} heparin (sbL-15). Macrophages (~83%) and neutrophils (~8%) constitute most of the inflamed peritoneal cell population, which also contains eosinophilic granular cells, lymphocytes and erythrocytes in small quantities [38].

Mouse bone marrow-derived macrophages (mBMDM) were obtained using an established protocol [69]. Briefly, to collect the bone marrow, muscle from mice femurs and tibias was removed, the extremities of the bones cut and the bone marrow cavities flushed with 5 mL of ice-cold HBSS per bone using a syringe with a 26G needle. The cell suspension was centrifuged (250 × *g*, 10 min, 4 °C) and the resulting pellet was resuspended in complete DMEM (cDMEM; DMEM supplemented with 10% (v/v) FBS, 10 mM L-glutamine, 10 mM HEPES, 1 mM sodium pyruvate and 1% (v/v) P/S) with 10% (v/v) of L929 cell conditioned medium (LCCM) as a source of M-CSF [70]. Cells were incubated overnight on a cell culture dish at 37 °C in a 7% CO_2 atmosphere to remove fibroblasts. Non-adherent cells were collected in HBSS, centrifuged, resuspended in cDMEM with 10% (v/v) LCCM and plated at a density of 5 × 10^5 cells/well in a 24-well plate with 1 mL per well. After 3 days, 10% (v/v) LCCM was added to each well and, at day 7, the medium was renewed. At day 10, mBMDM were ready to be used.

4.6. DNA constructs for recombinant protein production

AIP56: The construct encoding full-length AIP56 cloned into the NcoI/XhoI restriction sites of pET28a (Novagen) in frame with a C-terminal 6His-tag (pET28AIP56H+) is described in [1]. Constructs encoding $AIP56^{K350A}$, $AIP56^{K356A}$, $AIP56^{K365A}$, $AIP56^{R441A}$, $AIP56^{K467A}$, $AIP56^{K350A/R441A}$ were generated at Min Dong's lab by site-directed mutagenesis, using pET28AIP56H+ as template. His-tagged AIP56 metalloprotease mutant ($AIP56^{AAIVAA}$), corresponding to a full-length inactive version of the toxin was generated as described in [71] by site directed mutagenesis using QuickChange Site-Directed Mutagenesis Kit (Stratagene) following manufacturer's instructions. The DNA sequence encoding $AIP56^{T299-N497}$ and $AIP56^{N1-G256}$ were PCR amplified using pET28AIP56H+ as template and cloned into NcoI/XhoI restriction sites of pET28a in frame with a C-terminal 6His-tag.

AIP56-like toxins: The genes encoding full length AIP56-like proteins from *Vibrio azureus* ($_{Va}$AIP56, accession number WP_021710670.1) and *Vibrio tarriae* ($_{Vt}$AIP56, accession number WP_113604820.1; previously *Vibrio* sp. 2017V-1085, accession number WP_113602841.1) were amplified from *Vibrio azureus* LMG25266 and *Vibrio tarriae*, respectively, and cloned into the NdeI/XhoI restriction sites of pET28a in frame with a C-terminal 6His-tag. DNA sequences encoding full length AIP56-like toxins from *Arsenophonus nasoniae* ($_{An(WP251)}$AIP56, $_{An(WP919)}$AIP56 and $_{An(WP127)}$AIP56, accession numbers WP_135679251.1, WP_051296919 and WP_051297127.1, respectively) were synthesized *de novo* (GenScript Corporation, Piscataway, NJ, USA) with codon-optimization for expression in *E. coli* and cloned at the NcoI/XhoI restriction sites of pET28a in frame with a C-terminal 6His-tag. DNA sequences coding for truncated forms of the receptor-binding domains of AIP56-like proteins ($_{Va}$AIP56$^{S321\text{-}R518}$; $_{Vt}$AIP56$^{S321\text{-}S518}$; $_{An(WP251)}$AIP56$^{R318\text{-}I515}$; $_{An(WP919)}$AIP56$^{H295\text{-}L486}$; $_{An(WP127)}$AIP56$^{I376\text{-}L579}$) were amplified from the construct encoding the respective full-length protein and cloned into NcoI/XhoI restriction sites of pET28a in frame with a C-terminal 6His-tag.

AIP56-related toxins: DNA sequences encoding proteins of unknown function (PUF) from *Enterovibrio norvegicus* ($_{En}$PUF, accession number WP_017014894.1), *Danaus plexippus plexippus* ($_{Dpp}$PUF, accession number OWR44524.1), *Drosophila bipectinata* ($_{Db}$PUF, accession number XP_017099943.1) and hypothetical Protein D from bacteriophages APSE-2 ($_{APSE\text{-}2}$ProtD, accession number YP_002308522) and APSE-7 ($_{APSE\text{-}7}$ProtD, accession number CAB4327916.1) were synthetized *de novo* (GenScript Corporation, Piscataway, NJ, USA) and cloned into NcoI/XhoI restriction sites of pET28a in frame with a C-terminal 6His-tag. DNA sequences encoding the receptor-binding domain of AIP56-related proteins ($_{En}$PUF$^{A513\text{-}L704}$; $_{Dpp}$PUF$^{L244\text{-}S422}$; $_{Db}$PUF$^{K258\text{-}S458}$; $_{APSE\text{-}2}$ProtD$^{P49\text{-}S237}$, $_{APSE\text{-}7}$ProtD$^{M1\text{-}N219}$) were amplified from the constructs containing each respective full-length sequence and cloned into NcoI/XhoI restriction sites of pET28a in frame with a C-terminal 6His-tag.

LRP1 members: Constructs for expressing LRP1 and RAP proteins were generated at Min Dong's lab. DNA sequences encoding *Homo sapiens* LRP1 (Hs-LRP1) cluster 1, cluster 2, cluster 3 and cluster 4 (accession number NP_002323.2) and *Dicentrarchus Labrax* LRP1X1 (accession number XP_051280027.1) cluster 4 (Dl-LRP1X1-C4) and LRP1X2 (accession number XP_051270293.1) cluster 4 (Dl-LRP1X2-C4), were synthetized *de novo* (GenScript Corporation, Piscataway, NJ, USA) and cloned into the NcoI/XhoI restriction site of pET28a in frame with a N-terminal 6His-tag, thrombin site and AviTag. The sequences encoding Hs-RAP and Hs-RAP-D3 from accession number NP_002328.1 and Dl-RAP-D3

from accession number XP_051240455.1 were synthetized *de novo* and cloned into the NcoI/XhoI restriction sites of pET28a in frame with a N-terminal 6His-tag and thrombin site.

4.7. Production of recombinant proteins

Expression and purification conditions of the recombinant proteins used in this work are summarized in Table 1. AIP56, AIP56 mutant variants, inactive AIP56^{AAIVAA}, AIP56$^{N1\text{-}G256}$, $_{Vt}$AIP56, and $_{En}$PUF were expressed in *E. coli* BL21(DE3) (Invitrogen). $_{An(WP919)}$AIP56, $_{Va}$AIP56$^{S321\text{-}R518}$, $_{Vt}$AIP56$^{S321\text{-}S518}$, $_{An(WP251)}$AIP56$^{R318\text{-}I515}$, $_{An(WP919)}$AIP56$^{H295\text{-}L486}$, $_{An(WP127)}$AIP56$^{I376\text{-}L579}$, $_{En}$PUF$^{A513\text{-}L704}$, Hs-LRP1-C1, Hs-LRP1-C2, Hs-LRP1-C3, Hs-LRP1-C4, Dl-LRP1-C4 and Dl-LRPX1-C4 were expressed in *E. coli* BL21-CodonPlus(DE3) (Stratagene). $_{Dpp}$PUF$^{L244\text{-}S422}$, Hs-RAP and Hs-RAP-D3 were expressed in *E. coli* Rosetta(DE3) (Novagen). $_{Va}$AIP56, $_{Dpp}$PUF and Dl-RAP-D3 were expressed in *E. coli* BL21(DE3)-Star (Invitrogen). AIP56$^{T299\text{-}N497}$ and $_{An(WP251)}$AIP56 were expressed in *E. coli* SoluBL21(DE3) (Genlantis). Transformed *E. coli* cells were cultured at 37 °C in Luria Bertani (LB) broth with shaking (200 rpm) until $OD_{600} \approx 0.6$. IPTG was added to a final concentration of 0.5 mM and protein expression carried out at 17 °C for 18-20 h. After protein expression, bacteria were harvested by centrifugation (30 min, 4000 × *g*, 4 ºC) and resuspended in 40 ml of buffer (a) 50 mM Tris-HCl pH 8.0, 300 mM NaCl for $_{En}$PUF, $_{Va}$AIP56$^{S321\text{-}R518}$, $_{Vt}$AIP56$^{S321\text{-}S518}$, $_{An(WP251)}$AIP56$^{R318\text{-}I515}$, $_{An(WP919)}$AIP56$^{H295\text{-}L486}$, $_{An(WP127)}$AIP56$^{I376\text{-}L579}$, $_{Dpp}$PUF$^{L244\text{-}S422}$, AIP56$^{T299\text{-}N497}$, $_{An(WP251)}$AIP56, $_{Dpp}$PUF, Hs-RAP, Hs-RAP-D3, Dl-RAP-D3; (b) 50 mM Bis-tris pH 6.5, 300 mM NaCl for AIP56, AIP56 mutant variants, AIP56^{AAIVAA}, AIP56$^{N1\text{-}G256}$, $_{Vt}$AIP56, $_{An(WP919)}$AIP56 and $_{En}$PUF$^{A539\text{-}L730}$; (c) 50 mM Tris-HCl pH 7.5, 250 mM NaCl for $_{Vt}$AIP56; (d) 50 mM Tris-HCl pH 8.0, 300 mM NaCl, 1 mM DTT, 2.5 mM $CaCl_2$ for Hs-LRP1-C1, Hs-LRP1-C2, Hs-LRP1-C3, Hs-LRP1-C4, Dl-LRP1-C4 and Dl-LRP1X1-C4; and stored at -20 °C. After defrosting, cells were lysed by sonication on ice (three pulses of 30 s, duty cycle of 70-80 and energy of 300-400 J) and the lysates centrifuged (45 min, 35000 × *g*, 4 ºC). The recombinant proteins were purified from the supernatant using nickel-affinity chromatography (Ni-NTA agarose, ABT). In the case of $_{Vt}$AIP56 and Hs-RAP, affinity-purified proteins were subsequently subjected to size-exclusion chromatography (Superdex 200 increase 10/300, GE Healthcare). Inactive AIP56^{AAIVAA} was purified from inclusion bodies by metal affinity chromatography under denaturing conditions, refolded and subjected to size exclusion chromatography, as previously described [71]. After purification, proteins were analyzed by SDS-PAGE and purities determined by densitometry of Coomassie Blue-stained gels (Image Lab Software, BioRad). Purified recombinant proteins were maintained in the same buffer used for purification (Table 1), aliquoted, frozen in liquid nitrogen and stored at -80 °C.

Table 1. **Conditions used for recombinant protein expression and purification.**

Protein	Expression Strain	Expression Temperature	Buffer
AIP56 AIP56^{K350A} AIP56^{K356A} AIP56^{K365A} AIP56^{R441A} AIP56^{K467A} AIP56$^{K350A/R441A}$ AIP56^{AAIVAA} AIP56$^{N1-G256}$	*E. coli* BL21(DE3)	17°C	50 mM Bis-tris pH 6.5, 300 mM NaCl
AIP56$^{T299-N497}$ *An*(WP251)AIP56	*E. coli* SoluBL21(DE3)	17°C	50 mM Tris-HCl pH 8.0, 300 mM NaCl
*Va*AIP56	*E. coli* BL21(DE3)-Star	17°C	50 mM Bis-tris pH 6.5, 300 mM NaCl
*Vt*AIP56 *En*PUF	*E. coli* BL21(DE3)	17°C	50 mM Tris-HCl pH 7.5, 250 mM NaCl
*Va*AIP56$^{S321-R518}$ *Vt*AIP56$^{S321-S518}$ *An*(WP251)AIP56$^{R318-I515}$ *An*(WP919)AIP56$^{H295-L486}$ *An*(WP127)AIP56$^{I376-L579}$	*E. coli* BL21-CodonPlus(DE3)	17°C	50 mM Tris-HCl pH 8.0, 300 mM NaCl
An(WP919)AIP56 *En*PUF$^{A513-L704}$	*E. coli* BL21-CodonPlus(DE3)	17°C	50 mM Bis-tris pH 6.5, 300 mM NaCl
*Dpp*PUF Dl-RAP-D3	*E. coli* BL21(DE3)-Star	17°C	50 mM Tris-HCl pH 8.0, 300 mM NaCl
*Dpp*PUF$^{L244-S422}$ Hs-RAP Hs-RAP-D3	*E. coli* Rosetta(DE3)	17°C	50 mM Tris-HCl pH 8.0, 300 mM NaCl
Hs-LRP1-C1, C2, C3, C4 Dl-LRP1X1-C4 Dl-LRP1X2-C4	*E. coli* BL21-CodonPlus(DE3)	17°C	50 mM Tris-HCl pH 8.0, 300 mM NaCl, 1 mM DTT, 2.5 mM $CaCl_2$

4.8. Determination of protein concentration

Concentrations of recombinant proteins were determined by measuring absorbance at 280 nm using NanoDrop 1000 or NanoDrop One (Thermo Fisher Scientific) considering the extinction coefficient and the molecular weight calculated by the ProtParam tool (http://www.expasy.org/tools/protparam.htmL).

4.9. Fluorescent labelling of AIP56

AIP56 was labelled with Alexa Fluor 488 (AIP56-488), using the Molecular Probes® Alexa Fluor protein labelling kit (A10235, ThermoFisher Scientific) following the manufacturer's instructions, but with higher ratio AIP56:Alexa488 (57 nM:1 vial), since the recommended ratio inhibited AIP56-488 cell binding and NF-κB p65 cleavage [12].

4.10. Competition assays

Intoxication assays (NF-κB p65 cleavage): sbPL were plated on a 24-well plate at a density of 2 x 10^6 cells/well in sbL-15 without FBS and left to adhere at room temperature (RT) for 30 min. Before adding to the cells, 0.01 µM of AIP56 was pre-incubated with 400 x molar excess (4 µM) of LRP1 in sbL-15 without FBS for 15 min on ice. The medium of the cells was aspirated and replaced by the LRP1-AIP56 mixture of 250 µl of sbL-15 without FBS containing the competitors (RBD of AIP56-like and -related toxins, RAP molecules, lysine or arginine) at a molar concentration of 4 µM or 8 µM (lysine or arginine), followed by an incubation for 15 min on ice. AIP56 (0.01 µM final concentration) was then added to the wells containing the RBD of AIP56-like and -related toxins, RAP molecules, lysine or arginine and the plate incubated for further 15 min on ice. Afterwards, the plate was transferred to 22 ºC and incubated for 4 h. After two washes with sea bass PBS (sbPBS; 50 mM phosphate buffer pH 7.2 + 184 mM NaCl) cells were lysed with 30 µl SDS-PAGE gel loading buffer (50 mM Tris-HCl pH 8.8, 2% (w/v) SDS, 0.05% (w/v) bromophenol blue, 10% (v/v) glycerol, 2 mM EDTA, 100 mM DTT) and lysates analyzed by western blotting to assess NF-κB p65 cleavage.

Internalization assay (flow cytometry):

- sbPL: cells were plated at a density of 4 x 10^5 cells/well on a U-bottom 96-well plate (100 µl/well) in sbL-15 without FBS. Before adding to the cells, 0.09 µM of AIP56-488 were pre-incubated with 400 x molar excess (36 µM) of LRP1 for 15 min on ice. Then, this mixture, or 9 µM or 36 µM (i.e, 100 x and 400 x molar excess, respectively) of RAP molecules were added to the cells, followed by incubation for 15 min on ice. AIP56-488 was then added at a concentration of 0.09 µM to the wells containing the RAP molecules and plates incubated for further 15 min on ice, followed by 15 min at 22 ºC. Cells were then washed with sbPBS, centrifuged (3 min, 250 × *g*, 4 ºC), resuspended in sbFACS buffer (sbPBS with 2% (v/v) FBS) and filtered through a 35 µm nylon mesh cell strainer into flow cytometry tubes. Propidium iodide (PI; 5 µg/mL) was added to sbPL to access cell viability prior to analysis of AIP56-488 fluorescence by flow cytometry.

mBMDM: cells were used at a density of 5 x 10^5 cells/well on a flat-bottom 24-well plate. Cells were incubated for 15 min on ice with 9 µM of competitors in 250 µl of cDMEM without FBS. AIP56-488 was then added at a concentration of 0.09 µM (i.e, 400 times lower than the concentration of the competitor) and cells incubated for further 15 min on ice, followed by 30 min at 37 ºC. mBMDM were then washed with PBS and incubated in 100 µl of TripLE for 10 min to detach cells. To stop the reaction, 200 µl of FACS buffer (PBS with 2% (v/v) FBS) were added to the wells. Cells were collected into microcentrifuge tubes and centrifuged (5 min, 250 × g, 4 ºC). The cell pellets were resuspended in 200 µl of FACS buffer and filtered through a 35 µm nylon mesh cell strainer into flow cytometry tubes.

4.11. SDS-PAGE and western blotting

SDS-PAGE was performed using the Laemmli discontinuous buffer system [72]. Prior to loading, samples were heated for 5 min at 95 ºC in SDS-PAGE gel loading buffer. For sbPL samples, SDS-PAGE were stopped after 2/3 of the gel run. For western blotting, the proteins were transferred onto AmershamTM Protran 0.45 µm nitrocellulose membranes (10600002, Amersham). The protein loading on the membranes was controlled by Ponceau S staining. The membranes were blocked for 30 min at RT with blocking solution (5% (w/v) skimmed milk in TBS-T (Tris-buffered saline supplemented with 0.1% (v/v) Tween 20)) followed by 1 h incubation at RT with the anti-sea bass NF-κB p65 rabbit antibody (1:1500) or anti-actin mouse antibody (1:5000) diluted in blocking solution. After 3 washes of 5 min with TBS-T, membranes were incubated for 1 h at RT with anti-rabbit IgG or anti-mouse IgG alkaline phosphatase conjugated secondary antibodies diluted in blocking solution (1:10000). After 3 additional 5 min washes, the membrane was incubated with 5-bromo-4-chloro-3-indolyl-phosphate/nitro blue tetrazolium (BCIP/NBT, S3771, Promega). The quantification results are expressed as the density of the p65 band relative to the density of the β-actin band of the same lane. Each graph combines the results of three, four or six independent experiments.

4.12. Flow cytometry

Flow cytometry data was acquired on a BD FACSCanto™ II (BD Biosciences, San Jose, CA). Ten thousand events per sample of sea bass cells were analyzed at medium flow rate. Fluorescence was collected through a 530/30 nm (FITC) and 695/40 nm (PerCP-Cy5.5) detection filters. All data was analyzed using FlowJo™ software v10.6.1 (San Diego, CA).

SbPL and mBMDM were identified by differential gating based on their side scatter area (SSC-A) and forward scatter area (FSC-A), followed by elimination of duplets through its

forward scatter high (FSC-H) and FSC-A profile. The viable cells were selected as PI^- cells ($PerCP\text{-}Cy5.5^-$) and then, the percentage of $AIP56\text{-}488^+$ cells ($FITC^+$) was analyzed.

4.13. *In vivo* intoxication assays

Groups of 10 fish (average body weight of 15.2 ± 2.2 g) were inoculated with 100 µl of AIP56 at a dose of 0.3 µg toxin/g of body weight or AIP56 mixed with 300-fold molar excess of $AIP56^{T299\text{-}N497}$, $AIP56^{N1\text{-}G256}$, $_{Vt}AIP56^{S231\text{-}S518}$, $_{An(WP251)}AIP56^{R318\text{-}I515}$, $_{En}PUF^{A513\text{-}L704}$ or $_{Dpp}PUF^{L244\text{-}S422}$. Mortalities were recorded until three consecutive days with no mortality.

Groups of 10 fish (average body weight of 9.3 ± 4.3 g for experiment 1) or 6 fish (average body weight of 14.0 ± 3.7 g for experiment 2) were inoculated with 100 µl of AIP56 at a dose of 0.2 (experiment 1) or 0.3 (experiment 2) µg toxin/g of body weight or AIP56 mixed with 400-fold (experiment 1) or 300-fold (experiment 2) molar excess of the RBD of AIP56 *(*$AIP56^{T299\text{-}N497}$*)*, the catalytic domain of AIP56 ($AIP56^{N1\text{-}G256}$) or Dl-LRP1X1-C4. Sea bass were also injected with $AIP56^{AAIVAA}$ (at the same dose of AIP56) mixed with 300-fold molar excess of Dl-LRP1X1-C4, or 400-fold molar excess of Dl-LRP1X1-C4 alone. Mortalities were recorded until three consecutive days with no mortality.

Groups of 10 fish (average body weight of 51.0 ± 4.0 g and 68.3 ± 7.7 g for experiment 1 and 2, respectively) were inoculated with 100 µl AIP56, $AIP56^{K350A}$, $AIP56^{K356A}$, $AIP56^{K365A}$, $AIP56^{R441A}$, $AIP56^{K467A}$ or $AIP56^{K350A/R441A}$ at a dose of 0.15 µg toxin/g of body weight (experiment 1) or 0.1 µg toxin/g body weight (experiment 2). Mortalities were recorded until three consecutive days with no mortality.

5. Supplementary Data

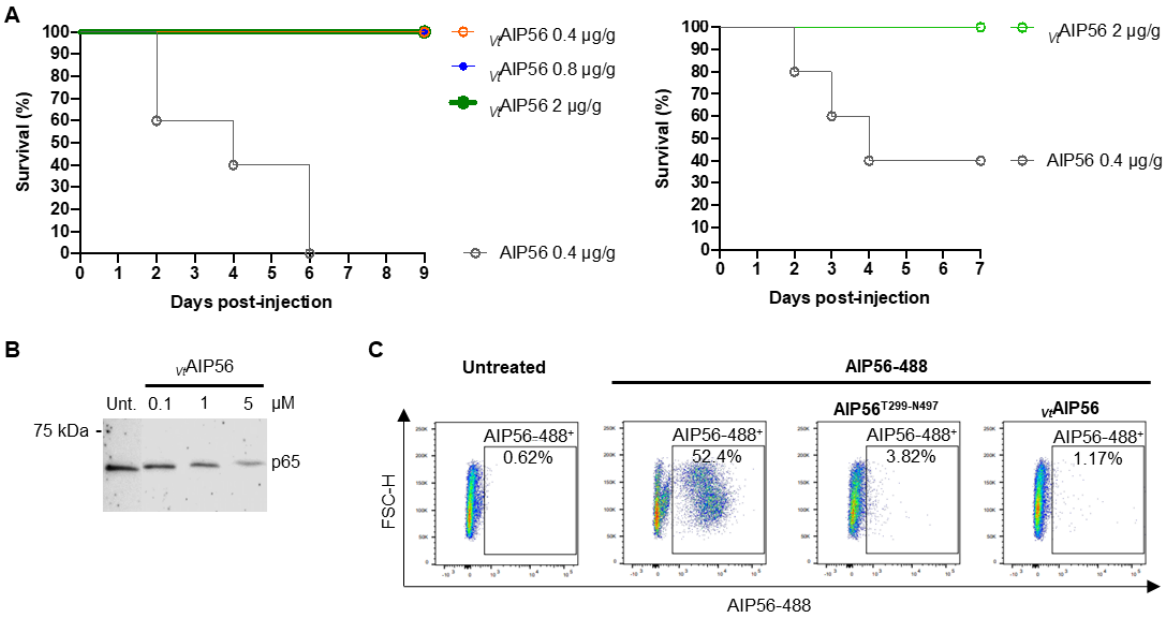

***Supplementary Figure 1.* $_{vt}$AIP56 is nontoxic for sea bass.** $_{vt}$AIP56 is secreted by *Vibrio tarriae*, a novel member of the *Cholerae* clade, which was isolated from humans [18,19]. As the putative RBD of $_{vt}$AIP56 competed for the same receptor as AIP56 in sbPL (Figure 2A), *in vivo* toxicity of $_{vt}$AIP56 in sea bass was tested, using AIP56 as positive control. **(A)** Kaplan-Meyer survival curves of sea bass injected with the indicated doses (µg/g of fish body weight) of $_{vt}$AIP56 or AIP56 (10 fish/treatment). Injection of sea bass with 0.4 µg AIP56 per gram of body weight resulted in 100% (experiment 1) and 60% (experiment 2) mortality, whereas no mortality was observed following injection of 0.4, 0.8 or 2 µg $_{vt}$AIP56 per gram of body weight. These data show that $_{vt}$AIP56 is not lethal for sea bass. **(B)** *In vitro* NF-κB p65 cleavage assay showing that the recombinant $_{vt}$AIP56 used in the *in vivo* intoxication challenges is catalytic active. HeLa cells lysates (2 × 10^6 cells/20 µl each condition) were left untreated or incubated at 22 ºC for 2 h with 0.1, 1 or 5 µM of $_{vt}$AIP56 in lysis buffer (10 mM Tris-HCl pH=8.0; 150 mM NaCl, 0.5% (v/v) Triton X-100; 10% (v/v) glycerol) and the cleavage of NF-κB p65 was analyzed by western blotting. **(C)** Representative flow cytometry plots of *ex vivo* competition assays for AIP56-488 internalization (n=2), showing that the recombinant $_{vt}$AIP56 used in the *in vivo* intoxication challenges binds to AIP56 receptor. sbPL were left untreated or pre-incubated on ice for 15 min with 18 µM $_{vt}$AIP56 or AIP56$^{T299-N497}$ (as control). AIP56-488 (0.09 µM) was added to the cells for 15 min on ice, followed by an incubation of 15 min at 22 ºC. Internalization of AIP56-488 was analyzed by flow cytometry. Untreated cells or cells incubated only with 0.09 µM AIP56 were used as controls.

These results suggest that the absence of $_{vt}$AIP56 toxicity in sea bass may be attributed to its eventual inability to translocate into the cytosol of target cells, possibly due to a differential interaction with an unknown co-receptor. Additionally, the complexity of biological processes occurring *in vivo* may contribute to this outcome

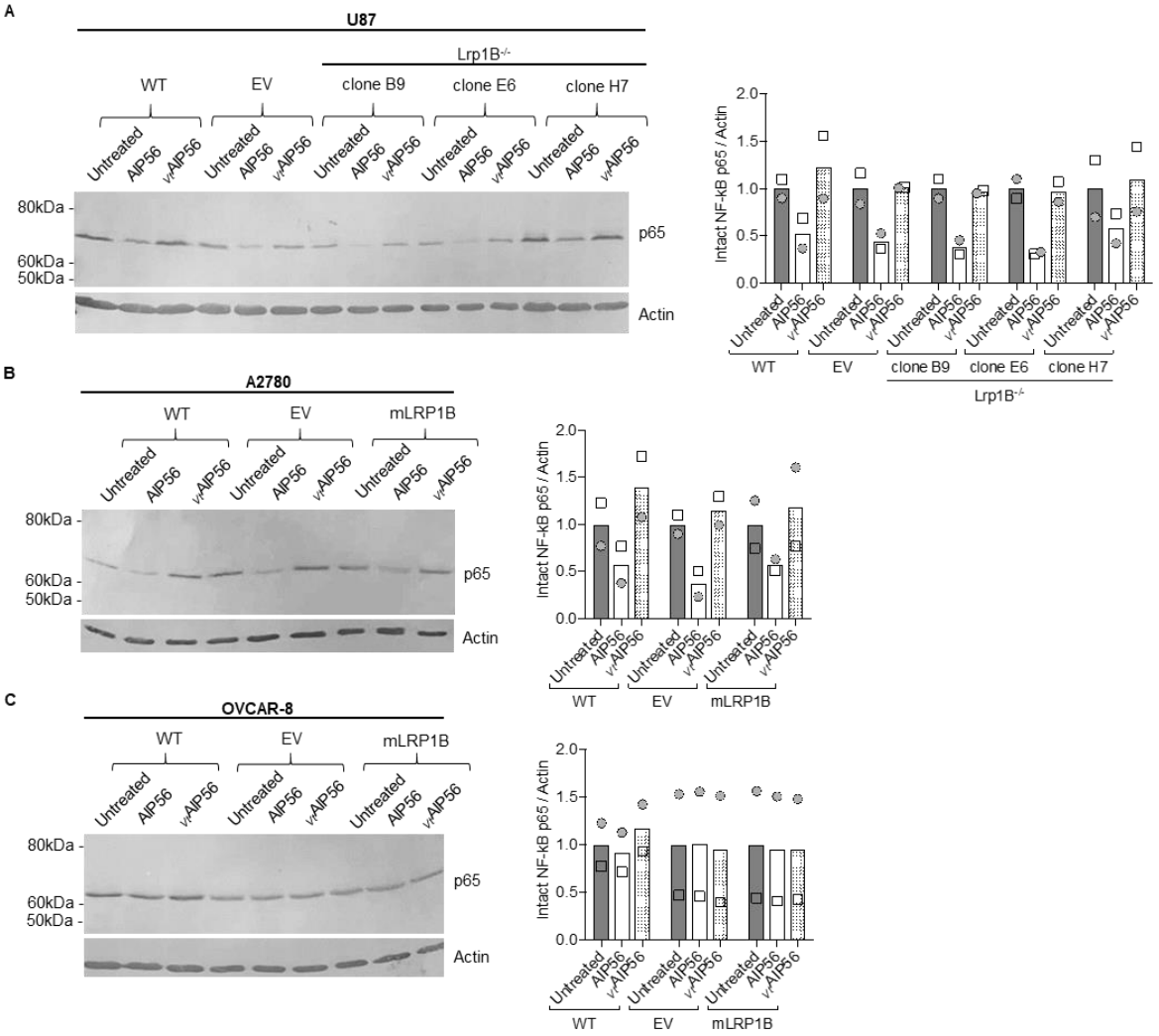

***Supplementary Figure 2*. LRP1B does not mediate AIP56 and $_{Vt}$AIP56 internalization in human cells.** To investigate whether LRP1B contributes to the internalization of AIP56, intoxication experiments were done using human cell lines in which *Lrp1B* has been knocked out (KO) (U87, human glioblastoma cell line) (Peixoto *et al*. IJMS. 2023; 24(14):11285. https://doi.org/10.3390/ijms241411285) or in which C4-containing mini-LRP1B (mLRP1BC4) has been overexpressed (A2780 and OVCAR-8, ovarian cancer cell lines) (Dionísio de Sousa IJ *et al*. Pathobiology. 2021;88(6):400-411. https://doi.org/10.1159/000517372). **(A)** U87 *Lrp1B* KO cells (three clones - B9, H6 and E7 - were chosen to represent different genetic backgrounds and phenotypic characteristics https://doi.org/10.3390/ijms241411285), alongside wild-type (WT) and empty vector (EV)-transformed control cells were incubated with 535 nM of AIP56 or $_{Vt}$AIP56 (AIP56-like toxin from *Vibrio tarriae*) for 6 h at 37 ºC with 5% CO_2 in DMEM high glucose medium supplemented with 10% (v/v) FBS and 1% (v/v) penicillin/streptomycin (P/S). The p65 cleavage was similar in *Lrp1B* KO and control cells, showing that in this cell type, LRP1B is dispensable for AIP56 intoxication. However, as U87 cells also express LRP1, it cannot be concluded whether this is because LRP1B is not a receptor for AIP56 or whether expression of LRP1 in U87 cells is sufficient for intoxication to occur. **(B)** A2780 or **(C)** OVCAR-8 cells overexpressing mLRP1B-C4, alongside WT and EV-transformed control cells were incubated with 535 nM of AIP56 or $_{Vt}$AIP56 for 6 h at 37 ºC with 5% CO_2 in RPMI 1640 medium supplemented with 10% (v/v) FBS and 1% (v/v) P/S. **(B)** Despite A2780 cells naturally express LRP1B and LRP1, they were transfected with mLRP1BC4 in order to evaluate whether its overexpression (confirmed by Dionísio de Sousa IJ *et al*. Pathobiology. 2021;88(6):400-411. https://doi.org/10.1159/000517372) would potentiate AIP56 intoxication, using p65 cleavage as read-out. Since there was no increase in p65

cleavage in A2780 overexpressing mLRP1BC4, the experiment was repeated in the OVCAR-8 cell line, which have minimal or no expression of LRP1B and LRP1 **(C)**. In this case, AIP56 did not cleave p65 neither in wild-type cells or in cells overexpressing mLRP1BC4, further supporting that LRP1B does not mediate AIP56 uptake. However, it must be considered that in the overexpression experiments only the mini receptor containing cluster 4 of LRP1B was overexpressed. Therefore, although AIP56 binds to cluster 4 of LRP1, we cannot rule out that, in the case of LRP1B, it may bind to other clusters. **(A, B and C)** Since *Vt*AIP56 is present in the genome of a *Vibrio* isolated from humans, the experiments mentioned above were also performed with *Vt*AIP56. Surprisingly, *Vt*AIP56 did not cleave p65 in any of the cell lines tested. This may be because although it blocks the internalization of AIP56 when used as a competitor, it may interact with a distinct co-receptor or factors required for its translocation that are absent in the tested cells.

For quantification, loading correction was achieved by dividing the density of intact p65 band by the density of actin band from the same lane. Results shown in the graph correspond to fold-changes in the normalized density of p65 band relative to the untreated control. Results from each independent experiment are represented by the same symbol (n=2).

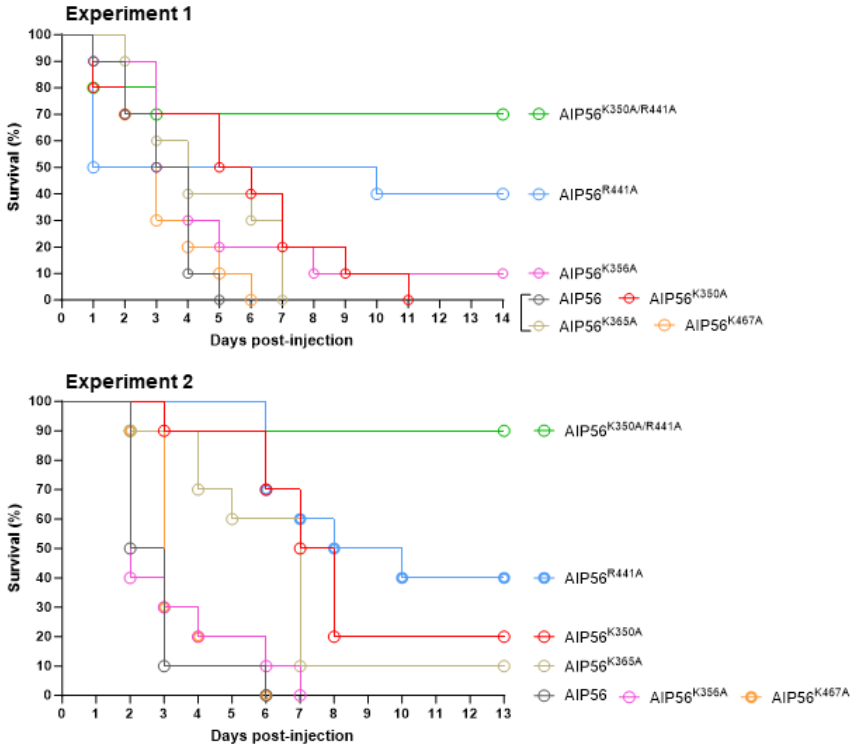

***Supplementary Figure 3*. Higher doses of AIP56 mutants confirm the involvement of residues K350 and R441 in AIP56 toxicity for sea bass.** Kaplan-Meyer survival curves of sea bass injected with 0.6 µg/g of body weight (experiment 1) or 0.4 µg/g of body weight (experiment 2) of AIP56 or AIP56 mutants. The two independent experiments (n=2) were performed using 10 fish/treatment and in parallel with experiments 1 and 2, respectively, shown in Figure 7. Despite overall lower survival rates observed in these experiments due to the higher doses used (i.e, 4-times higher than the doses used in experiments shown in Figure 7), fish injected with AIP56$^{K350A/R441A}$, AIP56^{K350A} or AIP56^{R441A} consistently showed higher survival than those injected with wild-type AIP56. These results reinforce the crucial role of the amino acid residues K350 and R441 for AIP56-induced lethality in sea bass.

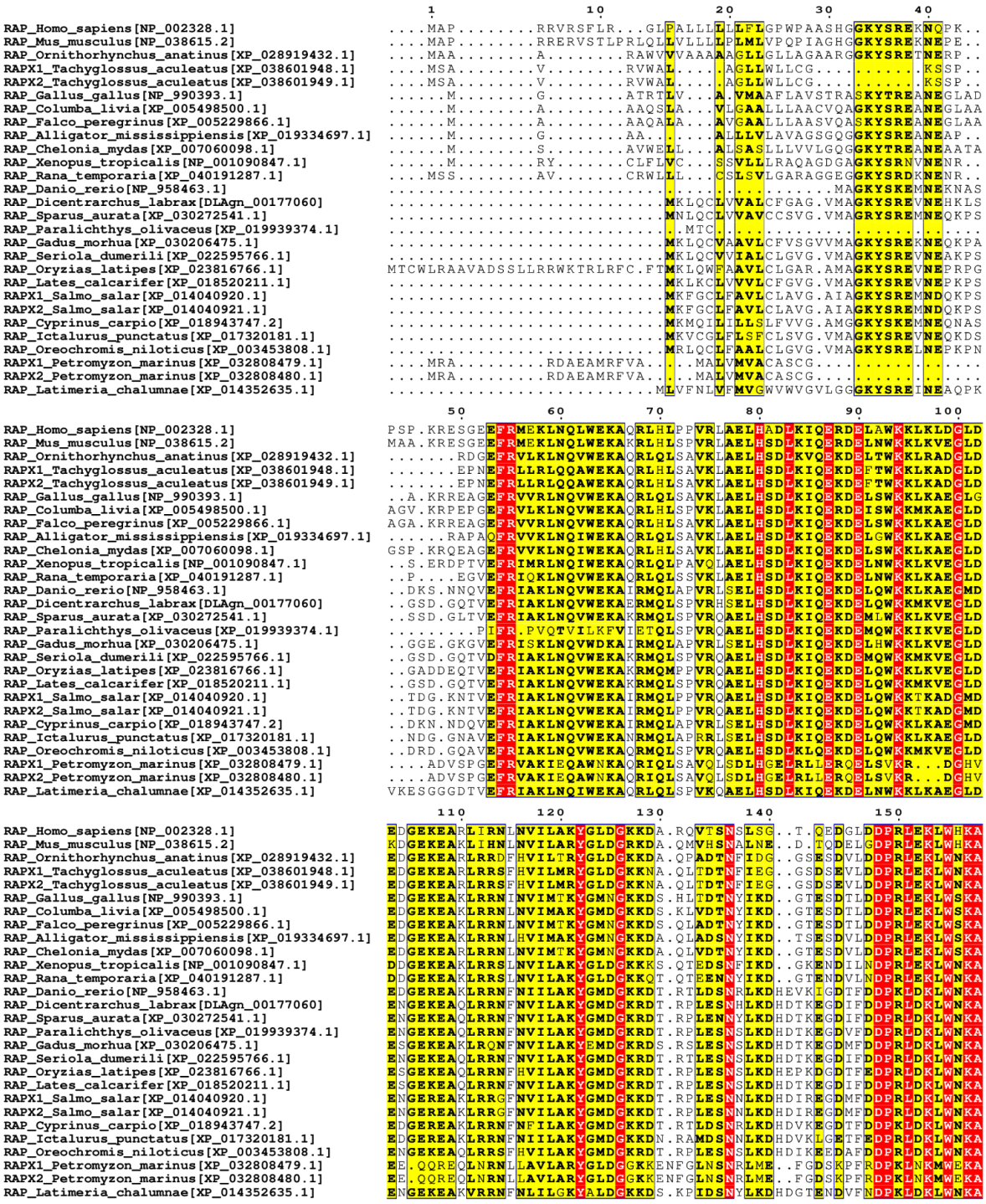
RAP_Homo_sapiens[NP_002328.1]
RAP_Mus_musculus[NP_038615.2]
RAP_Ornithorhynchus_anatinus[XP_028919432.1]
RAPX1_Tachyglossus_aculeatus[XP_038601948.1]
RAPX2_Tachyglossus_aculeatus[XP_038601949.1]
RAP_Gallus_gallus[NP_990393.1]
RAP_Columba_livia[XP_005498500.1]
RAP_Falco_peregrinus[XP_005229866.1]
RAP_Alligator_mississippiensis[XP_019334697.1]
RAP_Chelonia_mydas[XP_007060098.1]
RAP_Xenopus_tropicalis[NP_001090847.1]
RAP_Rana_temporaria[XP_040191287.1]
RAP_Danio_rerio[NP_958463.1]
RAP_Dicentrarchus_labrax[DLAgn_00177060]
RAP_Sparus_aurata[XP_030272541.1]
RAP_Paralichthys_olivaceus[XP_019939374.1]
RAP_Gadus_morhua[XP_030206475.1]
RAP_Seriola_dumerili[XP_022595766.1]
RAP_Oryzias_latipes[XP_023816766.1]
RAP_Lates_calcarifer[XP_018520211.1]
RAPX1_Salmo_salar[XP_014040920.1]
RAPX2_Salmo_salar[XP_014040921.1]
RAP_Cyprinus_carpio[XP_018943747.2]
RAP_Ictalurus_punctatus[XP_017320181.1]
RAP_Oreochromis_niloticus[XP_003453808.1]
RAPX1_Petromyzon_marinus[XP_032808479.1]
RAPX2_Petromyzon_marinus[XP_032808480.1]
RAP_Latimeria_chalumnae[XP_014352635.1]

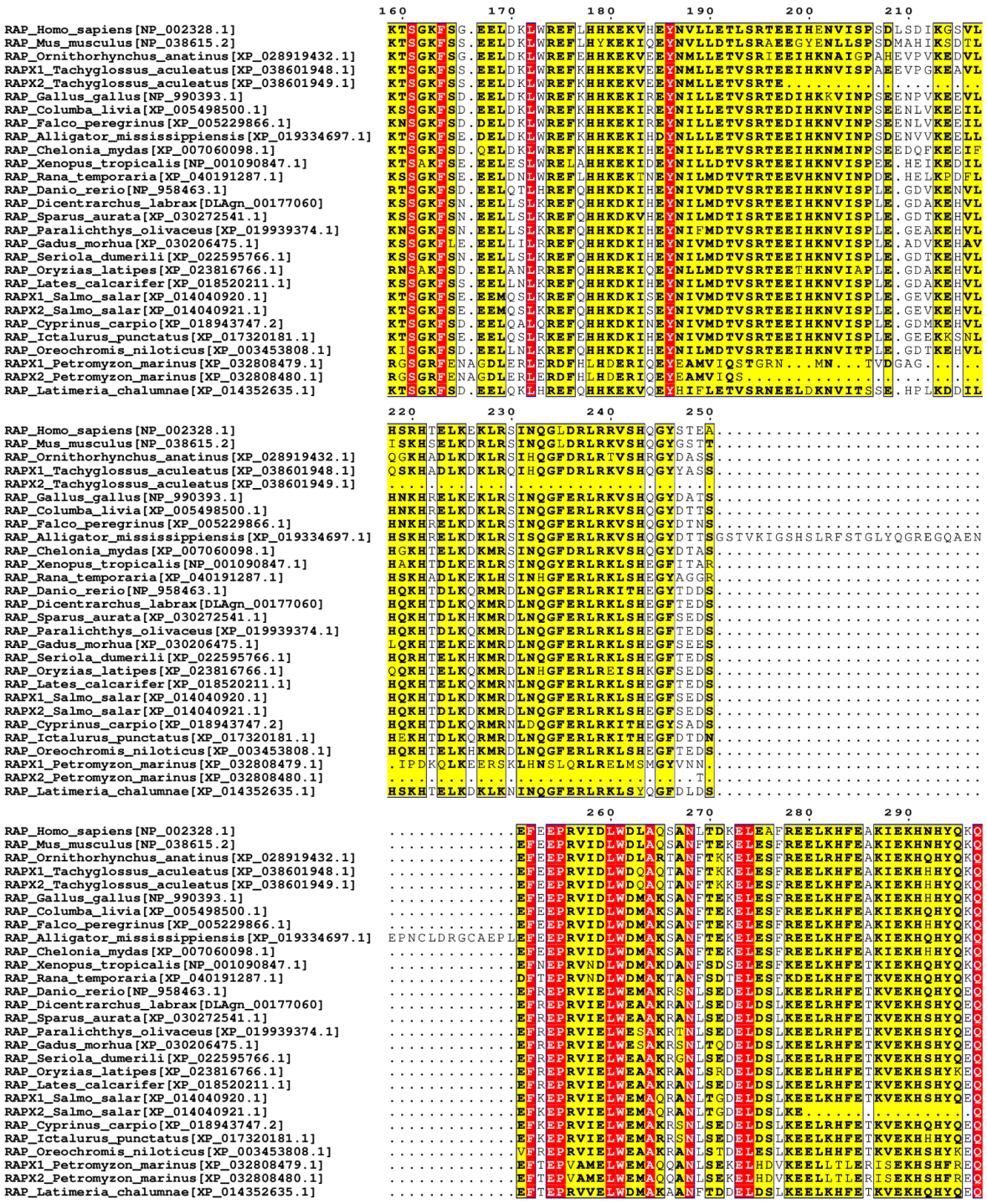
160 170 180 190 200 210
RAP_Homo_sapiens[NP_002328.1]
RAP_Mus_musculus[NP_038615.2]
RAP_Ornithorhynchus_anatinus[XP_028919432.1]
RAPX1_Tachyglossus_aculeatus[XP_038601948.1]
RAPX2_Tachyglossus_aculeatus[XP_038601949.1]
RAP_Gallus_gallus[NP_990393.1]
RAP_Columba_livia[XP_005498500.1]
RAP_Falco_peregrinus[XP_005229866.1]
RAP_Alligator_mississippiensis[XP_019334697.1]
RAP_Chelonia_mydas[XP_007060098.1]
RAP_Xenopus_tropicalis[NP_001090847.1]
RAP_Rana_temporaria[XP_040191287.1]
RAP_Danio_rerio[NP_958463.1]
RAP_Dicentrarchus_labrax[DLAgn_00177060]
RAP_Sparus_aurata[XP_030272541.1]
RAP_Paralichthys_olivaceus[XP_019939374.1]
RAP_Gadus_morhua[XP_030206475.1]
RAP_Seriola_dumerili[XP_022595766.1]
RAP_Oryzias_latipes[XP_023816766.1]
RAP_Lates_calcarifer[XP_018520211.1]
RAPX1_Salmo_salar[XP_014040920.1]
RAPX2_Salmo_salar[XP_014040921.1]
RAP_Cyprinus_carpio[XP_018943747.2]
RAP_Ictalurus_punctatus[XP_017320181.1]
RAP_Oreochromis_niloticus[XP_003453808.1]
RAPX1_Petromyzon_marinus[XP_032808479.1]
RAPX2_Petromyzon_marinus[XP_032808480.1]
RAP_Latimeria_chalumnae[XP_014352635.1]
220 230 240 250
RAP_Homo_sapiens[NP_002328.1]
RAP_Mus_musculus[NP_038615.2]
RAP_Ornithorhynchus_anatinus[XP_028919432.1]
RAPX1_Tachyglossus_aculeatus[XP_038601948.1]
RAPX2_Tachyglossus_aculeatus[XP_038601949.1]
RAP_Gallus_gallus[NP_990393.1]
RAP_Columba_livia[XP_005498500.1]
RAP_Falco_peregrinus[XP_005229866.1]
RAP_Alligator_mississippiensis[XP_019334697.1]
RAP_Chelonia_mydas[XP_007060098.1]
RAP_Xenopus_tropicalis[NP_001090847.1]
RAP_Rana_temporaria[XP_040191287.1]
RAP_Danio_rerio[NP_958463.1]
RAP_Dicentrarchus_labrax[DLAgn_00177060]
RAP_Sparus_aurata[XP_030272541.1]
RAP_Paralichthys_olivaceus[XP_019939374.1]
RAP_Gadus_morhua[XP_030206475.1]
RAP_Seriola_dumerili[XP_022595766.1]
RAP_Oryzias_latipes[XP_023816766.1]
RAP_Lates_calcarifer[XP_018520211.1]
RAPX1_Salmo_salar[XP_014040920.1]
RAPX2_Salmo_salar[XP_014040921.1]
RAP_Cyprinus_carpio[XP_018943747.2]
RAP_Ictalurus_punctatus[XP_017320181.1]
RAP_Oreochromis_niloticus[XP_003453808.1]
RAPX1_Petromyzon_marinus[XP_032808479.1]
RAPX2_Petromyzon_marinus[XP_032808480.1]
RAP_Latimeria_chalumnae[XP_014352635.1]
260 270 280 290
RAP_Homo_sapiens[NP_002328.1]
RAP_Mus_musculus[NP_038615.2]
RAP_Ornithorhynchus_anatinus[XP_028919432.1]
RAPX1_Tachyglossus_aculeatus[XP_038601948.1]
RAPX2_Tachyglossus_aculeatus[XP_038601949.1]
RAP_Gallus_gallus[NP_990393.1]
RAP_Columba_livia[XP_005498500.1]
RAP_Falco_peregrinus[XP_005229866.1]
RAP_Alligator_mississippiensis[XP_019334697.1]
RAP_Chelonia_mydas[XP_007060098.1]
RAP_Xenopus_tropicalis[NP_001090847.1]
RAP_Rana_temporaria[XP_040191287.1]
RAP_Danio_rerio[NP_958463.1]
RAP_Dicentrarchus_labrax[DLAgn_00177060]
RAP_Sparus_aurata[XP_030272541.1]
RAP_Paralichthys_olivaceus[XP_019939374.1]
RAP_Gadus_morhua[XP_030206475.1]
RAP_Seriola_dumerili[XP_022595766.1]
RAP_Oryzias_latipes[XP_023816766.1]
RAP_Lates_calcarifer[XP_018520211.1]
RAPX1_Salmo_salar[XP_014040920.1]
RAPX2_Salmo_salar[XP_014040921.1]
RAP_Cyprinus_carpio[XP_018943747.2]
RAP_Ictalurus_punctatus[XP_017320181.1]
RAP_Oreochromis_niloticus[XP_003453808.1]
RAPX1_Petromyzon_marinus[XP_032808479.1]
RAPX2_Petromyzon_marinus[XP_032808480.1]
RAP_Latimeria_chalumnae[XP_014352635.1]

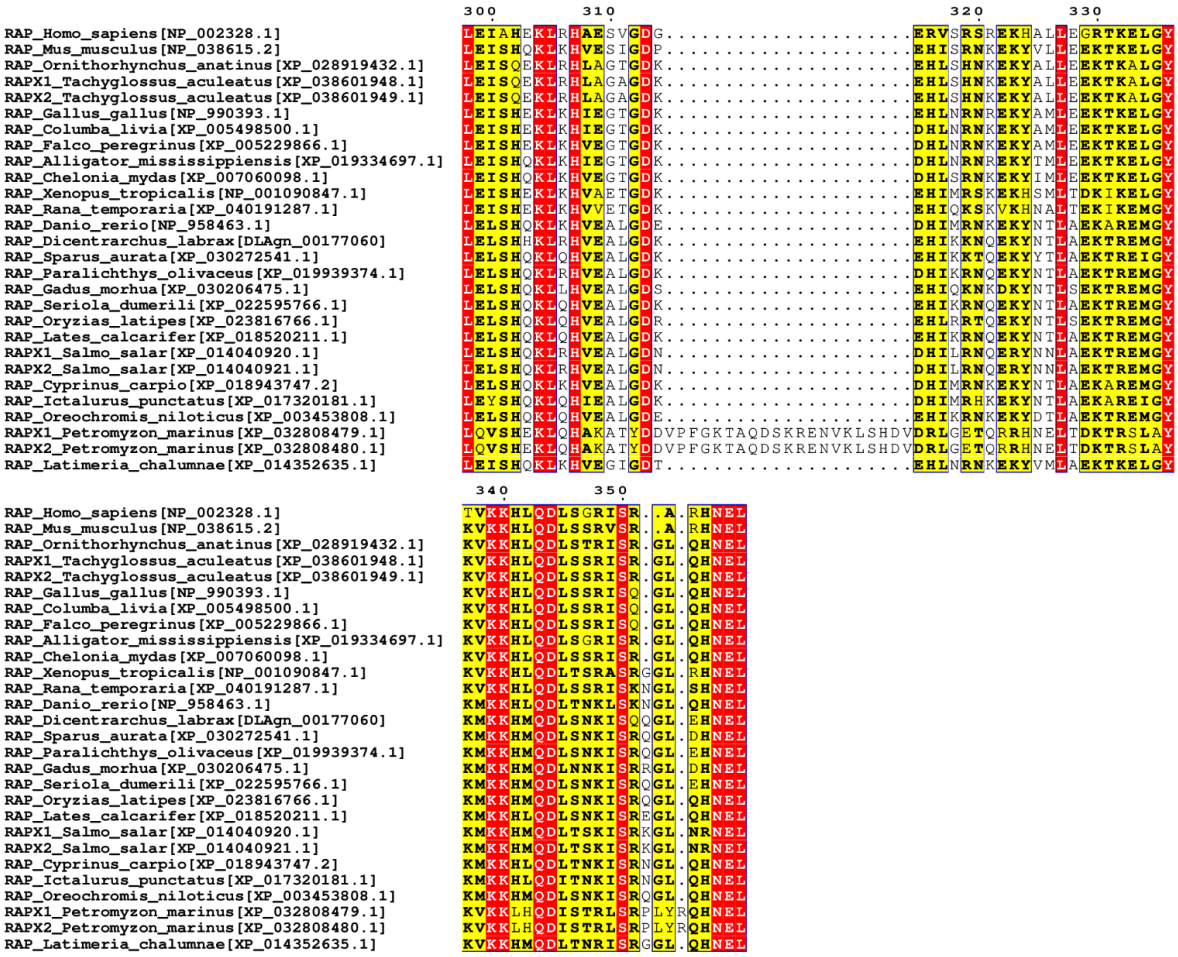

***Supplementary Figure 4*. RAP is conserved across different species.** Sequence alignment of the complete proteins was performed by Clustal Omega, with default parameters. Final image was obtained by ESPript. Identical and similar residues are highlighted in red and yellow, respectively.

Supplementary Table 1. Competition assay for AIP56-488 internalization in sbPL, using RAP molecules (n=3 for sbPL and n=2 for mBMDM. Values are average ± SD).

Cells	Condition	Percentage of AIP56-488$^+$ cells	MFI of AIP56-488$^+$ cells[1]
mBMDM	Untreated	0.00% ± 0.00	1.00 ± 0.15
	AIP56-488 (0.09 μM)	98.50% ± 0.00	14.58 ± 5.01
	AIP56$^{T299\text{-}N497}$ (9 μM) + AIP56-488 (0.09 μM)	53.45% ± 2.47	5.87 ± 2.13
	Hs-RAP (9 μM) + AIP56-488 (0.09 μM)	37.90% ± 2.97	4.47 ± 1.34
sbPL	Untreated	0.07% ± 0.09	1.00 ± 0.25
	AIP56-488 (0.09 μM)	42.38% ± 13.03	12.64 ± 5.11
	AIP56$^{T299\text{-}N497}$ (9 μM) + AIP56-488 (0.09 μM)	5.80% ± 5.22	1.85 ± 0.61
	Hs-RAP (9 μM) + AIP56-488 (0.09 μM)	36.83% ± 9.82	4.08 ± 1.80
sbPL	Untreated	0.62% ± 1.08	1.00 ± 0.13
	AIP56-488 (0.09 μM)	64.90% ± 4.78	13.53 ± 6.60
	AIP56$^{T299\text{-}N497}$ (9 μM) + AIP56-488 (0.09 μM)	7.64% ± 1.41	2.58 ± 0.72
	Hs-RAP-D3 (9 μM) + AIP56-488 (0.09 μM)	47.23% ± 16.73	4.41 ± 2.18
sbPL	Untreated	0.01% ± 0.01	1.00 ± 0.40
	AIP56-488 (0.09 μM)	67.33% ± 2.76	13.59 ± 4.01
	AIP56$^{T299\text{-}N497}$ (9 μM) + AIP56-488 (0.09 μM)	1.52% ± 1.13	2.70 ± 1.76
	Dl-RAP-D3 (9 μM) + AIP56-488 (0.09 μM)	56.35% ± 7.60	6.41 ± 1.52
sbPL	Untreated	0.01% ± 0.01	1.00 ± 0.19
	AIP56-488 (0.09 μM)	49.13% ± 4.79	9.32 ± 3.49
	AIP56$^{T299\text{-}N497}$ (9 μM) + AIP56-488 (0.09 μM)	3.95% ± 1.45	1.54 ± 0.38
	Hs-RAP-D3 (36 μM) + AIP56-488 (0.09 μM)	41.83% ± 5.52	2.97 ± 0.15
	Dl-RAP-D3 (36 μM) + AIP56-488 (0.09 μM)	51.6% ± 3.30	5.65 ± 2.26

[1]MFI (Median Fluorescence Intensity) results are presented as fold-change in fluorescence intensity relative to untreated cells (control).

Supplementary Table 2. Competition assay for AIP56-488 internalization in sbPL, using LRP1-C4 (n=4. Values are average ± SD).

Condition	Percentage of AIP56-488$^+$ cells	MFI of AIP56-488$^+$ cells[1]
Untreated	0.02% ± 0.00	1.00 ± 0.20
AIP56-488 (0.09 μM)	65.83% ± 0.06	7.34 ± 1.05
AIP56$^{T299\text{-}N497}$ (36 μM) + AIP56-488 (0.09 μM)	1.88% ± 0.01	1.25 ± 0.18
Dl-LRP1X1-C4 (36 μM) + AIP56-488 (0.09 μM)	0.83% ± 0.01	1.34 ± 0.37
Dl-LRP1X2-C4 (36 μM) + AIP56-488 (0.09 μM)	49.58% ± 0.13	1.49 ± 0.21
Hs-LRP1-C4 (36 μM) + AIP56-488 (0.09 μM)	67.50% ± 0.09	3.00 ± 0.29

[1]MFI (Median Fluorescence Intensity) results are presented as fold-change in fluorescence intensity relative to untreated cells (control).

References

1. do Vale, A.; Silva, M.T.; Dos Santos, N.M.S.; Nascimento, D.S.; Reis-Rodrigues, P.; Costa-Ramos, C.; Ellis, A.E.; Azevedo, J.E. AIP56, a Novel Plasmid-Encoded Virulence Factor of *Photobacterium Damselae* Subsp. *piscicida* with Apoptogenic Activity against Sea Bass Macrophages and Neutrophils. *Mol Microbiol* 2005, *58*, 1025–1038, doi:10.1111/j.1365-2958.2005.04893.x.
2. do Vale, A.; Pereira, C.; R. Osorio, C.; M. S. dos Santos, N. The Apoptogenic Toxin AIP56 Is Secreted by the Type II Secretion System of *Photobacterium Damselae* Subsp. *piscicida*. *Toxins (Basel)* 2017, *9*, 368, doi:10.3390/toxins9110368.
3. do Vale, A.; Marques, F.; Silva, M.T. Apoptosis of Sea Bass (*Dicentrarchus Labrax L.*) Neutrophils and Macrophages Induced by Experimental Infection with *Photobacterium Damselae* subsp. *piscicida*. *Fish Shellfish Immunol* 2003, *15*, 129–144, doi:10.1016/S1050-4648(02)00144-4.
4. Romalde, J.L. *Photobacterium Damselae* subsp. *piscicida*: An Integrated View of a Bacterial Fish Pathogen. *International Microbiology 2002 5:1* 2002, *5*, 3–9, doi:10.1007/S10123-002-0051-6.
5. Zorrilla, I.; Balebona, M.C.; Moriñigo, M.A.; Sarasquete, C.; Borrego, J.J. Isolation and Characterization of the Causative Agent of Pasteurellosis, *Photobacterium damsela* Ssp. *piscicida*, from Sole, Solea Senegalensis (Kaup). *J Fish Dis* 1999, *22*, 167–172, doi:10.1046/J.1365-2761.1999.00157.X.
6. Liu, P.C.; Lin, J.I.Y.; Lee, K.K. Virulence of *Photobacterium Damselae* subsp. *piscicida* in Cultured Cobia Rachycentron Canadum. *J Basic Microbiol* 2003, *43*, 499–507, doi:10.1002/JOBM.200310301.
7. Andreoni, F.; Magnani, M. Photobacteriosis: Prevention and Diagnosis. *J Immunol Res* 2014, *2014*, 793817, doi:10.1155/2014/793817.
8. Silva, D.S.; Pereira, L.M.G.; Moreira, A.R.; Ferreira-Da-Silva, F.; Brito, R.M. The Apoptogenic Toxin AIP56 Is a Metalloprotease A-B Toxin That Cleaves NF-κB P65. *PLoS Pathog* 2013, *9*, 1003128, doi:10.1371/journal.ppat.1003128.
9. Pereira, L.M.G.; Pinto, R.D.; Silva, D.S.; Moreira, A.R.; Beitzinger, C.; Oliveira, P.; Sampaio, P.; Benz, R.; Azevedo, J.E.; dos Santos, N.M.S.; et al. Intracellular Trafficking of AIP56, an NF-KB-Cleaving Toxin from *Photobacterium Damselae* subsp. *piscicida*. *Infect Immun* 2014, *82*, 5270–5285, doi:10.1128/IAI.02623-14.
10. Gilmore, T.D.; Wolenski, F.S. NF-JB: Where Did It Come from and Why? *Immunol Rev* 2012, *246*, 14–35.
11. do Vale, A.; Costa-Ramos, C.; Silva, A.; Silva, D.S.P.; Gärtner, F.; dos Santos, N.M.S.; Silva, M.T. Systemic Macrophage and Neutrophil Destruction by Secondary Necrosis

Induced by a Bacterial Exotoxin in a Gram-Negative Septicaemia. *Cell Microbiol* 2007, *9*, 988–1003, doi:10.1111/J.1462-5822.2006.00846.X.

12. Freitas, I.L.; Macedo, M.F.; Oliveira, L.; Oliveira, P.; do Vale, A.; dos Santos, N.M. AIP56, an AB Toxin Secreted by *Photobacterium Damselae* subsp. *piscicida*, Has Tropism for Myeloid Cells. *Front Immunol* 2025, *15*, 1527088, doi:10.3389/FIMMU.2024.1527088.
13. Lisboa, J.; Pereira, C.; Pinto, R.D.; Rodrigues, I.S.; Pereira, L.M.G.; Pinheiro, B.; Oliveira, P.; Pereira, P.J.B.; Azevedo, J.E.; Durand, D.; et al. Unconventional Structure and Mechanisms for Membrane Interaction and Translocation of the NF-KB-Targeting Toxin AIP56. *Nature Communications 2023 14:1* 2023, *14*, 1–16, doi:10.1038/s41467-023-43054-z.
14. Turco, M.M.; Sousa, M.C. The Structure and Specificity of the Type III Secretion System Effector NleC Suggest a DNA Mimicry Mechanism of Substrate Recognition. *Biochemistry* 2014, *53*, doi:10.1021/bi500593e.
15. Yen, H.; Ooka, T.; Iguchi, A.; Hayashi, T.; Sugimoto, N.; Tobe, T. NleC, a Type III Secretion Protease, Compromises NF-KB Activation by Targeting P65/RelA. *PLoS Pathog* 2010, *6*, e1001231, doi:10.1371/JOURNAL.PPAT.1001231.
16. Pereira, C.; Rodrigues, I.S.; Pereira, L.M.G.; Lisboa, J.; Pinto, R.D.; Araújo, L.; Oliveira, P.; Benz, R.; Santos, N.M.S.; Vale, A. Role of AIP56 Disulphide Bond and Its Reduction by Cytosolic Redox Systems for Efficient Intoxication. *Cell Microbiol* 2020, *22*, e13109, doi:10.1111/cmi.13109.
17. Duron, O. Arsenophonus Insect Symbionts Are Commonly Infected with APSE, a Bacteriophage Involved in Protective Symbiosis. *FEMS Microbiol Ecol* 2014, *90*, 184–194, doi:10.1111/1574-6941.12381.
18. Liang, K.; Islam, M.T.; Hussain, N.; Winkjer, N.S.; Im, M.S.; Rowe, L.A.; Tarr, C.L.; Boucher, Y. Draft Genome Sequences of Eight Vibrio Sp. Clinical Isolates from across the United States That Form a Basal Sister Clade to Vibrio Cholerae. *Microbiol Resour Announc* 2019, *8*, doi:10.1128/MRA.01473-18.
19. Islam, M.T.; Liang, K.; Orata, F.D.; Im, M.S.; Alam, M.; Lee, C.C.; Boucher, Y.F. Vibrio Tarriae Sp. Nov., a Novel Member of the Cholerae Clade. *Int J Syst Evol Microbiol* 2022, *72*, doi:10.1099/IJSEM.0.005571.
20. Brownlie, J.C.; Johnson, K.N. Symbiont-Mediated Protection in Insect Hosts. *Trends Microbiol* 2009, *17*, 348–354, doi:10.1016/J.TIM.2009.05.005.
21. Verster, K.I.; Cinege, G.; Lipinszki, Z.; Magyar, L.B.; Kurucz, É.; Tarnopol, R.L.; Ábrahám, E.; Darula, Z.; Karageorgi, M.; Tamsil, J.A.; et al. Evolution of Insect Innate Immunity through Domestication of Bacterial Toxins. *Proc Natl Acad Sci U S A* 2023,

120, e2218334120, doi:10.1073/PNAS.2218334120/SUPPL_FILE/PNAS.2218334120.SM01.AVI.

22. Thompson, F.L.; Hoste, B.; Thompson, C.C.; Goris, J.; Gomez-Gil, B.; Huys, L.; Vos, P. De; Swings, J. Enterovibrio Norvegicus Gen. Nov., Sp. Nov., Isolated from the Gut of Turbot (Scophthalmus Maximus) Larvae: A New Member of the Family Vibrionaceae. *Int J Syst Evol Microbiol* 2002, *52*, 2015–2022, doi:10.1099/00207713-52-6-2015.
23. Verster, K.I.; Wisecaver, J.H.; Karageorgi, M.; Duncan, R.P.; Gloss, A.D.; Armstrong, E.E.; Price, D.K.; Menon, A.R.; Ali, Z.M.; Whiteman, N.K.; et al. Horizontal Transfer of Bacterial Cytolethal Distending Toxin B Genes to Insects. *Mol Biol Evol* 2019, *36*, 2105–2110, doi:10.1093/MOLBEV/MSZ146.
24. Rouïl, J.; Jousselin, E.; Coeur d'acier, A.; Cruaud, C.; Manzano-Marın, A. The Protector within: Comparative Genomics of APSE Phages across Aphids Reveals Rampant Recombination and Diverse Toxin Arsenals. *Genome Biol Evol* 2020, *12*, 878–889, doi:10.1093/GBE/EVAA089.
25. Patel, V.; Lynn-Bell, N.; Chevignon, G.; Kucuk, R.A.; Higashi, C.H.V.; Carpenter, M.; Russell, J.A.; Oliver, K.M. Mobile Elements Create Strain-Level Variation in the Services Conferred by an Aphid Symbiont. *Environ Microbiol* 2023, *25*, 3333–3348, doi:10.1111/1462-2920.16520.
26. Príncipe, C.; de Sousa, I.J.D.; Prazeres, H.; Soares, P.; Lima, R.T. LRP1B: A Giant Lost in Cancer Translation. *Pharmaceuticals 2021, Vol. 14, Page 836* 2021, *14*, 836, doi:10.3390/PH14090836.
27. Dieckmann, M.; Dietrich, M.F.; Herz, J. Lipoprotein Receptors-an Evolutionarily Ancient Multifunctional Receptor Family. *Biol Chem* 2010, *391*, 1341–1363, doi:10.1515/BC.2010.129/MACHINEREADABLECITATION/RIS.
28. Gent, J.; Braakman, I. Low-Density Lipoprotein Receptor Structure and Folding. *Cellular and Molecular Life Sciences* 2004, *61*, 2461–2470, doi:10.1007/S00018-004-4090-3/METRICS.
29. Nykjaer, A.; Willnow, T.E. The Low-Density Lipoprotein Receptor Gene Family: A Cellular Swiss Army Knife? *Trends Cell Biol* 2002, *12*, 273–280, doi:10.1016/S0962-8924(02)02282-1.
30. Gonias, S.L.; Campana, W.M. LDL Receptor–Related Protein-1: A Regulator of Inflammation in Atherosclerosis, Cancer, and Injury to the Nervous System. *Am J Pathol* 2014, *184*, 18–27, doi:10.1016/J.AJPATH.2013.08.029.
31. Ganaie, S.S.; Schwarz, M.M.; Mcmillen, C.M.; Leung, D.W.; Amarasinghe, G.K.; Hartman, A.L.; Price, D.A.; Feng, A.X.; Albe, J.R.; Wang, W.; et al. Lrp1 Is a Host

Entry Factor for Rift Valley Fever Virus. *Cell* 2021, *184*, 5163–5178, doi:10.1016/j.cell.2021.09.001.

32. Sizova, O.; John, L.S.; Ma, Q.; Molldrem, J.J. Multi-Faceted Role of LRP1 in the Immune System. 2023, doi:10.3389/fimmu.2023.1166189.
33. Guo, S.; Chen, Y.; Liu, J.; Zhang, X.; Liu, Z.; Zhou, Z.; Wei, W. Low-Density Lipoprotein Receptor-Related Protein 1 Is a CROPs-Associated Receptor for Clostridioides Infection Toxin B. *Sci China Life Sci* 2022, *65*, 107–118, doi:10.1007/S11427-021-1943-9/METRICS.
34. Fisher, C.; Beglova, N.; Blacklow, S.C. Structure of an LDLR-RAP Complex Reveals a General Mode for Ligand Recognition by Lipoprotein Receptors. *Mol Cell* 2006, *22*, 277–283, doi:10.1016/J.MOLCEL.2006.02.021.
35. De Nardis, C.; Lossl, P.; Van Den Biggelaar, M.; Madoori, P.K.; Leloup, N.; Mertens, K.; Heck, A.J.R.; Gros, P.; Allewell, N. Recombinant Expression of the Full-Length Ectodomain of LDL Receptor-Related Protein 1 (LRP1) Unravels PH-Dependent Conformational Changes and the Stoichiometry of Binding with Receptor-Associated Protein (RAP). *Journal of Biological Chemistry* 2017, *292*, 912–924, doi:10.1074/JBC.M116.758862.
36. Neels, J.G.; Van Den Berg, B.M.M.; Lookene, A.; Olivecrona, G.; Pannekoekt, H.; Van Zonneveld, A.J. The Second and Fourth Cluster of Class A Cysteine-Rich Repeats of the Low Density Lipoprotein Receptor-Related Protein Share Ligand-Binding Properties. *J Biol Chem* 1999, *274*, 31305–31311, doi:10.1074/JBC.274.44.31305.
37. Prasad, J.M.; Migliorini, M.; Galisteo, R.; Strickland, D.K. Generation of a Potent Low Density Lipoprotein Receptor-Related Protein 1 (LRP1) Antagonist by Engineering a Stable Form of the Receptor-Associated Protein (RAP) D3 Domain. *Journal of Biological Chemistry* 2015, *290*, 17262–17268, doi:10.1074/JBC.M115.660084.
38. Freitas, I.L.; Teixeira, A.; Loureiro, I.; Lisboa, J.; Saraiva, A.; Dos Santos, N.M.S.; do Vale, A. Susceptibility of Sea Bream (*Sparus aurata*) to AIP56, an AB-Type Toxin Secreted by *Photobacterium Damselae* subsp. *piscicida*. *Toxins (Basel)* 2022, *14*, doi:10.3390/TOXINS14020119.
39. Pastrana, D. V.; Hanson, A.J.; Knisely, J.; Bu, G.; FitzGerald, D.J. LRP1B Functions as a Receptor for Pseudomonas Exotoxin. *Biochimica et Biophysica Acta (BBA) - Molecular Basis of Disease* 2005, *1741*, 234–239, doi:10.1016/J.BBADIS.2005.06.007.
40. Obermoeller-McCormick, L.M.; Li, Y.; Osaka, H.; FitzGerald, D.J.; Schwartz, A.L.; Bu, G. Dissection of Receptor Folding and Ligand-Binding Property with Functional Minireceptors of LDL Receptor-Related Protein. *J Cell Sci* 2001, *114*, 899–908, doi:10.1242/JCS.114.5.899.

41. Dionísio De Sousa, I.J.; Cunha, A.I.; Saraiva, I.A.; Portugal, R. V.; Gimba, E.R.P.; Guimarães, M.; Prazeres, H.; Lopes, J.M.; Soares, P.; Lima, R.T. LRP1B Expression as a Putative Predictor of Response to Pegylated Liposomal Doxorubicin Treatment in Ovarian Cancer. *Pathobiology* 2021, *88*, 400–411, doi:10.1159/000517372.
42. Van Den Biggelaar, M.; Madsen, J.J.; Faber, J.H.; Zuurveld, M.G.; Van Der Zwaan, C.; Olsen, O.H.; Stennicke, H.R.; Mertens, K.; Meijer, A.B. Factor VIII Interacts with the Endocytic Receptor Low-Density Lipoprotein Receptor-Related Protein 1 via an Extended Surface Comprising “Hot-Spot” Lysine Residues. *Journal of Biological Chemistry* 2015, *290*, 16463–16476, doi:10.1074/jbc.M115.650911.
43. Migliorini, M.; Li, S.H.; Zhou, A.; Emal, C.D.; Lawrence, D.A.; Strickland, D.K. High-Affinity Binding of Plasminogen-Activator Inhibitor 1 Complexes to LDL Receptor-Related Protein 1 Requires Lysines 80, 88, and 207. *Journal of Biological Chemistry* 2020, *295*, 212–222, doi:10.1074/jbc.RA119.010449.
44. Prasad, J.M.; Young, P.A.; Strickland, D.K. High Affinity Binding of the Receptor-Associated Protein D1D2 Domains with the Low Density Lipoprotein Receptorrelated Protein (LRP1) Involves Bivalent Complex Formation: Critical Roles of Lysines 60 and 191. *Journal of Biological Chemistry* 2016, *291*, 18430–18439, doi:10.1074/jbc.M116.744904.
45. Chen, K.; Martens, Y.A.; Meneses, A.; Ryu, D.H.; Lu, W.; Raulin, A.C.; Li, F.; Zhao, J.; Chen, Y.; Jin, Y.; et al. LRP1 Is a Neuronal Receptor for α-Synuclein Uptake and Spread. *Mol Neurodegener* 2022, *17*, doi:10.1186/s13024-022-00560-w.
46. Migliorini, M.M.; Behre, E.H.; Brew, S.; Ingham, K.C.; Strickland, D.K. Allosteric Modulation of Ligand Binding to Low Density Lipoprotein Receptor-Related Protein by the Receptor-Associated Protein Requires Critical Lysine Residues within Its Carboxyl-Terminal Domain. *Journal of Biological Chemistry* 2003, *278*, 17986–17992, doi:10.1074/jbc.M212592200.
47. Ramos-Pinto, L.; Azeredo, R.; Silva, C.; Conceição, L.E.C.; Dias, J.; Montero, D.; Torrecillas, S.; Silva, T.S.; Costas, B. Short-Term Supplementation of Dietary Arginine and Citrulline Modulates Gilthead Seabream (*Sparus aurata*) Immune Status. *Front Immunol* 2020, *11*, doi:10.3389/fimmu.2020.01544.
48. Herz, J.; Bock, H.H. Lipoprotein Receptors in the Nervous System. *Annu Rev Biochem* 2002, *71*, 405–434, doi:10.1146/ANNUREV.BIOCHEM.71.110601.135342.
49. Herz, J.; Strickland, D.K. LRP: A Multifunctional Scavenger and Signaling Receptor. *Journal of Clinical Investigation* 2001, *108*, 779–784, doi:10.1172/jci13992.
50. Kounnas, M.Z.; Morris, R.E.; Thompson, M.R.; FitzGerald, D.J.; Strickland, D.K.; Saelinger, C.B. The Alpha 2-Macroglobulin Receptor/Low Density Lipoprotein Receptor-Related Protein Binds and Internalizes Pseudomonas Exotoxin A. *Journal*

of Biological Chemistry 1992, *267*, 12420–12423, doi:10.1016/S0021-9258(18)42291-0.

51. Schorch, B.; Song, S.; Van Diemen, F.R.; Bock, H.H.; May, P.; Herz, J.; Brummelkamp, T.R.; Papatheodorou, P.; Aktories, K. LRP1 Is a Receptor for Clostridium Perfringens TpeL Toxin Indicating a Two-Receptor Model of Clostridial Glycosylating Toxins. *Proc Natl Acad Sci U S A* 2014, *111*, 6431–6436, doi:10.1073/PNAS.1323790111/SUPPL_FILE/PNAS.201323790SI.PDF.
52. Schöttelndreier, D.; Langejürgen, A.; Lindner, R.; Genth, H. Low Density Lipoprotein Receptor-Related Protein-1 (LRP1) Is Involved in the Uptake of Clostridioides Difficile Toxin A and Serves as an Internalizing Receptor. *Front Cell Infect Microbiol* 2020, *10*, 565465, doi:10.3389/FCIMB.2020.565465/BIBTEX.
53. Zhou, Y.; Li, D.; Li, D.; Chen, A.; He, L.; Luo, J.; Tao, L. LDLR, LRP1, and Megalin Redundantly Participate in the Uptake of Clostridium Novyi Alpha-Toxin. *Commun Biol* 2022, *5*, 906, doi:10.1038/S42003-022-03873-0.
54. Schoellkopf, J.; Mueller, T.; Hippchen, L.; Mueller, T.; Reuten, R.; Backofen, R.; Orth, J.; Schmidt, G. Genome Wide CRISPR Screen for Pasteurella Multocida Toxin (PMT) Binding Proteins Reveals LDL Receptor Related Protein 1 (LRP1) as Crucial Cellular Receptor. *PLoS Pathog* 2022, *18*, e1010781, doi:10.1371/JOURNAL.PPAT.1010781.
55. Blacklow, S.C. Versatility in Ligand Recognition by LDL Receptor Family Proteins: Advances and Frontiers. *Curr Opin Struct Biol* 2007, *17*, 419–426, doi:10.1016/J.SBI.2007.08.017.
56. Brown, M.S.; Herz, J.; Goldstein, J.L. Calcium Cages, Acid Baths and Recycling Receptors. *Nature 1997 388:6643* 1997, *388*, 629–630, doi:10.1038/41672.
57. Andersen, O.M.; Christensen, L.L.; Christensen, P.A.; Sørensen, E.S.; Jacobsen, C.; Moestrup, S.K.; Etzerodt, M.; Thøgersen, H.C. Identification of the Minimal Functional Unit in the Low Density Lipoprotein Receptor-Related Protein for Binding the Receptor-Associated Protein (RAP). *Journal of Biological Chemistry* 2000, *275*, 21017–21024.
58. Rauch, J.N.; Luna, G.; Guzman, E.; Audouard, M.; Challis, C.; Sibih, Y.E.; Leshuk, C.; Hernandez, I.; Wegmann, S.; Hyman, B.T.; et al. LRP1 Is a Master Regulator of Tau Uptake and Spread. *Nature 2020 580:7803* 2020, *580*, 381–385, doi:10.1038/s41586-020-2156-5.
59. Liu, S.; Meng, C.; Xu, G.; Jian, H.; Wang, F. Validation of Reference Genes for Reverse Transcription Real-Time Quantitative PCR Analysis in the Deep-Sea Bacterium Shewanella Psychrophila WP2. *FEMS Microbiol Lett* 2018, *365*, doi:10.1093/FEMSLE/FNY048.

60. Chiu, T.H.; Kao, L.Y.; Chen, M.L. Antibiotic Resistance and Molecular Typing of *Photobacterium Damselae* Subsp. Damselae, Isolated from Seafood. *J Appl Microbiol* 2013, *114*, 1184–1192, doi:10.1111/JAM.12104.
61. Lattos, A.; Giantsis, I.A.; Tsavea, E.; Kolygas, M.; Athanassopoulou, F.; Bitchava, K. Virulence Genes and *In vitro* Antibiotic Profile of *Photobacterium Damselae* Strains, Isolated from Fish Reared in Greek Aquaculture Facilities. *Animals (Basel)* 2022, *12*, doi:10.3390/ANI12223133.
62. Bras, A.; Roy, A.; Heckel, D.G.; Anderson, P.; Karlsson Green, K. Pesticide Resistance in Arthropods: Ecology Matters Too. *Ecol Lett* 2022, *25*, 1746–1759, doi:10.1111/ELE.14030.
63. Abreu, R.; Semedo-Lemsaddek, T.; Cunha, E.; Tavares, L.; Oliveira, M. Antimicrobial Drug Resistance in Poultry Production: Current Status and Innovative Strategies for Bacterial Control. *Microorganisms* 2023, *11*, doi:10.3390/MICROORGANISMS11040953.
64. do Vale, A.; Costa-Ramos, C.; Silva, D.S.P.; Macedo, P.M.; Fernandes, R.; Sampaio, P.; dos Santos, N.M.S.; Silva, M.T. Cytochemical and Ultrastructural Study of Anoikis and Secondary Necrosis in Enterocytes Detached *in vivo*. *Apoptosis* 2007, *12*, 1069–1083, doi:10.1007/S10495-006-0040-X/FIGURES/9.
65. Verster, K.I.; Tarnopol, R.L.; Akalu, S.M.; Whiteman, N.K. Horizontal Transfer of Microbial Toxin Genes to Gall Midge Genomes. *Genome Biol Evol* 2021, *13*, 197–205, doi:10.1093/GBE/EVAB202.
66. Conserving Monarch Butterflies and Their Habitats | Home Available online: https://www.usda.gov/about-usda/news/blog/conserving-monarch-butterflies-and-their-habitats (accessed on 22 April 2025).
67. dos Santos, N.M.S.; Taverne, N.; Taverne-Thiele, A.J.; De Sousa, M.; Rombout, J.H.W.M. Characterisation of Monoclonal Antibodies Specific for Sea Bass (Dicentrarchus LabraxL.) IgM Indicates the Existence of B Cell Subpopulations. *Fish Shellfish Immunol* 1997, *7*, 175–191, doi:10.1006/FSIM.1996.0073.
68. do Vale, A.; Afonso, A.; Silva, M.T. The Professional Phagocytes of Sea Bass (*Dicentrarchus Labrax L.*): Cytochemical Characterisation of Neutrophils and Macrophages in the Normal and Inflamed Peritoneal Cavity. *Fish Shellfish Immunol* 2002, *13*, 183–198, doi:10.1006/FSIM.2001.0394.
69. Gomes, M.S.; Fernandes, S.S.; Cordeiro, J. V; Gomes, S.S.; Vieira, A.; Appelberg, R. Engagement of Toll-like Receptor 2 in Mouse Macrophages Infected with Mycobacterium Avium Induces Non-Oxidative and TNF-Independent Anti-Mycobacterial Activity. *Eur J Immunol* 2008, *38*, 2180–2189, doi:10.1002/eji.200737954.

70. Englen, M.D.; Valdez, Y.E.; Lehnert, N.M.; Lehnert, B.E. Granulocyte/Macrophage Colony-Stimulating Factor Is Expressed and Secreted in Cultures of Murine L929 Cells. *J Immunol Methods* 1995, *184*, 281–283, doi:10.1016/0022-1759(95)00136-X.
71. Silva, D.S.; Pereira, L.M.G.; Moreira, A.R.; Ferreira-da-Silva, F.; Brito, R.M.; Faria, T.Q.; Zornetta, I.; Montecucco, C.; Oliveira, P.; Azevedo, J.E.; et al. The Apoptogenic Toxin AIP56 Is a Metalloprotease A-B Toxin That Cleaves NF-Kb P65. *PLoS Pathog* 2013, *9*, e1003128, doi:10.1371/journal.ppat.1003128.
72. Laemmli, U.K. Cleavage of Structural Proteins during the Assembly of the Head of Bacteriophage T4. *Nature 1970 227:5259* 1970, *227*, 680–685, doi:10.1038/227680a0.

GENERAL DISCUSSION

Virulence factors play a central role in bacterial infection and pathogenicity [1,2]. Among these, toxins are particularly significant due to their specificity and potency, targeting molecular components that cause cell dysfunction or death. They are frequently responsible for most of the symptoms and pathology associated with the disease [1,2]. This thesis contributes to advance the understanding of the specificity of the NF-κB targeting toxin AIP56 at the organismal, cellular, and molecular level. Specifically, it explores if AIP56 contributes to infection and pathology across different host species, describes–which immune cells are preferentially targeted and the consequences that arise from this and characterizes the receptor and receptor interaction mechanisms that provide this specificity. Moreover, with the growing identification of AIP56-like and -related toxins across a wide range of phylogenetically diverse organisms, a parallel was established between the discoveries made for AIP56 and this set of toxins that share a putative receptor-binding domain homologous to that of AIP56, providing insights into the evolution and speciation of this family of toxins.

AIP56, a key virulence factor secreted by *Photobacterium Damselae* subsp. *piscicida* (*Phdp*) [81], plays a crucial role in the pathogenesis and mortality observed in European sea bass, through cleavage of NF-κB p65 in macrophages, which leads to their lysis by post-apoptotic necrosis [81,125]. The scarcity of tools to identify specific cell populations in sea bass limited the study of the susceptibility to AIP56 to a few cell types. Nevertheless, the results obtained in this species, together with the results obtained in mice and humans suggest that the toxin exhibits a broad tropism for myeloid cells, preferentially macrophages (Chapter 2). A key finding in this thesis was that most of the neutrophil destruction that is also observed during *Phdp* infection or AIP56 intoxication [81,84,87,126] is not directly caused by AIP56, since only a small proportion of neutrophils internalize the toxin. Instead, neutrophils lysis is more likely the result of cell death pathways activated during their participation in the inflammatory response [127,128] triggered by the bacteria and/or its components (Chapter 2). This indirect immune-mediated cytotoxicity is a common feature in microbial pathogenesis [129,130]. Thus, widespread lysis of phagocytes by AIP56 has a negative impact on the host immune response, since myeloid cells play a fundamental role in innate immunity and make a bridge to adaptive immunity through antigen processing and presentation [131,132]. Another consequence is that host tissues are exposed to highly cytotoxic molecules released primarily by lysis of these cells, exacerbating the necrotic lesions typically seen in *Phdp* infections [81,126]. By selectively targeting and eliminating these key immune cells, AIP56 promotes bacterial proliferation, leading to septicemia and ultimately, host death [81,126].

Although similar histopathology features have been reported in *Phdp* infections across different fish species, including European sea bass [133], gilthead sea bream [134], sole [135], and striped bass (*Morone saxatilis*) [136], the role of AIP56 in the infection and pathology of species other than sea bass has not been thoroughly characterized. Surprisingly, this study reveals that AIP56 does not exert the same effect on gilthead sea bream (Chapter 1). Although AIP56 is internalized by sea bream phagocytes, its uptake is significantly lower compared to that in sea bass phagocytes. This reduced internalization may explain the resistance of sea bream phagocytes, and the fish itself, to AIP56 intoxication. Since LRP1 was identified in this study as the receptor for AIP56 (Chapter 3), it can be speculated that the lower susceptibility of sea bream to AIP56 may be due to a reduced affinity of the toxin for sea bream LRP1. However, this hypothesis is unlikely given that AIP56 also binds to human LRP1 (Chapter 3) and intoxicates macrophages from both humans and mice (Chapter 2), species phylogenetically more distant from sea bass than sea bream. Furthermore, an alignment of the amino acid sequences of LRP1 from sea bass and sea bream revealed a high degree of conservation (98% sequence identity, Supplementary Figure 1). Therefore, although the binding of AIP56 to sea bream LRP1 has not been confirmed, it is more plausible that the inability of AIP56 to intoxicate sea bream phagocytes is due to lower expression of this receptor on these cells. This is surprising, considering that, at least in mammals, LRP1 is ubiquitously expressed in immune cells, with highest levels in myeloid cells, particularly macrophages [137]. It also appears to be expressed in sea bass macrophages, since these cells are targeted by AIP56 in this species (Chapter 2 and [81,84,87]). An alternative explanation is that the association of a coreceptor with LRP1 is required for cell tropism and efficient internalization of the toxin. Coreceptor associations are known to promote the binding of a variety of macromolecules to LDLR, which include LRP1 [138]. Therefore, assessing the expression levels of LRP1, including in cells other than macrophages, is crucial to determine whether this receptor alone is sufficient to promote cell tropism and internalization of AIP56 or whether a coreceptor is necessary. For instance, this could help clarify why human neutrophils exhibit a higher rate of AIP56 internalization compared neutrophils from sea bass and mouse (Chapter 2). This increased uptake may be due to higher expression levels of LRP1 in human neutrophils, the presence of a coreceptor(s) that increases toxin entry, or the binding of AIP56 to a different receptor, such as a member of the LDLR family expressed on human neutrophils but not or less expressed on sea bass and mouse neutrophils. Findings suggesting that AIP56 may, indeed, have an alternative receptor were presented in Chapter 3 of these thesis: (1) Knocking out LRP1 in the human HEK 293T cell line reduced, but did not fully inhibit, intoxication by the ToxicMoiety-AIP56RBD chimera, and inhibiting AIP56 binding with RAP did not fully prevent p65

cleavage or cell death by the toxin, indicating that AIP56 might use another receptor for internalization; (2) RAP decreased toxicity in *Lrp1*-knockout HEK cells incubated with ToxicMoiety-AIP56RBD, which, considering that RAP is a universal inhibitor of the LDLR family [139–141], suggests that AIP56 may recognize another LDLR member. It is therefore critical to extend these studies on cellular susceptibility and receptor(s) interaction to other species susceptible to *Phdp*, in order to further elucidate the role of AIP56 for the infectious and pathological processes. Such studies should clarify which virulence factors play a more prominent role in different *Phdp*-susceptible species, thus informing the development of targeted prophylaxis and therapies aimed at neutralizing the specific virulence factors at play.

A significant finding uncovered in this thesis, which underscores the importance of the AIP56-LRP1 interaction in the intoxication process, is the identification of specific residues - K350 and R441 – on AIP56 that are critical for binding to the sea bass LRP1 receptor (Chapter 3). Mutation at these amino acid positions not only inhibited the interaction between AIP56 and sea bass LRP1 in biolayer interferometry (BLI) assays, but also significantly impaired the toxin's ability to intoxicate sea bass, with the double mutant nearly abolishing intoxication. This observation aligns with previous descriptions of ligand interaction with LRP1, where pairs of lysine and/or arginine residues interact with negatively charged amino acids in the complement-like repeats of LRP1 [55]. Understanding the mechanisms through which AIP56 interacts with its receptor(s) provides valuable insights for developing therapeutic strategies that could block the toxin's internalization and cytotoxic effects, thereby mitigating its impact on disease progression.

An interesting result that may contribute to this therapeutic approach is the observation that the addition of free lysine, and to some extent, arginine, to cultured sea bass macrophages inhibited AIP56 intoxication (Chapter 3). This suggests that dietary supplementation with these amino acids could potentially protect against AIP56 intoxication and mitigate the pathogenic effects of *Phdp* infection. In the same context, the finding that both the receptor-binding domain (RBD) of AIP56 [125] and cluster 4 of sea bass LRP1X1 (Chapter 3) inhibited AIP56 intoxication in sea bass macrophages is promising for the development of toxin blocking strategies. Even more compelling was the demonstration that the RBD of AIP56 effectively inhibited AIP56 intoxication in sea bass (Chapter 3), highlighting the urgent need to test its efficacy as a protective agent against *Phdp* infection and its potential as basis for the development of AIP56 inhibitors or blockers.

Another key contribution of this thesis was to show that the activity of AIP56-like and -related

toxins in their hosts is likely mediated through interactions with the respective LRP1 orthologs (Chapter 3). The structural homology of their putative receptor-binding domain to that of AIP56, along with their ability to interact with cluster 4 of human LRP1 and inhibit AIP56 internalization and intoxication in sea bass macrophages, supports this hypothesis. These findings also suggest that these toxins exhibit distinct affinities for different LRP1 orthologs, which may indicate speciation driven by toxin-host co-evolution.

The identification of LRP1 as a receptor for AIP56 and related toxins marks a significant breakthrough, paving the way for further characterization of the cellular specificity and internalization mechanisms of this growing family of toxins. These toxins are present in organisms from various phylogenetic branches, with hosts including insects, fish and humans. Consequently, understanding the molecular details underlying the interaction between these toxins and their cell receptors is crucial for advancing our knowledge of both the toxin-producing organisms and their hosts, as well as the coevolutionary dynamics shaped by toxin-receptor interactions. Specifically, the findings presented here will provide clarity on the intoxication and pathogenicity mechanisms of toxins produced by pathogenic or potentially pathogenic bacteria, such as AIP56 [125,126,142–144], AIP56-like toxins from *Vibrio* species, including strains isolated from humans [102,103] and the AIP56-related toxin from *Enterovibrio norvegicus* isolated from turbot [105]. A detailed understanding of the molecular interactions between these toxins and their receptors will provide a solid basis for the rational development of prophylactic and therapeutic strategies. These strategies could include vaccines capable of triggering the production of antibodies capable of blocking toxin-receptor binding or small-molecule inhibitors that prevent toxin-receptor interactions. Furthermore, these findings will contribute to the study of AIP56-related toxins from species such as *Danaus plexippus*, *Operophtera brumata*, *Drosophila bipectinata* and *D. ananassae*, which are likely involved in defense mechanisms against parasitoid wasps, as suggested for similar toxins encoded in the genomes of vinegar flies, aphids, and gall midges [108,145]. For example, a detailed understanding of the interaction between the *D. plexippus* toxin and LRP1 in parasitoid wasps could enhance our understanding of the butterfly's defense mechanisms and support the development of strategies to protect this vital pollinator [146]. Similarly, these insights may aid in the study of symbiont-mediated resistance to parasitism conferred by *Arsenophonus nasoniae* and *Hamiltonella defensa* in aphids, where the latter provides resistance to parasitoid wasps when infected with the APSE-2 bacteriophage [107]. APSE-2 produces a CdtB-like protein with DNase I activity, whose cellular specificity is thought to be mediated through association with Protein D, a protein homologous to the AIP56 RBD, encoded downstream of *cdtB* gene. Unraveling the mechanisms behind symbiont-mediated resistance to parasitism could have significant

implications for the biological control of herbivorous pests like aphids.

In broader terms, the work presented in this thesis provides a valuable foundation for the rational development of prophylactic and therapeutic strategies across multiple fields, including agriculture, aquaculture, and human health. This would ultimately contribute to the sustainability of aquatic and terrestrial ecosystems, and the production of safer, higher-quality food in a more sustainable manner.

Supplementary Data

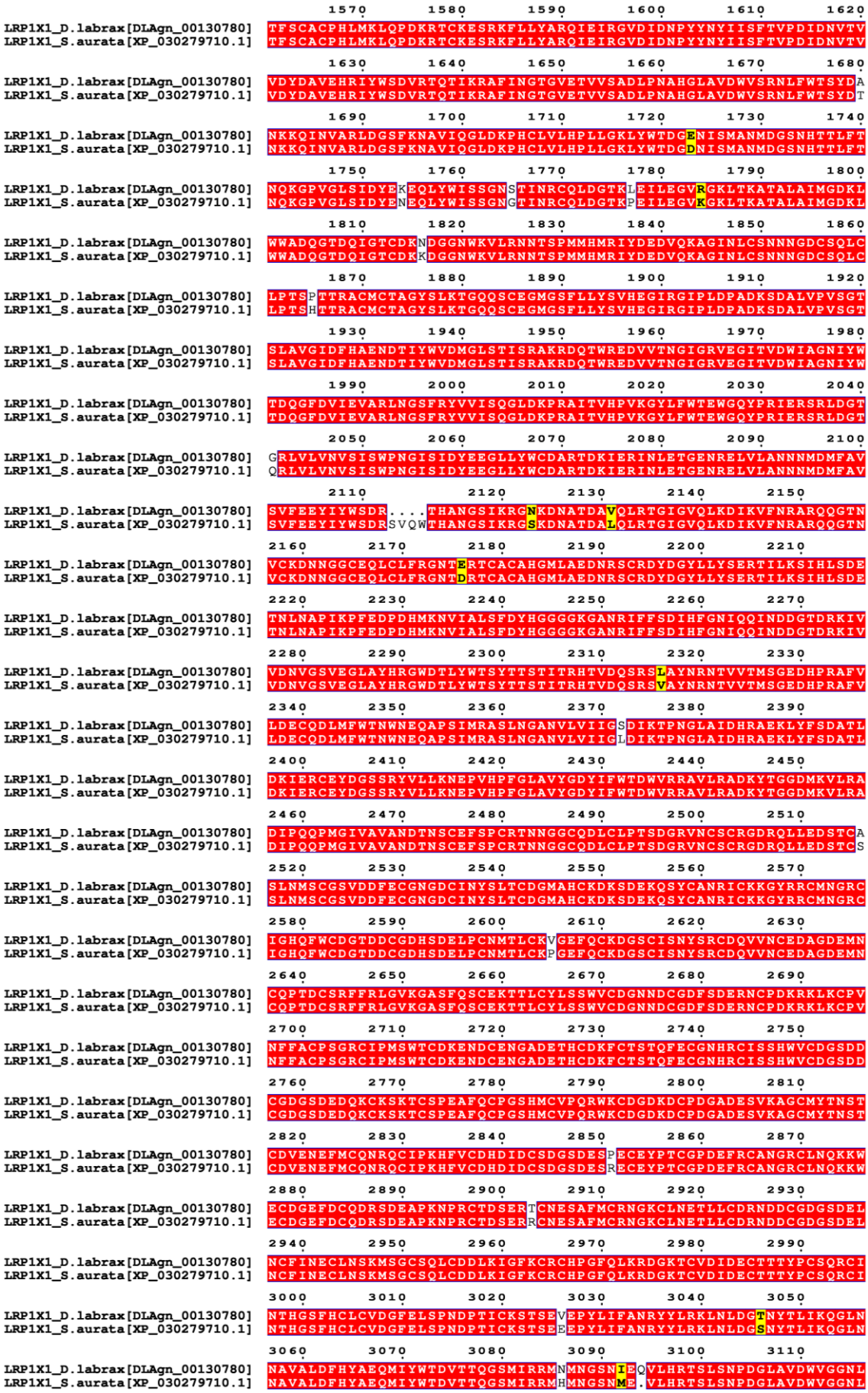
1570 1580 1590 1600 1610 1620
LRP1X1_D.labrax[DLAgn_00130780] TFSCACPHLMKLQPDKRTCKESRKFLLYARQIEIRGVDIDNPYYNYIISFTVPDIDNVTV
LRP1X1_S.aurata[XP_030279710.1] TFSCACPHLMKLQPDKRTCKESRKFLLYARQIEIRGVDIDNPYYNYIISFTVPDIDNVTV
1630 1640 1650 1660 1670 1680
LRP1X1_D.labrax[DLAgn_00130780] VDYDAVEHRIYWSDVRTQTIKRAFINGTGVETVVSADLPNAHGLAVDWVSRNLFWTSYDA
LRP1X1_S.aurata[XP_030279710.1] VDYDAVEHRIYWSDVRTQTIKRAFINGTGVETVVSADLPNAHGLAVDWVSRNLFWTSYDT
1690 1700 1710 1720 1730 1740
LRP1X1_D.labrax[DLAgn_00130780] NKKQINVARLDGSFKNAVIQGLDKPHCLVLHPLLGKLYWTDGENISMANMDGSNHTTLFT
LRP1X1_S.aurata[XP_030279710.1] NKKQINVARLDGSFKNAVIQGLDKPHCLVLHPLLGKLYWTDGDNISMANMDGSNHTTLFT
1750 1760 1770 1780 1790 1800
LRP1X1_D.labrax[DLAgn_00130780] NQKGPVGLSIDYEKEQLYWISSGNSTINRCQLDGTKLEILEGVRGKLTKATALAIMGDKL
LRP1X1_S.aurata[XP_030279710.1] NQKGPVGLSIDYENEQLYWISSGNGTINRCQLDGTKPEILEGVKGKLTKATALAIMGDKL
1810 1820 1830 1840 1850 1860
LRP1X1_D.labrax[DLAgn_00130780] WWADQGTDQIGTCDKNDGGNWKVLRNNTSPMMHMRIYDEDVQKAGINLCSNNNGDCSQLC
LRP1X1_S.aurata[XP_030279710.1] WWADQGTDQIGTCDKKDGGNWKVLRNNTSPMMHMRIYDEDVQKAGINLCSNNNGDCSQLC
1870 1880 1890 1900 1910 1920
LRP1X1_D.labrax[DLAgn_00130780] LPTSPTTRACMCTAGYSLKTGQQSCEGMGSFLLYSVHEGIRGIPLDPADKSDALVPVSGT
LRP1X1_S.aurata[XP_030279710.1] LPTSHTTRACMCTAGYSLKTGQQSCEGMGSFLLYSVHEGIRGIPLDPADKSDALVPVSGT
1930 1940 1950 1960 1970 1980
LRP1X1_D.labrax[DLAgn_00130780] SLAVGIDFHAENDTIYWVDMGLSTISRAKRDQTWREDVVTNGIGRVEGITVDWIAGNIYW
LRP1X1_S.aurata[XP_030279710.1] SLAVGIDFHAENDTIYWVDMGLSTISRAKRDQTWREDVVTNGIGRVEGITVDWIAGNIYW
1990 2000 2010 2020 2030 2040
LRP1X1_D.labrax[DLAgn_00130780] TDQGFDVIEVARLNGSFRYVVISQGLDKPRAITVHPVKGYLFWTEWGQYPRIERSRLDGT
LRP1X1_S.aurata[XP_030279710.1] TDQGFDVIEVARLNGSFRYVVISQGLDKPRAITVHPVKGYLFWTEWGQYPRIERSRLDGT
2050 2060 2070 2080 2090 2100
LRP1X1_D.labrax[DLAgn_00130780] GRLVLVNVSISWPNGISIDYEEGLLYWCDARTDKIERINLETGENRELVLANNNMDMFAV
LRP1X1_S.aurata[XP_030279710.1] QRLVLVNVSISWPNGISIDYEEGLLYWCDARTDKIERINLETGENRELVLANNNMDMFAV
2110 2120 2130 2140 2150
LRP1X1_D.labrax[DLAgn_00130780] SVFEEYIYWSDR....THANGSIKRGNKDNATDAVQLRTGIGVQLKDIKVFNRARQQGTN
LRP1X1_S.aurata[XP_030279710.1] SVFEEYIYWSDRSVQWTHANGSIKRGSKDNATDALQLRTGIGVQLKDIKVFNRARQQGTN
2160 2170 2180 2190 2200 2210
LRP1X1_D.labrax[DLAgn_00130780] VCKDNNGGCEQLCLFRGNTERTCACAHGMLAEDNRSCRDYDGYLLYSERTILKSIHLSDE
LRP1X1_S.aurata[XP_030279710.1] VCKDNNGGCEQLCLFRGNTDRTCACAHGMLAEDNRSCRDYDGYLLYSERTILKSIHLSDE
2220 2230 2240 2250 2260 2270
LRP1X1_D.labrax[DLAgn_00130780] TNLNAPIKPFEDPDHMKNVIALSFDYHGGGGKGANRIFFSDIHFGNIQQINDDGTDRKIV
LRP1X1_S.aurata[XP_030279710.1] TNLNAPIKPFEDPDHMKNVIALSFDYHGGGGKGANRIFFSDIHFGNIQQINDDGTDRKIV
2280 2290 2300 2310 2320 2330
LRP1X1_D.labrax[DLAgn_00130780] VDNVGSVEGLAYHRGWDTLYWTSYTTSTITRHTVDQSRSLAYNRNTVVTMSGEDHPRAFV
LRP1X1_S.aurata[XP_030279710.1] VDNVGSVEGLAYHRGWDTLYWTSYTTSTITRHTVDQSRSVAYNRNTVVTMSGEDHPRAFV
2340 2350 2360 2370 2380 2390
LRP1X1_D.labrax[DLAgn_00130780] LDECQDLMFWTNWNEQAPSIMRASLNGANVLVIIGSDIKTPNGLAIDHRAEKLYFSDATL
LRP1X1_S.aurata[XP_030279710.1] LDECQDLMFWTNWNEQAPSIMRASLNGANVLVIIGLDIKTPNGLAIDHRAEKLYFSDATL
2400 2410 2420 2430 2440 2450
LRP1X1_D.labrax[DLAgn_00130780] DKIERCEYDGSSRYVLLKNEPVHPFGLAVYGDYIFWTDWVRRAVLRADKYTGGDMKVLRA
LRP1X1_S.aurata[XP_030279710.1] DKIERCEYDGSSRYVLLKNEPVHPFGLAVYGDYIFWTDWVRRAVLRADKYTGGDMKVLRA
2460 2470 2480 2490 2500 2510
LRP1X1_D.labrax[DLAgn_00130780] DIPQQPMGIVAVANDTNSCEFSPCRTNNGGCQDLCLPTSDGRVNCSCRGDRQLLEDSTCA
LRP1X1_S.aurata[XP_030279710.1] DIPQQPMGIVAVANDTNSCEFSPCRTNNGGCQDLCLPTSDGRVNCSCRGDRQLLEDSTCS
2520 2530 2540 2550 2560 2570
LRP1X1_D.labrax[DLAgn_00130780] SLNMSCGSVDDFECGNGDCINYSLTCDGMAHCKDKSDEKQSYCANRICKKGYRRCMNGRC
LRP1X1_S.aurata[XP_030279710.1] SLNMSCGSVDDFECGNGDCINYSLTCDGMAHCKDKSDEKQSYCANRICKKGYRRCMNGRC
2580 2590 2600 2610 2620 2630
LRP1X1_D.labrax[DLAgn_00130780] IGHQFWCDGTDDCGDHSDELPCNMTLCKVGEFQCKDGSCISNYSRCDQVVNCEDAGDEMN
LRP1X1_S.aurata[XP_030279710.1] IGHQFWCDGTDDCGDHSDELPCNMTLCKPGEFQCKDGSCISNYSRCDQVVNCEDAGDEMN
2640 2650 2660 2670 2680 2690
LRP1X1_D.labrax[DLAgn_00130780] CQPTDCSRFFRLGVKGASFQSCEKTTLCYLSSWVCDGNNDCGDFSDERNCPDKRKLKCPV
LRP1X1_S.aurata[XP_030279710.1] CQPTDCSRFFRLGVKGASFQSCEKTTLCYLSSWVCDGNNDCGDFSDERNCPDKRKLKCPV
2700 2710 2720 2730 2740 2750
LRP1X1_D.labrax[DLAgn_00130780] NFFACPSGRCIPMSWTCDKENDCENGADETHCDKFCTSTQFECGNHRCISSHWVCDGSDD
LRP1X1_S.aurata[XP_030279710.1] NFFACPSGRCIPMSWTCDKENDCENGADETHCDKFCTSTQFECGNHRCISSHWVCDGSDD
2760 2770 2780 2790 2800 2810
LRP1X1_D.labrax[DLAgn_00130780] CGDGSDEDQKCKSKTCSPEAFQCPGSHMCVPQRWKCDGDKDCPDGADESVKAGCMYTNST
LRP1X1_S.aurata[XP_030279710.1] CGDGSDEDQKCKSKTCSPEAFQCPGSHMCVPQRWKCDGDKDCPDGADESVKAGCMYTNST
2820 2830 2840 2850 2860 2870
LRP1X1_D.labrax[DLAgn_00130780] CDVENEFMCQNRQCIPKHFVCDHDIDCSDGSDESPECEYPTCGPDEFRCANGRCLNQKKW
LRP1X1_S.aurata[XP_030279710.1] CDVENEFMCQNRQCIPKHFVCDHDIDCSDGSDESRECEYPTCGPDEFRCANGRCLNQKKW
2880 2890 2900 2910 2920 2930
LRP1X1_D.labrax[DLAgn_00130780] ECDGEFDCQDRSDEAPKNPRCTDSERTCNESAFMCRNGKCLNETLLCDRNDDCGDGSDEL
LRP1X1_S.aurata[XP_030279710.1] ECDGEFDCQDRSDEAPKNPRCTDSERRCNESAFMCRNGKCLNETLLCDRNDDCGDGSDEL
2940 2950 2960 2970 2980 2990
LRP1X1_D.labrax[DLAgn_00130780] NCFINECLNSKMSGCSQLCDDLKIGFKCRCHPGFQLKRDGKTCVDIDECTTTYPCSQRCI
LRP1X1_S.aurata[XP_030279710.1] NCFINECLNSKMSGCSQLCDDLKIGFKCRCHPGFQLKRDGKTCVDIDECTTTYPCSQRCI
3000 3010 3020 3030 3040 3050
LRP1X1_D.labrax[DLAgn_00130780] NTHGSFHCLCVDGFELSPNDPTICKSTSEVEPYLIFANRYYLRKLNLDGTNYTLIKQGLN
LRP1X1_S.aurata[XP_030279710.1] NTHGSFHCLCVDGFELSPNDPTICKSTSEEEPYLIFANRYYLRKLNLDGSNYTLIKQGLN
3060 3070 3080 3090 3100 3110
LRP1X1_D.labrax[DLAgn_00130780] NAVALDFHYAEQMIYWTDVTTQGSMIRRMNMNGSNIEQVLHRTSLSNPDGLAVDWVGGNL
LRP1X1_S.aurata[XP_030279710.1] NAVALDFHYAEQMIYWTDVTTQGSMIRRMHMNGSNME.VLHRTSLSNPDGLAVDWVGGNL

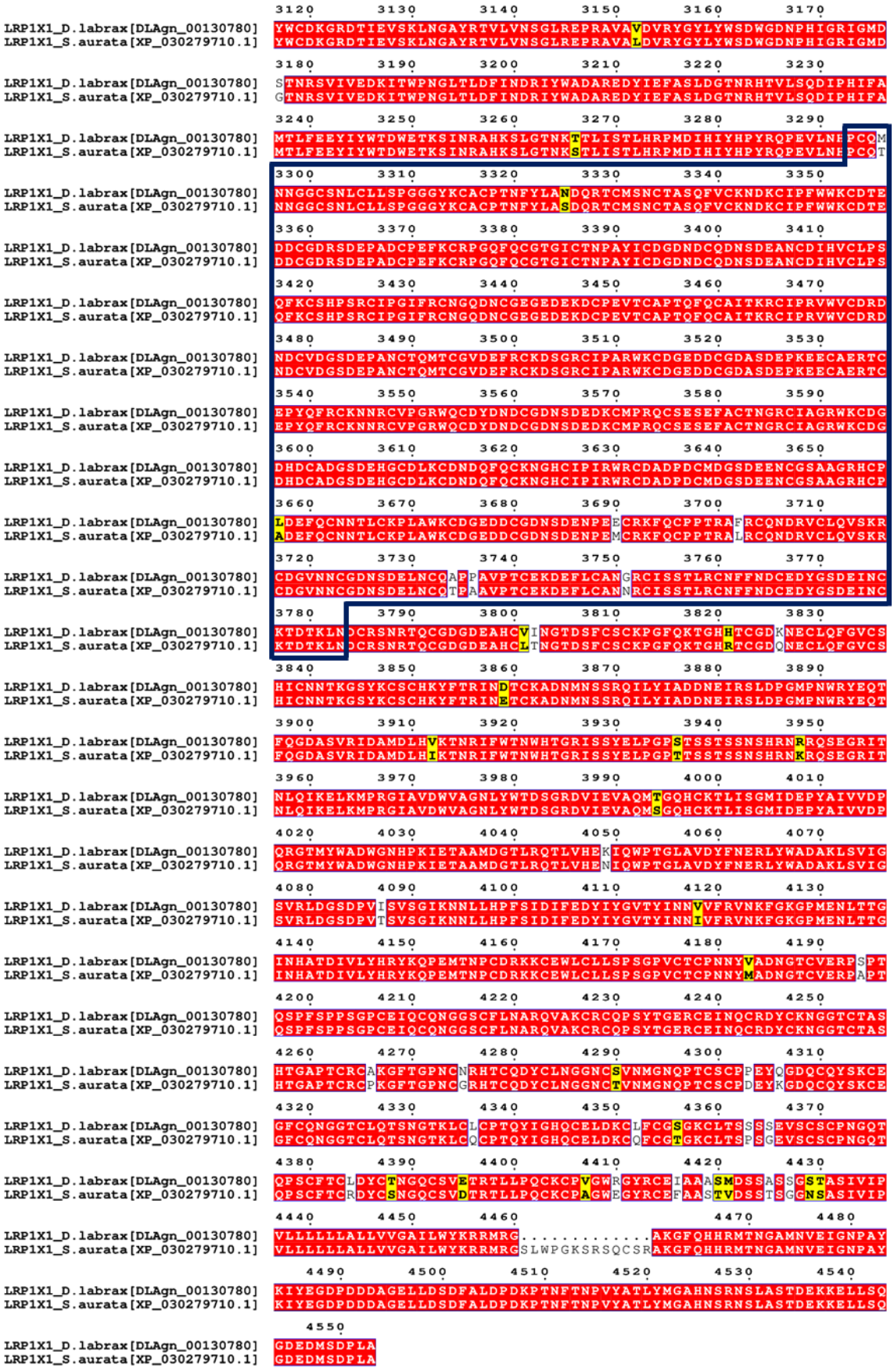

Figure S1. **Sea bass and sea bream LRP1X1 is conserved (98% sequence identity).** Sequence alignment

of the complete proteins was performed by Clustal Omega, with default parameters. Identical and similar residues are highlighted in red and yellow, respectively. Dark blue box is selecting the C4 region.

REFERENCES

1. Ghazaei, C. Advances in the Study of Bacterial Toxins, Their Roles and Mechanisms in Pathogenesis. *Malays J Med Sci* 2022, *29*, 4, doi:10.21315/MJMS2022.29.1.2.
2. Lemichez, E.; Barbieri, J.T. General Aspects and Recent Advances on Bacterial Protein Toxins. 2013, doi:10.1101/cshperspect.a013573.
3. Fabbri, A.; Travaglione, S.; Falzano, L.; Fiorentini, C. Bacterial Protein Toxins: Current and Potential Clinical Use. *Curr Med Chem* 2008, *15*, 1116–1125, doi:10.2174/092986708784221430.
4. Masignani, V.; Pizza, M.; Rappuoli, R. Bacterial Toxins. In *The Prokaryotes*; 2006 ISBN 9781626239777.
5. Hajra, D.; Nair, A.V.; Chakravortty, D. An Elegant Nano-Injection Machinery for Sabotaging the Host: Role of Type III Secretion System in Virulence of Different Human and Animal Pathogenic Bacteria. *Phys Life Rev* 2021, *38*, 25–54, doi:10.1016/J.PLREV.2021.05.007.
6. Cheng, H.C.; Skehan, B.M.; Campellone, K.G.; Leong, J.M.; Rosen, M.K. Structural Mechanism of WASP Activation by the Enterohaemorrhagic E. Coli Effector EspFU. *Nature* 2008, *454*, 1009–1013, doi:10.1038/nature07160.
7. Nadler, C.; Baruch, K.; Kobi, S.; Mills, E.; Haviv, G.; Farago, M.; Alkalay, I.; Bartfeld, S.; Meyer, T.F.; Ben-Neriah, Y.; et al. The Type III Secretion Effector NleE Inhibits NF-KB Activation. *PLoS Pathog* 2010, *6*, doi:10.1371/journal.ppat.1000743.
8. Hemrajani, C.; Berger, C.N.; Robinson, K.S.; Marchès, O.; Mousnier, A.; Frankel, G. NleH Effectors Interact with Bax Inhibitor-1 to Block Apoptosis during Enteropathogenic *Escherichia Coli* Infection. *Proc Natl Acad Sci U S A* 2010, *107*, 3129–3134, doi:10.1073/pnas.0911609106.
9. Baruch, K.; Gur-Arie, L.; Nadler, C.; Koby, S.; Yerushalmi, G.; Ben-Neriah, Y.; Yogev, O.; Shaulian, E.; Guttman, C.; Zarivach, R.; et al. Metalloprotease Type III Effectors That Specifically Cleave JNK and NF-KB. *EMBO Journal* 2011, *30*, 221–231, doi:10.1038/emboj.2010.297.
10. Wong Fok Lung, T.; Pearson, J.S.; Schuelein, R.; Hartland, E.L. The Cell Death Response to Enteropathogenic *Escherichia Coli* Infection. *Cell Microbiol* 2014, *16*, 1736–1745.
11. Yen, H.; Ooka, T.; Iguchi, A.; Hayashi, T.; Sugimoto, N.; Tobe, T. NleC, a Type III Secretion Protease, Compromises NF-KB Activation by Targeting P65/RelA. *PLoS Pathog* 2010, *6*, e1001231, doi:10.1371/JOURNAL.PPAT.1001231.
12. Tam, V.C.; Serruto, D.; Dziejman, M.; Brieher, W.; Mekalanos, J.J. A Type III Secretion System in *Vibrio Cholerae* Translocates a Formin/Spire Hybrid-like Actin Nucleator to Promote Intestinal Colonization. *Cell Host Microbe* 2007, *1*, 95–107, doi:10.1016/j.chom.2007.03.005.

13. Goehring, U.M.; Schmidt, G.; Pederson, K.J.; Aktories, K.; Barbieri, J.T. The N-Terminal Domain of *Pseudomonas Aeruginosa* Exoenzyme S Is a GTPase-Activating Protein for Rho GTPases. *Journal of Biological Chemistry* 1999, *274*, 36369–36372, doi:10.1074/jbc.274.51.36369.
14. Janjusevic, R.; Abramovitch, R.B.; Martin, G.B.; Stebbins, C.E. A Bacterial Inhibitor of Host Programmed Cell Death Defenses Is an E3 Ubiquitin Ligase. *Science (1979)* 2006, *311*, 222–226, doi:10.1126/science.1120131.
15. Hardt, W.D.; Urlaub, H.; Galán, J.E. A Substrate of the Centisome 63 Type III Protein Secretion System of Salmonella Typhimurium Is Encoded by a Cryptic Bacteriophage. *Proc Natl Acad Sci U S A* 1998, *95*, 2574–2579, doi:10.1073/pnas.95.5.2574.
16. Diao, J.; Zhang, Y.; Huibregtse, J.M.; Zhou, D.; Chen, J. Crystal Structure of SopA, a *Salmonella* Effector Protein Mimicking a Eukaryotic Ubiquitin Ligase. *Nat Struct Mol Biol* 2008, *15*, 65–70, doi:10.1038/nsmb1346.
17. Rytkönen, A.; Poh, J.; Garmendia, J.; Boyle, C.; Thompson, A.; Liu, M.; Freemont, P.; Hinton, J.C.D.; Holden, D.W. SseL, a *Salmonella* Deubiquitinase Required for Macrophage Killing and Virulence. *Proc Natl Acad Sci U S A* 2007, *104*, 3502–3507, doi:10.1073/pnas.0610095104.
18. Hernandez, L.D.; Hueffer, K.; Wenk, M.R.; Galán, J.E. *Salmonella* Modulates Vesicular Traffic by Altering Phosphoinositide Metabolism. *Science (1979)* 2004, *304*, 1805–1807, doi:10.1126/science.1098188.
19. Steele-Mortimer, O.; Knodler, L.A.; Marcus, S.L.; Scheid, M.P.; Goh, B.; Pfeifer, C.G.; Duronio, V.; Finlay, B.B. Activation of Akt/Protein Kinase B in Epithelial Cells by the *Salmonella Typhimurium* Effector SigD. *Journal of Biological Chemistry* 2000, *275*, 37718–37724, doi:10.1074/jbc.M008187200.
20. Ohlson, M.B.; Huang, Z.; Alto, N.M.; Blanc, M.P.; Dixon, J.E.; Chai, J.; Miller, S.I. Structure and Function of *Salmonella* SifA Indicate That Its Interactions with SKIP, SseJ, and RhoA Family GTPases Induce Endosomal Tubulation. *Cell Host Microbe* 2008, *4*, 434–446, doi:10.1016/j.chom.2008.08.012.
21. Alto, N.M.; Shao, F.; Lazar, C.S.; Brost, R.L.; Chua, G.; Mattoo, S.; McMahon, S.A.; Ghosh, P.; Hughes, T.R.; Boone, C.; et al. Identification of a Bacterial Type III Effector Family with G Protein Mimicry Functions. *Cell* 2006, *124*, 133–145, doi:10.1016/j.cell.2005.10.031.
22. Izard, T.; Tran Van Nhieu, G.; Bois, P.R.J. *Shigella* Applies Molecular Mimicry to Subvert Vinculin and Invade Host Cells. *Journal of Cell Biology* 2006, *175*, 465–475, doi:10.1083/jcb.200605091.

23. Von Pawel-Rammingen, U.; Telepnev, M. V.; Schmidt, G.; Aktories, K.; Wolf-Watz, H.; Rosqvist, R. GAP Activity of the *Yersinia* YopE Cytotoxin Specifically Targets the Rho Pathway: A Mechanism for Disruption of Actin Microfilament Structure. *Mol Microbiol* 2000, *36*, 737–748, doi:10.1046/j.1365-2958.2000.01898.x.
24. Barth, H.; Stiles, B.G. Protein Toxins from Bacteria. In *Comprehensive Natural Products II: Chemistry and Biology*; Elsevier Ltd, 2010; Vol. 5, pp. 149–173 ISBN 9780080453828.
25. Henkel, J.S.; Baldwin, M.R.; Barbieri, J.T. *Toxins from Bacteria*; 2013;
26. Brito, C.; Cabanes, D.; Sarmento Mesquita, F.; Sousa, S. Mechanisms Protecting Host Cells against Bacterial Pore-Forming Toxins. *Cell Mol Life Sci* 2018, *76*, 1319, doi:10.1007/S00018-018-2992-8.
27. Schmitt, C.K.; Meysick, K.C.; O'Brien, A.D. Bacterial Toxins: Friends or Foes? *Emerg Infect Dis* 1999, *5*, 224–234, doi:10.3201/eid0502.990206.
28. Falnes, P.; Sandvig, K. Penetration of Protein Toxins into Cells. *Curr Opin Cell Biol* 2000, *12*, 407–413, doi:10.1016/S0955-0674(00)00109-5.
29. Garred, O.; Van Deurs, B.; Sandvig, K. Furin-Induced Cleavage and Activation of Shiga Toxin. *Journal of Biological Chemistry* 1995, *270*, 10817–10821, doi:10.1074/jbc.270.18.10817.
30. Sun, J. Roles of Cellular Redox Factors in Pathogen and Toxin Entry in the Endocytic Pathways. In *Molecular Regulation of Endocytosis*; InTech, 2012.
31. Tsuneoka, M.; Nakayama, K.; Hatsuzawa, K.; Komada, M.; Kitamura, N.; Mekada, E. Evidence for Involvement of Furin in Cleavage and Activation of Diphtheria Toxin. *Journal of Biological Chemistry* 1993, *268*, 26461–26465, doi:10.1016/s0021-9258(19)74337-3.
32. Shen, A. Autoproteolytic Activation of Bacterial Toxins. *Toxins (Basel)* 2010, *2*, 963–977.
33. Silva, D.S.; Pereira, L.M.G.; Moreira, A.R.; Ferreira-da-Silva, F.; Brito, R.M.; Faria, T.Q.; Zornetta, I.; Montecucco, C.; Oliveira, P.; Azevedo, J.E.; et al. The Apoptogenic Toxin AIP56 Is a Metalloprotease A-B Toxin That Cleaves NF-Kb P65. *PLoS Pathog* 2013, *9*, e1003128, doi:10.1371/journal.ppat.1003128.
34. Cao, X.; Lilla, S.; Cao, Z.; Pringle, M.A.; Oka, O.B.V.; Robinson, P.J.; Szmaja, T.; Van Lith, M.; Zanivan, S.; Bulleid, N.J. The Mammalian Cytosolic Thioredoxin Reductase Pathway Acts via a Membrane Protein to Reduce ER-Localised Proteins. *J Cell Sci* 2020, *133*, doi:10.1242/jcs.241976.
35. Beddoe, T.; Paton, A.W.; Le Nours, J.; Rossjohn, J.; Paton, J.C. Structure, Biological Functions and Applications of the AB5 Toxins. *Trends Biochem Sci* 2010, *35*, 411–418.

36. Kronhardt, A.; Rolando, R.; Beitzinger, C.; Stefani, C.; Leuber, M.; Flatau, G.; Popoff, M.; Benz, R.; Lemichez, E.; Rolando, M.; et al. Cross-Reactivity of Anthrax and C2 Toxin: Protective Antigen Promotes the Uptake of Botulinum C2I Toxin into Human Endothelial Cells. *PLoS ONE, Public Library of Science* 2011, *6*, 23133, doi:10.1371/journal.pone.0023133ï.
37. Young, J.A.T.; Collier, R.J. Anthrax Toxin: Receptor Binding, Internalization, Pore Formation, and Translocation. *Annu Rev Biochem* 2007, *76*, 243–265, doi:10.1146/ANNUREV.BIOCHEM.75.103004.142728/CITE/REFWORKS.
38. Singh, Y.; Klimpel, K.R.; Goel, S.; Swain, P.K.; Leppla, S.H. Oligomerization of Anthrax Toxin Protective Antigen and Binding of Lethal Factor during Endocytic Uptake into Mammalian Cells. *Infect Immun* 1999, *67*, 1853–1859, doi:10.1128/IAI.67.4.1853-1859.1999.
39. Song, J.; Gao, X.; Galán, J.E. Structure and Function of the *Salmonella Typhi* Chimaeric A 2 B 5 Typhoid Toxin. *Nature* 2013, *499*, 350–354, doi:10.1038/nature12377.
40. Martin, O.C.B.; Frisan, T. Bacterial Genotoxin-Induced DNA Damage and Modulation of the Host Immune Microenvironment. *Toxins 2020, Vol. 12, Page 63* 2020, *12*, 63, doi:10.3390/TOXINS12020063.
41. Bezine, E.; Vignard, J.; Mirey, G. The Cytolethal Distending Toxin Effects on Mammalian Cells: A DNA Damage Perspective. *Cells* 2014, *3*, 592–615, doi:10.3390/cells3020592.
42. Geny, B.; Popoff, M.R. Bacterial Protein Toxins and Lipids: Role in Toxin Targeting and Activity. *Biol Cell* 2006, *98*, 633–651, doi:10.1042/BC20060038.
43. Ulloa-Aguirre, A.; Maya-Núñez, G.; Timossi, C. Membrane Receptor Signaling in Health and Disease. In *Encyclopedia of Hormones*; Elsevier, 2003; pp. 644–657.
44. Westerfield, J.M.; Barrera, F.N. Membrane Receptor Activation Mechanisms and Transmembrane Peptide Tools to Elucidate Them. *Journal of Biological Chemistry* 2020, *295*, 1792–1814.
45. Horiguchi, Y.; Mekada, E. Toxin Receptors. In *The Comprehensive Sourcebook of Bacterial Protein Toxins*; Elsevier Inc., 2006; pp. 106–119 ISBN 9780120884452.
46. Holmgren, J.; Lonnroth, I.; Mansson, J.E.; Svennerholm, L. Interaction of Cholera Toxin and Membrane Gm1 Ganglioside of Small Intestine. *Proc Natl Acad Sci U S A* 1975, *72*, 2520–2524, doi:10.1073/pnas.72.7.2520.
47. Odumosu, O.; Nicholas, D.; Yano, H.; Langridge, W. AB Toxins: A Paradigm Switch from Deadly to Desirable. *Toxins (Basel)* 2010, *2*, 1612–1645.

48. Sethi, A.; Wands, A.M.; Mettlen, M.; Krishnamurthy, S.; Wu, H.; Kohler, J.J. Cell Type and Receptor Identity Regulate Cholera Toxin Subunit B (CTB) Internalization. *Interface Focus* 2019, *9*, doi:10.1098/rsfs.2018.0076.
49. Melton-Celsa, A.R. Shiga Toxin (Stx) Classification, Structure, and Function. *Microbiol Spectr* 2014, *2*, doi:10.1128/microbiolspec.ehec-0024-2013.
50. Cheng, B.; Liu, Y.; Zhao, Y.; Li, Q.; Liu, Y.; Wang, J.; Chen, Y.; Zhang, M. The Role of Anthrax Toxin Protein Receptor 1 as a New Mechanosensor Molecule and Its Mechanotransduction in BMSCs under Hydrostatic Pressure. *Sci Rep* 2019, *9*, 1–17, doi:10.1038/s41598-019-49100-5.
51. Mitamura, T.; Higashiyama, S.; Taniguchi, N.; Klagsbrunll, M.; Mekadall, E. *THE JOURNAL OF BIOLOGICAL CHEMISTRY Diphtheria Toxin Binds to the Epidermal Growth Factor (EGF)-like Domain of Human Heparin-Binding EGF-like Growth Factor/Diphtheria Toxin Receptor and Inhibits Specifically Its Mitogenic Activity**; 1995; Vol. 270;.
52. Berntsson, R.P.A.; Peng, L.; Dong, M.; Stenmark, P. Structure of Dual Receptor Binding to Botulinum Neurotoxin B. *Nat Commun* 2013, *4*, 2058, doi:10.1038/ncomms3058.
53. Osicka, R.; Osickova, A.; Hasan, S.; Bumba, L.; Cerny, J.; Sebo, P. Bordetella Adenylate Cyclase Toxin Is a Unique Ligand of the Integrin Complement Receptor 3. *Elife* 2015, *4*, doi:10.7554/eLife.10766.
54. Schöttelndreier, D.; Langejürgen, A.; Lindner, R.; Genth, H. Low Density Lipoprotein Receptor-Related Protein-1 (LRP1) Is Involved in the Uptake of Clostridioides Difficile Toxin A and Serves as an Internalizing Receptor. *Front Cell Infect Microbiol* 2020, *10*, 565465, doi:10.3389/FCIMB.2020.565465/BIBTEX.
55. Gonias, S.L.; Campana, W.M. LDL Receptor–Related Protein-1: A Regulator of Inflammation in Atherosclerosis, Cancer, and Injury to the Nervous System. *Am J Pathol* 2014, *184*, 18–27, doi:10.1016/J.AJPATH.2013.08.029.
56. Obermoeller-McCormick, L.M.; Li, Y.; Osaka, H.; FitzGerald, D.J.; Schwartz, A.L.; Bu, G. Dissection of Receptor Folding and Ligand-Binding Property with Functional Minireceptors of LDL Receptor-Related Protein. *J Cell Sci* 2001, *114*, 899–908, doi:10.1242/JCS.114.5.899.
57. Morgan, R.N.; Saleh, S.E.; Farrag, H.A.; Aboshanab, K.M. New Insights on *Pseudomonas Aeruginosa* Exotoxin A-Based Immunotoxins in Targeted Cancer Therapeutic Delivery. *Ther Deliv* 2023, *14*, 31–60, doi:10.4155/TDE-2022-0055.
58. Pastrana, D. V.; Hanson, A.J.; Knisely, J.; Bu, G.; FitzGerald, D.J. LRP1B Functions as a Receptor for Pseudomonas Exotoxin. *Biochimica et Biophysica Acta (BBA) -*

Molecular Basis of Disease 2005, *1741*, 234–239, doi:10.1016/J.BBADIS.2005.06.007.

59. Williams, J.M.; Tsai, B. Intracellular Trafficking of Bacterial Toxins. 2016, doi:10.1016/j.ceb.2016.03.019.
60. Harper, C.B.; McCluskey, A.; Robinson, P.J.; Meunier, F.A. Exploiting Endocytic Pathways to Prevent Bacterial Toxin Infection. In *The Comprehensive Sourcebook of Bacterial Protein Toxins*; Elsevier Inc., 2015; pp. 1072–1094 ISBN 9780128005897.
61. Kumari, S.; Mg, S.; Mayor, S. Diversity of Endocytic Mechanisms 256 Endocytosis Unplugged: Multiple Ways to Enter the Cell. *Cell Research* | 2010, *20*, 256–275, doi:10.1038/cr.2010.19.
62. Sandvig, K.; Kavaliauskiene, S.; Skotland, T. Clathrin-Independent Endocytosis: An Increasing Degree of Complexity. *Histochem Cell Biol* 2018, *150*, 107–118.
63. El-Sayed, A.; Harashima, H. Endocytosis of Gene Delivery Vectors: From Clathrin-Dependent to Lipid Raft-Mediated Endocytosis. *Molecular Therapy* 2013, *21*, 1118–1130.
64. Mayor, S.; Parton, R.G.; Donaldson, J.G. Clathrin-Independent Pathways of Endocytosis. *Cold Spring Harb Perspect Biol* 2014, *6*, doi:10.1101/cshperspect.a016758.
65. Johannes, L.; Decaudin, D. Protein Toxins: Intracellular Trafficking for Targeted Therapy. *Gene Ther* 2005, *12*, 1360–1368.
66. Kaksonen, M.; Roux, A. Mechanisms of Clathrin-Mediated Endocytosis. *Nat Rev Mol Cell Biol* 2018, *19*, 313–326.
67. Kabbani, A.M.; Raghunathan, K.; Lencer, W.I.; Kenworthy, A.K.; Kelly, C. V. Structured Clustering of the Glycosphingolipid GM1 Is Required for Membrane Curvature Induced by Cholera Toxin. *Proc Natl Acad Sci U S A* 2020, *117*, 14978–14986, doi:10.1073/pnas.2001119117.
68. Sharma, N.C.; Efstratiou, A.; Mokrousov, I.; Mutreja, A.; Das, B.; Ramamurthy, T. Diphtheria. *Nat Rev Dis Primers* 2019, *5*, 1–18, doi:10.1038/s41572-019-0131-y.
69. Abrami, L.; Bischofberger, M.; Kunz, B.; Groux, R.; Van Der Goot, F.G. Endocytosis of the Anthrax Toxin Is Mediated by Clathrin, Actin and Unconventional Adaptors. *PLoS Pathog* 2010, *6*, doi:10.1371/journal.ppat.1000792.
70. Machen, A.; Fisher, M.; Freudenthal, B. Anthrax Toxin Translocation Complex Reveals Insight into the Lethal Factor Unfolding and Refolding Mechanism. *bioRxiv* 2020, 2020.04.20.049601, doi:10.1101/2020.04.20.049601.
71. Mayor, S.; Parton, R.G.; Donaldson, J.G. Clathrin-Independent Pathways of Endocytosis. *Cold Spring Harb Perspect Biol* 2014, *6*, doi:10.1101/cshperspect.a016758.

72. Imre, N.; Hetényi, A.; Szabó, E.; Bodnár, B.; Szkalisity, A.; Gróf, I.; Bocsik, A.; Deli, M.A.; Horvath, P.; Czibula, Á.; et al. Routing Nanomolar Protein Cargoes to Lipid Raft-Mediated/Caveolar Endocytosis through a Ganglioside GM1-Specific Recognition Tag. *Advanced Science* 2020, *7*, doi:10.1002/advs.201902621.
73. Shafaq-Zadah, M.; Dransart, E.; Johannes, L. Clathrin-Independent Endocytosis, Retrograde Trafficking, and Cell Polarity. *Curr Opin Cell Biol* 2020, *65*, 112–121.
74. Nagahama, M.; Takehara, M.; Seike, S.; Sakaguchi, Y. Cellular Uptake and Cytotoxicity of Clostridium Perfringens Iota-Toxin. *Toxins (Basel)* 2023, *15*.
75. Harper, C.B.; McCluskey, A.; Robinson, P.J.; Meunier, F.A. Exploiting Endocytic Pathways to Prevent Bacterial Toxin Infection. In *The Comprehensive Sourcebook of Bacterial Protein Toxins*; Elsevier Inc., 2015; pp. 1072–1094 ISBN 9780128005897.
76. Badizadegan, K.; Wheeler, H.E.; Fujinaga, Y.; Lencer, W.I. Trafficking of Cholera Toxin-Ganglioside G M1 Complex into Golgi and Induction of Toxicity Depend on Actin Cytoskeleton. *Am J Physiol Cell Physiol* 2004, *287*, 1453–1462, doi:10.1152/ajpcell.00189.2004.-Intesti.
77. Renard, H.F.; Simunovic, M.; Lemiere, J.; Boucrot, E.; Garcia-Castillo, M.D.; Arumugam, S.; Chambon, V.; Lamaze, C.; Wunder, C.; Kenworthy, A.K.; et al. Endophilin-A2 Functions in Membrane Scission in Clathrin-Independent Endocytosis. *Nature* 2015, *517*, 493–496, doi:10.1038/nature14064.
78. Inoue, T.; Moore, P.; Tsai, B. How Viruses and Toxins Disassemble to Enter Host Cells. 2011, doi:10.1146/annurev-micro-090110-102855.
79. Nowakowska-Gołacka, J.; Sominka, H.; Sowa-Rogozińska, N.; Słomińska-Wojewódzka, M. Toxins Utilize the Endoplasmic Reticulum-Associated Protein Degradation Pathway in Their Intoxication Process. *Int J Mol Sci* 2019, *20*.
80. Barnes, A.C.; dos Santos, N.M.S.; Ellis, A.E. Update on Bacterial Vaccines: *Photobacterium Damselae* Subsp. *piscicida*. In Proceedings of the Developments in Biologicals; January 1 2005; Vol. 121, pp. 75–84.
81. do Vale, A.; Silva, M.T.; dos Santos, N.M.S.; Nascimento, D.S.; Reis-Rodrigues, P.; Costa-Ramos, C.; Ellis, A.E.; Azevedo, J.E. AIP56, a Novel Plasmid-Encoded Virulence Factor of *Photobacterium Damselae* Subsp. *piscicida* with Apoptogenic Activity against Sea Bass Macrophages and Neutrophils. *Mol Microbiol* 2005, *58*, 1025–1038, doi:10.1111/j.1365-2958.2005.04893.x.
82. do Vale, A.; Cabanes, D.; Sousa, S. Bacterial Toxins as Pathogen Weapons against Phagocytes. *Front Microbiol* 2016, *7*, 172814, doi:10.3389/FMICB.2016.00042/XML.
83. Costa-Ramos, C.; do Vale, A. do; Ludovico, P.; dos Santos, N.M.S.; Silva, M.T. The Bacterial Exotoxin AIP56 Induces Fish Macrophage and Neutrophil Apoptosis Using

Mechanisms of the Extrinsic and Intrinsic Pathways. *Fish Shellfish Immunol* 2011, *30*, 173–181, doi:10.1016/j.fsi.2010.10.007.

84. Pereira, L.M.G.; Pinto, R.D.; Silva, D.S.; Moreira, A.R.; Beitzinger, C.; Oliveira, P.; Sampaio, P.; Benz, R.; Azevedo, J.E.; dos Santos, N.M.S.; et al. Intracellular Trafficking of AIP56, an NF-KB-Cleaving Toxin from *Photobacterium Damselae* Subsp. *piscicida*. *Infect Immun* 2014, *82*, 5270–5285, doi:10.1128/IAI.02623-14.
85. Silva, M.T.; dos Santos, N.M.S.; do Vale, A. AIP56: A Novel Bacterial Apoptogenic Toxin. *Toxins 2010, Vol. 2, Pages 905-918* 2010, *2*, 905–918, doi:10.3390/TOXINS2040905.
86. Jongeneel, C.V.; Bouvier, J.; Bairoch, A. A Unique Signature Identifies a Family of Zinc-Dependent Metallopeptidases. *FEBS Lett* 1989, *242*, 211–214, doi:10.1016/0014-5793(89)80471-5.
87. Silva, D.S.; Pereira, L.M.G.; Moreira, A.R.; Ferreira-da-Silva, F.; Brito, R.M.; Faria, T.Q.; Zornetta, I.; Montecucco, C.; Oliveira, P.; Azevedo, J.E.; et al. The Apoptogenic Toxin AIP56 Is a Metalloprotease A-B Toxin That Cleaves NF-Kb P65. *PLoS Pathog* 2013, *9*, e1003128, doi:10.1371/journal.ppat.1003128.
88. Silva, M.T.; dos Santos, N.M.S.; do Vale, A. AIP56: A Novel Bacterial Apoptogenic Toxin. *Toxins (Basel)* 2010, *2*, 905–918.
89. Lisboa, J.; Pereira, C.; Pinto, R.D.; Rodrigues, I.S.; Pereira, L.M.G.; Pinheiro, B.; Oliveira, P.; Pereira, P.J.B.; Azevedo, J.E.; Durand, D.; et al. Unconventional Structure and Mechanisms for Membrane Interaction and Translocation of the NF-KB-Targeting Toxin AIP56. *Nature Communications 2023 14:1* 2023, *14*, 1–16, doi:10.1038/s41467-023-43054-z.
90. Richards, S.; Gibbs, R.A.; Gerardo, N.M.; Moran, N.; Nakabachi, A.; Stern, D.; Tagu, D.; Wilson, A.C.C.; Muzny, D.; Kovar, C.; et al. Genome Sequence of the Pea Aphid Acyrthosiphon Pisum. *PLoS Biol* 2010, *8*, e1000313, doi:10.1371/journal.pbio.1000313.
91. Yen, H.; Ooka, T.; Iguchi, A.; Hayashi, T.; Sugimoto, N.; Tobe, T. NleC, a Type III Secretion Protease, Compromises NF-KB Activation by Targeting P65/RelA. *PLoS Pathog* 2010, *6*, e1001231, doi:10.1371/JOURNAL.PPAT.1001231.
92. Oeckinghaus, A.; Ghosh, S. The NF-KappaB Family of Transcription Factors and Its Regulation. *Cold Spring Harb Perspect Biol* 2009, *1*.
93. Gilmore, T.D.; Wolenski, F.S. NF-KB: Where Did It Come from and Why? *Immunol Rev* 2012, *246*, 14–35.
94. Riedlinger, T.; Liefke, R.; Meier-Soelch, J.; Jurida, L.; Nist, A.; Stiewe, T.; Kracht, M.; Lienhard Schmitz, M. NF-κB P65 Dimerization and DNA-binding Is Important for

Inflammatory Gene Expression. *The FASEB Journal* 2019, *33*, 4188–4202, doi:10.1096/fj.201801638R.

95. Rossetto, O.; Pirazzini, M.; Lista, F.; Montecucco, | Cesare The Role of the Single Interchains Disulfide Bond in Tetanus and Botulinum Neurotoxins and the Development of Antitetanus and Antibotulism Drugs. 2019, doi:10.1111/cmi.13037.
96. Pereira, C.; Rodrigues, I.S.; Pereira, L.M.G.; Lisboa, J.; Pinto, R.D.; Araújo, L.; Oliveira, P.; Benz, R.; Santos, N.M.S.; Vale, A. Role of AIP56 Disulphide Bond and Its Reduction by Cytosolic Redox Systems for Efficient Intoxication. *Cell Microbiol* 2020, *22*, e13109, doi:10.1111/cmi.13109.
97. Magarinos, B.; Romalde, J.L.; Bandin, I.; Fouz, B.; Toranzo, A.E. Phenotypic, Antigenic, and Molecular Characterization of *Pasteurella piscicida* Strains Isolated from Fish. *Appl Environ Microbiol* 1992, *58*, 3316–3322, doi:10.1128/aem.58.10.3316-3322.1992.
98. Fahrer, J.; Kuban, J.; Heine, K.; Rupps, G.; Kaiser, E.; Felder, E.; Benz, R.; Barth, H. Selective and Specific Internalization of Clostridial C3 ADP-Ribosyltransferases into Macrophages and Monocytes. *Cell Microbiol* 2010, *12*, 233–247, doi:10.1111/J.1462-5822.2009.01393.X.
99. Finkelstein, A. The Channel Formed in Planar Lipid Bilayers by the Protective Antigen Component of Anthrax Toxin. *Toxicology* 1994, *87*, 29–41, doi:10.1016/0300-483X(94)90153-8.
100. Rodrigues, I.S.; Pereira, L.M.G.; Lisboa, J.; Pereira, C.; Oliveira, P.; dos Santos, N.M.S.; do Vale, A. Involvement of Hsp90 and Cyclophilins in Intoxication by AIP56, a Metalloprotease Toxin from *Photobacterium Damselae* Subsp. *piscicida*. *Sci Rep* 2019, *9*, 1–13, doi:10.1038/s41598-019-45240-w.
101. Foster, F.M.; Traer, C.J.; Abraham, S.M.; Fry, M.J. The Phosphoinositide (PI) 3-Kinase Family. *J Cell Sci* 2003, *116*, 3037–3040, doi:10.1242/jcs.00609.
102. Liang, K.; Islam, M.T.; Hussain, N.; Winkjer, N.S.; Im, M.S.; Rowe, L.A.; Tarr, C.L.; Boucher, Y. Draft Genome Sequences of Eight *Vibrio* Sp. Clinical Isolates from across the United States That Form a Basal Sister Clade to *Vibrio Cholerae*. *Microbiol Resour Announc* 2019, *8*, doi:10.1128/MRA.01473-18.
103. Islam, M.T.; Liang, K.; Orata, F.D.; Im, M.S.; Alam, M.; Lee, C.C.; Boucher, Y.F. *Vibrio Tarriae* Sp. Nov., a Novel Member of the *Cholerae* Clade. *Int J Syst Evol Microbiol* 2022, *72*, doi:10.1099/IJSEM.0.005571.
104. Verster, K.I.; Cinege, G.; Lipinszki, Z.; Magyar, L.B.; Kurucz, É.; Tarnopol, R.L.; Ábrahám, E.; Darula, Z.; Karageorgi, M.; Tamsil, J.A.; et al. Evolution of Insect Innate Immunity through Domestication of Bacterial Toxins. *Proc Natl Acad Sci U S*

A 2023, *120*, e2218334120, doi:10.1073/PNAS.2218334120/SUPPL_FILE/PNAS.2218334120.SM01.AVI.

105. Thompson, F.L.; Hoste, B.; Thompson, C.C.; Goris, J.; Gomez-Gil, B.; Huys, L.; Vos, P. De; Swings, J. *Enterovibrio Norvegicus* Gen. Nov., Sp. Nov., Isolated from the Gut of Turbot (Scophthalmus Maximus) Larvae: A New Member of the Family *Vibrionaceae*. *Int J Syst Evol Microbiol* 2002, *52*, 2015–2022, doi:10.1099/00207713-52-6-2015.
106. Frisan, T. Bacterial Genotoxins: The Long Journey to the Nucleus of Mammalian Cells. *Biochimica et Biophysica Acta (BBA) - Biomembranes* 2016, *1858*, 567–575, doi:10.1016/J.BBAMEM.2015.08.016.
107. Rouïl, J.; Jousselin, E.; Coeur d'acier, A.; Cruaud, C.; Manzano-Marın, A. The Protector within: Comparative Genomics of APSE Phages across Aphids Reveals Rampant Recombination and Diverse Toxin Arsenals. *Genome Biol Evol* 2020, *12*, 878–889, doi:10.1093/GBE/EVAA089.
108. Verster, K.I.; Wisecaver, J.H.; Karageorgi, M.; Duncan, R.P.; Gloss, A.D.; Armstrong, E.E.; Price, D.K.; Menon, A.R.; Ali, Z.M.; Whiteman, N.K.; et al. Horizontal Transfer of Bacterial Cytolethal Distending Toxin B Genes to Insects. *Mol Biol Evol* 2019, *36*, 2105–2110, doi:10.1093/MOLBEV/MSZ146.
109. Rodrigues, I.S.; Pereira, L.M.G.; Lisboa, J.; Pereira, C.; Oliveira, P.; dos Santos, N.M.S.; do Vale, A. Involvement of Hsp90 and Cyclophilins in Intoxication by AIP56, a Metalloprotease Toxin from *Photobacterium Damselae* Subsp. *piscicida*. *Sci Rep* 2019, *9*, 1–13, doi:10.1038/s41598-019-45240-w.
110. Peres, J.M.O. Development of Tools for the Study of AIP56 Binding/Translocation Domain. 2014.
111. Chenal, A.; Ladant, D. Bioengineering of *Bordetella Pertussis* Adenylate Cyclase Toxin for Antigen-Delivery and Immunotherapy. *Toxins (Basel)* 2018, doi:10.3390/toxins10070302.
112. Ladant, D. Bioengineering of *Bordetella Pertussis* Adenylate Cyclase Toxin for Vaccine Development and Other Biotechnological Purposes. *Toxins (Basel)* 2021, *13*.
113. Bröker, M.; Costantino, P.; DeTora, L.; McIntosh, E.D.; Rappuoli, R. Biochemical and Biological Characteristics of Cross-Reacting Material 197 (CRM197), a Non-Toxic Mutant of Diphtheria Toxin: Use as a Conjugation Protein in Vaccines and Other Potential Clinical Applications. *Biologicals* 2011, *39*, 195–204, doi:10.1016/J.BIOLOGICALS.2011.05.004.

114. Shaw, C.A.; Starnbach, M.N. Stimulation of CD8+ T Cells Following Diphtheria Toxin-Mediated Antigen Delivery into Dendritic Cells. *Infect Immun* 2006, *74*, 1001–1008, doi:10.1128/IAI.74.2.1001-1008.2006.
115. Guan, J.; Zhang, Z.; Hu, X.; Yang, Y.; Chai, Z.; Liu, X.; Liu, J.; Gao, B.; Lu, W.; Qian, J.; et al. Cholera Toxin Subunit B Enabled Multifunctional Glioma-Targeted Drug Delivery. *Adv Healthc Mater* 2017, *6*, 1700709, doi:10.1002/ADHM.201700709.
116. Lin, D.; He, H.; Sun, J.; He, X.; Long, W.; Cui, X.; Sun, Y.; Zhao, S.; Zheng, X.; Zeng, Z.; et al. Co-Delivery of PSMA Antigen Epitope and MGM-CSF with a Cholera Toxin-like Chimeric Protein Suppressed Prostate Tumor Growth via Activating Dendritic Cells and Promoting CTL Responses. *Vaccine* 2021, *39*, 1609–1620, doi:10.1016/J.VACCINE.2021.02.002.
117. Liu, S.; Netzel-Arnett, S.; Birkedal-Hansen, H.; Leppla, S.H. Tumor Cell-Selective Cytotoxicity of Matrix Metalloproteinase-Activated Anthrax Toxin. *Cancer Res* 2000, *60*, 6061–6067.
118. Liu, S.; Bugge, T.H.; Leppla, S.H. Targeting of Tumor Cells by Cell Surface Urokinase Plasminogen Activator-Dependent Anthrax Toxin. *Journal of Biological Chemistry* 2001, *276*, 17976–17984, doi:10.1074/JBC.M011085200.
119. Arora, N.; Leppla, S.H. Fusions of Anthrax Toxin Lethal Factor with Shiga Toxin and Diphtheria Toxin Enzymatic Domains Are Toxic to Mammalian Cells. *Infect Immun* 1994, *62*, 4955–4961, doi:10.1128/IAI.62.11.4955-4961.1994.
120. Kostova, V.; Dransart, E.; Azoulay, M.; Brulle, L.; Bai, S.K.; Florent, J.C.; Johannes, L.; Schmidt, F. Targeted Shiga Toxin-Drug Conjugates Prepared via Cu-Free Click Chemistry. *Bioorg Med Chem* 2015, *23*, 7150–7157, doi:10.1016/J.BMC.2015.10.010.
121. Mohseni, Z.; Sedighian, H.; Halabian, R.; Amani, J.; Behzadi, E.; Imani Fooladi, A.A. Potent in Vitro Antitumor Activity of B-Subunit of Shiga Toxin Conjugated to the Diphtheria Toxin against Breast Cancer. *Eur J Pharmacol* 2021, *899*, 174057, doi:10.1016/J.EJPHAR.2021.174057.
122. Ryou, J.H.; Sohn, Y.K.; Hwang, D.E.; Park, W.Y.; Kim, N.; Heo, W. Do; Kim, M.Y.; Kim, H.S. Engineering of Bacterial Exotoxins for Highly Efficient and Receptor-Specific Intracellular Delivery of Diverse Cargos. *Biotechnol Bioeng* 2016, *113*, 1639–1646, doi:10.1002/BIT.25935.
123. Da Silva, D.M.; Skeate, J.G.; Chavez-Juan, E.; Lühen, K.P.; Wu, J.M.; Wu, C.M.; Kast, W.M.; Hwang, K.K. Therapeutic Efficacy of a Human Papillomavirus Type 16 E7 Bacterial Exotoxin Fusion Protein Adjuvanted with CpG or GPI-0100 in a Preclinical Mouse Model for HPV-Associated Disease. *Vaccine* 2019, *37*, 2915, doi:10.1016/J.VACCINE.2019.04.043.

124. do Vale, A.; Afonso, A.; Silva, M.T. The Professional Phagocytes of Sea Bass (*Dicentrarchus Labrax* L.): Cytochemical Characterisation of Neutrophils and Macrophages in the Normal and Inflamed Peritoneal Cavity. *Fish Shellfish Immunol* 2002, *13*, 183–198, doi:10.1006/FSIM.2001.0394.
125. Silva, D.S.; Pereira, L.M.G.; Moreira, A.R.; Ferreira-Da-Silva, F.; Brito, R.M. The Apoptogenic Toxin AIP56 Is a Metalloprotease A-B Toxin That Cleaves NF-κB P65. *PLoS Pathog* 2013, *9*, 1003128, doi:10.1371/journal.ppat.1003128.
126. do Vale, A.; Costa-Ramos, C.; Silva, A.; Silva, D.S.P.; Gärtner, F.; dos Santos, N.M.S.; Silva, M.T. Systemic Macrophage and Neutrophil Destruction by Secondary Necrosis Induced by a Bacterial Exotoxin in a Gram-Negative Septicaemia. *Cell Microbiol* 2007, *9*, 988–1003, doi:10.1111/J.1462-5822.2006.00846.X.
127. Singhal, A.; Kumar, S. Neutrophil and Remnant Clearance in Immunity and Inflammation. *Immunology* 2022, *165*, 22–43, doi:10.1111/IMM.13423.
128. Nauseef, W.M. Human Neutrophils ≠ Murine Neutrophils: Does It Matter? *Immunol Rev* 2022, doi:10.1111/IMR.13154.
129. Horowitz, A.; Stegmann, K.A.; Riley, E.M. Activation of Natural Killer Cells during Microbial Infections. *Front Immunol* 2012, *2*.
130. Newman, K.C.; Korbel, D.S.; Hafalla, J.C.; Riley, E.M. Cross-Talk with Myeloid Accessory Cells Regulates Human Natural Killer Cell Interferon-γ Responses to Malaria. *PLoS Pathog* 2006, *2*, 1120–1133, doi:10.1371/journal.ppat.0020118.
131. Stegelmeier, A.A.; van Vloten, J.P.; Mould, R.C.; Klafuric, E.M.; Minott, J.A.; Wootton, S.K.; Bridle, B.W.; Karimi, K. Myeloid Cells during Viral Infections and Inflammation. *Viruses* 2019, *11*, doi:10.3390/V11020168.
132. McDaniel, M.M.; Meibers, H.E.; Pasare, C. Innate Control of Adaptive Immunity and Adaptive Instruction of Innate Immunity: Bi-Directional Flow of Information. *Curr Opin Immunol* 2021, *73*, 25, doi:10.1016/J.COI.2021.07.013.
133. European Seabass - Cultured Aquatic Species Available online: https://www.fao.org/fishery/en/culturedspecies/dicentrarchus_labrax/en (accessed on 6 May 2025).
134. Gilthead Seabream - Cultured Aquatic Species Available online: https://www.fao.org/fishery/en/culturedspecies/sparus_aurata/en (accessed on 6 May 2025).
135. Common Sole - Cultured Aquatic Species Available online: https://www.fao.org/fishery/en/culturedspecies/solea_spp/en (accessed on 6 May 2025).
136. Morone Saxatilis - Introduced Species Fact Sheets Available online: https://www.fao.org/fishery/en/introsp/1460/en (accessed on 6 May 2025).

137. Sizova, O.; John, L.S.; Ma, Q.; Molldrem, J.J. Multi-Faceted Role of LRP1 in the Immune System. 2023, doi:10.3389/fimmu.2023.1166189.
138. Nykjaer, A.; Willnow, T.E. The Low-Density Lipoprotein Receptor Gene Family: A Cellular Swiss Army Knife? *Trends Cell Biol* 2002, *12*, 273–280, doi:10.1016/S0962-8924(02)02282-1.
139. De Nardis, C.; Lossl, P.; Van Den Biggelaar, M.; Madoori, P.K.; Leloup, N.; Mertens, K.; Heck, A.J.R.; Gros, P.; Allewell, N. Recombinant Expression of the Full-Length Ectodomain of LDL Receptor-Related Protein 1 (LRP1) Unravels PH-Dependent Conformational Changes and the Stoichiometry of Binding with Receptor-Associated Protein (RAP). *Journal of Biological Chemistry* 2017, *292*, 912–924, doi:10.1074/JBC.M116.758862.
140. Ganaie, S.S.; Schwarz, M.M.; Mcmillen, C.M.; Leung, D.W.; Amarasinghe, G.K.; Hartman, A.L.; Price, D.A.; Feng, A.X.; Albe, J.R.; Wang, W.; et al. Lrp1 Is a Host Entry Factor for Rift Valley Fever Virus. *Cell* 2021, *184*, 5163–5178, doi:10.1016/j.cell.2021.09.001.
141. Prasad, J.M.; Migliorini, M.; Galisteo, R.; Strickland, D.K. Generation of a Potent Low Density Lipoprotein Receptor-Related Protein 1 (LRP1) Antagonist by Engineering a Stable Form of the Receptor-Associated Protein (RAP) D3 Domain. *Journal of Biological Chemistry* 2015, *290*, 17262–17268, doi:10.1074/JBC.M115.660084.
142. do Vale, A.; Silva, M.T.; dos Santos, N.M.S.; Nascimento, D.S.; Reis-Rodrigues, P.; Costa-Ramos, C.; Ellis, A.E.; Azevedo, J.E. AIP56, a Novel Plasmid-Encoded Virulence Factor of *Photobacterium Damselae* Subsp. *piscicida* with Apoptogenic Activity against Sea Bass Macrophages and Neutrophils. *Mol Microbiol* 2005, *58*, 1025–1038, doi:10.1111/j.1365-2958.2005.04893.x.
143. do Vale, A.; Costa-Ramos, C.; Silva, D.S.P.; Macedo, P.M.; Fernandes, R.; Sampaio, P.; dos Santos, N.M.S.; Silva, M.T. Cytochemical and Ultrastructural Study of Anoikis and Secondary Necrosis in Enterocytes Detached *in Vivo*. *Apoptosis* 2007, *12*, 1069–1083, doi:10.1007/S10495-006-0040-X/FIGURES/9.
144. do Vale, A.; Pereira, C.; R. Osorio, C.; M. S. dos Santos, N. The Apoptogenic Toxin AIP56 Is Secreted by the Type II Secretion System of *Photobacterium Damselae* Subsp. *piscicida*. *Toxins (Basel)* 2017, *9*, 368, doi:10.3390/toxins9110368.
145. Verster, K.I.; Tarnopol, R.L.; Akalu, S.M.; Whiteman, N.K. Horizontal Transfer of Microbial Toxin Genes to Gall Midge Genomes. *Genome Biol Evol* 2021, *13*, 197–205, doi:10.1093/GBE/EVAB202.

146. Conserving Monarch Butterflies and Their Habitats | Home Available online: https://www.usda.gov/about-usda/news/blog/conserving-monarch-butterflies-and-their-habitats (accessed on 22 April 2025).